The Synthesis of Shape-Persistent Macrocycles Towards the Rational Design of Stable Large-Pore Metal-Organic Frameworks

by

© Mohsen Shayan

A Thesis submitted to the School of Graduate Studies in partial fulfillment of the requirements for the degree of

Doctor of Philosophy

Faculty of Science

Department of Chemistry
Memorial University of Newfoundland

November 2021
St. John's, Newfoundland and Labrador

Abstract

Metal-organic frameworks (MOFs) are porous materials that have attracted substantial attention due to their exciting features and applications. Synthesis of MOFs involves the self-assembly of organic linkers and metal-containing inorganic nodes through coordination bonds. Given the porous structure of MOFs, it is not surprising that the targeted design of different pore architecture and functionality is of great importance. With that in mind, the pore can be designed and controlled on the molecular level by judicious choice of linkers, nodes, and controlling synthesis conditions.

MOFs with large pore sizes can provide porous materials with higher surface areas that are of interest for several applications. For example, in heterogeneous catalysis, larger pores result in faster mass transfer rates of the substrate and products. Moreover, tuning the pore size for larger molecules can accommodate larger reactants inside the pore. In order to design a MOF with larger pore size and surface area, researchers need to utilize larger linkers. However, extension of the organic linker imparts challenges in the resultant MOF structure. The two most common concerns when large linkers are used are robustness (i.e., stability) as well as the formation of interpenetrated networks, which reduces the porosity of the MOF. To make large-pore MOFs that are stable (i.e., do not collapse upon removal of guest molecules from the pore) and non-interpenetrated structures, thereby providing as much pore volume as possible, one approach is to use linkers that are both large and rigid. These large and rigid linkers have very few degrees of conformation freedom that should result in a more stable structure and are sufficiently bulky to prevent interpenetration. When combined with an inorganic node of high connectivity, the linker can result in a stable framework. One of the options is shape-persistent macrocycle scaffolds (e.g., *m*-phenylene ethynylene

macrocycle (PEM)). Another set of rigid and bulky linkers are phthalocyanines (Pc). The aim of this thesis was to synthesize PEM and Pc linkers and explore MOF synthesis with these linkers.

PEM is a shape-persistent macrocyclic compound that we were interested in as a linker scaffold due to its rigid structure and large size. I embarked on the synthesis of a tetratopic carboxylate-based PEM through Sonogashira coupling reaction and a final cyclization that is discussed in Chapter 2. The PEM was synthesized with an overall yield of 6%, which is comparable to previously reported compounds; however, our method involves less steps and can be achieved faster.

Pcs are aromatic macrocyclic compounds that have structural similarities to porphyrins. What makes Pcs and porphyrins so attractive is that the central ring of these compounds is highly conjugated, bulky, rigid, and many metal ions can be coordinated in the central cavity of these molecule. As such, these linkers are attractive choices for the development of large-pore and robust MOFs for various applications. Porphyrins have received a great deal of attention in MOF chemistry with many different types of porphyrinic linkers synthesized and applied in MOF synthesis. Pcs, on the other hand, have rarely been reported in the MOF field and the existing examples to date are limited to MOFs with a limited number of structures and applications. As such, we opted for the introductions of a new family of Pc linkers. In Chapter 3, I will discuss the synthesis of tetraimidazophthalocyanine linkers that can be used in MOF synthesis. In this thesis, I demonstrate that the strategy for the tunable synthesis of tetraimidazophthalocyaniens through the tetracyclization of imidazophthalonitrile derivatives can make both carboxylate-based and imidazolate-based linkers. Also, the synthesis is flexible to make Pc linkers with other coordination groups. These new linkers provide an opportunity for the synthesis of new PcMOFs, which are lacking in the field.

Finally in Chapter 4, I demonstrate the synthesis of PcMOF using the carboxylate-based tetraimidazophthalocyanie linker with zirconium containing nodes. As such, I explored the synthesis of PcMOFs under various condition. The aim was to explore the reaction space associated with this linker to determine if, and how, these MOFs can be formed. These conditions include temperature; different ligands and node precursors, concentrations, and ratios; reaction time; use of different modulators and the modulator concentrations; use of varying concentrations of hydrochloric acid as additive; different solvents and solvents mixture; and sonication of the reaction mixture. Powder X-ray diffraction (PXRD) and N_2 gas adsorption of the synthesized samples were evaluated as our metric for the quality of the material. As such, the highest Brunauer-Emmett-Teller (BET) surface area for PcMOF was 1220 m^2/g. Pore size distribution (PSD) and PXRD show that the synthesized materials that were obtained under different reaction conditions share similar features in terms of pore size and diffraction pattern. This finding suggests that when a porous material was obtained, the synthesis produced the same material although they have different surface areas. Therefore, the synthesized material needs a better activation method and more efficient removal of the starting materials from the pores.

To my wife, Saba.

Acknowledgments

I would like to thank my supervisor Dr. Michael Katz for his guidance and being supportive through my doctoral studies. He was an excellent supervisor that taught me to be a better chemist by triggering curiosity in fields that I didn't know about. The people within Katz research group, the MOFia research group, were always supportive and knowledgeable. Brandon, Mason, Devon, Ellan, Craig, Nathan, and Victoria, these people were awesome teammates that helped me whenever I reached out to them. Special thanks to my friends and teammates Brandon Furlong and Devon McGrath, who helped me both inside the lab with chemistry and outside with my life.

I would like to thank my supervisory committee, Dr. Bottaro and Dr. Young. Special thanks to Dr. Jian-Bin Lin for training me on PXRD and for answering my questions patiently and with details. Dr. Celine Schneider for training me and answering my questions with NMR spectroscopy and Dr. Stefana Egli for training me on MS. Dr. Randy Whittal from the University of Alberta for ESI-MS analysis. The Department of Chemistry and the School of Graduate Studies at the Memorial University of Newfoundland for the academic and financial support.

I would like to express my sincere gratitude to Dr. Ali Golbabanezhad and Fereshteh Shahhosseini for their insightful discussion and enjoyable conversation we had on mass spectrometry and chemistry in general. Ali and Fereshteh were more than just colleagues and friends. They had become like a family for me and my wife. They will be always in my memory.

Finally, I would like to convey my appreciation to my wonderful wife Saba. Saba went above and beyond to make an environment filled with love for me to stay productive and write my thesis. Without her none of this would have been possible.

List of Tables

List of Figures

List of Abbreviations and Symbols

a. u.	arbitrary units
ATR-FTIR	attenuated total reflectance-Fourier transform infrared
BET	Brunauer-Emmett-Teller
DBU	1,8-diazabicyclo[5.4.0]undec-7-ene
DEF	*N*,*N*-diethylformamide
DFT	density functional theory
DMA	*N*,*N*-dimethylacetamide
DMF	*N*,*N*-dimethylformamide
DMSO	dimethylsulfoxide
EDTA	ethylenediaminetetraacetic acid
EDX	energy dispersive X-ray
ESI-MS	electrospray ionization mass spectrometry
H_2BCPBD	1,4-bis-*p*-carboxyphenylbuta-1,3-diene
H_2BDC	1,4-benzenedicaroboxylic acid
H_2BPDC	4,4′-biphenyldicarboxylic acid
H_2TPDC	4,4′′-terphenyldicarboxylic acid
H_3BBC	4,4′,4″-[benzene-1,3,5-triyl-tris(benzene-4,1-diyl)]tribenozoic acid
H_3BTB	4,4′,4″-benzene-1,3,5-triyl-tribenzoic acid
H_3BTC	1,3,5-benzenetricarboxylic acid
H_3BTE	4,4′,4″-[benzene-1,3,5-triyl-tris(ethyne-2,1-diyl)]tribenzoic acid
H_4Py-PTP	4,4',4",4"'-((pyrene-1,3,6,8-tetrayltetrakis(benzene-4,1 diyl))tetrakis(ethyne-2,1diyl))tetrabenzoic acid

H_4TBAPy	1,3,6,8-tetrakis(*p*-benzoic acid)pyrene
H_4TCPP	tetrakis(4-carboxyphenyl)porphyrin
IUPAC	international union of pure and applied chemistry
LD-MS	laser desorption mass spectrometry
MOF	metal-organic framework
MPc	metallophthalocyanine
NMP	*N*-Methyl-2-pyrrolidone
NMR	nuclear magnetic resonance
OER	oxygen evolution reaction
ORR	oxygen reduction reaction
Pc	phthalocyanines
PcMOF	Phthalocyanine-based MOF
PEM	*m*-phenylene ethynylene macrocycle
PSD	pore size distribution
PXRD	powder X-ray diffraction
RBF	round-bottom flask
SBU	secondary building unit
SEM	scanning electron microscopy
SSA	specific surface area
TBAF	tetrabutylammonium fluoride
TEA	triethylamine
TEM	transmission electron microscopy
THF	tetrahydrofuran

TLC	thin-layer chromatography
UV-Vis	ultraviolet-visible
VOCs	volatile organic compounds
XRD	X-ray diffraction
ZIF	zeolitic-imidazolate framework
δ	chemical shift
d	doublet
dba	dibenzylideneacetone
dd	doublet of doublets
ddd	doublet of doublet of doublets
ddt	doublet of doublet of triplets
dt	doublet of triplets
Hz	hertz
J	coupling constant
m	multiplet
m/z	mass-to-charge ratio
MHz	megahertz
ppm	parts per million
q	quartet
s	singlet
t	triplet
td	triplet of doublets

TABLE OF CONTENTS

1 Introduction

1.1 Porous materials

Porous materials contain void space that is not occupied by the molecules making up the material.[1] These materials, which are characterized by their porosity, are a class of solid-state materials that play an important role in our lives such as in gas storage,[2] filtration,[3] and catalysis.[4] Therefore, the study and the development of porous materials is an important area of research among materials scientists and chemists.

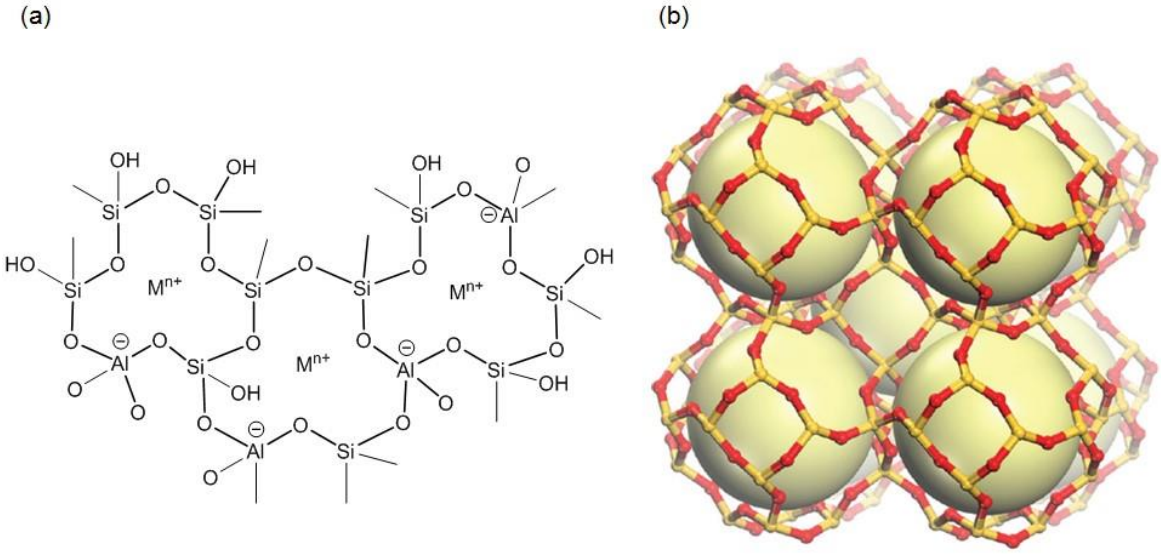

Figure 1.1 (a) Two-dimensional illustration of a zeolite framework. M^{n+} shows the counter ion of the framework. (b) Three-dimensional representation of a zeolite. Si and Al atoms are in yellow, oxygen is in red. Light yellow spheres show the pores created by the cages. Figures reprinted with permission from reference 5, Copyright (2006) Elsevier and reference 6, Copyright (2018) Royal Society of Chemistry.

One of the most popular and frequently used porous materials are zeolites. Zeolites are naturally occurring materials that can be viewed as purely inorganic coordination polymers.[5] As shown in Figure 1.1 zeolites are a class of crystalline aluminosilicates that contain group I or II

elements (Na, K, Mg, Ca) as charge compensating cations.[7, 8] The framework of the zeolite is formed via AlO_4^{5-} and SiO_4^{4-} units. The units are connected to each other via bridging oxygen groups (i.e., one of the oxygen atoms in AlO_4^{5-} is the same oxygen in the SiO_4^{4-} unit). As shown in Figure 1.1, this connectivity continues in 3-D to form a crystalline framework that contains cavities that are accessible from the external portion of the crystal (i.e., pores). The frameworks are often negatively charged and are thus charge compensated by the cations. Due to their porosity and their mechanical and thermal stability, zeolites have found numerous applications such as in petroleum refining, catalysis, ion exchange, molecular adsorption, and gas separation.[9] Since the first synthesis of zeolites reported by Barrer in 1948,[10] a wide range of structures have been synthesized.[11, 12] Furthermore, several methods have been developed for their functionalization.[13-16] However, the challenge with zeolites is that their synthesis is a practice of trial and error, and their atomic composition and functionality are limited. Moreover, zeolites have limited surface areas, that range from 400 to 600 m^2/g, and small pore sizes, mostly smaller than 1 nm,[17] which restricts their applications to molecules with kinetic diameters larger than 1 nm. Considering these limitations of zeolites, researchers have been focused on finding alternative methods of making porous materials.

Looking at the structure of a zeolite (Figure 1.1), the oxygen atom can be considered as a bridging unit. The bridging unit bridges silicon and aluminum to one another to form the overall 3-D structure. If we could extend the size of the bridging unit, this would lead to a structure with larger pores. If the length of the bridging unit can be tuned, then that offers the versatility to tune the size of the pore to any applications. Secondly, if we could design this new linker in a way that would enable researchers to also incorporate functional groups that would decorate the pores, then we would have a way to tailor the pores towards specific applications. Lastly, if we could select

the atom or group of atoms that was responsible for the attachment to the Al or Si, then we would have a truly versatile bridging group. The new linker would be versatile enough that we could explore other cations such as d-block metals in order to study how the coordination chemistry of these metals affects the pore properties of the material. Compared with zeolites, the synthesis of this newly designed material would be more flexible in terms of choices for the atomic composition, functionality, and architecture. This concept opens the realm of coordination polymers, and especially the theme of this thesis, metal-organic frameworks (MOFs).

1.2 Metal Organic Frameworks (MOFs)

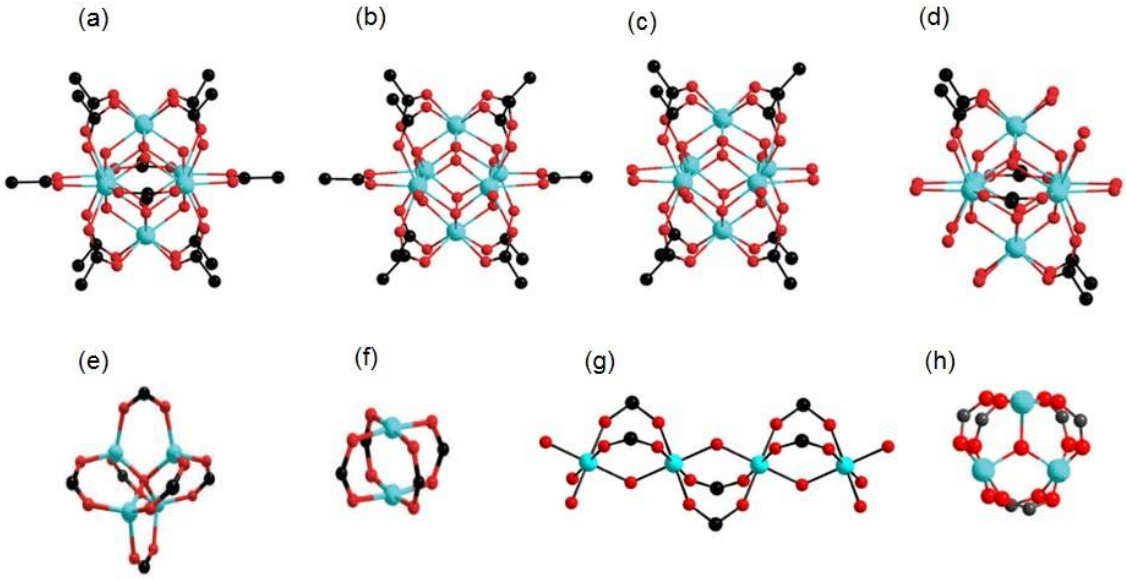

Figure 1.2 Some secondary building units (SBUs) observed in MOFs. (a) to (d) Zr_6 clusters with different connectivity. Depending on the ligand connectivity requirement and reaction conditions, this SBU can (a) 12-connected (b) 10-connected (c) 8-connected, and (d) 6-connected. (e) Zn_4O cluster. (f) paddlewheel cluster observed with Zn^{2+} or Cu^{2+} as metal. (g) chain-like SBU and (h) trinuclear SBU observed with M^{3+} metals. Atoms are color coded as Carbon: black, Oxygen: red, Metal: blue. Hydrogen atoms are omitted for clarity. Figures reprinted with permission from reference 18, Copyright (2016) Royal Society of Chemistry, reference 19, Copyright (2014) Royal Society of Chemistry, and reference 20, Copyright (2014) American Chemical Society.

In the last two decades a new class of porous materials known as MOFs have emerged and the scientific community witnessed an explosion of publications on the topic.[21] MOFs are composed of two parts, inorganic and organic. As shown in Figure 1.2, the metal component of the MOF, also known as the node or a secondary building unit (SBU) can contain an isolated metal centre (not shown), a dimer (Figure 1.2f), a trimer (Figure 1.2h), a tetramer of metal nodes (Figure 1.2e), a cluster of metal cations that contain oxo/hydroxo bridges (Figure 1.2a-d) or even chains of metal nodes (Figure 1.2g).[22] These metal nodes are linked to one another via polytopic organic bridging ligands (Figure 1.4). For example, MOF-5 (Figure 1.3a) is formed via the reaction between zinc nitrate and 1,4-benzenedicaroboxylic acid (also known as terephthalic acid; H_2BDC).[23] While zinc nitrate is used in the synthesis, the node of MOF-5 contains a Zn_4O^{6+} unit (Figure 1.2e and Figure 1.3b) that can connect to six BDC^{2-} ligands to make a cubic framework.

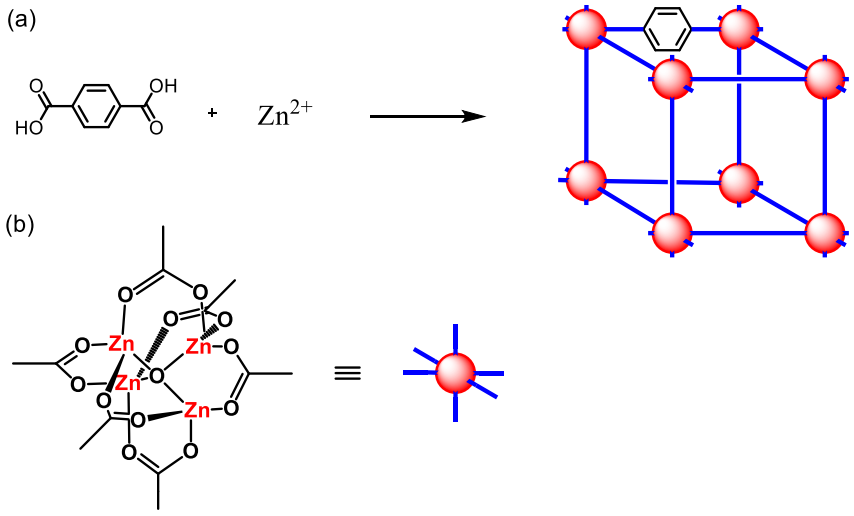

Figure 1.3 Synthesis of MOF-5 from zinc ions and benzenedicarboxylic acid. (b) Structure of the SBU in MOF-5.

The central theme of the linker is, as described above, a stable core that contains two or more locations (Lewis-base sites) for metal ions to coordinate and promote metal-metal bridging rather than metal chelation (e.g., 4,4′-bipyridine *vs.* 2,2′-bipyridine). Figure 1.4a shows some

important features of an organic linker. Organic ligands that are used for the construction of MOFs can include carboxylates, phosphonates, sulfonates, and N-donor heterocyclic compounds such as azolates, imidazolates, and pyridyl (Figure 1.4).[24] Although employing organic ligands with single N-donor groups on each side such as 4,4′-bipyridine and appropriate metal ions can lead to the creation of open frameworks, in most cases, the framework collapses upon evacuating or exchanging the guests filling inside the pores (which is a required process in MOFs activation). In contrast, multidentate ligands such as carboxylates, make it possible to form more stable frameworks, because of their ability to form rigid SBUs instead of connecting to single metal ions. Besides, organic ligands can have a variety of geometries such as trigonal planar, and square planar which can have different connectivity to the node.[25] These ligands often range from ditopic, tritopic, to tetratopic (Figure 1.4 b, c, and d). These can affect the size and shape of the pore. The addition of non-node coordinating functional groups on the organic linker can have an important effect on the properties and applications of MOF.[26] These functional groups decorate the pore and thus play a critical role in modifying the properties between the host and guest. This approach has been used in a multitude of applications such as in CH_4/CO_2 separation,[27] and mercury sorption in water treatment.[28] In addition to introducing ligand functional groups, the length of the organic linkers can be extended to make larger linkers such as 4,4′-biphenyldicarboxylic acid (H_2BPDC) and 4,4′′-terphenyldicarboxylic acid (H_2TPDC).[19] These longer linkers allow the chemist to study how an increased pore size changes the observed property. From just these two variables (i.e., changing the length of the linker and the linkers functional group) a vast range of structure-property relationships can be examined; therefore, an endless number of linkers can be designed for use in MOF synthesis.

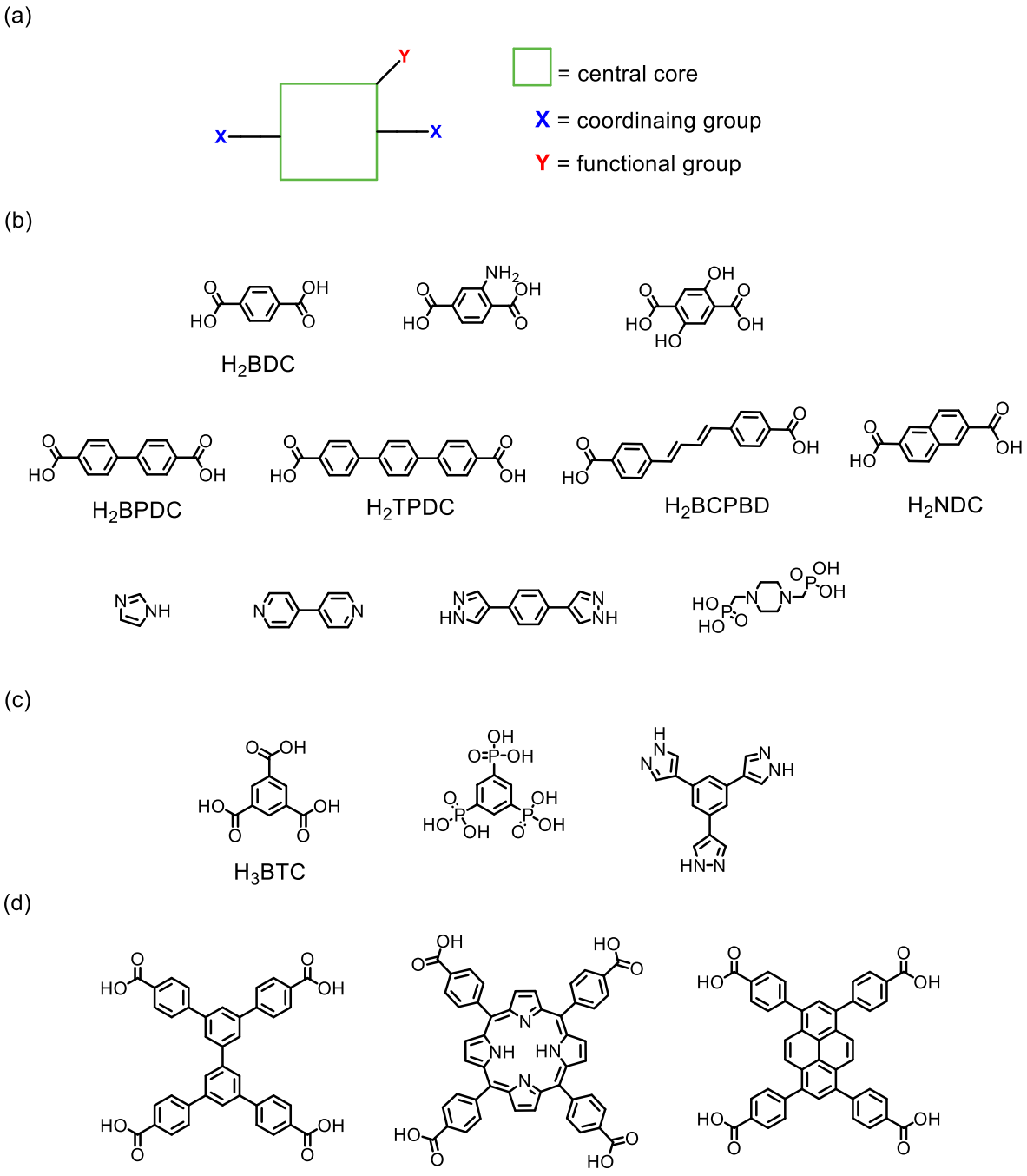

Figure 1.4 (a) Schematic representation of a linker used in MOF synthesis. The central core must have more than one coordination cite that is shown as X, and the core may have functional groups that is shown as Y. (b) to (d) select examples of linkers used in MOF synthesis. (b) ditopic linkers. (c) tritopic linkers, and (d) tetratopic linkers.

For the inorganic component of MOFs, there is a wide variety of metal cations to choose. As such, many of the metals in the periodic table can be used in MOF synthesis.[29] Often, the metal chosen for the work is related to the stability that it imparts on the resultant framework. The weakest point in a MOF framework is usually the metal–ligand bond. For example, the ionic character of the alkaline earth metals makes MOFs based on these metals more vulnerable to hydrolysis. In applications where the presence of moisture is inevitable, for example in adsorption of CO_2 from the flue gas, using M-MOF-74 (M is the metal in the SBU, crystal structure of this MOF is shown in Figure 1.5) Mg has been shown to be more humidity-sensitive than other isostructural analogues.[30] As such alkaline earth-based MOFs are less favorable in that sense. On the other hand, trivalent and tetravalent metals have better chemical/hydrothermal stability compared with MOFs made from other metals.[31] For example, MOF-5 (Figure 1.3a) and UiO-66[32] both use H_2BDC as the linker, but the Zn_4O^{6+} SBU in MOF-5 is considerably more sensitive to moisture than the $Zr_6O_4(OH)_4^{12+}$ node in UiO-66.[33] The first reason for this chemical stability is that tri-and tetravalent metal ions are hard Lewis-acids due to their high charge and charge to size ratio; the coordination bond between the hard Lewis-base carboxylate ligand and the hard Lewis-acid metal ion is stronger. Additionally, the higher nuclearity SBUs is responsible for the higher degree of chemical stability.[18] It is for this reason that Zr^{4+}, Hf^{4+} and other high-charge metal-based cluster nodes (Figure 1.2) are so prevalent in the literature today.

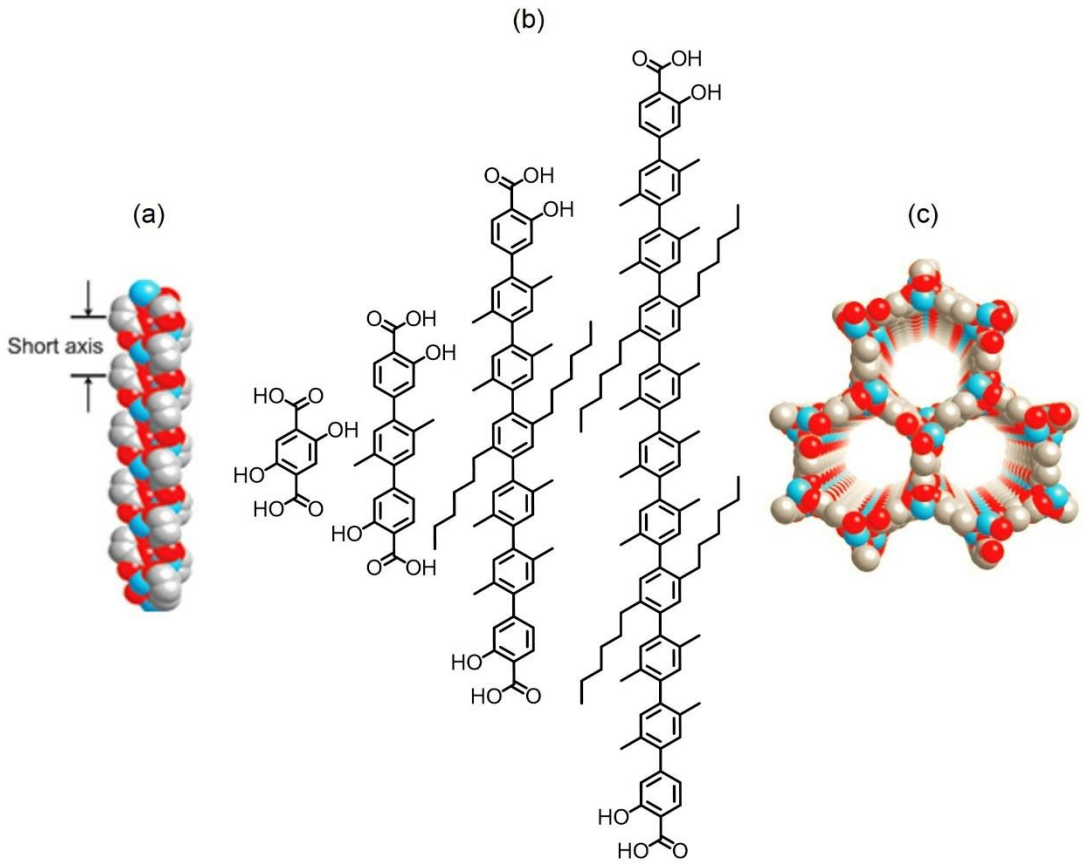

Figure 1.5 a) Metal oxide SBU chain-like structure. Atoms are color codes as Carbon: grey, Oxygen: red, and Metal: blue. (b) Some ligands used for the synthesis of M-MOF-74 series. (c) M-MOF-74 crystal structure made by coordination of ligand to the metal oxide SBU. Adapted with permission from reference 34, Copyright (2019) Elsevier.

Beside acting as connecting points in MOFs, SBUs can have other functions. For example, open metal cites (vacant Lewis-acid sites) can act as interaction site for gas molecules in gas uptake applications.[35] These coordinatively unsaturated sites can be produced upon activation process of the MOF, which is the removal of the solvent molecules from the MOF framework, or MOFs can be engineered to form open metal sites during the synthesis. For example, M-MOF-74 (shown in Figure 1.5) has abundant of open metal sites (one per metal). For M-MOF-74, different divalent metals can be incorporated (M = Mg, Mn, Fe, Co, Ni, Zn). This has enabled researchers to study

the role of each metal on the gas adsorption properties. For CO_2 adsorption applications, lighter metals such as Mg cause Mg-MOF-74 to have a higher gravimetric uptake (CO_2 per gram of material). Gravimetric uptake is important when the weight of the material (i.e., in transportation applications) is important. In addition to gas adsorption, MOFs with accessible open metal cites have been used in catalytic applications[36].

What makes MOFs attractive for different applications is a combination of the high surface areas that can be achieved as well as the tunable size and functionality that can be introduced to the pore. This is important because these features make it possible to tailor MOFs for specific applications. Furthermore, since the materials are traditionally crystalline, it is easy to determine a structure-property relationship.

1.3 Designing of MOFs

One of the goals of MOF chemistry is to enable researchers to design the topology and pore properties (shape, size, aperture, and functionality) by judiciously choosing the SBU, ligand, and functional group that present into the pore. It is the combination of the geometry of the SBU as well as that of the organic ligands that indicates the topology and pore structure of the framework and ultimately the properties of the resultant MOFs. By strategically selecting ligands and SBUs, MOFs with controlled pore functionality, shape, and size can be made. This approach introduced by Yaghi and colleagues, which is known as "reticular synthesis", allows for the synthesis of various MOF structures through the modification of the ligand or SBUs.[37] Once SBUs are formed with fixed linking geometries, predesigned ligands assembly to the SBUs will result in the construction of MOFs with ideally predicted structural topologies. In summary, the ultimate framework topology is defined by the combined effect of the both likers and the SBUs.

1.3.1 Influence of SBU and ligand on the MOF topology

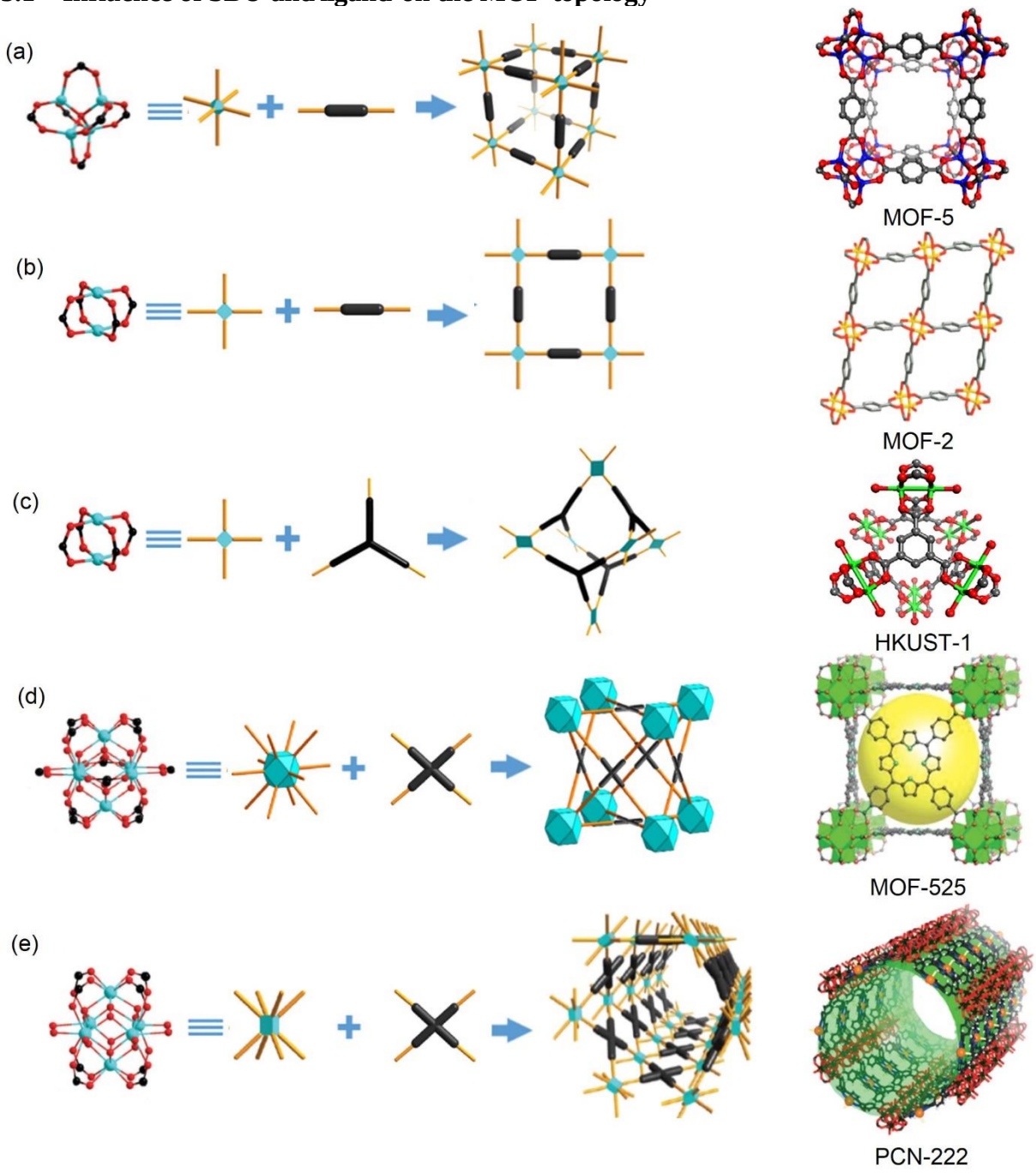

Figure 1.6 Schematic representation of selected examples showing construction of MOFs from some SBUs and ligands. Crystal structure of representative MOFs are shown on the right side of each example. Figures adapted with permission from references 19 and 18, Copyright (2014) and (2016) Royal Society of Chemistry, reference 38, 39 and 40, Copyright (2015), (2012), and (2001) American Chemical Society, reference 41, Copyright (2010) Taylor & Francis, and reference 42 Copyright (2012) Wiley.

Different metal ions as well as different reaction conditions can produce SBUs of varied geometry and connectivity.[43] Therefore, change in SBU geometry, while the ligand is unchanged, leads to different topologies. For example, MOF-5 is the product of the solvothermal reaction between zinc nitrate and H_2BDC. However, when at room temperature, a mixture of zinc nitrate and H_2BDC in *N*,*N*-dimethyl formamide (DMF):toluene mixture, which is exposed to slow vapor diffusion of triethylamine (TEA), yields prism-shaped crystals of MOF-2 (Figure 1.6b).[44] The difference between the topologies of these two MOFs originates from the square planar dizinc paddlewheel that has four points of extension in MOF-2 as opposed to the octahedral SBUs that has six points of extension in MOF-5. In MOF-5, as is shown in Figure 1.3b, four Zn^{2+} ions form a cluster around an oxygen atom to form Zn_4O^{6+} units. These four zinc atoms are bridged by six carboxylates to form the SBU component of the MOF. This SBU is in the form of an octahedral-directing node and the points of extension, that are the carbon atom of the carboxylate, lie on the corners of this octahedron. It is the combination of this octahedral-directing node and the linear BDC^{2-} ligand that construct the cubic framework of MOF-5. In principle, it would be possible to make such cubic framework with any linear ditopic ligand and any SBU that the points of extension are on the edges of an octahedral. Other examples presenting the effect of the change in SBU on MOF structure are shown in Figure 1.6 d and e. Therefore, the geometry of SBU, that depends both on the nature of the metal ion and the synthesis conditions, has an important effect on the topology of the MOF.

While SBUs are one method of changing the topology of the MOF, ligands are traditionally the method that is investigated first.[19] This is because SBUs are generated *in situ* so that the geometry and composition of the SBU are not always predictable. Hence, the geometry, connectivity, and length of the organic ligand, which are at the synthetic control of the chemist, are more wildly investigated in designing MOFs. Therefore, designing organic likers is critical to

obtain MOFs with desired functions. For example, when using tritopic 1,3,5-benzenetricarboxylic acid (H_3BTC) instead of H_2BDC, HKUST-1[45] which is a 3-D MOF can be formed with the node in Figure 1.6c (4-connected square planar dicopper paddlewheel); this contrasts with H_2BDC, which forms a 2-D MOF (MOF-2) with the same node. Thus, it is very easy to see how new topologies can be investigated by simply changing the number of types of connection groups on the ligand.

1.4 Mesoporous MOFs

The majority of MOFs made are microporous.[6] As categorized by International Union of Pure and Applied Chemistry (IUPAC), micropores are pores that are less than 2 nm. MOFs with pores larger than 2 nm are of interest to chemists.[46] In applications such as catalysis and separation, mass transfer through the micropores hinders the application of MOFs. In addition to these applications, if larger pores MOFs could be made, then inclusion of enzymes or nanoparticles inside the pore of these MOFs can enable new applications of catalyst-based MOFs. For these new applications, rational design and synthesis of mesoporous MOFs (pore size 2-50 nm) are important. Extending the MOF network can be achieved by choosing longer organic ligands. However, making MOFs with large pore size and big enough apertures for the inclusion and passage of large molecules is challenging. Attempts to extend the pore size by choosing larger ligands usually yield interpenetrating structures, thereby largely reduces the size of the pores. In some other cases, using extended ligands may cause the formation of fragile frameworks prone to collapse and disintegration upon removal of solvent molecules.[46] Since the first report of mesoporous IRMOF-16, which was made utilizing H_2TPDC,[47] new mesoporous MOFs have been continuously reported. There are various methods of making mesoporous MOFs, among which some of the relevant examples selected and included here.

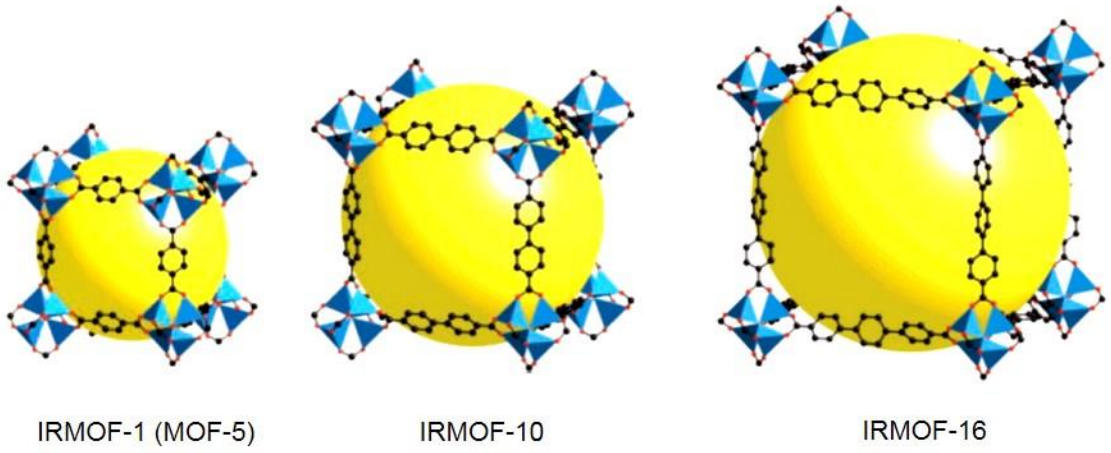

Figure 1.7 A series of isostructural MOFs made of Zn_4O^{6+} SBU and extension of the linear ditopic ligand BDC^{2-}. The spheres show the empty space of pores. Reprinted with permission from reference 48, Copyright (2019) American Chemical Society.

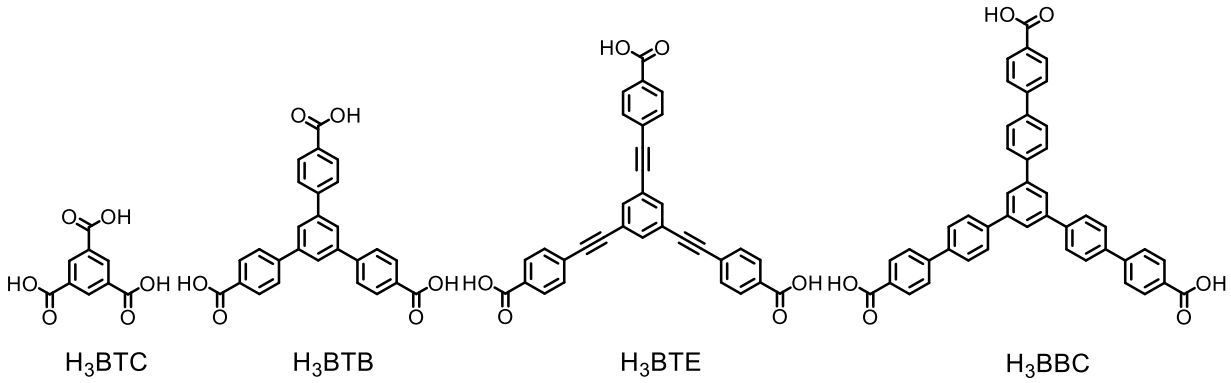

Figure 1.8 Some tritopic linkers used in the synthesis of MOFs.

IRMOF-16 that was reported by Yaghi and co-workers in 2002 was the first 3-D mesoporous MOF.[47] This MOF was made by extending the ligand length of the prototype MOF-5 by employing H_2TPDC instead of H_2BDC (Figure 1.7). This breakthrough example proved that reticular chemistry can be employed in the realm of fully ordered mesoporous MOFs. However, no further information regarding the N_2 adsorption of the IRMOF-16 was reported. As previously mentioned, a common issue in designing large-pore MOFs by extending the ligand length is

interpenetration. However, if linkers and nodes that create non-interpenetrated topologies are used, then this problem can be avoided.[49] For example, the topology formed between tritopic linkers such as H_3BTC and the prototypical Zn_4O^{6+} SBU cannot interpenetrate. With that in mind, researchers have used longer tritopic linkers (Figure 1.8) to form non-interpenetrated MOFs.[49] MOF-177, MOF-180, and MOF-200 (Figure 1.9) are examples of such isostructural frameworks that are made of Zn_4O^{6+} as SBU and 4,4′,4″-benzene-1,3,5-triyl-tribenzoate (BTB^{3-}), 4,4′,4″-[benzene-1,3,5-triyl-tris(ethyne-2,1-diyl)]tribenzoate (BTE^{3-}), and 4,4′,4″-[benzene-1,3,5-triyl-tris(benzene-4,1-diyl)]tribenozate (BBC^{3-}) as ligand respectively. These MOFs are on the border of mesoporous frameworks, with cage sizes as large as 18×28 Å and Brunauer-Emmett-Teller (BET) surface areas as high as 4530 m^2/g.

To further pursue the goal of mesoporous MOFs, it has been shown that tritopic linkers can be used in combination with ditopic linkers in a mixed ligand strategy to make non-interpenetrated mesoporous MOFs with high surface area. For example, Yaghi and co-workers made MOF-210 (Figure 1.9) by linking Zn_4O^{6+} SBUs with a mixture of BTE^{3-} and $BPDC^{2-}$ as ligand.[49] The largest pore size in this MOF is 30×48 Å. The highest record of specific surface area for a MOF to date belongs to DUT-60 (Figure 1.9) with BET surface area of 7800 m^2/g;[50] this MOF contains Zn_4O^{6+} SBUs linked via tritopic BBC^{3-} ligand and the bridging ditopic ligand 1,4-bis-*p*-carboxylatephenylbuta-1,3-diene ($BCPBD^{2-}$). The resultant MOF has two kinds of mesopores with dimensions of 37×42 and 15×27 Å. In MOF-210 and DUT-60 examples, the ditopic ligands act as auxiliary ligands that cross-link between the large pores and prevent interpenetration as well as the collapse of the framework upon activation.

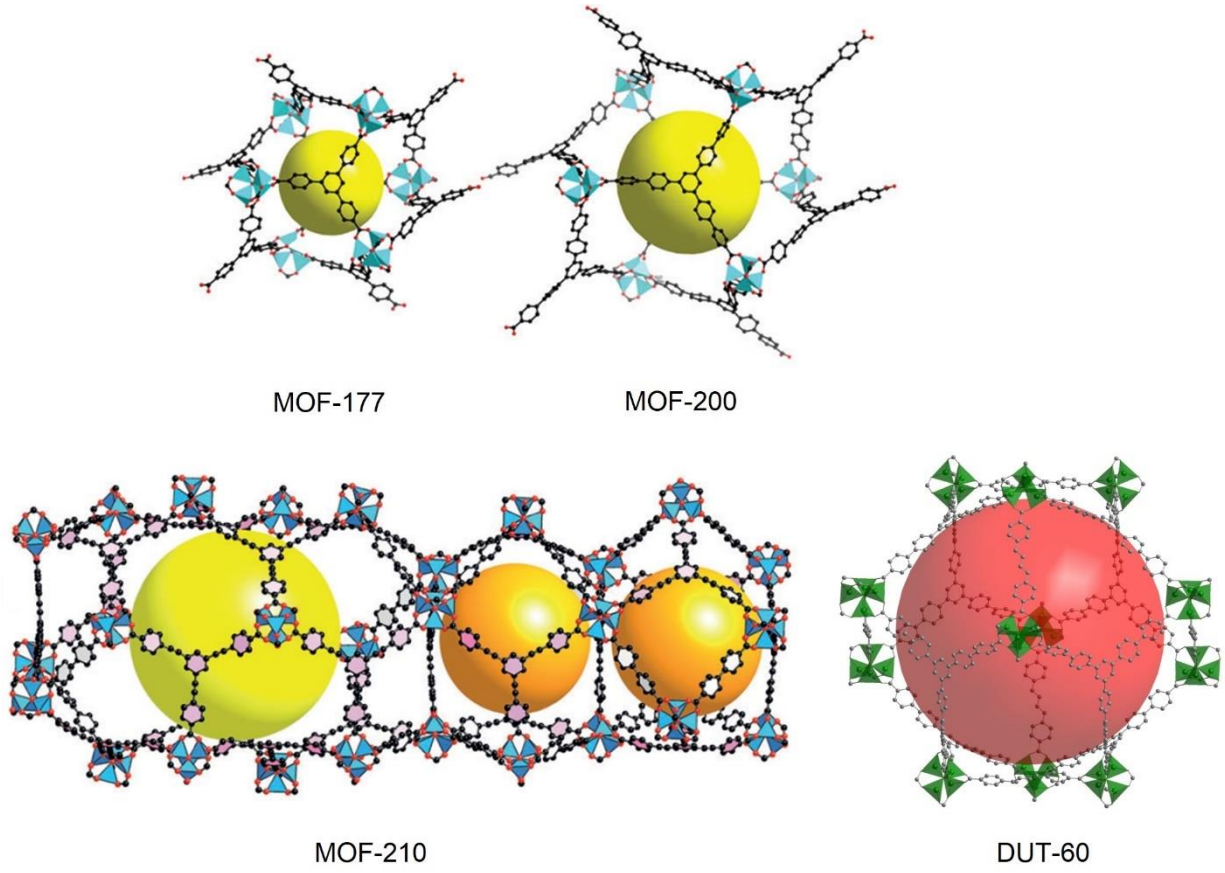

Figure 1.9 Crystal structure of some selected examples of MOFs made of Zn_4O^{6+} SBU and triangular tritopic ligands. The spheres show the empty space of pores. Figures reprinted with permission from reference 19, Copyright (2014) Royal Society of Chemistry, reference 51, Copyright (2015) Wiley, and reference 52, Copyright (2020) Nature.

Mesoporous MOFs with 1-D channels can be synthesized using rod-packing SBUs.[53] An example of a MOF with rod-packing SBU that forms 1-D channels is M-MOF-74 (Figure 1.5) and its derivatives.[54] M-MOF-74 is composed of dicationic metal centers linked to one another by dihydroxy-BDC, which is deprotonated on the carboxylic acid as well as the hydroxyl units to make the tetra-anionic 2,5-dioxido-1,4-benzene-dicarboxylate. It has been shown that by increasing the length of the ligand, it is possible to make a series of isostructural non-interpenetrating frameworks with pore sizes up to 98 Å. As shown in Figure 1.5a, connecting

points on the SBU are spaced so close from each other that coordinating organic ligands, which are aligned perpendicular to the rod-packing SBU, form a tightly packed wall. The small space between the parallel ligands is insufficient to allow another ligand to start a secondary framework. This enables the formation of mesopores without the danger of forming interpenetrated frameworks.

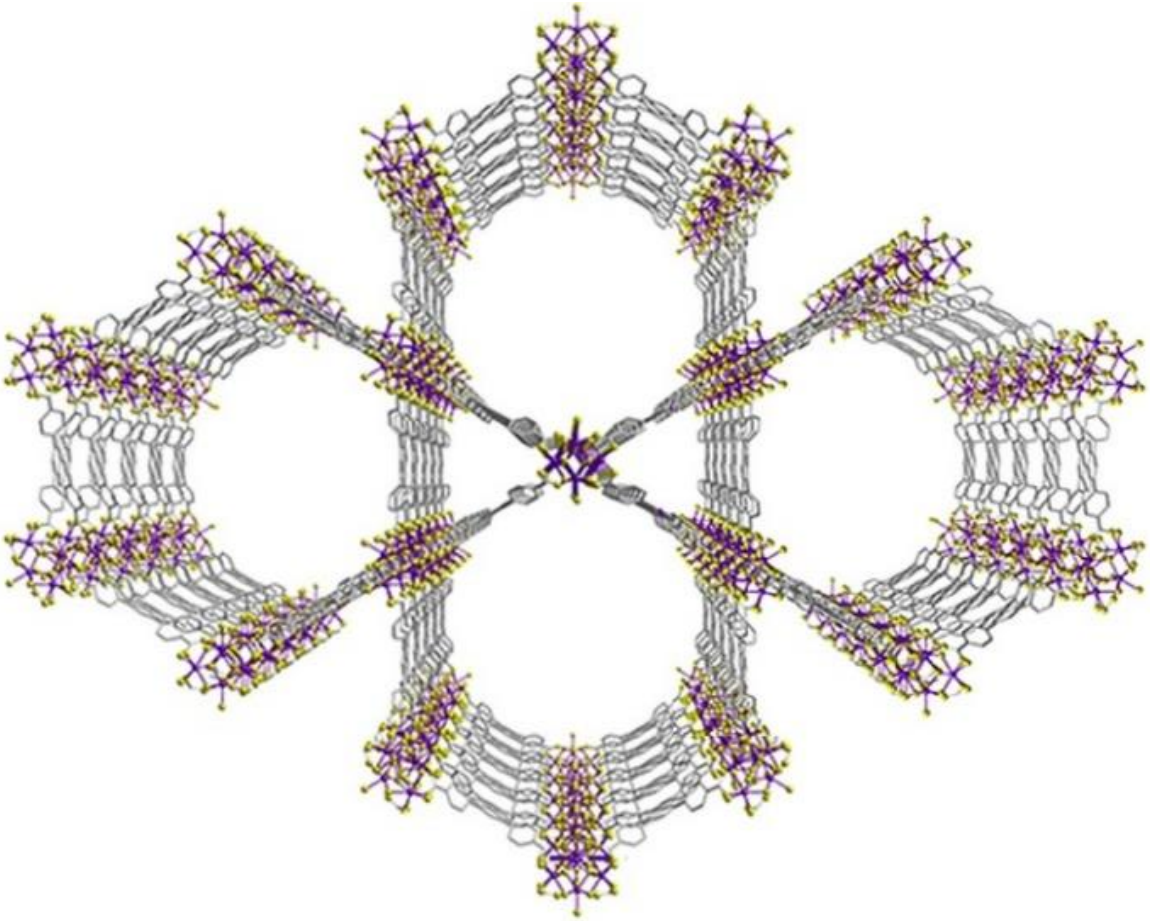

Figure 1.10 Crystal structure of NU-1000 made of 8-conneded Zr_6 SBUs and $TBAPy^{4-}$ ligands. SBUs are at the vertices and the ligands form the sides of the hexagons or trigons. Adapted with permission from reference 55, Copyright (2013) American Chemical Society.

There is a handful of MOFs with 1-D mesopores that are made using tetratopic ligands and versatile connectivity of Zr_6 clusters.[18] Pyrene-based ligands are among the most explored ligands in this field. NU-1000 is an iconic MOF with 1-D channels (31 Å hexagonal mesopore channels and 12 Å trigonal micropore channels. Figure 1.10) and high surface area (2300 m^2/g).[55] This MOF is composed of 8-connected Zr_6 cluster (Figure 1.2c) and tetratopic ligand 1,3,6,8-tetrakis(*p*-benzoate)pyrene ($TBAPy^{4-}$) (Figure 1.11). As expected, larger pyrene-based ligands (Figure 1.11) give MOFs isostructural with NU-1000 such as NU-1003, NU-1004, NU-1005, NU-1006, and NU-1007 among which NU-1007 has the widest hexagonal channel of 67 Å.[56]

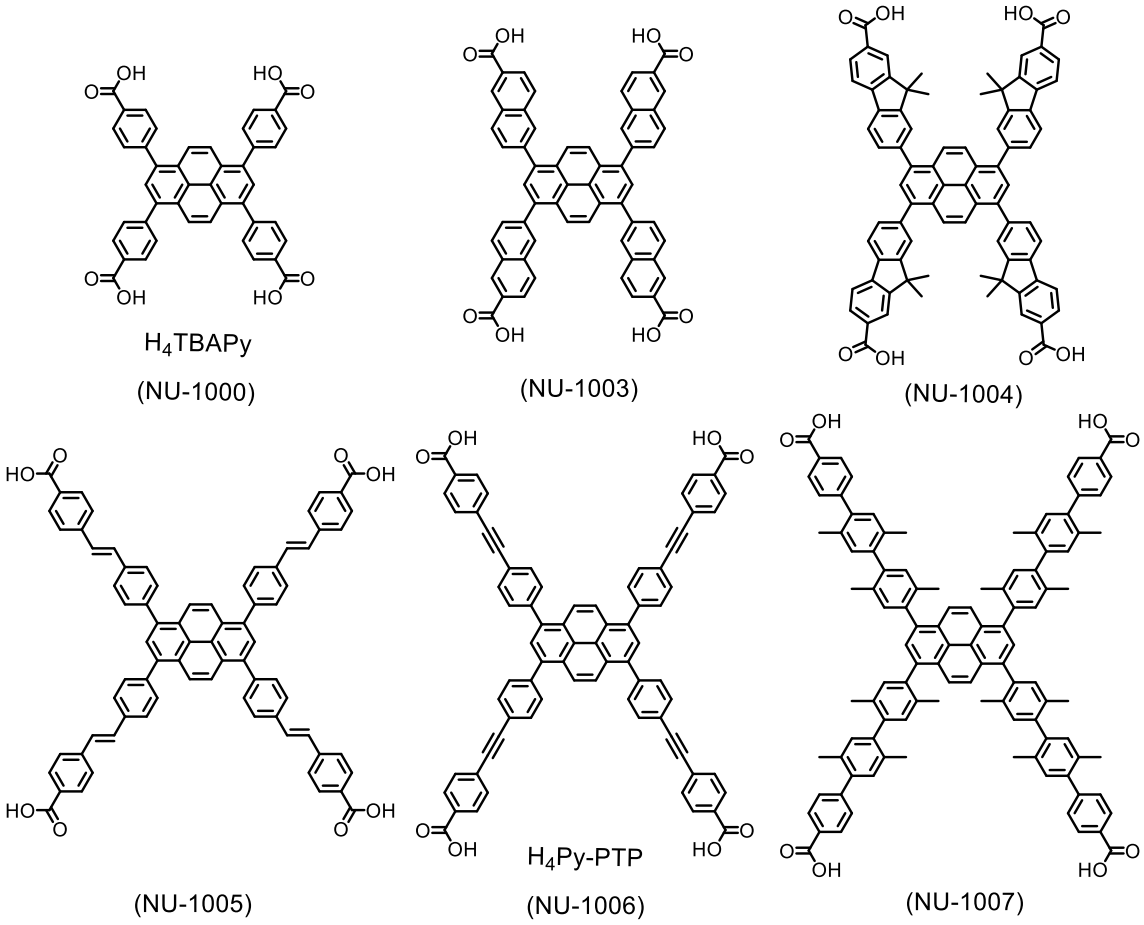

Figure 1.11 Some tetratopic pyrene-based linkers used in the synthesis of Zr-based MOFs with1-D channel hexagonal pores. Labels in parentheses show the MOF in which the associated linker is used.

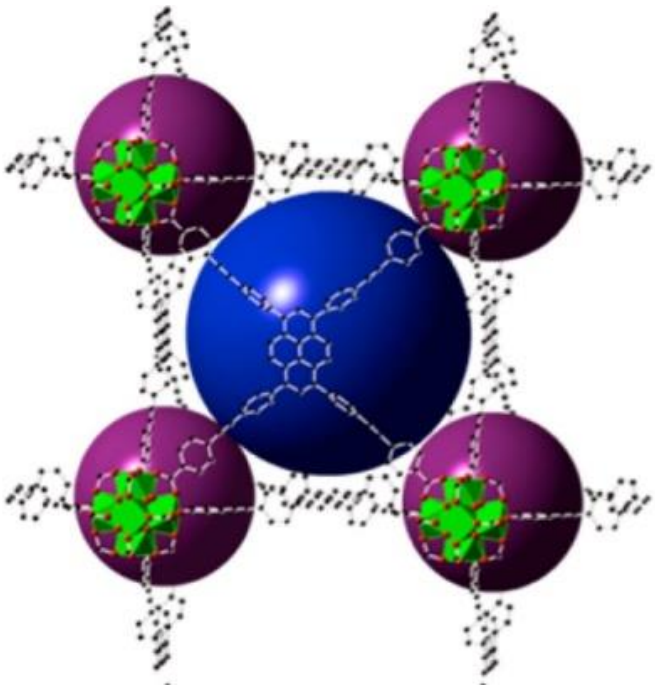

Figure 1.12 Crystal structure of NU-1103 made of 12-conneded Zr_6 SBUs and Py-PTP^{4-} ligand. SBUs are shown in green at the vertices and the ligands form the sides of the cube. Purple spheres show the smaller pore, and the blue sphere shows the larger pore. Reprinted with permission from reference 57, Copyright (2015) American Chemical Society.

Pyrene-based ligands can also be used for making MOFs with 3-D mesopore cages. The versatile connectivity regimes of Zr_6 cluster provides the opportunity of synthesis of different MOF topologies with the same building blocks. For example, MOFs with a cubic structure (Figure 1.12) can be made using tetratopic pyrene-based ligands (Figure 1.13) and 12-connected Zr_6 cluster (Figure 1.2a). This isostructural series of MOFs (NU-110x series = NU-1106,[58] NU-1100,[59] NU-1101,[57] and NU-1103[57]) have increasing larger pore sizes. Among these MOFs, NU-1103 that uses 4,4',4",4"'-((pyrene-1,3,6,8-tetrayltetrakis(benzene-4,1-diyl))tetrakis(ethyne-2,1diyl))tetrabenzoic acid (H_4Py-PTP) as linker is mesoporous with two types of pores (Figure 1.12), the larger one is 22.7 Å and the smaller one is 12.7 Å.

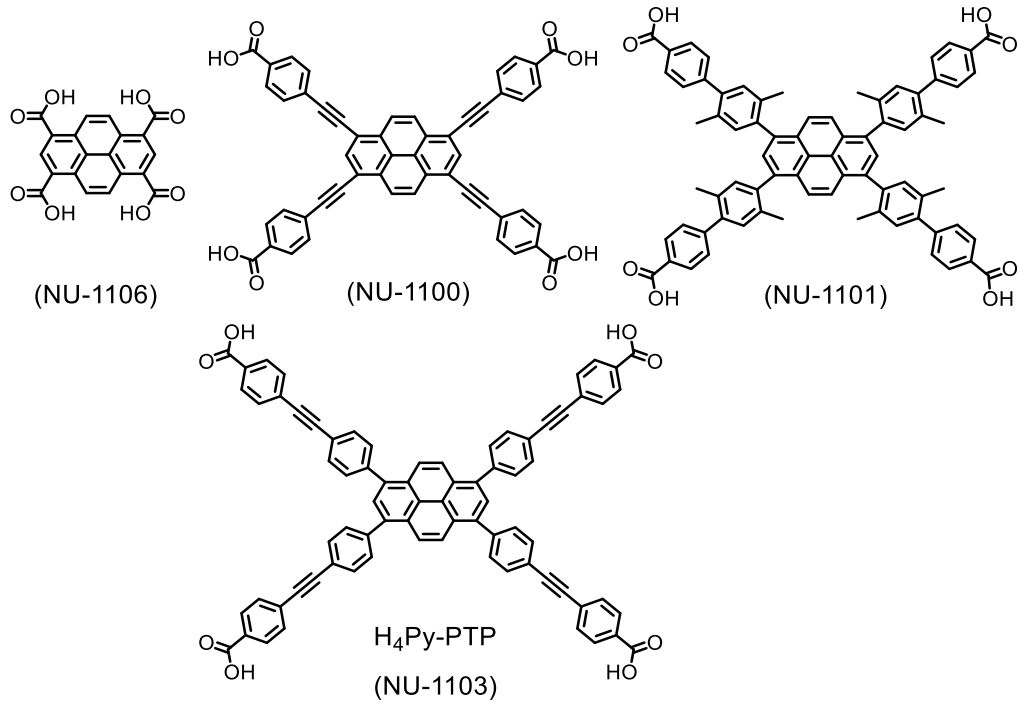

Figure 1.13 Some tetratopic pyrene-based linkers used in the synthesis of Zr-based MOFs with 3-D cubic cage pores. Labels in parentheses show the MOF in which the associated linker is used.

1.5 Rigid macrocyclic ligands for the synthesis of MOFs

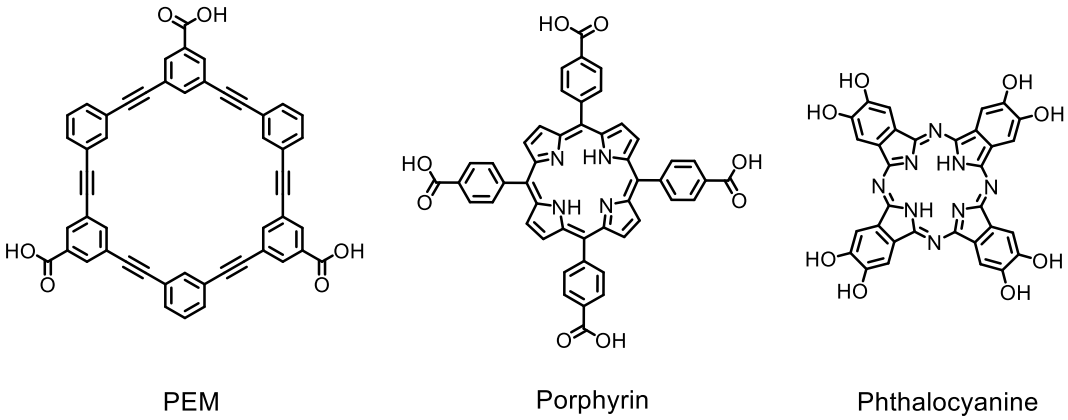

Figure 1.14 Macrocyclic ligands used in MOF synthesis. Phthalocyanine, *m*-phenylene ethynylene macrocycle (PEM), and porphyrin are selected examples representative of these families of ligands.

Macrocyclic ligands are bulky, therefore when used in MOF synthesis, these ligands can potentially make MOFs with large pores without interpenetration. However, the macrocycle used

for this purpose needs to be rigid as well for the MOF to have a robust structure. The rigid macrocyclic ligands that have been used so far in MOF synthesis are *m*-phenylene ethynylene macrocycle (PEM),[60, 61] porphyrins,[62] and phthalocyanines (Pc)[63] (Figure 1.14).

1.5.1 *m*-phenylene ethynylene macrocycle-containing MOFs

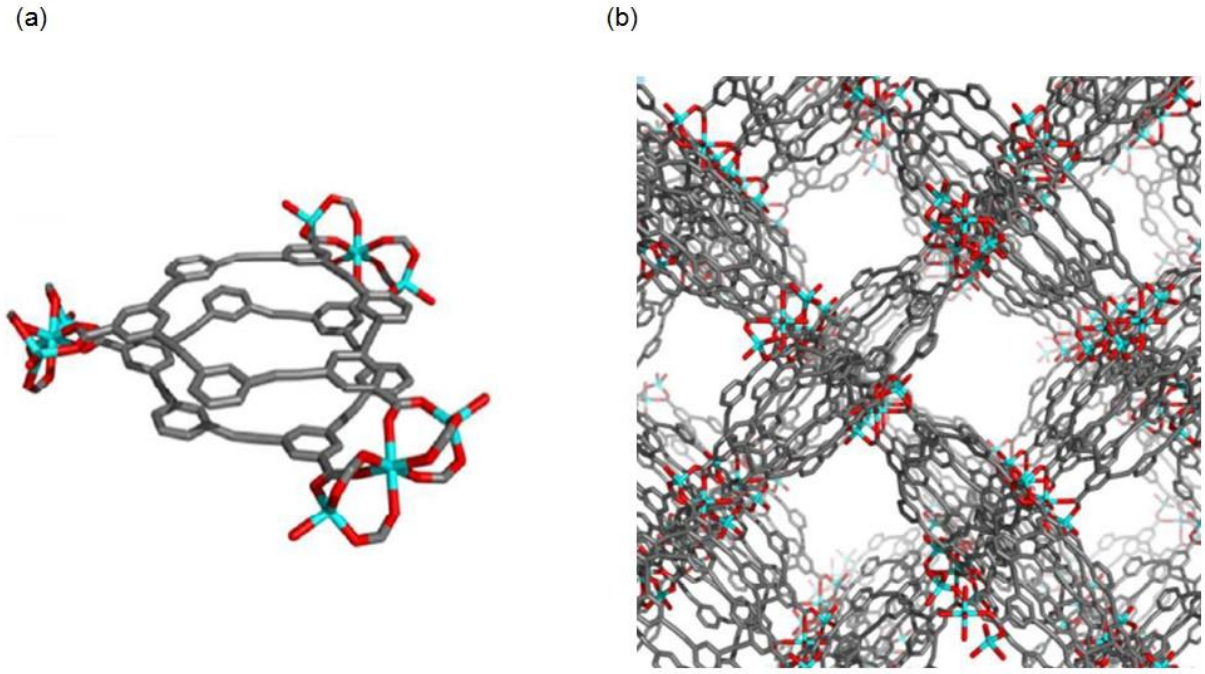

Figure 1.15 Crystal structure of Zn-MCMOF. (a) Stack of PEM coordinated to the Zn_3 SBU. (b) 1-D aperture in the structure with 20 Å size. Atoms are color codes as Carbon: grey, Oxygen: red, and Zn: blue. Reprinted with permission from reference 60, Copyright (2015) Royal Society of Chemistry.

Miljanic and co-workers synthesized and used PEM ligand for the first time in MOF synthesis.[60, 61] This ligand is a shape-persistent molecule that has a cavity of 8.6 Å. In their first report of using this ligand in MOF synthesis, they made a mesoporous MOF, Zn-MCMOF, that is composed of PEM as ligand and Zn_3 cluster as SBU (Figure 1.15).[60] In the structure of this MOF, every two PEMs are [π-π] stacked with a distance of 3.64 Å and the MOF has 3-D channels that are connected to each other. The largest aperture of these channels is around 20 Å. Although the expected surface

area based on the crystal structure of this MOF is calculated 4203 m^2/g, the experimental value is only 518 m^2/g that is attributed to the collapse of pores in the activation process.

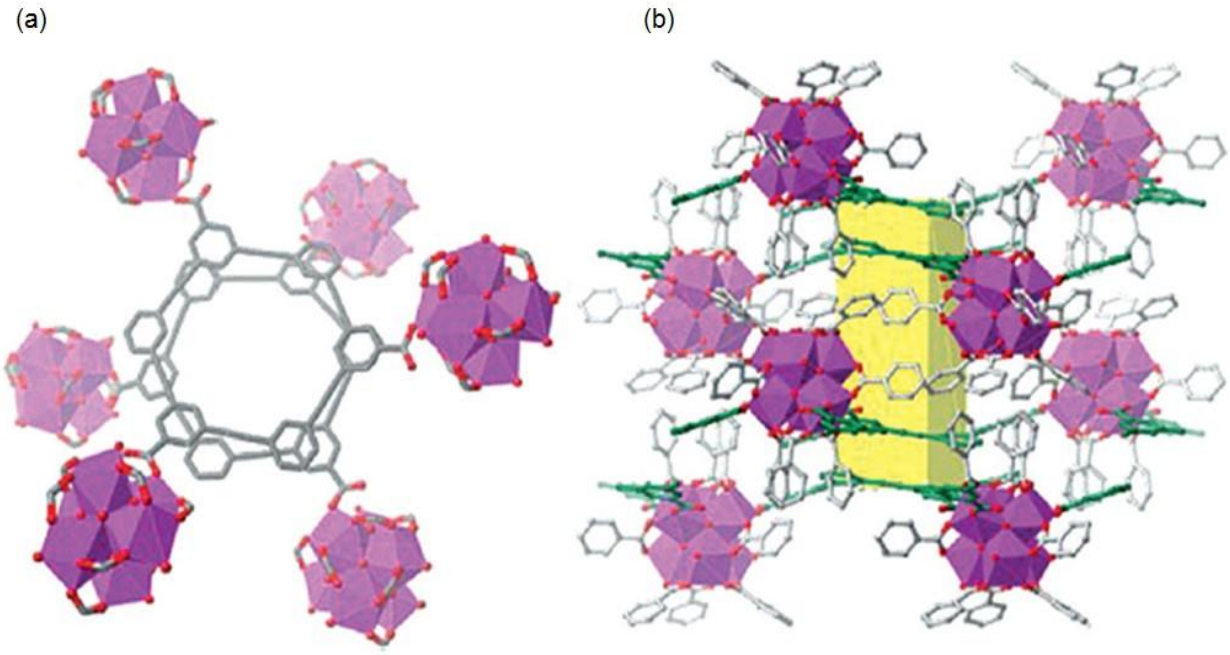

Figure 1.16 Crystal structure of Zr-MCMOF. (a) Stack of PEM coordinated to Zr_6 SBU. (b) 1-D channel (in yellow) in the structure with 9 Å aperture size. Atoms are color coded. Zr is shown as purple polyhedral, Carbon: grey, and Oxygen: red. Reprinted with permission from reference 61 Copyright (2017) Wiley.

In the second report by Miljanic and co-workers, using PEM as linker and 3-connected Zr_6 cluster as SBU resulted 3-D framework microporous Zr-MCMOF (Figure 1.16) that has 1-D channels with 9 Å aperture and BET surface area of 317 m^2/g.[61] In this MOF, it is the macrocycle void size that acts as a predesigned pore and dictates the 1-D channel aperture size. Similar to Zn-MCMOF, the ligands are [π-π] stacked with a distance of 3.45 Å. this stacking force the Zr_6 cluster to form layered structure. Interestingly, single crystal X-ray reveals that only one oxygen of each carboxylate group is coordinated to the Zr_6 SBU; as a result, this MOF shows less chemical stability compared with what is expected from a Zr-based MOF.

1.5.2 Porphyrins as macrocyclic ligands

Porphyrins are a class of highly conjugated N-heterocyclic macrocycles that can be found in nature. This can be in the form of the visible light active site molecules in chlorophyll that is involved in photosynthesis, in the active units of other enzymatic systems such as in cytochromes that perform oxidative reactions, vitamin B_{12} that is active in metabolism, or hemoglobin as oxygen carrying entity.[62] Porphyrins are one of the attractive macrocyclic ligands for the synthesis of large-pore MOFs because of their bulky and rigid character, as well as the versatile functionality of the porphyrin molecule.[64] As such, there are many reports of porphyrinic MOFs, where porphyrin is incorporated as a building block in MOF structure, with a wide range of applications such as in photocatalysis, bio-mimetics catalysis, electrocatalysis, biomedicine, and sensing.[62, 65, 66] Considering catalytic applications of porphyrinic MOFs, when incorporated as ligand in the MOF structure, the porphyrin molecules are isolated as discreet units. Thus, every single porphyrin molecule would be ideally available as a catalyst site. The resultant MOF catalyst is a heterogenous system with a higher efficiency compared with direct use of porphyrin where there is a high risk of aggregation of porphyrin molecules. Additionally, the well-defined pores of the MOF can act as a microreactor environment for the catalyst that potentially reducing side reactions. A further advantage of the heterogeneous chemistry of MOFs is that the MOF can be easily separated and recovered after the completion of the reaction.

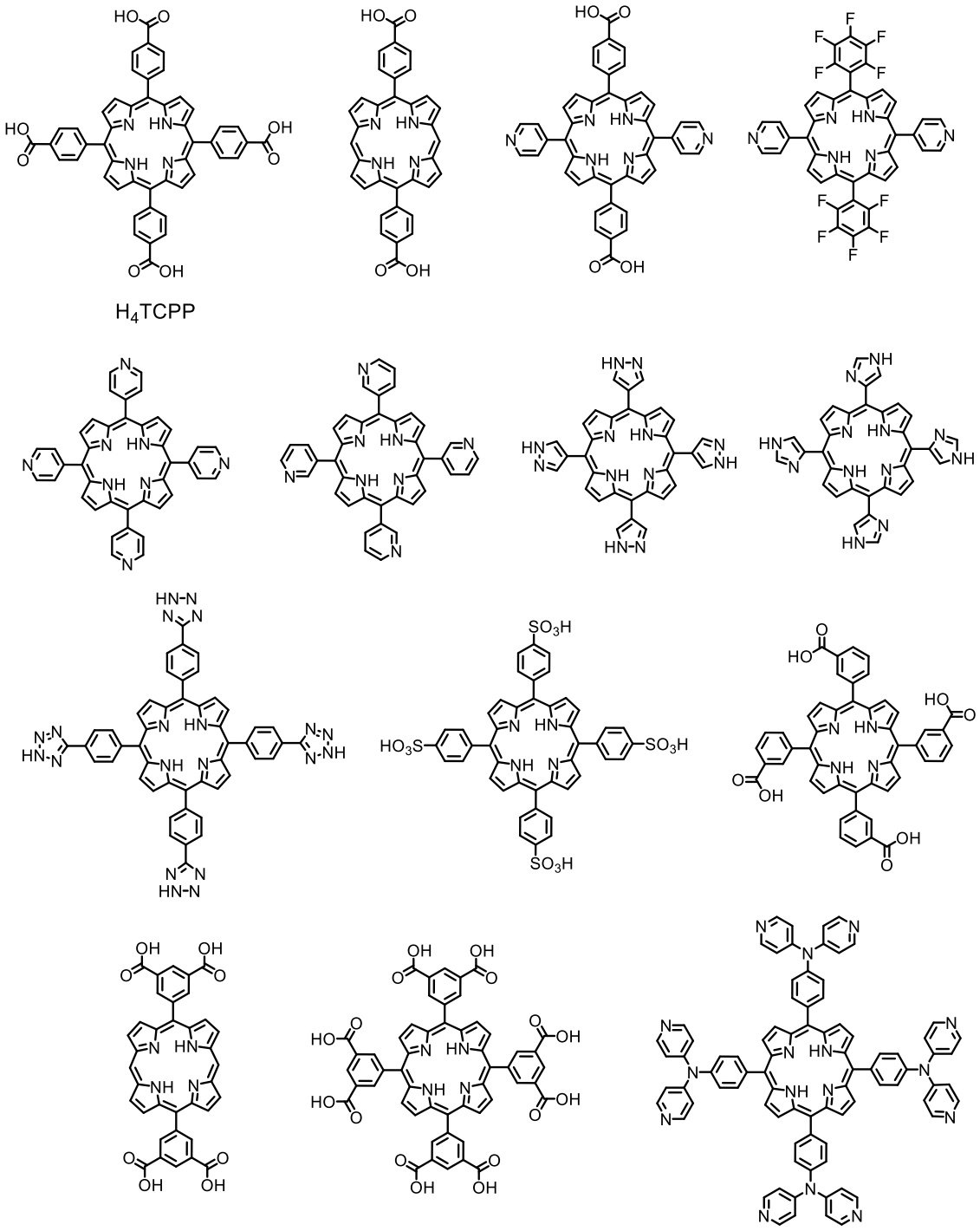

Figure 1.17 Selected examples of porphyrin-based linkers used in MOF synthesis.

Synthetic tunability of the porphyrin ligand is another aspect that makes this molecule attractive to MOF chemists. As such, free-base and metallo-porphyrins with different topicity,

donor groups, and geometries have been used for the synthesis of MOFs. Figure 1.17 includes some of these porphyrin-based linkers, among which tetrakis(4-carboxyphenyl)porphyrin (H_4TCPP) is the most popular linker. Much like other MOFs, when neutral ligands such as pyridyl-based porphyrins are used to coordinate to metal ions,[67-69] although the resulting framework can have large channels, the MOF loses its crystallinity upon solvent removal. On the other hand, carboxylate-based porphyrin ligands make stronger bonds and therefore more stable MOFs. Achieving more robust frameworks is feasible by using hard Lewis-acid metal cations such as Al^{3+}, Fe^{3+}, and Zr^{4+} when carboxylate-based porphyrins (hard Lewis-base) are used as ligand.[64] Enhanced stability of the resultant coordinating bonds can lead to the development of water stable porphyrinic MOFs suitable for use in catalysis applications such as in aqueous media with a wide range of pH.

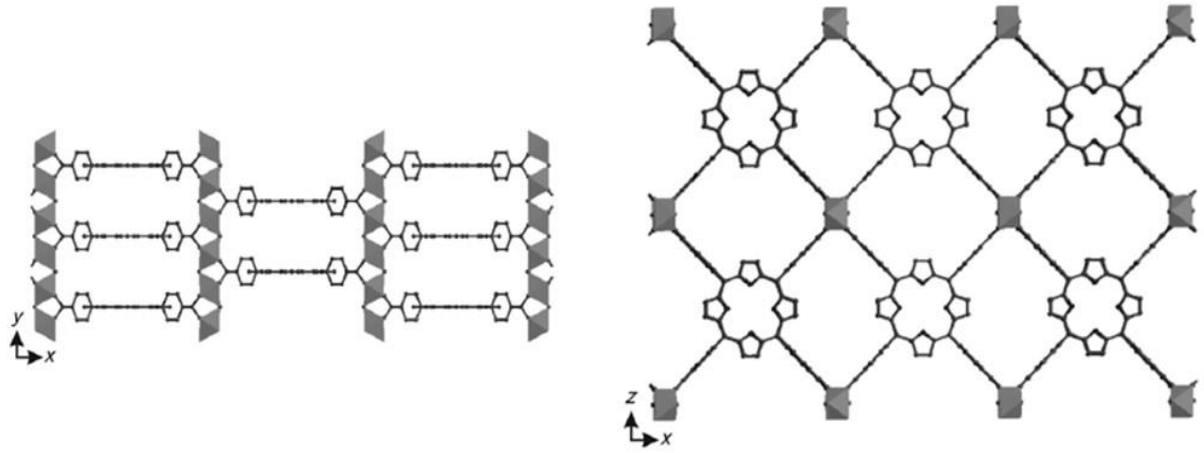

Figure 1.18 Crystal structure of Al-PMOF shown from two different directions. Grey octahedra represent Al atoms. Reprinted with permission from reference 70, Copyright (2012) Wiley.

One of the first examples of a water stable porphyrinic MOFs is microporous Al-PMOF that is made of $TCPP^{4-}$ and rod-packing infinite $Al(OH)O_4$ chains (Figure 1.18) that has a BET surface area of 1400 m^2/g.[70] This MOF is stable in water in pH up to 5 and is used for visible light

photocatalysis for hydrogen generation from water. Similarly, a series of MOFs named as PCN-600 (M) (where M is the metal center of H_4TCPP. M = Fe, Co, Ni, Cu) is formed when six-connected Fe_3 SBU clusters in trigonal prismatic geometry (Figure 1.2h) are connected to the tetratopic $TCPP^{4-}$ ligand.[20] These MOFs have BET surface areas up to 2350 m^2/g and 1-D channels with sizes of up to 31 Å with hexagonal cross-section shape (Figure 1.19). Moreover, PCN-600 has good stability in a wide range of pH (1-12).

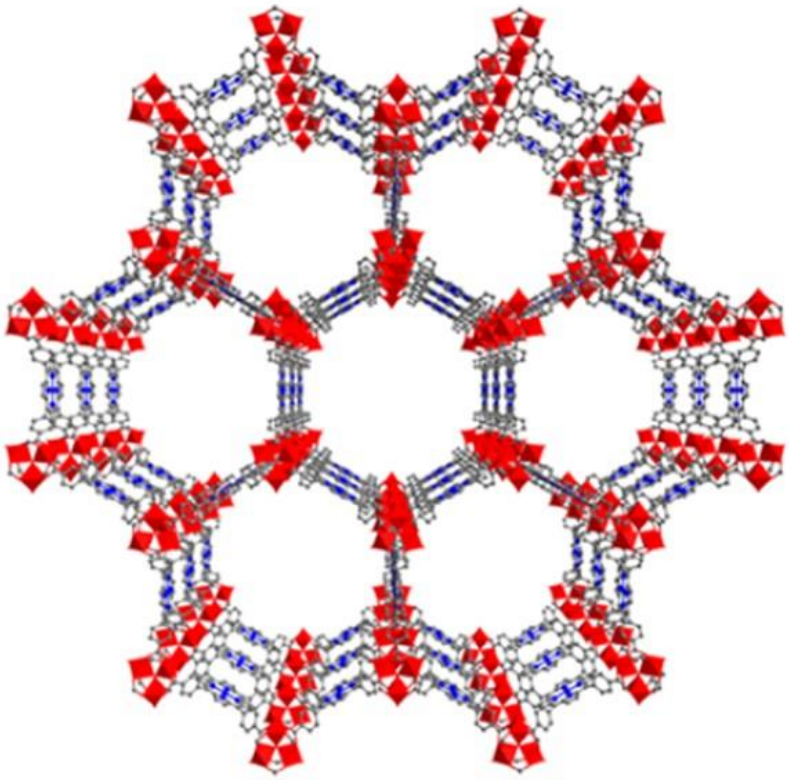

Figure 1.19 Crystal structure of PCN-600. Red octahedra are Fe^{3+} atoms of the trinuclear SBU. Blue: nitrogen atoms of $TCPP^{4-}$, Grey: carbon. Reprinted with permission from reference 20, Copyright (2014) American Chemical Society.

Compared with other hard Lewis-acid cations, Zr-based porphirinic MOFs gained more attention because of their higher stability and the variety of Zr SBUs. As such, there are many reports of Zr-based porphyrinic MOFs and their application in different fields such as

photocatalysis, electrocatalysis, biomimetic catalysis, biomedical, and sensing.[71] For example, MOF-545 (also known as PCN-222 and is isostructural with NU-1000) is a mesoporous porphyrinic MOF that is made of $TCPP^{4-}$ and 8-connected Zr_6 cluster.[42] This MOF has 1-D hexagonal-shaped channels of 36 Å diameter, as well as triangular 1-D micropore channels of 8 Å size and BET surface area of 2260 m^2/g (Figure 1.20a). Without changing the linker, and by only taking advantage of the various connectivity regimes of the Zr-based node, as well as the different structures of these nodes, different MOF topologies can be synthesized. For example, when the same inorganic and organic precursors (Zr^{4+} and $TCPP^{4-}$) for the synthesis of MOF-545 are used under different reaction conditions, MOF-525 is formed.[39] MOF-525 is isostructural with NU-110x series and has a cubic structure (Figure 1.20b) with 3-D cage pores that are made of 12-connected Zr_6 cluster rather than 8-connected SBU (which is in MOF-545). The pore diameter of MOF-525 is 20 Å and its BET surface area is reported as 2620 m^2/g. In MOF-545 the benzoates of the linker are in an angle (54°) with respect to the core porphyrin ring (Figure 1.20c),[42] while in MOF-525 the peripheral phenyl rings on porphyrin (benzoates) have to be in the plane of the central porphyrin ring to fulfill the connection angle requirements between the carboxylate groups and the 12-connected Zr_6 oxocluster (Figure 1.20d). However, the steric effect because of the repulsion between hydrogens of the core porphyrin ring and hydrogens of phenyl forces the peripheral phenyl ring to rotate, while rotation of the carboxylate group is not favorable regarding the destruction of the aromaticity of the system.[38, 56] Therefore, the porphyrin ligands in MOF-525 are under torsion stress when the peripheral benzene rings are fixed in the plane of the porphyrin ring.

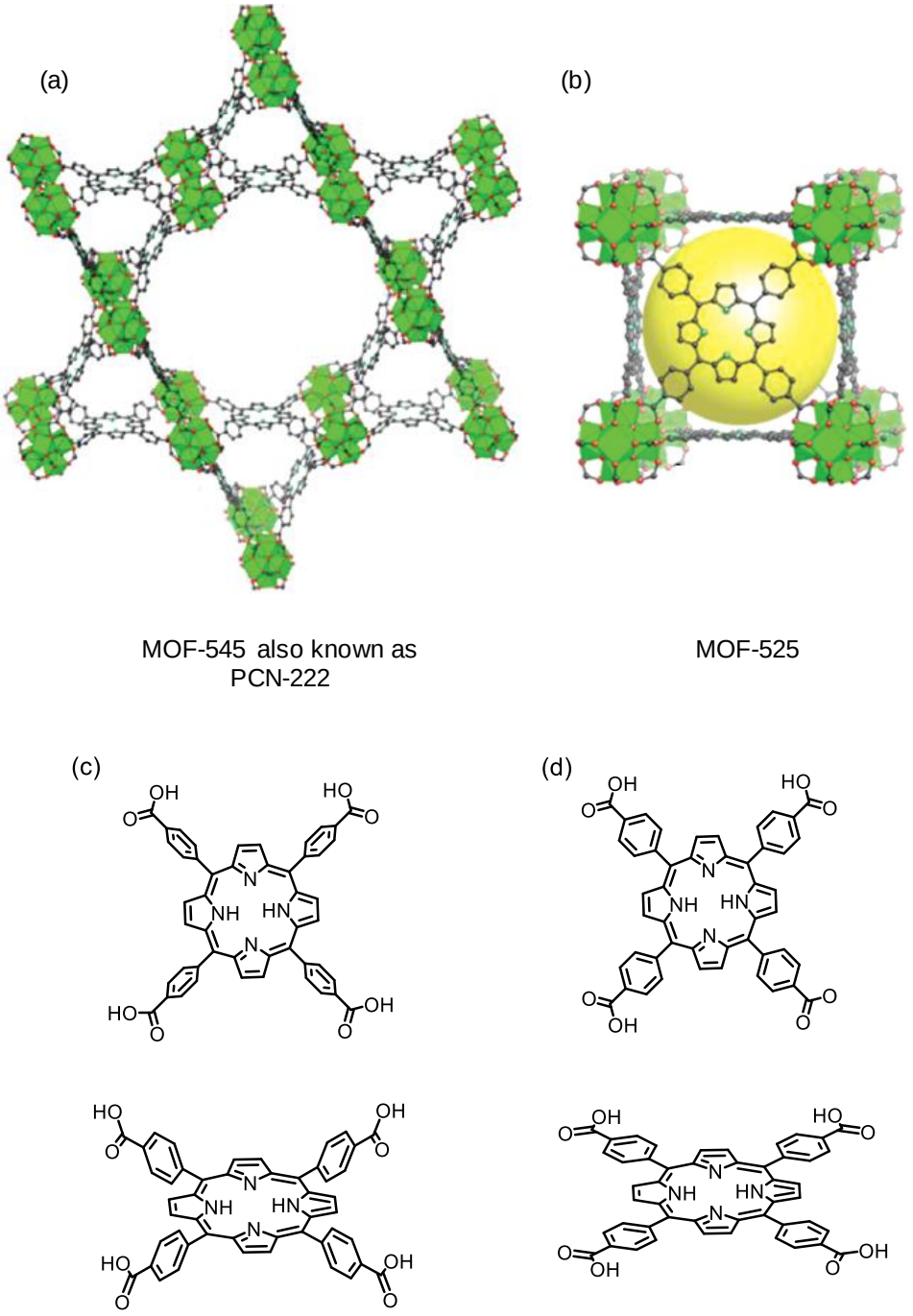

Figure 1.20 (a) Crystal structure of MOF-545 (PCN-222) (b) Crystal structure of MOF-525 (c) and (d) H_4TCPP conformation from two perspectives in MOF-545 and MOF-525 respectively. Reprinted with permission from reference 39, Copyright (2012) American Chemical Society.

Increasing the size of the porphyrin, by extending the length of the peripheral groups has been proved to be a successful strategy for making non-interpenetrated mesoporous MOFs with exceptionally high surface area.[38, 57] Besides, by extending the length of the peripheral groups of the porphyrin, the inner peripheral phenyl rings can rotate to minimize the steric effect mentioned above while the outermost benzoate can stay in the plane of the porphyrin core to fulfill the connection angle requirement to the 12-connected Zr_6 SBU. This makes the porphyrin-based ligands with longer peripheral groups to be incorporated in the MOF structure with less torsion stress compared with H_4TCPP. [38, 57] As such, all the reported carboxylate-based porphyrinic Zr-based MOFs with extended ligand (these ligands are shown in Figure 1.21) are isostructural and have cubic networks with 12-connected Zr_6 SBU (NU-1102 (CPM-99),[57, 72] PCN-228,[38] PCN-229,[38] NU-1104,[57] and PCN-230[38]). PCN-230 has the largest porphyrin ligand among all the reported porphyrinic MOFs. This MOF has BET surface area of 4455 m^2/g and cubic cage pore with the size of 38 Å and is reported stable in a wide range of pH (0-12), which is attributed to the high connectivity of the 12-connected Zr_6 cluster. This is in contrast with PCN-222, which is made of 8-connected Zr_6 and is reported to be only stable under acidic conditions.

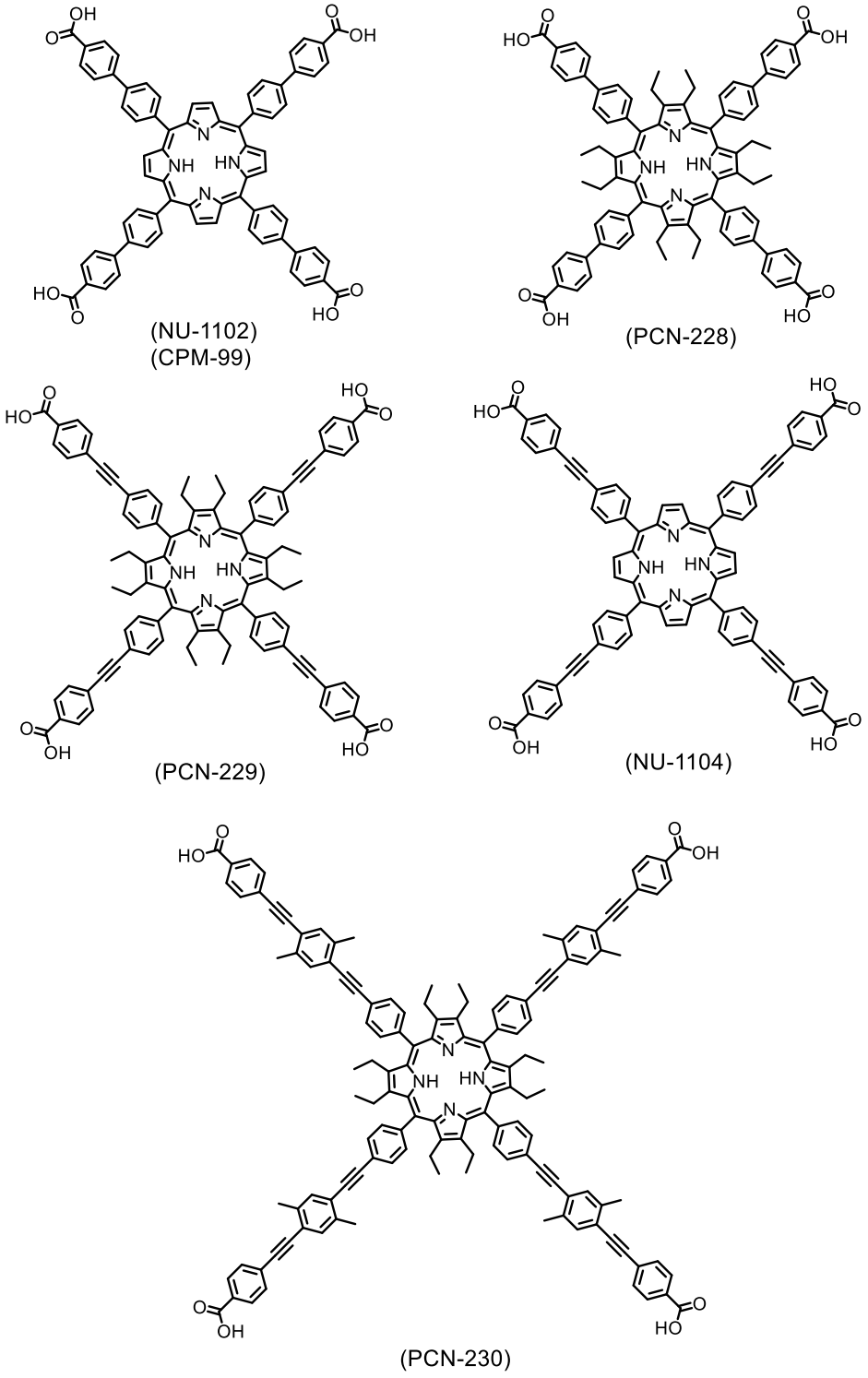

Figure 1.21 Porphyrin-based linkers with extended length used in the synthesis of porphyrinic MOFs. Labels in parentheses show the MOF in which the associated linker is used.

1.5.3 Phthalocyanines as macrocyclic ligands

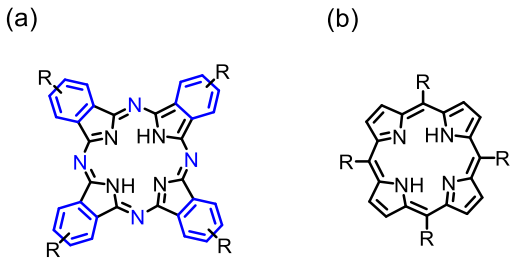

Figure 1.22 (a) Structure of phthalocyanine showing the nitrogen atoms and phenyl rings compared with (b) structure of porphyrin.

Phthalocyanines (Pcs) are conjugated macrocyclic molecules with some structural similarity to porphyrins. However, phthalocyanines have differences with porphyrins and are not found in natural systems.[73] Compared with porphyrins, Pcs have four extra nitrogen atoms in the core aromatic (porphyrin-like) ring and four arenes fused to the exterior of the core (Figure 1.22); therefore, Pcs have higher thermal stability than porphyrins.[74] Besides, Pcs absorb longer wavelength radiation in the red region.[75, 76] Additionally, compared with porphyrins, the larger conjugated system of Pcs causes stronger stacking that results in aggregation and reduces their solubility that can limit their applications.[74] Using Pcs as linkers in the synthesis of MOFs to make Pc-based MOFs (PcMOF), similar to porphyrinc MOFs, is an approach to take advantage of the chemistry of Pcs in a micro/nano reactor environment while preventing aggregation. Just like with PEMs and porphyrins, the macrocyclic and rigid character of Pc makes this molecule an attractive choice as ligand for the synthesis of large-pore MOFs.

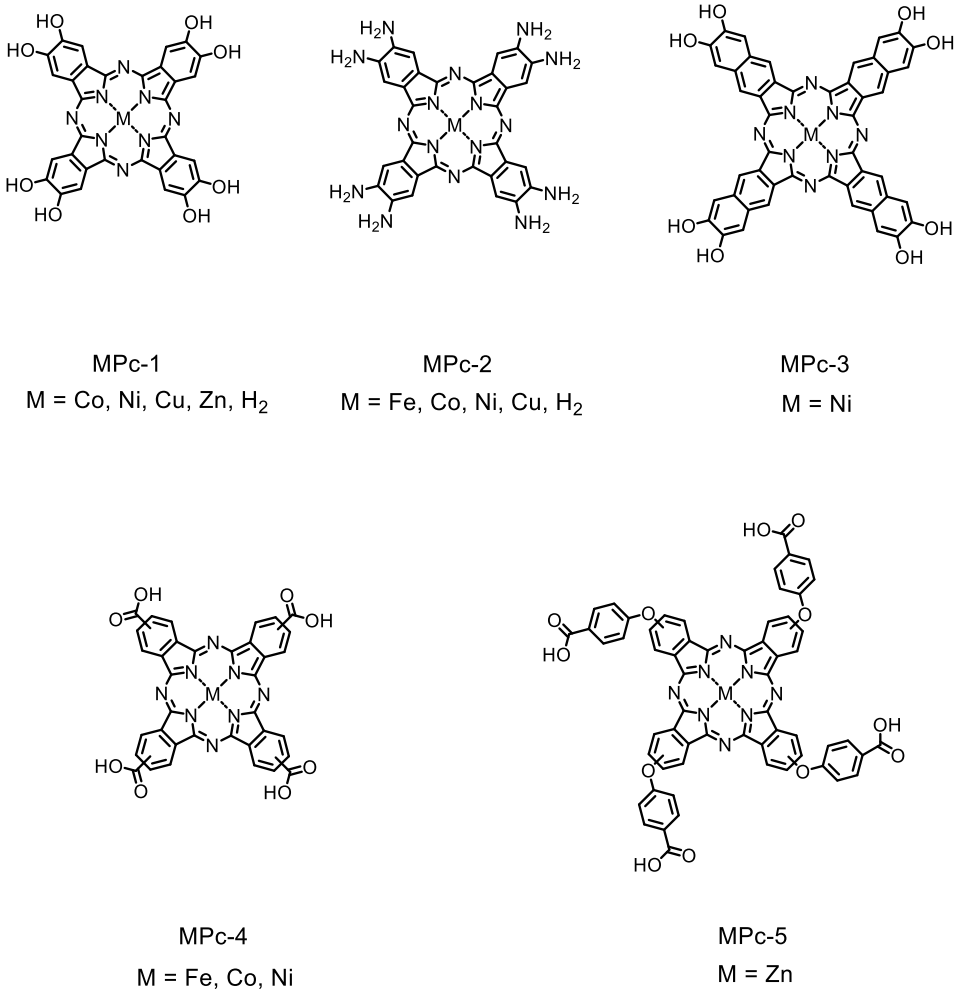

Figure 1.23 Phthalocyanine-based linkers used in the synthesis of PcMOFs.

Compared with the vast group of porphyrinic MOFs, there aren't many examples of PcMOFs reported. Additionally, the coordinating groups on these Pc ligands are limited to diamino and catechol (in symmetrically substituted Pcs). With unsymmetrical ones, however, there are three reports,[77-79] but no crystal structure is reported for these MOFs. Figure 1.23 shows all the Pc ligands used in the synthesis of PcMOFs. A brief review of PcMOFs is discussed below. It is noteworthy that reports in which Pc is not a building block of the MOF (encapsulated or partially anchored examples) are not included. A list of all the reported PcMOFs, with their corresponding application is shown in Table 1.1.

Table 1.1 Reported PcMOFs.

Entry	Linker	Node	SSA[a]	Pore Size (Å)	Application	Ref.
1	CuPc-1	Cu	358	14	Cathode for Li-ion battery	80
2	NiPc-2	Ni	593	-	Electrochemical OER[b]	81
3	CuPc-1	Fe, Co, Ni, Cu	412 (Co)	15	Electrochemical ORR[c] and cathode for Zn-air battery	82
4	FePc-1	Fe	206	14	Superparamagnetic properties	83
5	CuPc-1	Fe, Ni, Zn	-	-	Cathode for Na-I_2 battery	84
6	NiPc-3	Ni, Cu	174 (Ni), 267 (Cu)	-	Chemiresistive sensing of NO, NH_3, and H_2S	85
7	NiPc-1	Ni, Cu	101 (Ni), 284 (Cu)	-	Chemiresistive sensing of NO, NH_3, and H_2S	85
8	CuPc-1 ZnPc-1	Cu, Zn	378 (CuPc-1, Zn^{2+} SBU)	14	Electrochemical CO_2 reduction	86
9	CuPc-2	Ni	659	15	Supercapacitor electrode material	87
10	CoPc-2 NiPc-2	Cu	349 (Co), 628 (Ni)	-	Electrochemical CO_2 reduction	88
11	CoPc-1 NiPc-1	Cu	582 (Co), 421 (Ni)	-	Electrochemical CO_2 reduction	88
12	H_2Pc-2	Cu	181	-	Electrochemical CO_2 reduction	88
13	H_2Pc-1	Cu	364	-	Electrochemical CO_2 reduction	88
14	NiPc-1	Ni	180	12	Electrochemical CO_2 reduction	89
15	NiPc-2	Ni	172	17	Electrochemical CO_2 reduction	90
16	NiPc-2	Ni	543	-	Electrochemical nitrite sensing	91
17	NiPc-2 CuPc-2	Ni	-	12.3	Chemiresistive sensing of water and VOCs[d]	92
18	CoPc-1	Fe	1471	10.7, 14.6	Electrochemical CO_2 reduction	93
19	FePc-4	Fe	-	-	Electrochemical sensing of vanillin	79
20	CoPc-4 NiPc-4	Zr	-	-	Visible light photocatalytic oxidation of anthracene	78
21	ZnPc-5	Zr	1789	10.8	Visible light photocatalytic oxidation of naphthols to naphthoquinones	77

[a] specific surface area
[b] oxygen evolution reaction
[c] oxygen reduction reaction
[d] volatile organic compound

The first PcMOF was reported by Nagatomi *et al.* in 2018 where they used CuPc-1 as the linker and Cu^{2+} as the linking node (Figure 1.24).[80] This MOF has a 2-D structure where the 2-D layers are stacked through π-π interactions that form 1-D square channels. Because of the large delocalized π-conjugated system of Pc, combined with the Pc electroactive nature of the bond between catecholate and metal node, the formed 2-D MOF is electrically conductive. As such, mixed with carbon black, this MOF can be used as active material for the cathode of Li-ion battery. In all of the reported PcMOFs when MPc-1, MPc-2, and MPc-3 are used as linkers (Figure 1.23),

and the node is a single metal ion that can form square planar complexes with the linker, the synthesized PcMOF has a 2-D structure similar to Figure 1.24.[81-92] One of the most important characteristics that makes this series of PcMOFs attractive is their conductivity; therefore, it is not surprising that almost all the applications of these 2-D PcMOFs (except for one report, see Entry 4 in Table 1.1) is investigated in electrochemical or electron conductive applications.

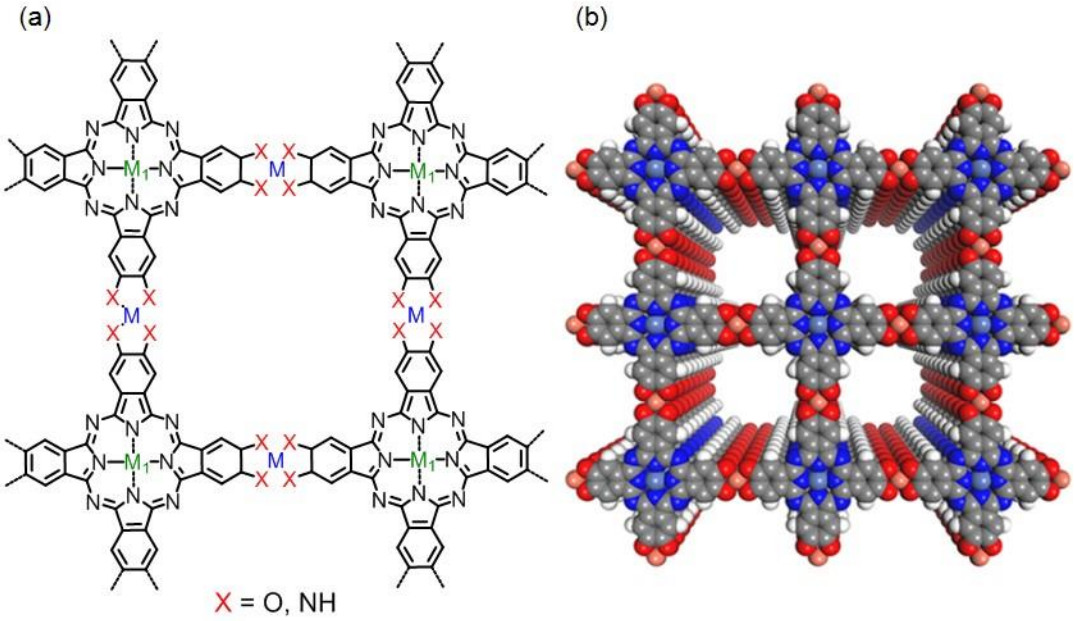

Figure 1.24 (a) Structure of PcMOF with M_1Pc-1 or M_1Pc-2 linker and M^{2+}node. (b) PcMOF with NiPc-1 linker and Cu^{2+}node showing stacked structure of the MOF. Reprinted with permission from reference 85, Copyright (2019) American Chemical Society.

The first and only 3-D PcMOF, MOF-1992, that has a well-defined crystal structure was reported by Yaghi and co-workers in 2019.[93] Linker in this MOF is CoPc-1 and the SBU is Fe^{3+} trimer $Fe_3(\text{-}C_2O_2\text{-})_6(OH_2)_2$ that provides 6-connection points along its axis (Figure 1.25). Although Pc ligands in this MOF are isolated from each other in a 3-D framework with no π-π interaction, both the catecholate-iron bonds and the Pc ligand have electron conductive properties; therefore, MOF-1992 is the first electrically conductive 3-D MOF that has molecular catalyst in its structure

(CoPc is known for its CO_2 reduction catalytic activity). As a result, MOF-1992 mixed with carbon black shows high electrocatalytic activity towards CO_2 reduction to CO in aqueous solution.

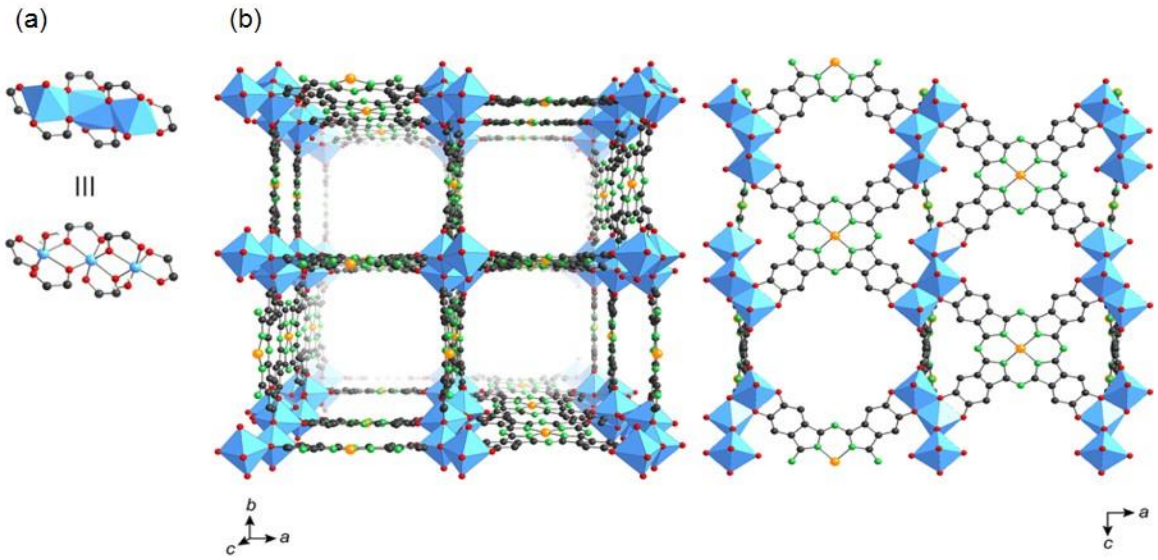

Figure 1.25 Crystal structure of MOF-1992 made of CoPc-1 and Fe^{3+} trimer. (a) $Fe_3(-C_2O_2-)_6(OH_2)_2$ SBU (b) 3-D framework of MOF-1992 showing 3-D pores. Atoms are color coded. Fe is shown in blue, Carbon: grey, Nitrogen: green, Co: orange, and Oxygen: red. Reprinted with permission from reference 93, Copyright (2019) American Chemical society.

The first report of using carboxylate-based Pc ligand in MOF synthesis was in 2020 by Yu and co-workers.[78] Mixed ligand strategy is used for the synthesis of this MOF in which CoPc-4 is mixed with H_3BTB and $ZrCl_4$ to yield PCN-135(Co-TCPC). BTB^{3-} forms 2-D metal organic layers (Figure 1.26a) by coordinating to hexagonal planar 6-connected Zr_6 cluster (SBU is shown in Figure 1.2d). These coordinatively unsaturated Zr_6 clusters in the mentioned 2-D layers are pillared by CoPc-4 to make the PcMOF Figure 1.26b. However, there is no single crystal structure characterization reported for this MOF. Considering the well-known photocatalytic activity of Pcs, PCN-135(Co-TCPC) is used as heterogenous photocatalyst for the oxidation of anthracene under visible light. In 2020, Peng *et al.* reported the use of FePc-4 as linker along with

$[Fe_3O(OOCCH_3)_6OH]•2H_2O$ as the meal source to make a PcMOF.[79] Although no surface area and MOF structure characterization except for scanning electron microscopy (SEM) and transmission electron microscopy (TEM) images is reported, the synthesized PcMOF is used as a porous electrocatalyst for the detection of vanillin.

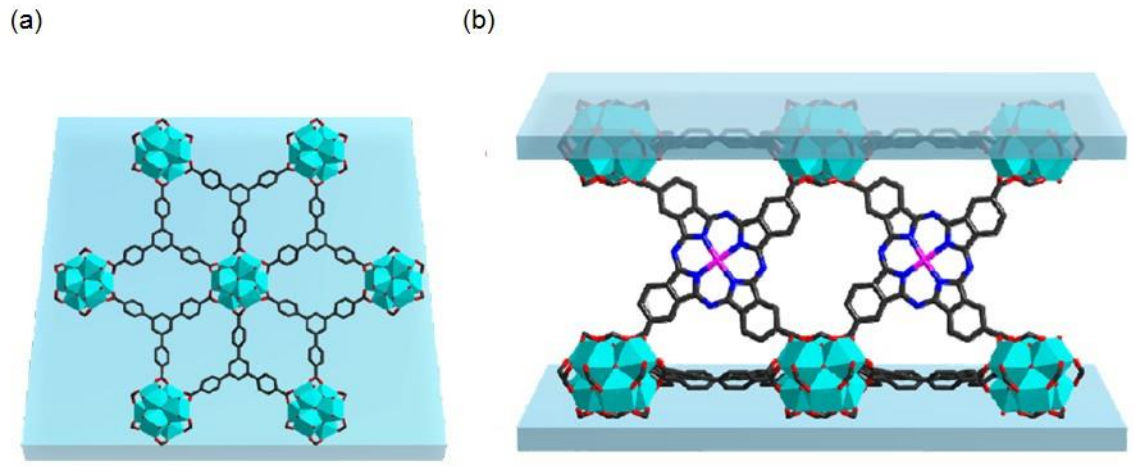

Figure 1.26 (a) Structure of 2-D metal organic layer showing BTB^{3-} coordinated to Zr_6 SBU. (b) schematic illustration of PCN-135(Co-TCPC) showing 2-D metal organic layers pillared by CoPc-4. Reprinted with permission from reference 78, Copyright (2020) Wiley.

The last report of using carboxylate-based Pc ligand in MOF synthesis is was 2020 by Wu and co-workers where they used ZnPc-5 mixed with H_2BPDC as linkers and $ZrCl_4$ as the metal source to make UiO-67-ZnPc.[77] This MOF is formed by the partial replacement of $BPDC^{2-}$ with ZnPc-5 in the UiO-67 structure (Figure 1.27a). UiO-67 is a Zr-based MOF that is composed of $BPDC^{2-}$ ligand and 12-connected Zr_6 SBU (Figure 1.27b). $BPDC^{2-}$ and ZnPc-5 have different coordination modes; therefore, it is likely that UiO-67-ZnPc has structural defects. However, powder X-ray diffraction (PXRD) and SEM analysis indicate that UiO-67-ZnPc has the same structure and morphology (octahedron microcrystals) as that of UiO-67. Although no crystal information is reported to prove that ZnPc-5 is incorporated as a part of the MOF backbone, even

distribution of elements in the UiO-67-ZnPc which is evidenced by energy dispersive X-ray spectroscopy (EDX) analysis is used as a proof to show that ZnPc-5 is not trapped or aggregated in the UiO-67. Finally, light-induced generation of singlet oxygen from ZnPc-5 ligand in the UiO-67-ZnPc is used for the photocatalytic oxidation of naphthols under visible light and in the presence of O_2.

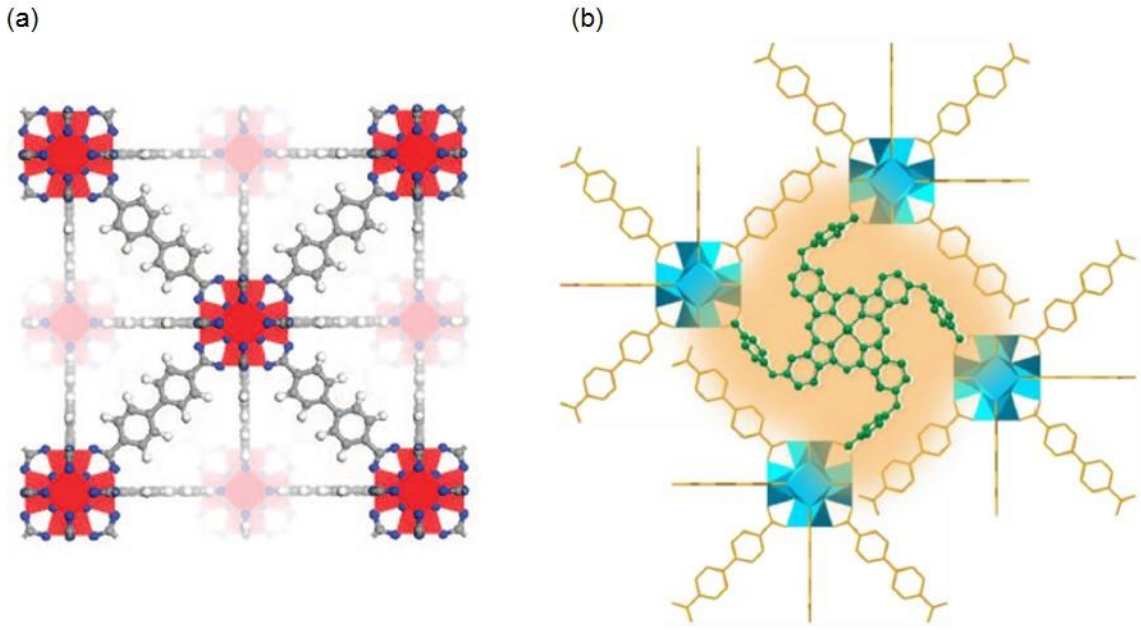

Figure 1.27 (a) Crystal structure of UiO-67 showing $BPDC^{2-}$ ligand coordinated to 12-connected Zr_6. Atoms are color coded as Zirconium: red, Oxygen: blue, Carbon: gray, and Hydrogen: white. (b) Schematic illustration of UiO-67-ZnPc showing incorporation of ZnPc-5 in UiO-67 structure. Zirconium is shown in blue. Reprinted with permission from reference 32, Copyright (2008) American Chemical Society and reference 77, Copyright (2020) Elsevier.

1.6 Conclusion

The large variety of choices for inorganic and organic constituents, when further combined with varying reaction conditions, lead to an extensive array of MOF structures to make. As new MOFs with new structural and functional diversity are being discovered, many new applications for these materials in different technologies such as gas storage, catalysis, and sensing are reported.

Interestingly, the variable parameters in MOFs synthesis can be tuned not only towards application, but also towards understanding the structure-property relationship. This understanding gives the chemist a high degree of insight regarding what structure factors are responsible for the properties being studied. Therefore, engineering MOFs through a judicious design of the framework structure, to gain structural and compositional control, is an important endeavor.

In this thesis we investigate the synthesis of macrocyclic rigid linkers that can be used for the design and synthesis of mesoporous MOFs. Among the rigid macrocyclic linkers, PEM and Pc are my interest. These linkers are poorly explored in comparison to other macrocyclic linkers such as porphyrins. Furthermore, these linkers can be functionalized, and their size can be extended, making them an ideal platform for new chemistry with these linkers. Therefore, with these new linkers, there are opportunities to introduce numerous new MOFs and their associated applications to the field.

2 Synthesis of *m*-phenylene ethynylene macrocycle

2.1 Introduction

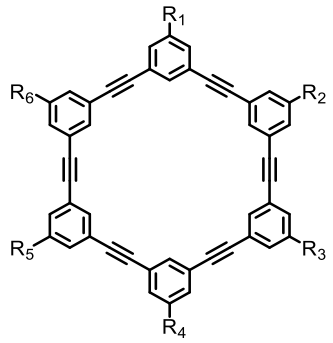

Figure 2.1 Hexamer *m*-phenylene ethynylene macrocycle.

As stated in Chapter 1, to make large-pore MOFs that have stable structure (i.e., does not collapse upon removal of guest molecules from the pore) and non-interpenetrated structure, thereby providing as much pore volume as possible, one approach is to use ligands that are both large and rigid. Shape-persistent macrocycle scaffolds (e.g., PEM shown in Figure 2.1), provide such an opportunity.[60, 94] These molecules have very few degrees of conformation freedom that should result in a more stable structure and are sufficiently large to prevent interpenetration. In Figure 2.1, R_n can be a desired coordinating group that provides connectivity to the nodes. In addition to having a rigid structure and large size, PEMs can be used to synthesize MOFs where we can guarantee that there is an opening (pore aperture); this is because the cavity of the PEM is around 9 Å in size,[60, 61] which is sufficient to allow most gases to enter the pores. Therefore, PEMs are an interesting class of molecules to consider as ligands in MOFs. However, despite these interesting characteristics, PEMs have not been explored in the MOFs chemistry, except for two reports,[60, 61] there aren't other reports of using such linkers in MOF synthesis.

Synthesis of PEMs can be achieved through different methods. In the following sections we have categorized these methods into three groups with a short literature review and examples for each.

2.1.1 Single pot synthesis of macrocycle

Single pot method of forming a PEM can be accomplished in several ways. Generally, this process requires intermolecular coupling that starts by forming oligomers and subsequently undergoes an intramolecular ring closure. There are several methods that this reaction can be accomplished. For example, as shown in Figure 2.2a, alkyne metathesis in which exchange of substituents occurs can result in the desired product.[95, 96] It has been shown that this reaction can result in as high as 77% yield using a single monomer component.[96] Given the fact that this reaction is a single pot reaction, and it provides the potential to form polymers rather than a macrocycle, 77% yield is considered to be excellent. The challenge with this work is that only a single R group can be installed in the periphery of the molecule. As such, derivatization is an all or nothing methodology.

To address the limitations of a single component one-pot reaction, chemists have explored the ability to form these macrocycles using two different precursors.[97, 98] Although this method is prone to the formation of a mixture of different products and oligomers, controlling the reaction conditions can produce the desired product. For example, two monomer methods have been attempted by Gleiter and co-workers[98] by tuning the solubility of the precursors and controlling the addition rate (5 mL/h) of a dilute solution (4 mM) of precursors to the catalyst mixture ($Pd(PPh_3)_4$ and CuI) over several hours to produce the macrocycle in Figure 2.2b with 23% yield.

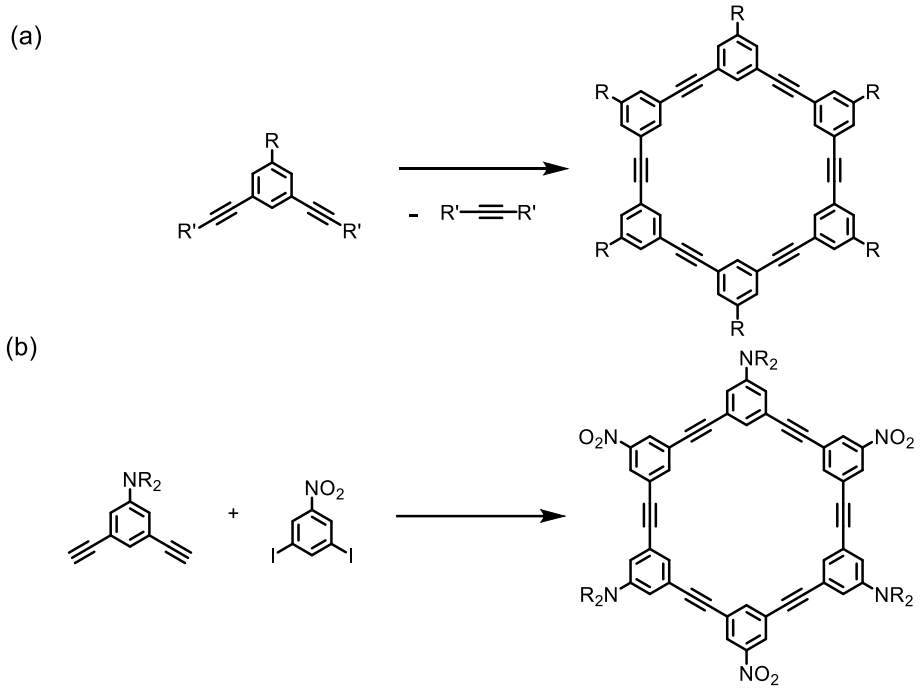

Figure 2.2 One-pot synthesis of PEMs. (a) alkyne metathesis. (b) two-monomer approach.

2.1.2 Cyclization (double cross-coupling) between two precursors

In another approach to the synthesis of PEMs, first two halves of the macrocycle are synthesized separately through intermolecular coupling, then the macrocycle is synthesized through coupling reactions between the two halves that require two new bonds to form.[98-103] The precursors are usually reacted in dilute solutions (1-10 mM) to decrease the chance of oligomer and polymer formation. For example, Huang and co-workers synthesized the macrocycle shown in Figure 2.3a with 32% yield by the reaction between 1 mM solutions of precursors at the presence of $Pd_2(dba)_3$ as catalyst and CuI as co-catalyst.[101] Likewise, Yamasaki *et al.* synthesized the macrocycle in Figure 2.3b by slow addition (0.054 mL/h) of a solution (10 mM) of precursor to the catalyst ($Pd(CH_3CN)_2Cl_2$) to make the macrocycle in Figure 2.3b with 24% yield.[102]

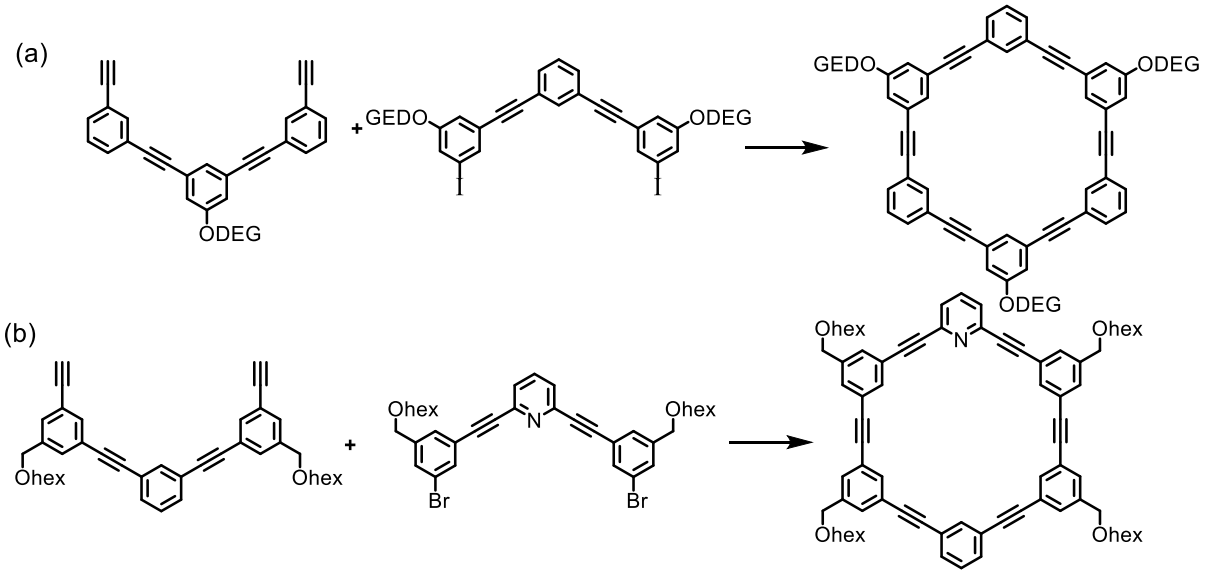

Figure 2.3 Synthesis of PEM with cyclization between two precursors. DEG = $(CH_2CH_2O)_2CH_2CH_3$.

2.1.3 Ring-closure of a single component

Another method for the synthesis of PEMs is the ring-closure of a pre-assembled precursor.[104-106] This is accomplished by slow addition of a solution of the precursor to the catalyst. The precursor is synthesized in a sequential approach by intermolecular coupling with the desired length and functionality. Intramolecular ring closure is done thorough a Sonogashira cross-coupling reaction that entails the formation of one new bond; therefore, compared with the other methods that was discussed in the previous sections, ring-closure is achieved in good yield, however synthesis of the precursor needs many steps. For example, Moore and co-workers synthesized the macrocycle in Figure 2.4a where R = *tert*-butyl with 75% yield by slowly adding (2.5 mL/h) a 11 mM solution of the precursor to the catalyst mixture ($Pd(dba)_2$ and CuI).[105] In this example, synthesis of the precursor involves 10 steps with 51% total yield. Although these yields are acceptable for such cyclization reactions, it seems like that this is not always the case. For example, Miljanic and co-workers used a similar method to synthesize the macrocycle in Figure 2.4a where R = $COOCEt_3$ with 21% yield.[106] They used slow addition (0.5 mL/h) of a 25 mM solution of the precursor to the

catalyst mixture ($Pd(PPh_3)_4$ and CuI). In this example, synthesis of the precursor involves 13 steps with 24% total yield to achieve the final product needed for cyclization.

Stepwise synthesis of the precursor makes it possible to synthesize a macrocycle with not only the desired functional groups but also with the desired size. For example, Moore and co-workers synthesized the macrocycle in Figure 2.4b with 70% yield by slow addition (2.5 mL/h) of a 5 mM solution of the precursor to the catalyst mixture ($Pd(dba)_2$ and CuI).[105] In this example, stepwise synthesis of the precursor involves 12 steps with 35% total yield to achieve the final product needed for cyclization.

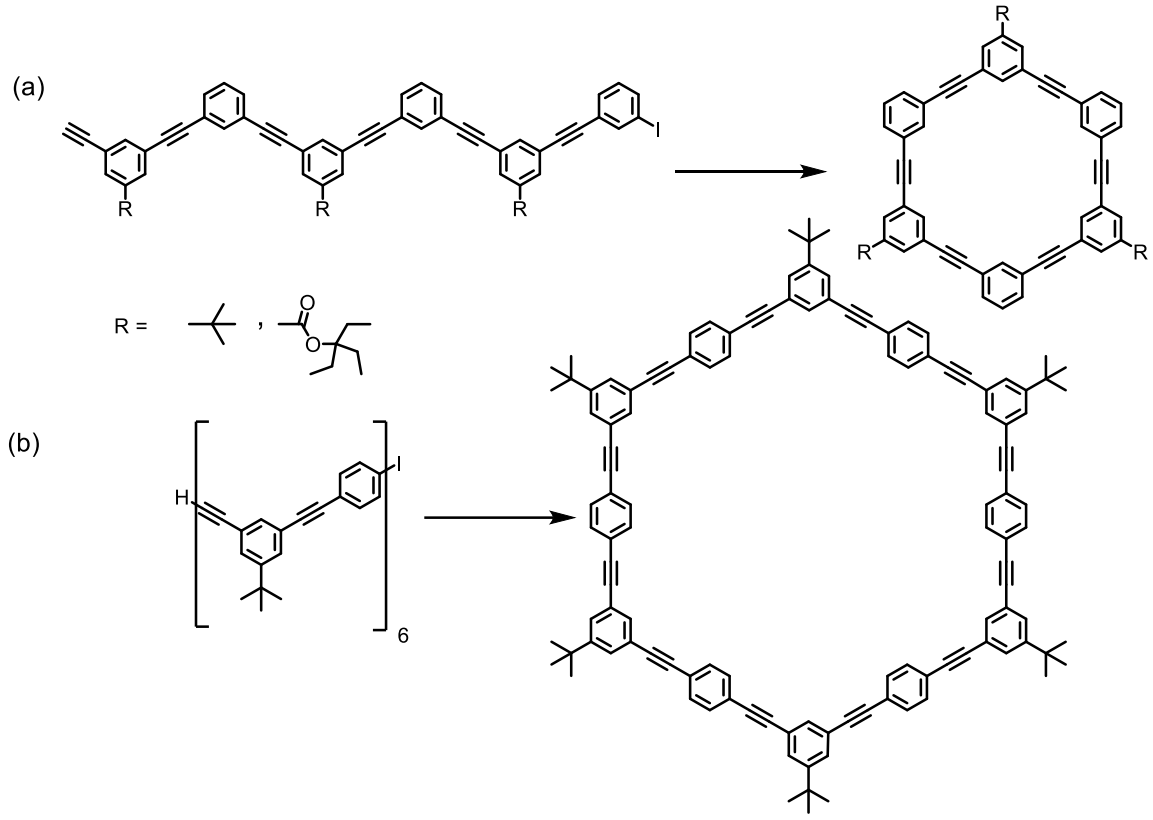

Figure 2.4 Ring-closure of a pre-assembled precursor for the synthesis of PEM.

With the different methods identified for the synthesis of phenylene ethynylene macrocycles, we turn our attention to the synthesis of macrocycle and the required precursors. Here we aimed at hexamer PEM ligand (Figure 2.4a) where R = -COOH groups.

2.2 Results and discussion

2.2.1 Synthesis options for making the PEM ligand

Among the discussed methods in the previous sections, as options for the synthesis of PEM ligand, alkyne metathesis is ruled out because we can't control the position of R group. The one-pot method based on two monomers (Figure 2.5) is not an optimal approach either. Although the synthesis is simple, it is prone to oligomerization and polymerization because it needs five intermolecular couplings before the final intramolecular reaction to close the ring.

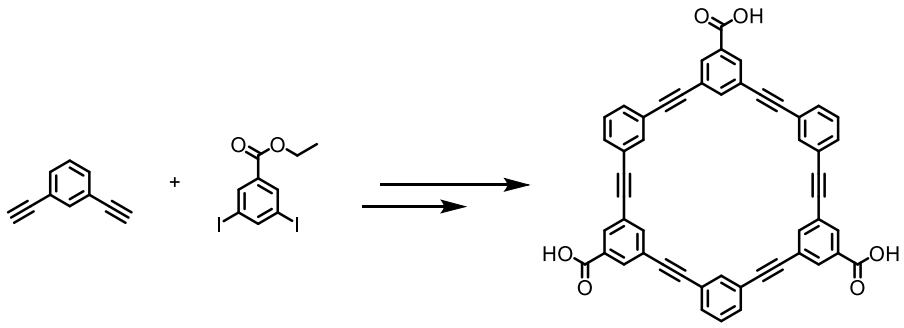

Figure 2.5 One-pot synthesis of PEM followed by hydrolysis to make the PEM ligand.

As an alternative approach (Figure 2.6), the precursor 5 can be synthesised in five steps. Using this precursor, synthesis of the macrocycle needs two inter- and one intra-molecular coupling reaction. Although still simple with seven steps in total and lower risk of side product and polymerization compared with the one-pot option in Figure 2.5, there is still risk of polymerization with this method.

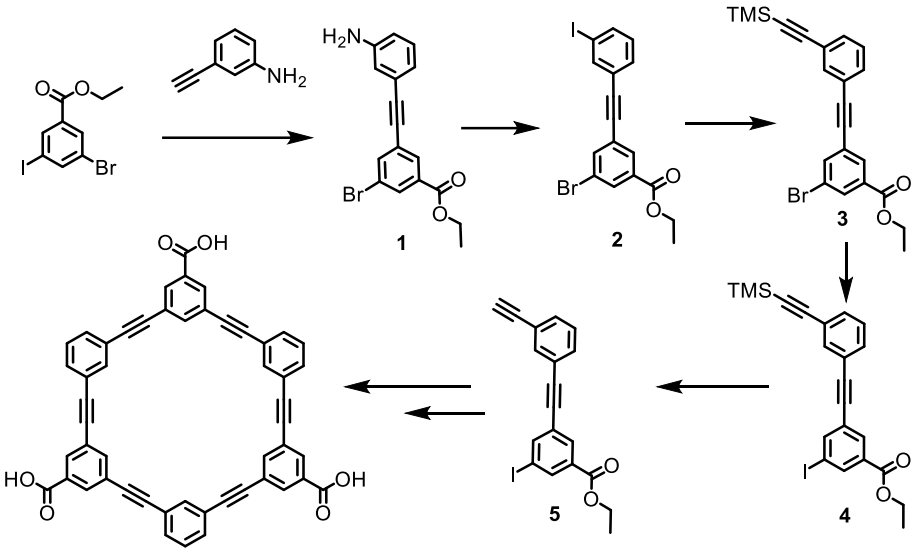

Figure 2.6 Stepwise synthesis of precursors for the synthesis of PEM ligand.

As discussed in the introduction section, ring-closure of a single component is a potentially viable approach for the synthesis of PEMs with good yield. It is clear from Figure 2.7 that making the macrocycle needs only one intra-molecular coupling; therefore, there is a lower risk of side products formation and polymerization compared with the previous options. However, starting from compound **2-4** (in Figure 2.8) but using a similar procedure reported by Miljanic and co-workers, it requires 12 steps to make the ligand.

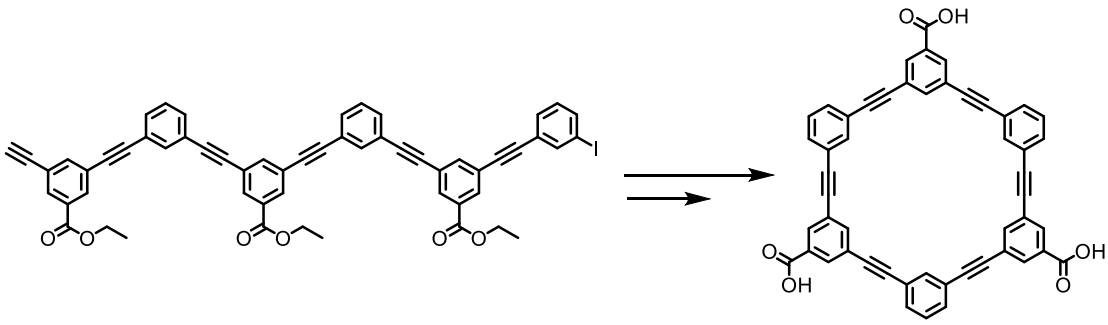

Figure 2.7 Ring-closure of a single component for the synthesis of PEM ligand.

The final option is cyclization between two precursors. As is shown in Figure 2.8, this method needs seven steps to make the PEM ligand; therefore, this option is comparable with the

method in Figure 2.6, but with lower risk of polymerization because it needs formation of two new bonds, one inter- and one intra-molecular coupling to close the cycle.

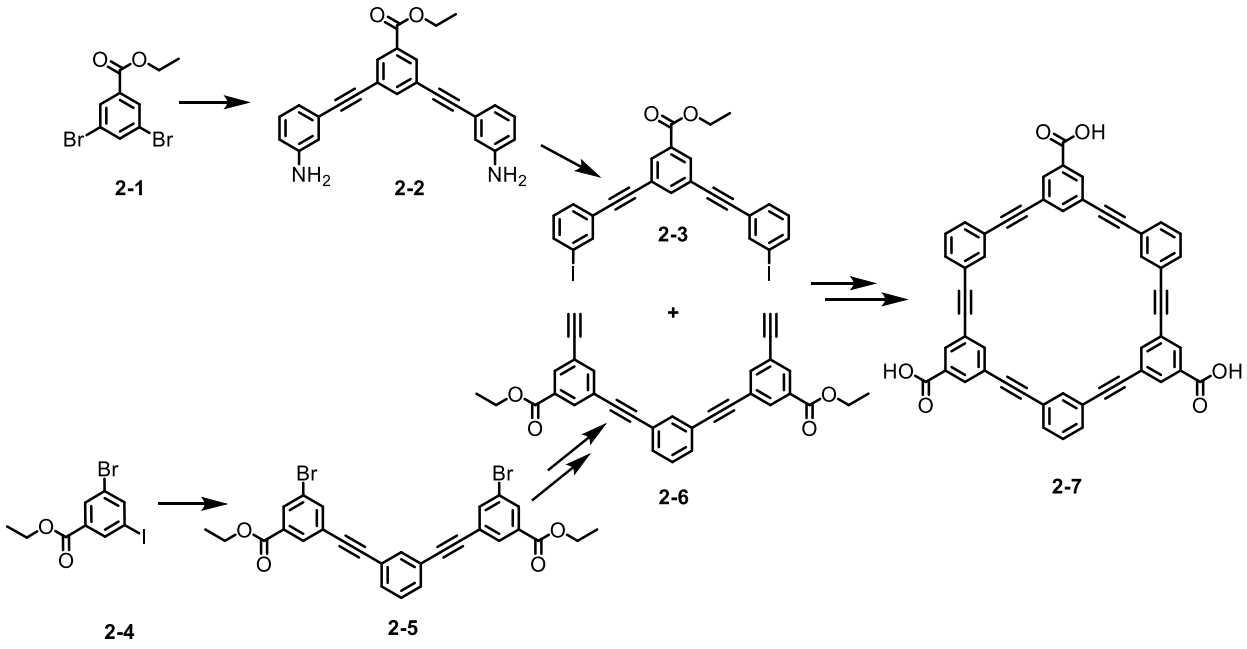

Figure 2.8 Synthesis of precursors and cyclization between two precursors (**2-3** and **2-6**) for the synthesis of PEM ligand (**2-7**).

Comparing these options, we chose the cyclization between two precursors (Figure 2.8) to place three carboxylic acid groups in a symmetrical fashion on the macrocycle (compound **2-7**). This method for the ligand synthesis is shorter than other options (seven steps, can be done in five pots) and theoretically the cyclization can be done with relatively lower chance of side-products formation while the synthesis done by Miljanic and co-workers requires 14 steps in 14 pots to make the same PEM ligand (compound **2-7**). In the following sections we will first discuss the synthesis of precursors needed for the final cross-coupling reaction, then we elaborate on the cyclization reaction.

2.2.2 Synthesis of precursors

2.2.2.1 Synthesis of 2-2

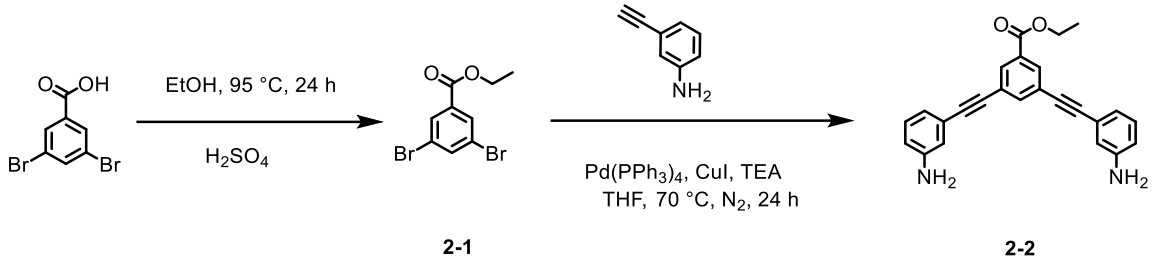

Figure 2.9 Two-step synthesis of **2-2**. First step is esterification of 3,5-dibromobenzoic acid to make **2-1**, and the second step is Sonogashira cross-coupling between **2-1** and 3-ethynylaniline.

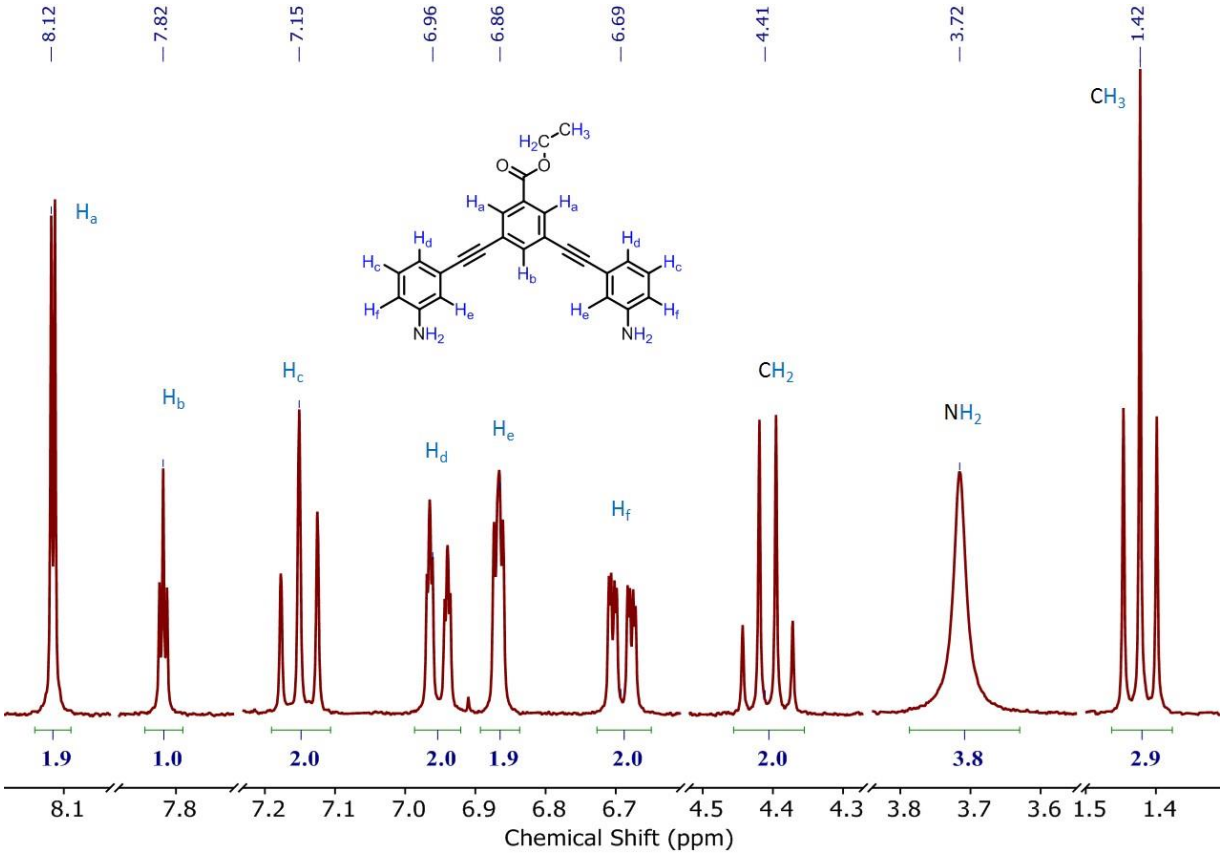

Figure 2.10 ^{1}H-NMR (300 MHz, $CDCl_3$) of compound **2-2**.

The synthesis of **2-1** can be achieved in 92% yield under standard reaction conditions. Sonogashira cross-coupling reaction on **2-1** was done by using 3-ethynylaniline as reagent (Figure 2.9). As it is

common in the Sonogashira cross-coupling reactions,[107] we used $Pd(PPh_3)_4$ as the Pd^0 catalyst, CuI as co-catalyst, TEA as the base, and the reaction was performed under inert (N_2) atmosphere. Under these conditions, the product **2-2** was obtained in high yield of 81% as a beige powder. ^{1}H-NMR spectrum of the product is shown in Figure 2.10 with the chemical shifts of the assigned protons and the correlated integrations. Figure 2.11 shows a comparison of the ^{1}H-NMR spectrum to those of the starting materials. This comparison indicates that the obtained product has protons with chemical shifts different from those of the starting materials; therefore, the desired product is synthesized successfully.

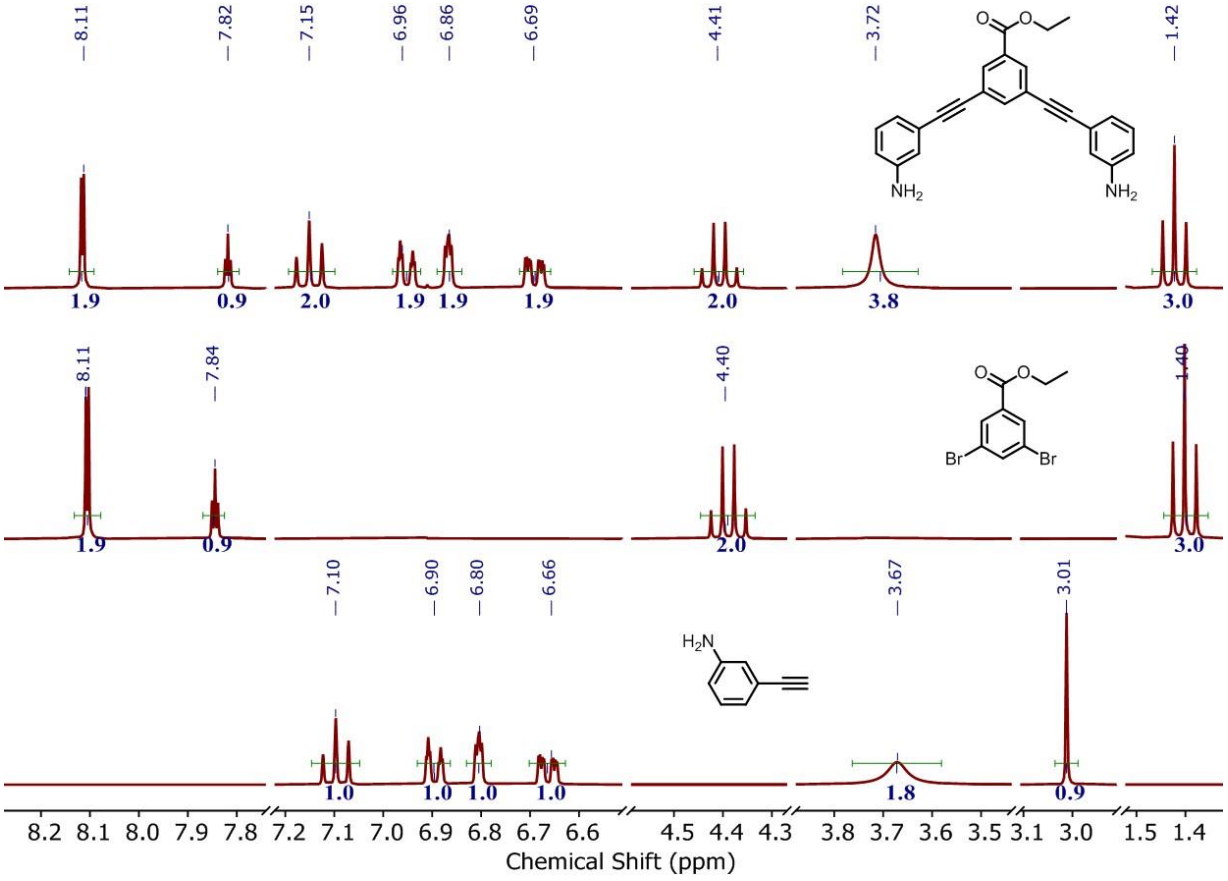

Figure 2.11 ^{1}H-NMR (300 MHz, $CDCl_3$) of compound **2-2** (top) in comparison with the spectrum of starting material (middle and bottom).

2.2.2.2 Synthesis of 2-3

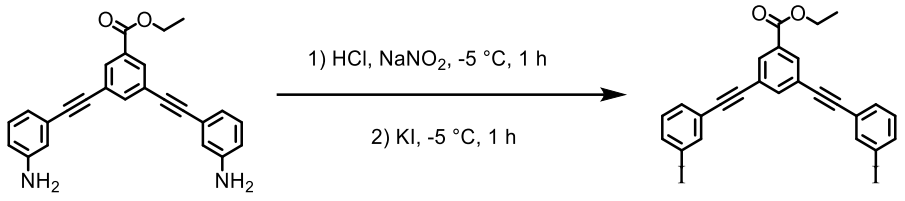

2-2 **2-3**

Figure 2.12 Synthesis of **2-3** from **2-2**.

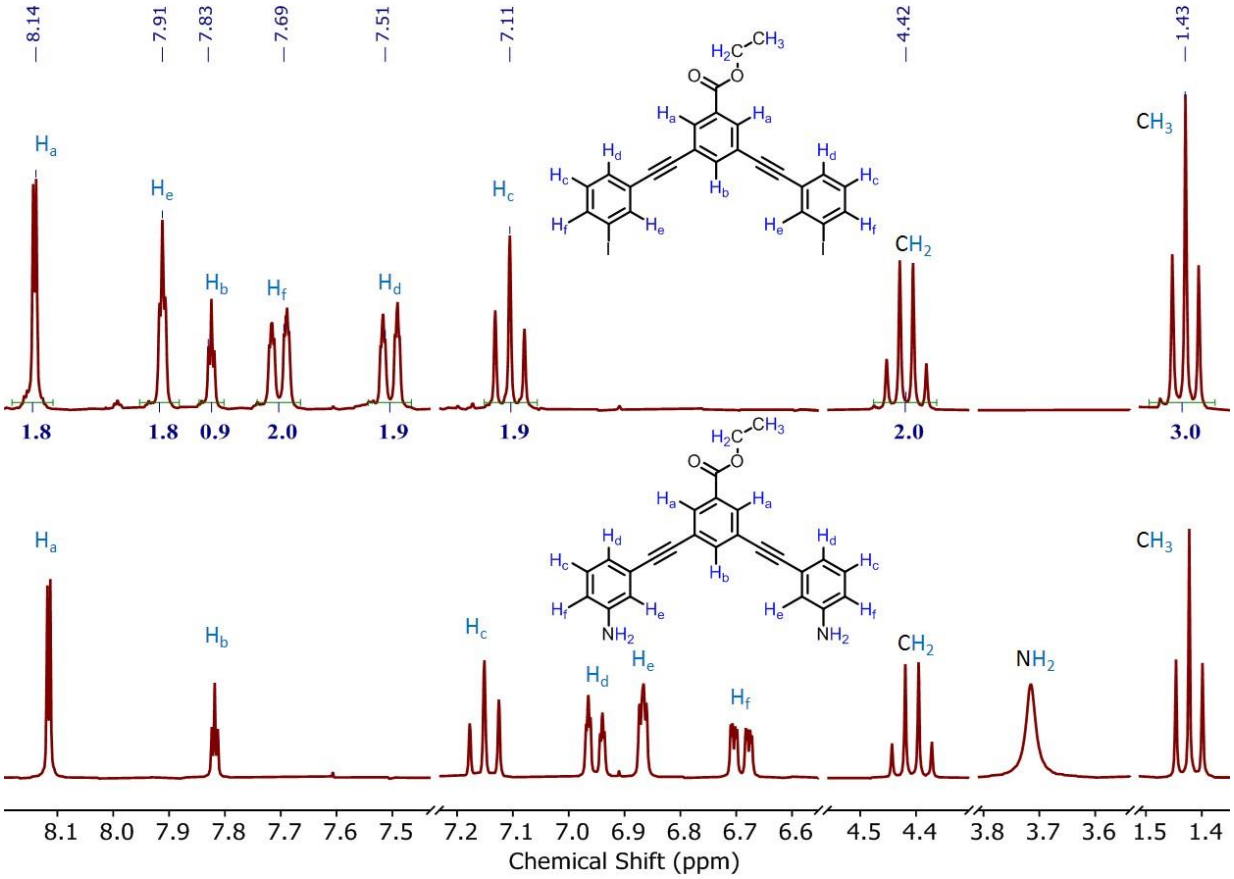

Figure 2.13 ^{1}H-NMR (300 MHz, $CDCl_3$) of the product **2-3** (top) compared with the starting material **2-2** (bottom).

As it is shown in Figure 2.12, synthesis of **2-3** from **2-2** goes through two steps of one-pot reactions. The first step is the formation of a diazonium intermediate by reacting **2-2** with a cold solution of sodium nitrite and hydrochloric acid. The second step is the substitution of the

diazonium groups with the iodo groups by treating the reaction mixture with a cold solution of potassium iodide. This procedure resulted in **2-3** with 44% yield as a light-yellow solid. ^{1}H-NMR spectrum of **2-3** and its comparison with the starting material **2-2** is shown in Figure 2.13. It is clear from Figure 2.13 that the peak correlated to the amine protons of **2-2** at chemical shift of 3.7 ppm do not exist in the spectrum of **2-3**. Additionally, due to the electronegative iodo groups, there is a considerable shift of H_d, H_f, and H_e proton resonances, which are deshielded, as expected, relative to the starting material **2-2**. Moreover, peaks integration correlated to the assigned protons of the molecule show the expected values. Thus, we conclude that **2-3** was synthesized successfully.

2.2.2.3 Synthesis of 2-5

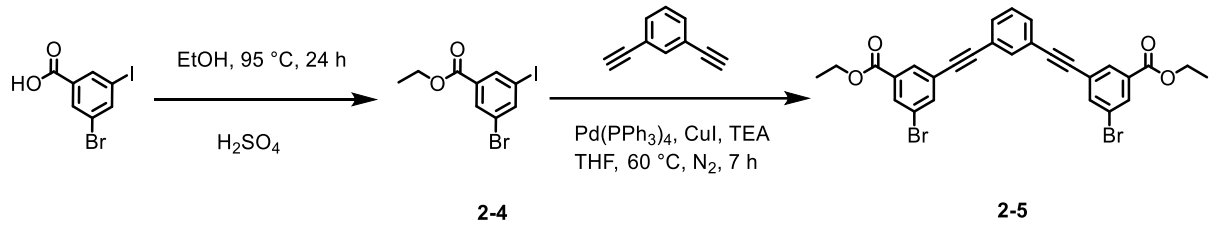

Figure 2.14 Two-step synthesis of **2-5**. First step is esterification of 3-bromo-5-iodobenzoic acid to make **2-4**, and the second step is Sonogashira cross-coupling between **2-4** and 1,3-diethynylbenzene.

After the synthesis of **2-4** that was achieved in 81% yield, synthesis of **2-5** was carried out in a similar fashion to the synthesis of **2-2** using Sonogashira reaction (Figure 2.14). Although compound **2-4** has both the iodide and bromide groups, Sonogashira cross-coupling reaction on the iodide side of the molecule proceeds much faster;[107] therefore, when 1,3-diethynylbenzene is the limiting reagent, the main product is **2-5**. ^{1}H-NMR spectrum of **2-5** is shown in Figure 2.15 with the assigned peaks and the correlated integrations. Figure 2.16 shows the comparison between the ^{1}H-NMR spectrum of the product with the starting materials. This comparison clearly shows that compound **2-5** is synthesized successfully.

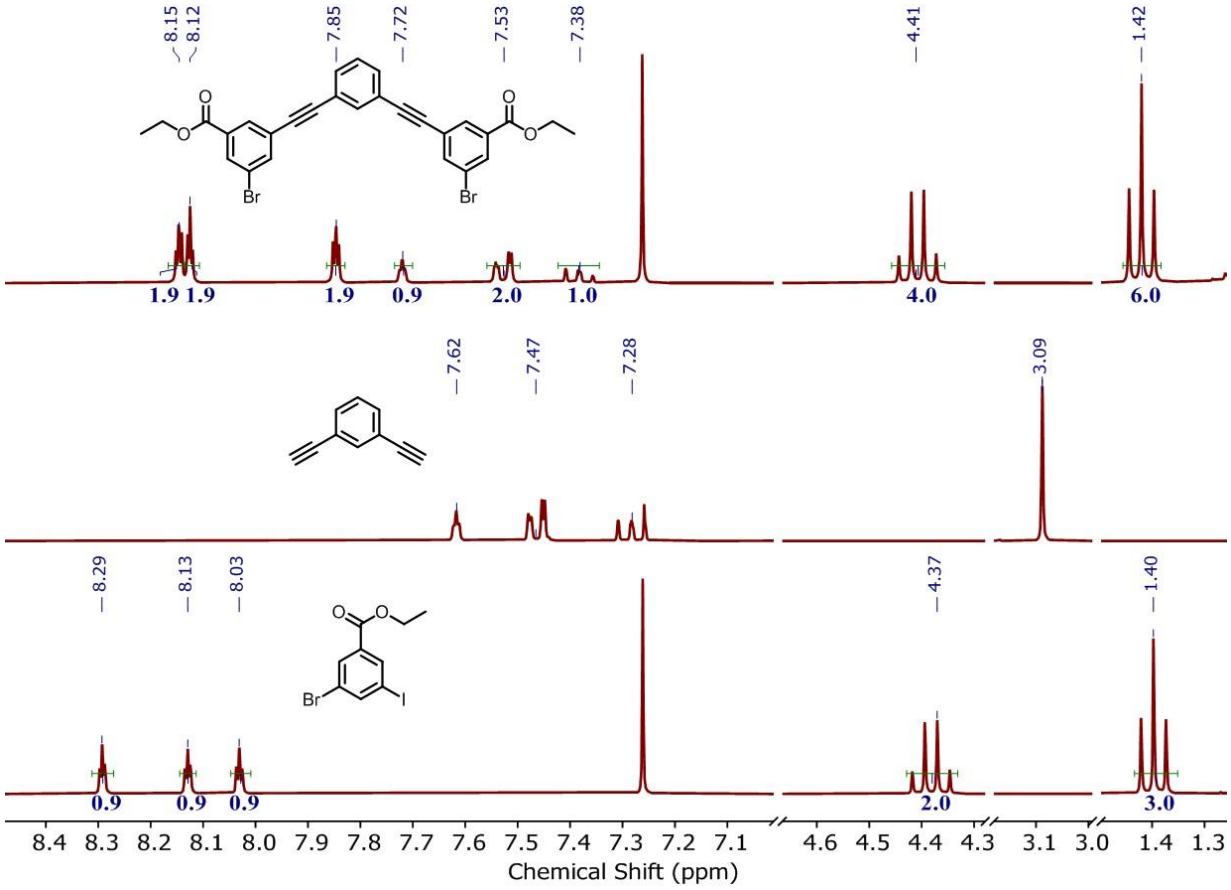

Figure 2.15 ^{1}H-NMR (300 MHz, $CDCl_3$) of compound **2-5** (top) and comparison with the spectrum of starting materials (middle and bottom). The signal at 7.26 ppm is the solvent residual peak.

2.2.2.4 Synthesis of 2-6

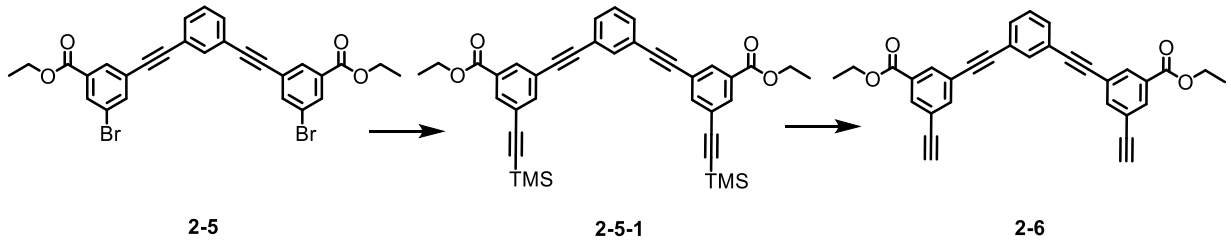

Figure 2.16 Synthesis route of **2-6** from **2-5**.

As it is shown in Figure 2.17, synthesis of **2-6** from **2-5** needs cross-coupling reaction of trimethylsilylacetylene with **2-5** to make **2-5-1**. Finally, the desilylation of the trimethylsilyl groups on **2-5-1** gives the product **2-6**. Here we describe each step separately with more details.

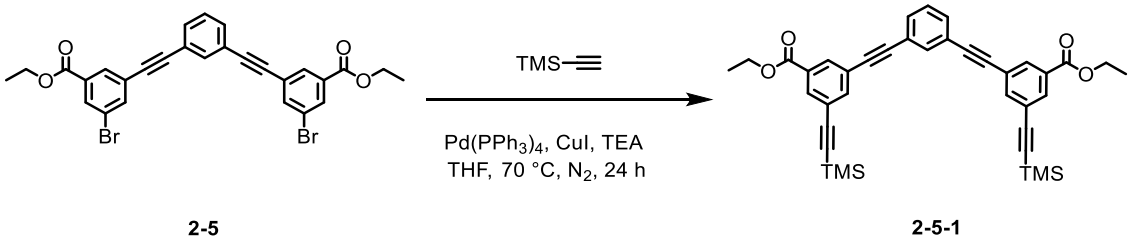

Figure 2.17 Synthesis of **2-5-1** from **2-5** with Sonogashira cross-coupling reaction between **2-5** and trimethylsilylacetylene.

Synthesis of **2-5-1** (Figure 2.18) proceeds in a way similar to the previous Sonogashira reactions already discussed in this thesis. Synthesis of **2-5-1** was accomplished in high yield (96%) and the product was obtained as a light-yellow solid that was purified by column chromatography. ^{1}H-NMR spectrum of the compound **2-5-1** along with the spectrum of the starting material **2-5** with the assigned peaks and the correlated integrations are shown in Figure 2.19. The presence of the strong peak at 0.26 ppm chemical shift that corresponds to the protons of the trimethylsilyl groups of the compound **2-5-1**. Additionally, the observed changes in the chemical shift of all the peaks related to the phenyl protons compared with those of the starting material **2-5** illustrate that the product **2-5-1** is successfully synthesized.

Although synthesis of both **2-5** and **2-5-1** were achieved in high yields (86 and 96% respectively), based on our experience, making **2-5-1** starting from **2-4** in a one-pot procedure (Figure 2.20) eliminates extra workups. This makes the synthesis of **2-5-1** easier by doing the workup only in the last step. For this purpose, the procedure discussed in Section 2.2.2.3 and Figure 2.14 for the synthesis of **2-5** from **2-4** was followed and subsequently trimethylsilylacetylene and TEA were added to the reaction mixture (no more catalyst was added). This procedure resulted in **2-5-1** with higher yield (94%) compared with the two-pot method (83% total yield).

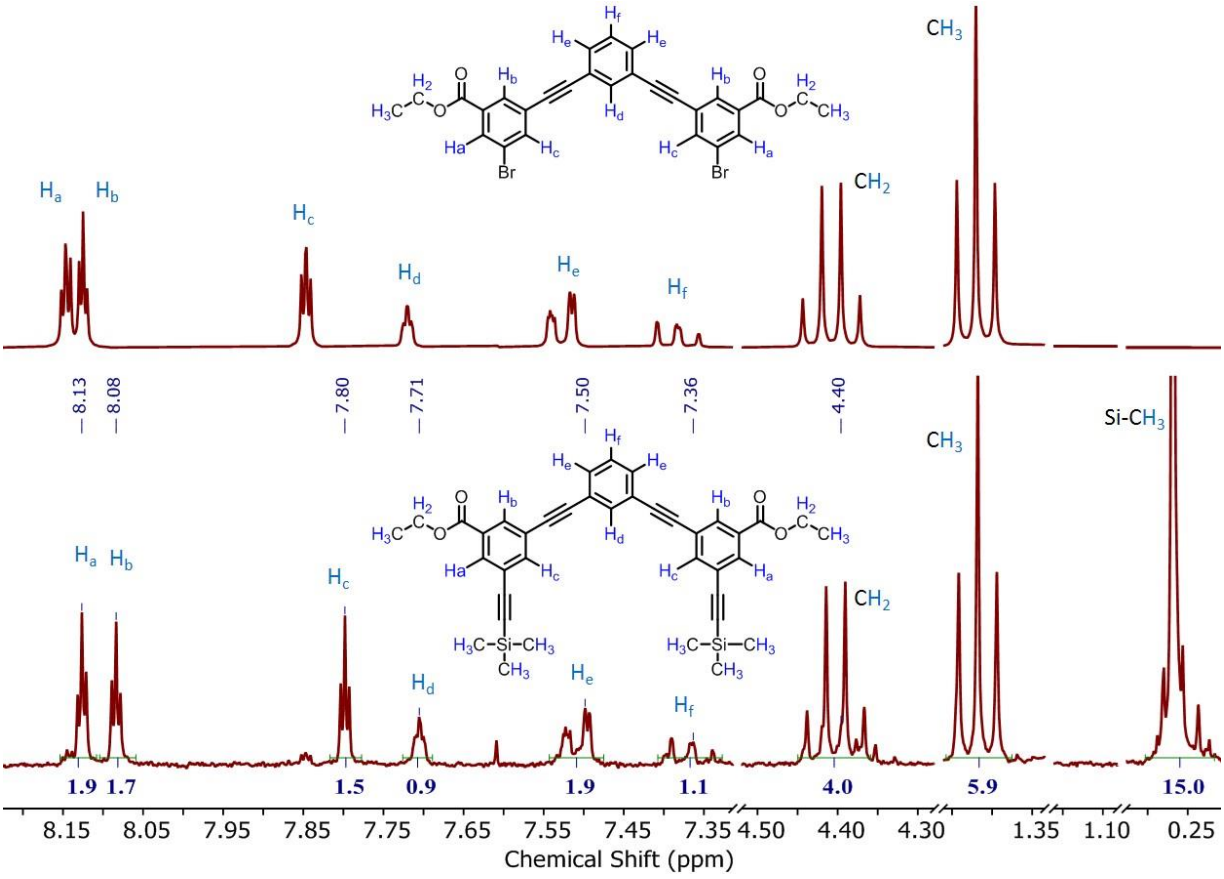

Figure 2.18 ^{1}H-NMR (300 MHz, $CDCl_3$) of compound **2-5-1** (bottom) compared with the spectrum of the starting material **2-5** (top).

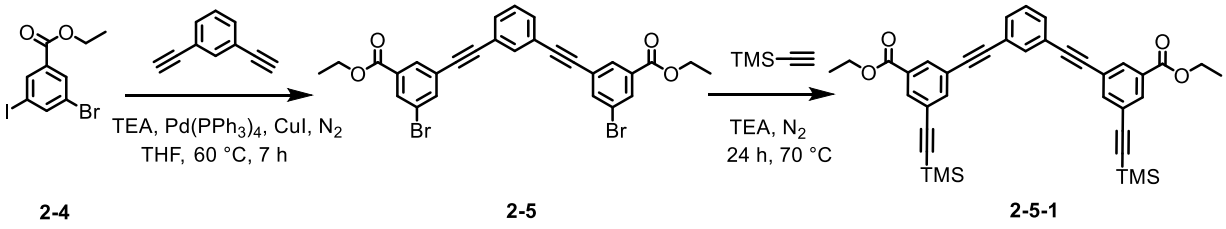

Figure 2.19 One-pot synthesis of **2-5-1** from **2-4**. The first step is done by Sonogashira cross-coupling between **2-4** and 1,3-diethynylbenzene. The second step is done by adding trimethylsilylacetylene and TEA to the reaction pot containing **2-5** and catalysts from the first step.

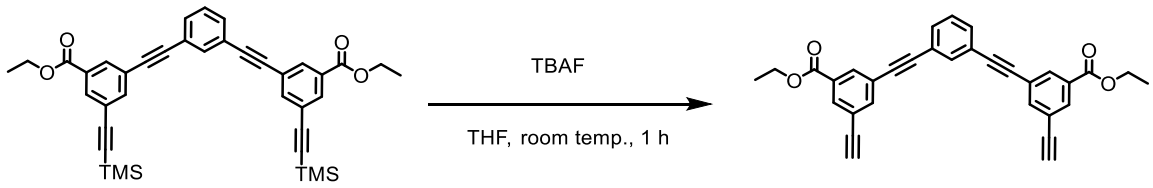

2-5-1 **2-6**

Figure 2.20 Synthesis of **2-6** by desylilation of **2-5-1** using TBAF.

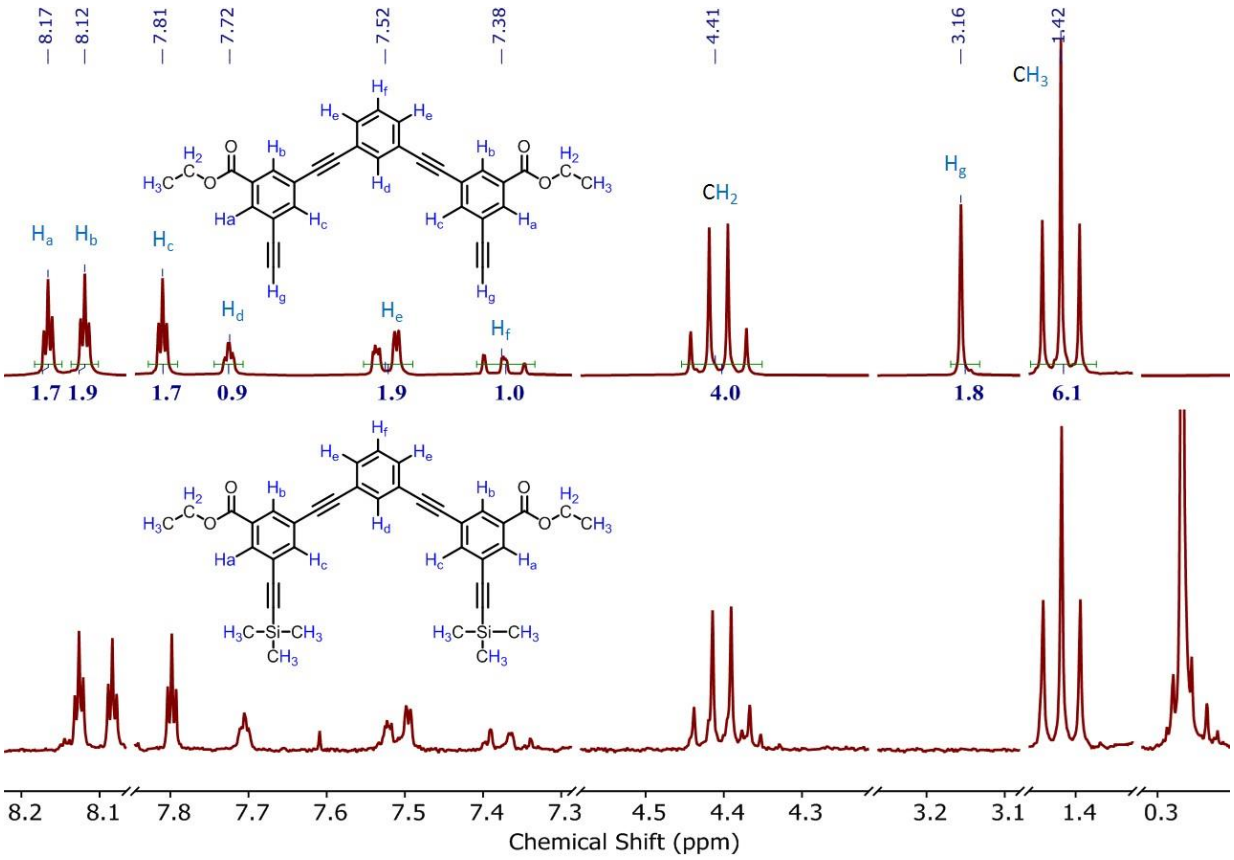

Figure 2.21 ^{1}H-NMR (300 MHz, $CDCl_3$) of compound **2-6** (top) compared with the spectrum of the starting material **2-5-1** (bottom).

As illustrated in Figure 2.21, the synthesis of **2-6** was achieved through desilylation of **2-5-1** with tetrabutylammonium fluoride (TBAF) that resulted in **2-6** as a white solid with 55% yield. ^{1}H-NMR spectrum of compound **2-6** along with the spectrum of the starting **2-5-1** with the assigned peaks and the correlated integrations are shown in Figure 2.22. It can be seen that the peak at 0.26 ppm corresponding to the trimethylsilyl groups of the starting material **2-5-1** cannot

be found in the spectrum of the product **2-6**. Instead, as expected, a new peak at 3.16 ppm corresponding to the acetylene proton is observed in the spectrum of the product **2-6**. Besides, phenyl protons of the product **2-5** are slightly shifted compared with the starting material **2-5-1**. All of this evidence, as well as the relative peak integrations, indicate the successful synthesis of the compound **2-6**.

With the successful synthesis of the starting materials **2-3** and **2-6** that are required for the synthesis of the PEM ligand, as illustrated in the general scheme in Figure 2.8, we proceeded to the more challenging step which is the synthesis of the macrocycle through coupling between these two precursors.

2.2.3 Synthesis of the macrocycle 2-6-1

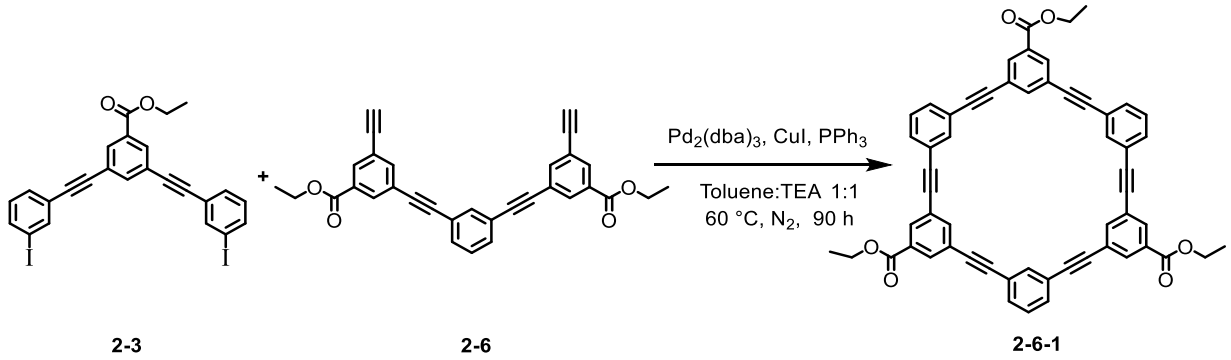

2-3 **2-6** **2-6-1**

Figure 2.22 Synthesis of macrocycle **2-6-1** with cross-coupling and cyclization between two precursors **2-3** and **2-6**.

As it was discussed in Section 2.2.1, our strategy for the synthesis of PEM is the cross-coupling between two precursors. For this purpose, we synthesized compounds **2-3** and **2-6** as the precursors of PEM. Sonogashira cross-coupling between these two compounds was carried out to make the PEM. For this purpose, we slowly added a solution of compound **2-6** to a mixture of the catalyst and a solution of compound **2-3**.

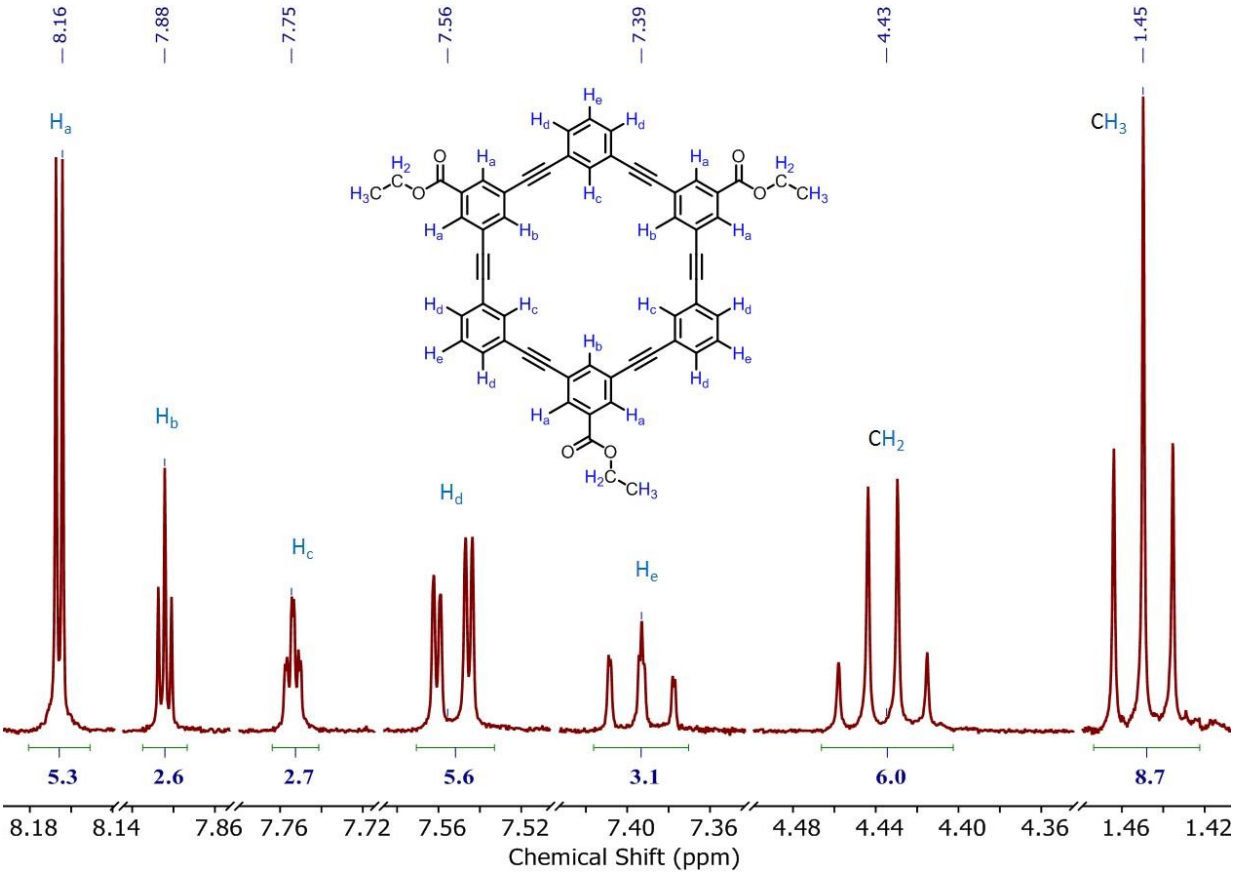

Figure 2.23 ^{1}H-NMR (500 MHz, $CDCl_3$) of **2-6-1**.

The synthesis was performed under N_2 and the cyclization reaction was performed under reaction conditions similar to literature (temperature, concentration range, and use of a syringe pump for the slow addition of the precursor).[98, 101, 102, 105, 106] With these measures, compound **2-6-1** was obtained as a white solid (purified with column chromatography) in 19% yield. ^{1}H-NMR spectrum of **2-6-1** is shown in Figure 2.24 and illustrates the assigned protons with the corresponding integrations. Comparison between the ^{1}H-NMR spectrum of one of the macrocycles synthesized by Moore and co-workers[105] (Figure 2.4a where R = *tert*-butyl) and our PEM shows that the spectrum of both molecules contains peaks with the same coupling patterns for the phenyl protons. Likewise, comparing the ^{1}H-NMR spectrum of the macrocycle synthesized by Miljanic and co-workers[106] (Figure 2.4a where R = $COOCEt_3$) with our PEM shows that the peaks

correlated to the phenyl protons of both molecules have chemical shifts similar to each other. Furthermore, the order of these proton resonances with the correlated integrations are the same as our synthesized compound **2-6-1**. Figure 2.25 shows the ^{1}H-NMR spectrum of the PEM compared with the spectrum of the precursors. It can be seen that the chemical shifts of the proton resonance of the product are different from those of the precursors used in the reaction. All these pieces of evidence point to the formation of the expected PEM.

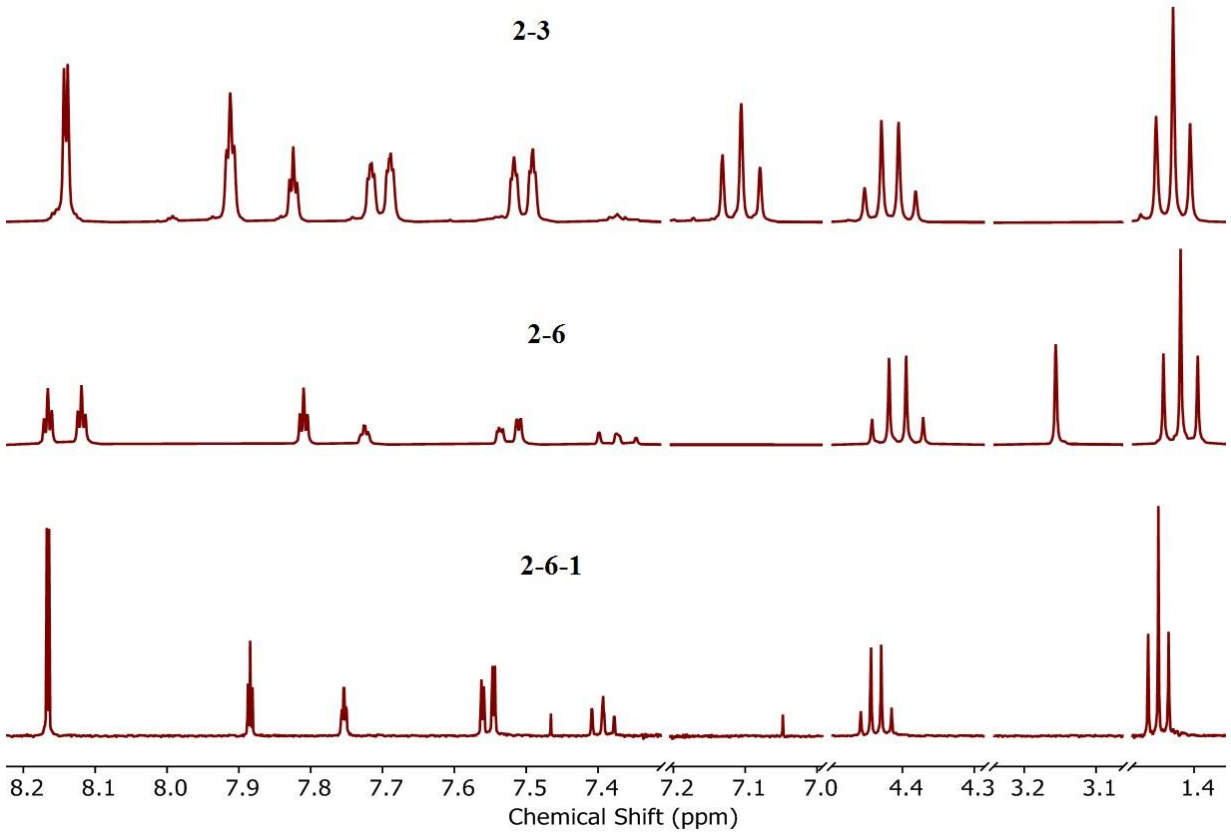

Figure 2.24 ^{1}H-NMR (500 MHz, $CDCl_3$) of the macrocycle **2-6-1** (bottom) compared with the ^{1}H-NMR (300 MHz, $CDCl_3$) spectrum of the starting materials **2-6** (middle) and **2-3** (top).

2.3 Conclusion

We synthesized a macrocyclic molecule (**2-6-1**) from which a macrocyclic linker (**2-7**) can be made. This macrocyclic linker can be used for the synthesis of large-pore MOFs in which

interpenetration is avoided, therefore larger pores and high surface area can be achieved. The overall yield for the synthesized macrocycle molecule (**2-6-1**) is 6% which is comparable to the overall yield (5%) for a similar molecule (Figure 2.4a, R = $COOCEt_3$) previously reported by Miljanic and co-workers. However, our method involves 8 steps and can be achieved in total of 6 pots while synthesis reported by Miljanic is done in 13 steps and 13 pots. Therefore, with our approach, synthesis of the macrocyclic linker **2-7** can be achieved in a more facile way compared with work reported by Miljanic. While the goal of the project was to deprotect **2-6-1** and utilize it as a linker in MOF synthesis, shortly after our synthesis of **2-6-1** was complete, Miljanic and co-workers published two reports of the use of the deprotected macrocycle as a linker were reported with the nodes that we were interested in exploring.[60, 61] Although the surface areas obtained are lower than what is expected which is, as reported by the authors, due to collapse of the framework in the case of Zn-MCMOF and incomplete activation in the case of Zr-MCMOF, it could be possible that the stacking of PEM itself dictates the SBU connectivity and therefore the structure of the resultant MOF. This suggest that there is still room for improvement by the synthesis of a substituted PEM linker to prevent aggregation and obtain a different MOF topology with potentially higher surface area. However, with regard to the low yield of the PEM (**2-6-1**) we synthesized in this thesis and the two MOF reports by Miljanic and co-workers, we opted to focus on another linker system.

2.4 Experimental details

2.4.1 General procedures, materials, and instrumentation

Reagents and solvents were purchased from commercial sources and used without purification. ^{1}H-NMR spectra were recorded on a Bruker 300 MHz AVANCE III or Bruker AVANCE 500 MHz spectrometers using $CDCl_3$ as the NMR solvent.

2.4.2 Synthesis of 2-1

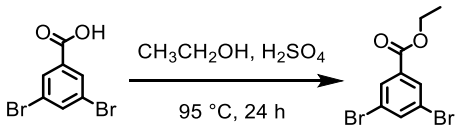

2-1

4.46 g 3,5-dibromobenzoic acid (15.5 mmol) and 110 mL anhydrous ethanol, along with a magnetic stir bar were added to a 250 mL round-bottom flask (RBF). The solid was dissolved by stirring the mixture then 2.0 mL of concentrated sulfuric acid was added to the flask and the solution was heated under reflux for 24 h. After cooling down to room temperature, 100 mL deionized water was added to the flask and the product was extracted from the mixture by dichloromethane. The collected dichloromethane extracts were washed with 3×50 mL of aqueous solution of 2.0% sodium carbonate (made by dissolving 5.0 g Na_2CO_3 in 250 mL deionized water) then the organic solution was dried with $MgSO_4$, and the solvent was evaporated using rotary evaporator to obtain 4.37 g product 2-1 as an off-white solid (14.2 mmol, 92% yield. ^{1}H-NMR (300 MHz, $CDCl_3$) δ 8.11 (d, J = 1.8 Hz, 2H), 7.84 (t, J = 1.8 Hz, 1H), 4.39 (q, J = 7.1 Hz, 2H), 1.40 (t, J = 7.1 Hz, 3H).

2.4.3 Synthesis of 2-4

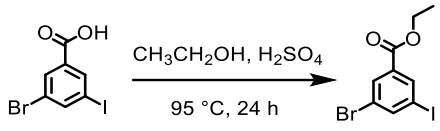

2-4

14.8 g 3-bromo-5-iodobenzoic acid (43.9 mmol) and 250 mL anhydrous ethanol, along with a magnetic stir bar were added to a 500 mL RBF. The solid was dissolved by stirring the mixture then 5.6 mL of concentrated sulfuric acid was added to the flask and the solution was heated under reflux for 24 h. A workup procedure similar to what was done for the synthesis of **2-1** was followed

to obtain 12.6 g product **2-4** as an off-white solid (35.5 mmol, 81% yield). ^{1}H-NMR (300 MHz, $CDCl_3$) δ (t, *J* = 1.5 Hz, 1H), 8.13 (t, *J* = 1.6 Hz, 1H), 8.03 (t, *J* = 1.7 Hz, 1H), 4.38 (q, *J* = 7.1 Hz, 2H), 1.40 (t, *J* = 7.2 Hz, 3H).

2.4.4 Synthesis of 2-2

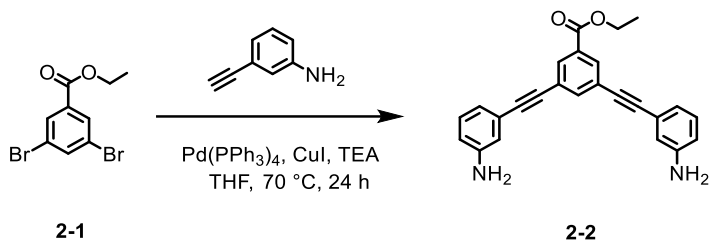

2-1 **2-2**

1.23 g of **2-1** (4.00 mmol), 91.7 mg $Pd(PPh_3)_4$ (0.0794 mmol), and 16.1 mg CuI (0.0845 mmol) along with a magnetic stir bar were added to a 20 mL vial. The vial was sealed with a crimpable septa-containing cap, and subsequently sparged using a needle punctured through the septa with N_2; a second needle was pierced through the septa to vent the gas. In a second 20 mL vial was added 1.1600 g (around 1100 μL) 3-ethynylaniline (9.90 mmol) and 2.2 mL of dry TEA. The vial was crimped and sealed with a septa-containing cap. Using a canula, approximately 15 mL of dry tetrahydrofuran (THF) was transferred to the vial using N_2 gas to pressurize the transfer. Once dissolved, the contents of this vial were then transferred to the first vial using a cannula transfer using N_2 as the carrier gas and thereby ensuring that the sealed vial was under an inert atmosphere. The vial was then heated and stirred in an oil bath at 70 °C for 24 h using a hot plate equipped with a temperature probe. The reaction was followed by TLC (hexanes:ethyl acetate 7:3). After cooling down to room temperature, the vial contents were poured into 100 mL deionized water in a beaker and the product was extracted from the mixture with dichloromethane. The collected dichloromethane extracts were further washed with 3×50 mL deionized water then the organic solution was dried with $MgSO_4$, and the solvent was evaporated using rotary evaporator to obtain 1.45 g crude product **2-2** as a beige solid. The crude product was further purified by column

chromatography as follows. The crude product **2-2** was dissolved in minimum amount of dichloromethane then it was mixed with 4.5 g silica to absorb on it and left for dichloromethane to evaporate. The absorbed material on silica was dry loaded into a column then using eluent gradient of hexanes:ethylacetate (1:1-1:2), and subsequent solvent evaporation resulted in 1.23 g product **2-2** as an off-white solid (3.23 mmol, 81% yield). ^{1}H-NMR (300 MHz, $CDCl_3$) δ 8.12 (d, *J* = 1.6 Hz, 2H), 7.82 (t, *J* = 1.6 Hz, 1H), 7.15 (t, *J* = 7.8 Hz, 2H), 6.95 (dt, *J* = 7.7, 1.2 Hz, 2H), 6.87 (dd, *J* = 2.3, 1.4 Hz, 2H), 6.69 (ddd, *J* = 8.0, 2.5, 1.0 Hz, 2H), 4.41 (q, *J* = 7.1 Hz, 2H), 3.72 (s, 4H), 1.42 (t, *J* = 7.1 Hz, 3H).

2.4.5 Synthesis of 2-5

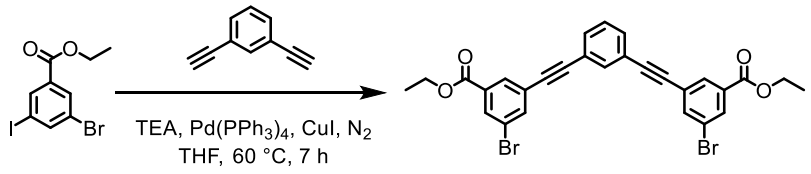

2-4 **2-5**

2.434 g of **2-4** (6.86 mmol), 81.2 mg $Pd(PPh_3)_4$ (0.0701 mmol), and 20.4 mg CuI (0.107 mmol) along with a magnetic stir bar were placed in a 20 mL vial The vial was sealed with a crimpable septa-containing cap, and subsequently sparged using a needle punctured through the septa with N_2; a second needle was pierced through the septa to vent the gas. In a second 20 mL vial was added 393 mg (around 405 μL) 1,3-diethynylbenzene (3.02 mmol), and 1.172 g (around 1.7 mL) of dry triethyamine. The vial was crimped and sealed with a septa-containing cap. Using a canula, approximately 15 mL of dry THF was transferred to the vial using N_2 gas to pressurize the transfer. Once dissolved, the contents of this vial were then transferred to the first vial using a cannula transfer using N_2 as the carrier gas and thereby ensuring that the sealed vial was under an inert atmosphere. The vial was heated and stirred in an oil bath at 60 °C for 7 h using a hot plate equipped with a temperature probe. The reaction was followed by TLC (hexanes:ethylacetate 2:1) . After

cooling down to room temperature, the vial contents were poured into 100 mL deionized water in a beaker and the product was extracted from the mixture by dichloromethane. The collected dichloromethane extracts were further washed with 3×50 mL water then the organic solution was dried with $MgSO_4$, and the solvent was evaporated using rotary evaporator to obtain 1.50 g product **2-5** as a yellow solid (2.59 mmol, 86% yield). ^{1}H-NMR (300 MHz, $CDCl_3$) δ 8.15 (t, *J* = 1.7 Hz, , 2H), 8.12 (t, *J* = 1.5 Hz, 2H), 7.85 (t , *J* = 1.7, Hz, 2H), 7.72 (t, *J* = 1.7 Hz, 1H), 7.56 – 7.49 (m, 2H), 7.38 (t , *J* = 7.6 Hz, 1H), 4.41 (q, *J* = 7.1 Hz, 4H), 1.42 (t, *J* = 7.1 Hz, 6H).

2.4.6 Synthesis of 2-3

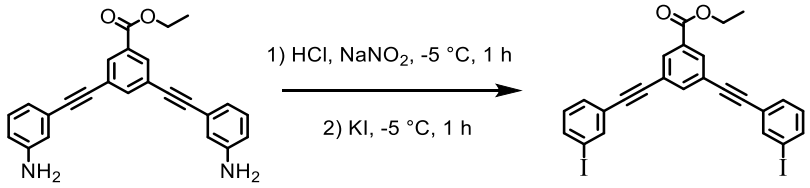

2-2 **2-3**

385 mg **2-2** (1.01 mmol) was added to a 250 mL RBF containing 10 mL 20% HCl solution (made by diluting 12.4 mL concentrated HCl to 25.0 mL) and a magnetic stir bar, then the mixture was stirred. The flask was placed in an ice bath containing NaCl. The initial temperature of the salt bath was -10 to -5 °C. To the RBF was added 0.30 g $NaNO_2$ (4.3 mmol) dissolved in 3 mL ice-cold 20% HCl solution. This solution was added dropwise to the first RBF in a fume hood while stirring the mixture (the mixture foams and gradually turns into a clear brown solution). Stirring the mixture in the ice bath was continued for 1 h. Subsequently, 0.97 g KI (5.8 mmol) was dissolved in 3 mL ice-cold water. This solution was added dropwise to the RBF in the ice bath, and it was stirred for 30 min. Then a solution of 183 mg $NaHSO_3$ in 2 mL deionized water was added to the RBF at room temperature and it was stirred; this reacted with any formed I_2. Subsequently, 100 mL deionized water was added to the flask and the product was extracted with dichloromethane. The organic solution was dried with $MgSO_4$, and the solvent was evaporated

using rotary evaporator. The crude product (dark brown sticky substance) was purified by column chromatography using hexanes:ethylacetate with the ratio of 1:0 then 95:5 as eluent. Finally, the solvent was evaporated using rotary evaporator to give 269 mg product **2-3** as a light-yellow solid (0.447 mmol, 44% yield). ^{1}H-NMR (300 MHz, $CDCl_3$) δ 8.14 (d, *J* = 1.6 Hz, 2H), 7.91 (t, *J* = 1.7 Hz, 2H), 7.82 (t, *J* = 1.6 Hz, 1H), 7.70 (dt, *J* = 8.0, 1.4 Hz, 2H), 7.50 (dt, *J* = 7.7, 1.3 Hz, 2H), 7.11 (t, *J* = 7.9 Hz, 2H), 4.42 (q, *J* = 7.1 Hz, 2H), 1.43 (t, *J* = 7.1 Hz, 3H).

2.4.7 Synthesis of 2-5-1

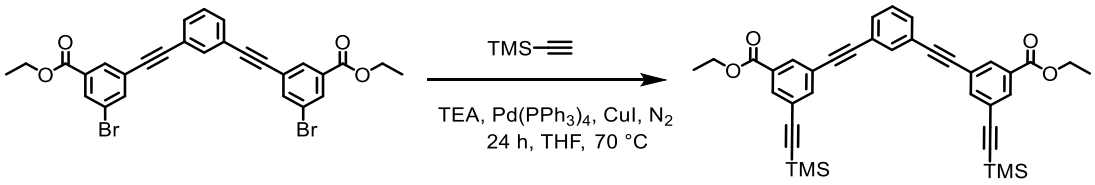

2-5 **2-5-1**

2.03 g of **2-5** (3.50 mmol), 91.8 mg $Pd(PPh_3)_4$ (0.0795 mmol), and 16.3 mg CuI (0.0855 mmol) along with a magnetic stir bar were placed in a 20 mL vial The vial was sealed with a crimpable septa-containing cap, and subsequently sparged using a needle punctured through the septa with N_2; a second needle was pierced through the septa to vent the gas. In a second 20 mL vial was added 1.21 g (around 1840 μL) trimethylsilylacetylene **(**12.1 mmol) and 2.2 mL of dry TEA. The vial was crimped and sealed with a septa-containing cap. Using a canula, approximately 15 mL of dry THF was transferred to the vial using N_2 gas to pressurize the transfer. Once dissolved, the contents of this vial were then transferred to the first vial using a cannula transfer using N_2 as the carrier gas and thereby ensuring that the sealed vial was under an inert atmosphere. The vial was heated and stirred in an oil bath at 70 °C for 24 h using a hot plate equipped with a temperature probe. The reaction was followed by TLC (hexanes:ethylacetate 6:1). After cooling down to room temperature, the vial contents were poured into 100 mL deionized water in a beaker and the product was extracted from the mixture by dichloromethane. The collected dichloromethane extracts were

further washed with water then the organic solution was dried with $MgSO_4$, and the solvent was evaporated using rotary evaporator to obtain a brown sticky crude product. The crude product was purified by column chromatography using hexanes:ethylacetate (1:12) as eluent. The solvent was evaporated using rotary evaporator to obtain 2.06 g product **2-5-1** as a light-yellow solid (3.35 mmol, 96% yield). ^{1}H-NMR (300 MHz, $CDCl_3$) δ 8.13 (t, *J* = 1.6 Hz, 2H), 8.08 (t, *J* = 1.6 Hz, 2H), 7.80 (t, *J* = 1.6 Hz, 2H), 7.71 (t, *J* = 1.6 Hz, 1H), 7.54 – 7.48 (m, 2H), 7.36 (t, *J* = 7.6 Hz, 1H), 4.40 (q, *J* = 7.1 Hz, 4H), 1.42 (t, *J* = 7.2 Hz, 6H), 0.27 (s, 18H).

2.4.8 One-pot synthesis of 2-5-1

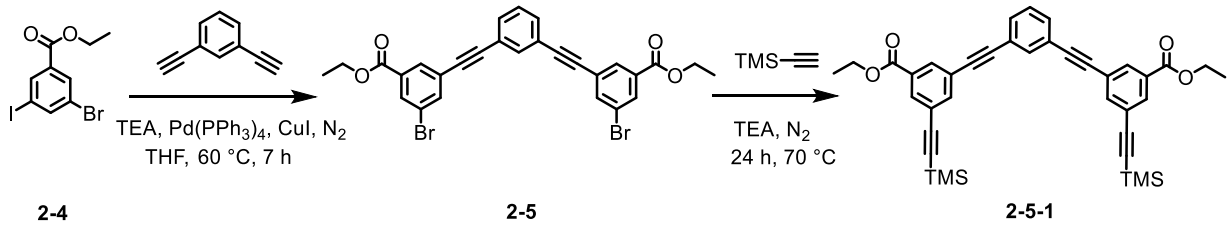

2-4 **2-5** **2-5-1**

3.246 g of **2-4** (9.14 mmol), 108 mg $Pd(PPh_3)_4$ (0.0935 mmol), and 27.2 mg CuI (0.143 mmol) along with a magnetic stir bar were placed in a 20 mL vial, The vial was sealed with a crimpable septa-containing cap, and subsequently sparged using a needle punctured through the septa with N_2; a second needle was pierced through the septa to vent the gas. In a second 20 mL vial was added 524 mg (around 540 µL) 1,3-diethynylbenzene (4.02 mmol), and 1.562 g (around 2.2 mL) dry triethyamine. The vial was crimped and sealed with a septa-containing cap. Using a canula, approximately 15 mL of dry THF was transferred to the vial using N_2 gas to pressurize the transfer. Once dissolved, the contents of this vial were then transferred to the first vial using a cannula transfer using N_2 as the carrier gas and thereby ensuring that the sealed vial was under an inert atmosphere. The vial was heated and stirred in an oil bath at 60 °C for 7 h using a hot plate equipped with a temperature probe. The reaction was followed by TLC (hexanes:ethylacetate 2:1). After cooling down to room temperature, 2.2 mL dry TEA and 2.1 g (around 3.2 mL)

trimethylsilylacetylene (21 mmol) was added to the vial through the septa seal using syringe and needle. The vial was then backfilled with N_2 and heated and stirred in an oil bath at 70 °C for 24 h. The reaction was followed by TLC (hexanes:ethylacetate 6:1). After cooling down to room temperature, the vial contents were poured into 100 mL of a saturated aqueous solution of NH_4Cl, and the product was extracted from the mixture by dichloromethane. The collected dichloromethane extracts were further washed with deionized water then the organic solution was dried with $MgSO_4$, and the solvent was evaporated using rotary evaporator. The crude product was purified by column chromatography using hexanes:ethylacetate (1:12) as eluent. The solvent was evaporated using rotary evaporator to obtain 2.32 g product **2-5-1** as a light-yellow solid (3.77 mmol, 94% yield based on 1,3-diethynylbenzene).

2.4.9 Synthesis of 2-6

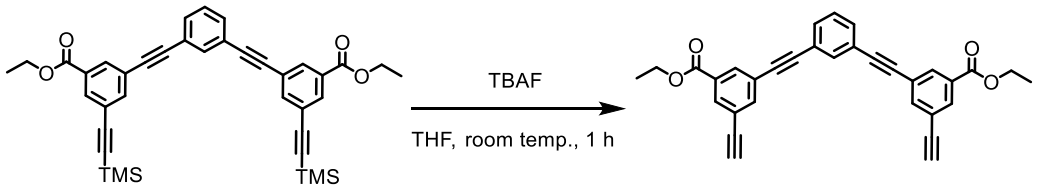

2-5-1 **2-6**

307.7 mg of **2-5-1** (0.5004 mmol) along with a magnetic stir bar was added to a 100 mL RBF, then 33 mL THF was added to dissolve the solid. 1.5 mL of 1.0 M of TBAF solution was added dropwise to the flask. Upon addition of TBAF solution, the reaction solution turns into a light-brown clear solution. The solution was stirred for 1 h at room temperature and the reaction was followed by TLC (hexanes:ethylacetate 4:1). Subsequently, 100 mL deionized water was added to the reaction mixture in a beaker and the product was extracted from the mixture with dichloromethane. The organic solvent was evaporated using rotary evaporator to obtain 266.0 mg dark brown sticky substance. The crude product was purified using column chromatography with

silica gel as stationary phase (the crude product was dry-loaded into the column) and hexanes:ethylacetate (8:1) was used as eluent. The solvent was evaporated using a rotary evaporator to obtain 130.0 mg product **2-6** as a white solid (0.2763 mmol, 55% yield). ^{1}H-NMR (300 MHz, $CDCl_3$) δ 8.17 (t, *J* = 1.6 Hz, 2H), 8.12 (t, *J* = 1.6 Hz, 2H), 7.81 (t, *J* = 1.6 Hz, 2H), 7.73 (t, *J* = 1.7 Hz, 1H), 7.55-7.49 (m, 2H), 7.37 (t, *J* = 7.6 Hz, 1H), 4.41 (q, *J* = 7.1 Hz, 4H), 3.16 (s, 2H), 1.42 (t, *J* = 7.2 Hz, 6H).

2.4.10 Synthesis of 2-6-1

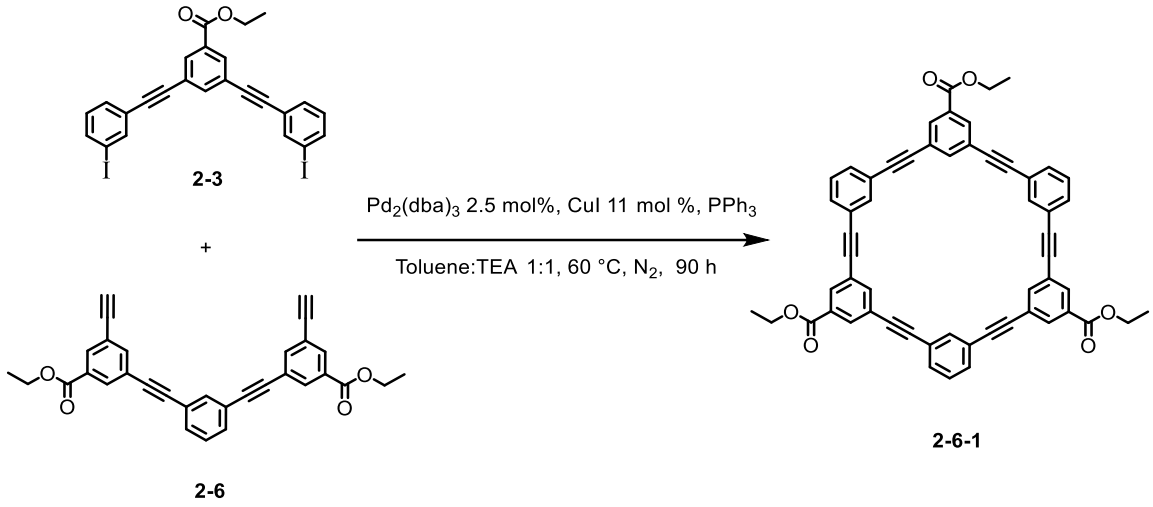

64.7 mg of **2-3** (0.107 mmol) was dissolved in 10 mL dry toluene, then this solution was transferred to a 500 mL RBF along with a magnetic stir bar. 5.2 mg $Pd_2(dba)_3$ (0.0054 mmol, 5.0 mol%), 4.4 mg CuI (0.022 mmol, 21 mol%), and 11.4 mg PPh_3 (0.0435 mmol) were added to the 500 mL RBF. Then the flask was evacuated and filled with N_2 gas for three cycles. 70 mL dry toluene was transferred to the flask using a syringe through the septa on the flask. Around 130 mL dry TEA (from the original sure-sealed bottle) was transferred to a preheated and dry 250 mL RBF using cannula transfer. Then TEA was transferred from the 250 mL RBF to the 500 mL RBF using cannula transfer. 45.6 mg of **2-6** (0.0969 mmol) was dissolved in 60 mL dry toluene, then this solution (1.62 mM) was taken to a 60 mL syringe (inner diameter 29.2 mm) under N_2 atmosphere.

The 500 mL RBF was gently heated and stirred using a mantle and stirrer plate with a thermometer showing 60 °C for the solution inside the flask while a continuous flow of N_2 gas was maintained though the flask. After the temperature was stabilized, the solution in the 60 mL syringe (containing 1.62 mM **2-6**) was added to the 500 mL RBF through a stainless steel canula (fit into the syringe) using a programmable syringe pump with the flow of 46.3 µL/min (this setting delivers around 4.5 µmol **2-6** per hour and 60 mL is delivered in around 22 h). The solution in the 500 mL RBF was further stirred for 70 h at 60 °C. After cooling to room temperature, 200 mL deionized water was added to the flask and the product was extracted with dichloromethane. The organic solvent was evaporated with a rotary evaporator then the solid was dissolved in minimum amount of dichloromethane followed by adding methanol to precipitate the product. The obtained suspension was filtered to obtain 77 mg of a grey solid. The crude product was purified using column chromatography with silica gel as stationary phase and dichloromethane:hexanes gradient as eluent (started with 7:3, finished with 100% dichloromethane). After evaporating the solvent, 15.1 mg product **2-6-1** was obtained as a white solid (0.0185 mmol, 19% yield). ^{1}H-NMR (500 MHz, $CDCl_3$) δ 8.17 (d, *J* = 1.6 Hz, 6H), 7.88 (t, *J* = 1.6 Hz, 3H), 7.75 (td, *J* = 1.7, 0.6 Hz, 3H), 7.55 (dd, *J* = 7.7, 1.6 Hz, 6H), 7.39 (ddd, *J* = 8.1, 7.4, 0.6 Hz, 3H), 4.44 (q, *J* = 7.1 Hz, 6H), 1.45 (t, *J* = 7.1 Hz, 9H).

3 Synthesis of phthalocyanine linkers

3.1 Introduction

As stated in Chapter 1, one of the ways to prevent interpenetration is to utilize sterically crowded ligands. Macrocyclic ligands like phthalocyanines (Figure 3.1) provide such an opportunity. Pcs share similar structural properties with porphyrins.[74-76] Just like their porphyrin counterparts, the ability to incorporate a wide range of metals at the center of the Pc makes them an ideal choice for examining metal-based catalysis and photochemistry, but with a different chemical/electronic environment (Figure 3.1). Despite all these characteristics, with the exception of a few reports of PcMOFs since 2018 (Chapter 1), Pcs as ligands for MOF building blocks have not been well-explored. However, if similar ligand features can be designed for Pc as in the existing porphyrin literature, then it should be possible to access PcMOFs with similar structural characteristics to porphyrinic MOFs.

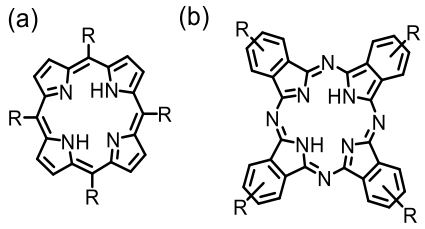

Figure 3.1 (a) structure of porphyrin showing the common substitution points. (b) Pc showing the common substitution points.

The challenge with Pcs, relative to porphyrins, is that their planarity and larger conjugated system cause stronger stacking, and subsequent aggregation, through π-π interaction.[74] This is problematic in some applications (e.g., catalysis and photochemistry-related applications) because only the surface of the aggregate can be addressed. Although Pcs are synthetically more attainable than porphyrins, they have lower solubility in common organic solvents.[74, 108] This makes

purification and characterization of these molecules difficult, further limiting their applications. In Pc chemistry, aggregation can be greatly reduced by introducing solubilizing groups onto the periphery of the core (R groups in Figure 3.1). This introduces a synthetic demand that limits the ability to use these positions as a method of introducing other necessary functionality to the core. The detriment of Pcs can, in principle, be removed by incorporating Pcs in a MOF framework. Much similar to porphyrinic MOFs, the inclusion of these macrocycles into a porous structure enables researchers to take advantage of the chemistry of Pcs in a micro/nanoreactor environment. This produces a high density of active sites with large pores and a high surface area for various applications while preventing aggregation.

Despite the rationale for using Pc's in MOFs, as Chapter 1 indicates, there is not a lot of PcMOFs. Comparatively, porphyrinic MOFs have been widely adopted by many research groups for applications in photocatalysis, electrocatalysis, biomimetic catalysis, biomedical, and sensing.[62] The challenge here is in the symmetry of Pc *vs.* porphyrins, coupled with the structural features necessary for a good MOF linker are not as readily available in Pcs (Figure 3.1). It is not to say that PcMOFs have not been made, but they are mostly limited to diamino and catechol-based Pcs (Chapter 1). With a focus on MOFs, an ideal Pc linker would contain carboxylic acids (or other MOF-based metal coordination groups) substituted around a core in a highly symmetric fashion. Additionally, for the linker to be adopted by the MOF community, the core of the structure has to offer the ability to (a) easily install longer linkers or linkers with different carboxylic acid substitution patterns (Figure 3.2c) and (b) easy add-in functional groups for different chemistry; the diamino and catechol-based Pcs do not easily offer these features.

Looking at Figure 3.2, it is easy to see why porphyrins are so readily available for MOF synthesis. A simple reaction between pyrrole and an aldehyde can easily result in the C_4-symmetric

porphyrin. Similarly, it is easy to see how *para*-substituted on the *meso*-carbons of the porphyrins can generate the ideal C_2-symmetric porphyrin with the other two groups used to add functionality to the structure. Looking at Pc, it is more difficult to see the pathway to a similar C_4 or C_2 symmetric linker. Substitution on one of the carbon atoms may yield the Pc in Figure 3.2b, but it may also result in one of three other isomers, at least two of which are not ideal for MOF synthesis. In contrast, the related porphyrin would produce just one isomer (Figure 3.1a). Thus, for PcMOFs to reach their full potential, we must first determine a synthetic pathway that offers all the features that make porphyrin MOFs popular, without any of the isomer challenges that come with Pcs.

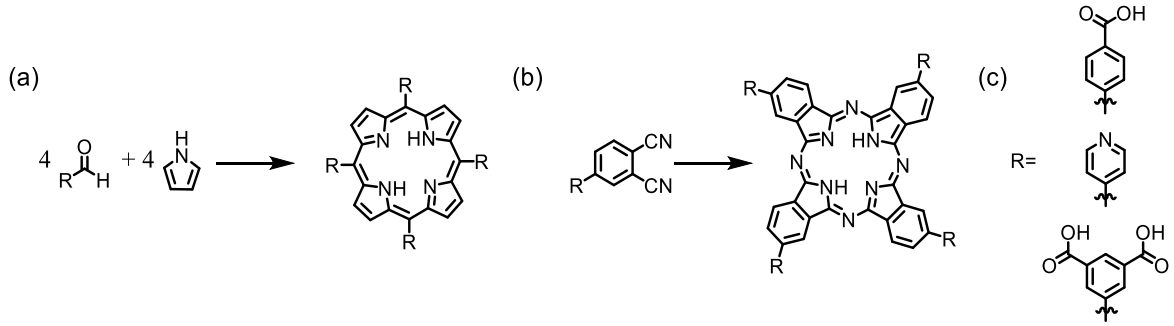

Figure 3.2 (a) Synthesis of a porphyrin. (b) synthesis of a metal-free Pc linker for MOFs. (c) potential R groups to use as metal attachment points.

3.1.1 Synthesis of Phthalocyanines

There are two general methods for the synthesis of peripherally substituted Pcs. One method is to utilize electrophilic aromatic substitution chemistry on existing Pcs (Figure 3.3a).[109] The challenge with this approach is that the low solubility of unfunctionalized Pcs and the number of available substitution sites leads to a complex mixture of products. The second method relies on the tetracyclization reaction to form the Pc (Figure 3.3b).[108, 109] In this method, the substitution pattern on the aryl ring can be synthetically tuned prior to the formation of the Pc. In comparison with the first method, this enhances the solubility of the reagents while also reducing the number of

potential isomers that can be formed. Furthermore, as shown in Figure 3.3b, there are lots of precursors that can be used to directly form the desired Pc or can be converted to other reagents that can directly form Pc. Thus, the synthetic landscape to access the desired product is rich with opportunities. For this method, tetracyclization of phthalonitriles is one of the most common methods. In this synthesis, usually a high boiling alcohol like 1-pentanol is used as the solvent. As shown in Figure 3.4, an excess amount of 1,8-diazabicyclo[5.4.0]undec-7-ene (DBU) is used to deprotonate the alcohol and form the alkoxide (RO^-).[110] The formed alkoxide initiates the cyclization by nucleophilic attack to the phthalonitrile, forming monomeric alkoxyiminoisoindolenine.[111] This isoindolenine goes on a sequence of nucleophilic attacks with phthalonitrile molecules to make dimeric, and trimeric indolenine intermediates. Tetrameric indolenine can form by either the attack of a trimeric intermediate to a phthalonitrile molecule or by self-condensation of two dimeric indolenine. Finally, the tetrameric intermediate goes through a nucleophilic attack of the imide group to the aryl ether, which necessitates a two-electron reduction reaction of the ring upon ring-cyclization to yield 18π electron Pc and formation of aldehyde (from the leaving ether) as the oxidation product. In the presence of a metal ion, coordination by the indole nitrogen at any time can lead to a desirable template effect that brings the reactants in close contact with each other in the right orientation to form a metalated phthalocyanine (metallophthalocyanine, MPc).[112]

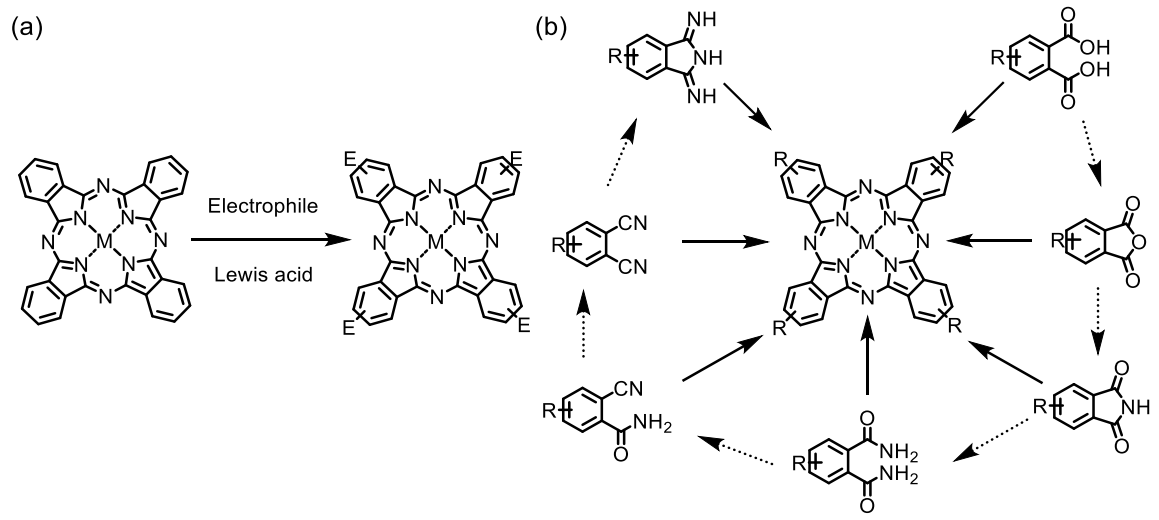

Figure 3.3 different routes to the synthesis of substituted phthalocyanine. (a) Electrophilic aromatic substitution (b) Tetracyclization.

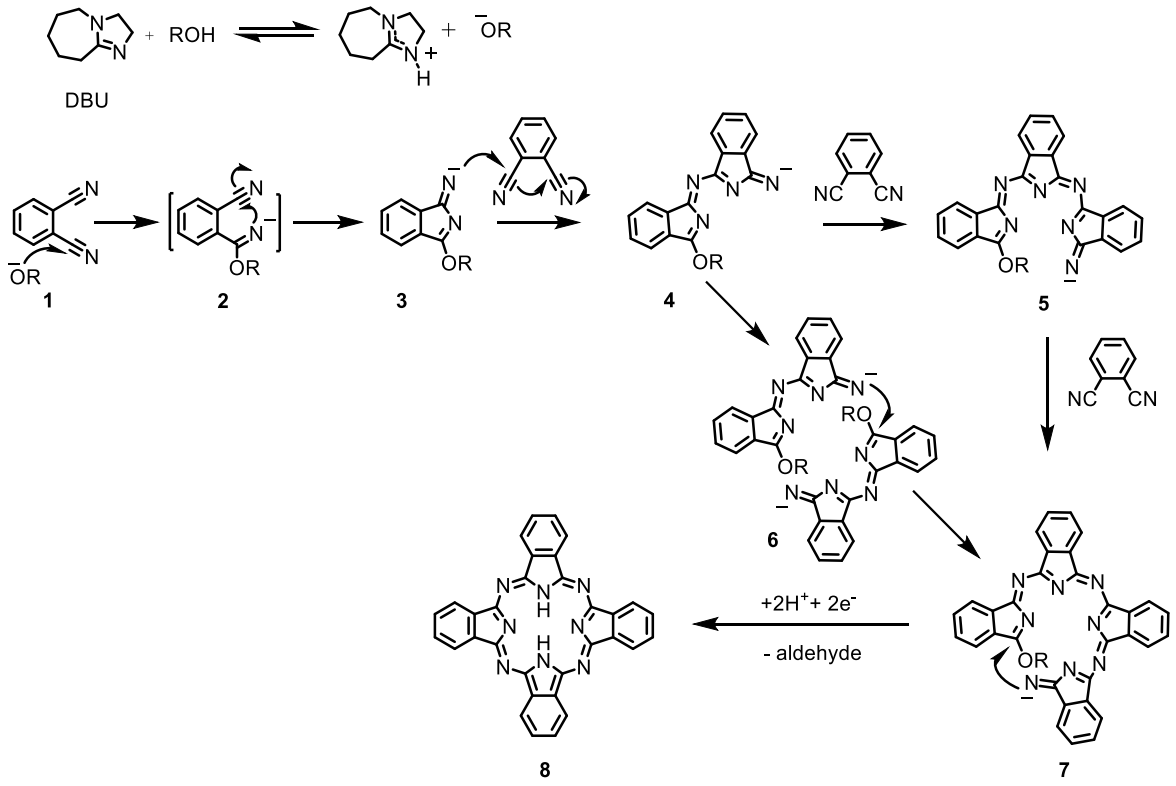

Figure 3.4 Mechanism of the formation of metal-free and metalated (not shown) phthalocyanine from phthalonitrile. The addition of a metal cation can lead to a template effect from molecule **3** onward.

Although the cyclization reaction is the preferred method for producing Pc/MPc, it can still form a mixture of isomers (Figure 3.5). However, compared with the electrophilic substitution that leads to 16 positions for substitution with only a limited number of accessible substituents, the cyclization reaction offers more diversity with fewer isomers. If the precursor of the cyclization reaction is symmetrically substituted, then the tetracyclization reaction provides synthetic flexibility to make a single isomer. With a focus on MOF ligands, the tetracyclization of nitriles, where the isoindole ring contains one carboxylic acid for MOF formation, can lead to four potential isomers. In principle, linkers with D_{4h} and D_{2h} symmetry (Figure 3.5) have the potential to form MOFs due to their higher symmetry, but the other two isomers are likely not ideal for MOF synthesis. This requires the separation of the low-solubility isomers, and the formation of wasteful undesired products.

With the different methods for the synthesis of substituted phthalocyanine identified, we turn our attention to making a phthalonitrile that has the necessary features for MOF chemistry without the possibility for isomers.

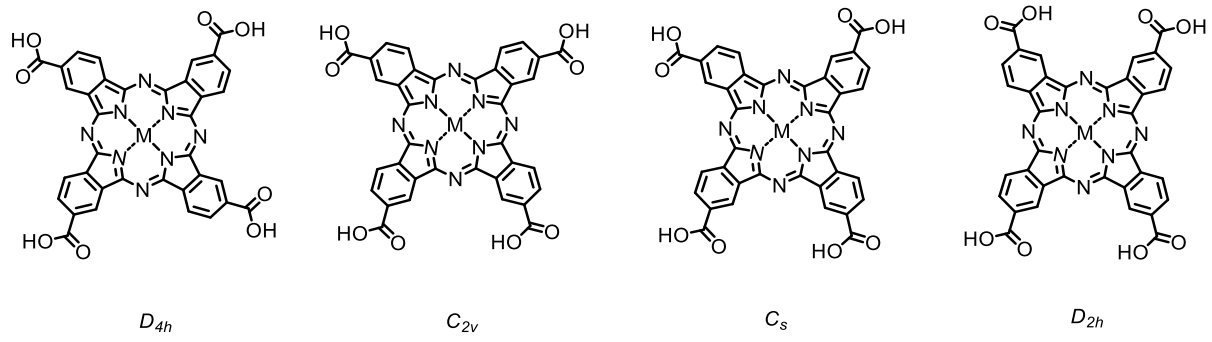

Figure 3.5 Isomeric mixture in the synthesis of tetrasubstituted carboxylate phthalocyanine from cyclization reaction.

3.1.2 Design of the target linker

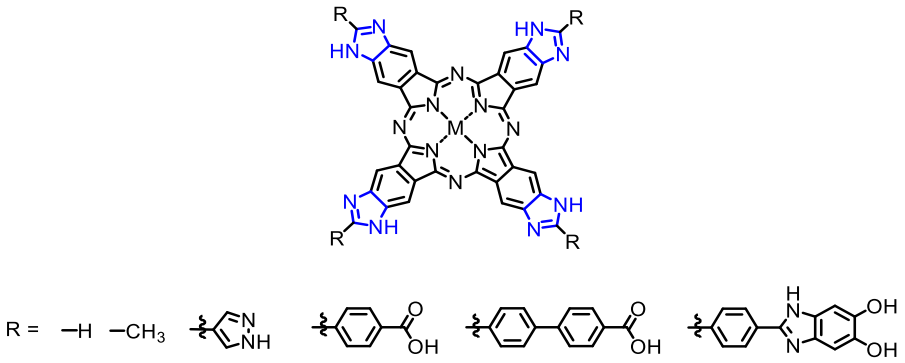

Figure 3.6 Phthalocyanine ligand with symmetrical R substituted. Examples of R groups are presented but are not limited to these groups.

To circumvent the mentioned problems associated with the phthalocyanine linker, we need the product of the cyclization reaction to not only make one Pc/MPc with symmetric carboxylic acid distribution but to also allow for synthetic modification to make longer linkers, or linkers with additional functionality; this enables future development of the field of PcMOFs by enabling the tailorability of the linker. To achieve this, we chose a linker where the structure of the substituted Pc ligand would have a five-membered ring fused to the indole ring of the Pc. Five membered heterocyclic rings (e.g., pyrrole, indole, thiophene, and imidazole) would result in a symmetric Pc that would not yield isomers. Ultimately, imidazole (Figure 3.6) was chosen for this work as it is synthetically more amendable for the desirable chemistry by enabling the central carbon to be modified to introduce carboxylic acids or even left unfunctionalized to make imidazolate-based MOFs. If left unfunctionalized for metal coordination, the R group (Figure 3.6) can be used to introduce functionality to the pore of the MOF. If functionalized with the focus of installing a carboxylic acid-containing group in the R position, then the imidazole nitrogens can be further functionalized, even post MOF formation, to introduce functional groups to the pore.

The present chapter will explore the synthesis and purification pathways to the formation of the Pc core in Figure 3.6. The particular focus will be on the design and synthesis of two families of Pc linkers. The first family occurs when R = H. In this case, the metal nodes of the MOF can only be coordinated via the imidazole nitrogens. Imidazole-based MOFs have been well-explored with simple imidazoles (i.e., imidazole, nitroimidazole, methyl imidazole), but complex imidazoles such as Pc-imidazole (Figure 3.6 where R = H) have not been explored. MOFs that rely on imidazoles as the metal connection points are known as zeolitic-imidazolate frameworks (ZIFs) due to the similar M-imidazole-M bond angles (145°) to that of M-O-M angle in zeolites (where M is the metal ion).[113, 114] In the second family of MOFs, the R group will be a benzoic acid (R = -C_6H_4COOH). In this family of MOFs, the carboxylic acid can coordinate to the metal ion. For this to work, the chosen metal has to prefer to bind to oxygen donor groups rather than nitrogen donor groups.

3.2 Results and discussion

3.2.1 General synthesis route to the Pc ligands

Figure 3.7 gives a general scheme of the routes that were explored for the synthesis of Pc ligands in this thesis. As it is shown in this figure, two pathways (pathway **A** and pathway **B**) were explored to reach **3-3**. Pathway **A** first focuses on the synthesis that results in the desired imidazole and subsequently introducing the necessary cyanide groups that would be necessary to form the desired Pc. The advantage of this method is that the synthetic work to form the desired imidazole can be explored at the start, and once the reaction conditions are optimized, the cyanide groups can be installed via existing chemistry. This also opens up the potential to focus on some of the other precursors outlined in Figure 3.3b. The disadvantage is that the cyanation reaction condition is harsh, which may result in a low yield. Pathway **B**, on the other hand, aims to first make

4,5-diaminophthalonitrile (**3-2**) and subsequently introduce the necessary imidazole. The advantage here is that once **3-2** is formed, it can be used to introduce many different imidazole substitutions without having to go through the cumbersome cyanation reaction and workup.

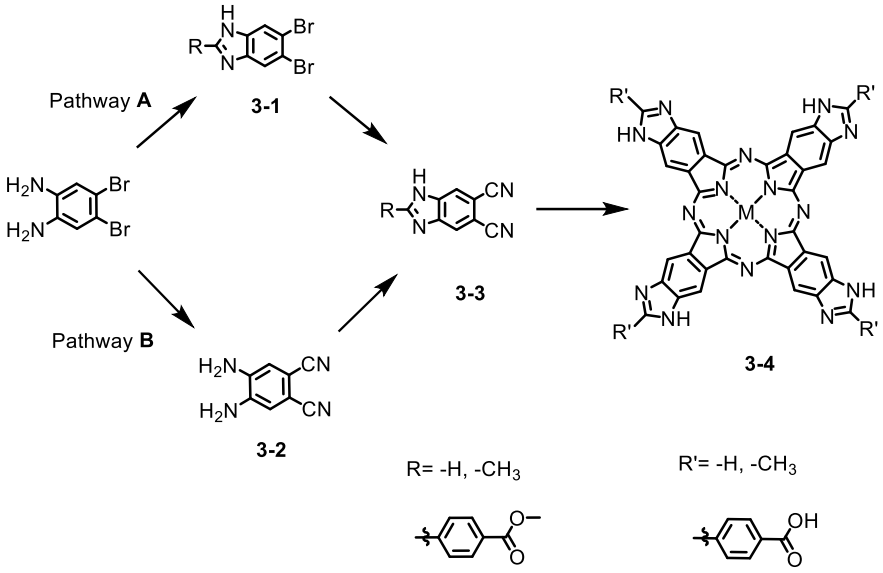

Figure 3.7 General synthesis route to phthalocyanine ligand with symmetric coordination sites.

In brief, after many attempts for the synthesis of **3-3** using pathway **A**, the difficulties associated with the extraction of **3-3**, and the low purification yield, pathway **A** was eventually abandoned. While disappointing, the chemistry that was learned in pathway **A** was directly amendable in pathway **B.** Pathway **B** resulted in the formation of **3-3** that was easier to extract from the reaction mixture in a shorter time with a higher yield. Finally, phthalocyanine linker **3-4** was synthesized from cyclotetramerization of **3-3**. The following sections will discuss details of each pathway and the synthesis of **3-4** from **3-3**.

3.2.2 Synthesis of benzimidazophthalonitriles using pathway A

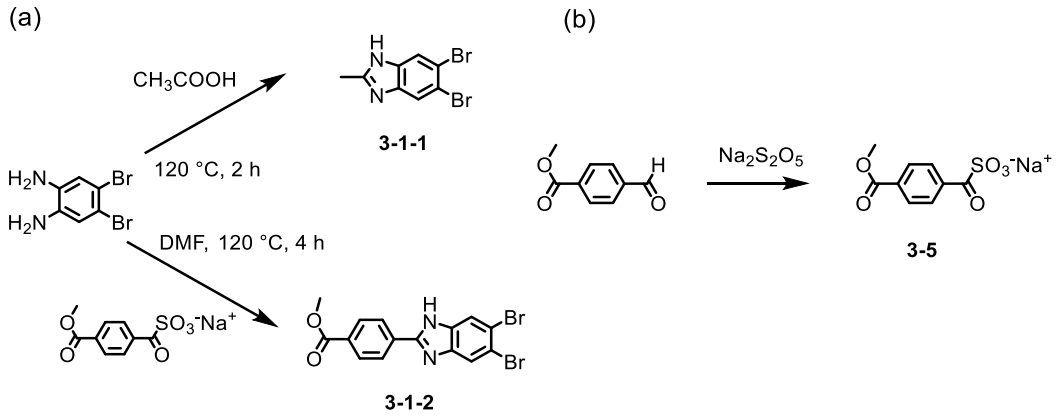

Figure 3.8 (a) Synthesis of benzimidazole derivatives (b) synthesis of the bisulfite adduct.

As discussed in the previous sections, benzimidazole derivatives are good candidates as precursors for the synthesis of symmetrical Pc ligands. Since we were aiming to make two families of Pc ligands, one with imidazole group and the other one with carboxylate group as the node-ligating moieties, we needed to make two kinds of benzimidazole precursors. With the commercially available 4,5-dibromobenzene-1,2-diamine and well-known synthetic procedures, we synthesized **3-1-1** and **3-1-2** (Figure 3.8a). Details of the synthesis of each are discussed accordingly.

3.2.2.1 Synthesis of 3-1-1

Condensation of *o*-phenylenediamine or its derivatives with aldehydes or carboxylic acids is among the most common method in the synthesis of benzimidazoles.[115, 116] Here we synthesized **3-1-1** with 77% yield through a condensation reaction between 4,5-dibromobenzene-1,2-diamine and glacial acetic acid, which acts as both solvent and reagent. This reaction was complete in 2 h at 120 °C as reported for these condensation reactions. To work up the reaction, the contents of the reaction were poured into dichloromethane. Subsequently, a 0.5 M aqueous solution of $NaHCO_3$ was added to the mixture and stirred to neutralize the excess acetic acid. The product was extracted with dichloromethane resulting in a yellow-orange powder obtained in a 77% yield. The

product was characterized by ^{1}H-NMR (Figure 3.9). The NMR of **3-1-1** is consistent with what we would expect. A new resonance at 2.48 ppm is consistent with the formation of a methyl imidazole, the aromatic protons are deshielded as would be expected, and a broad resonance at 12.48 ppm is present for the N-H proton of the imidazole.

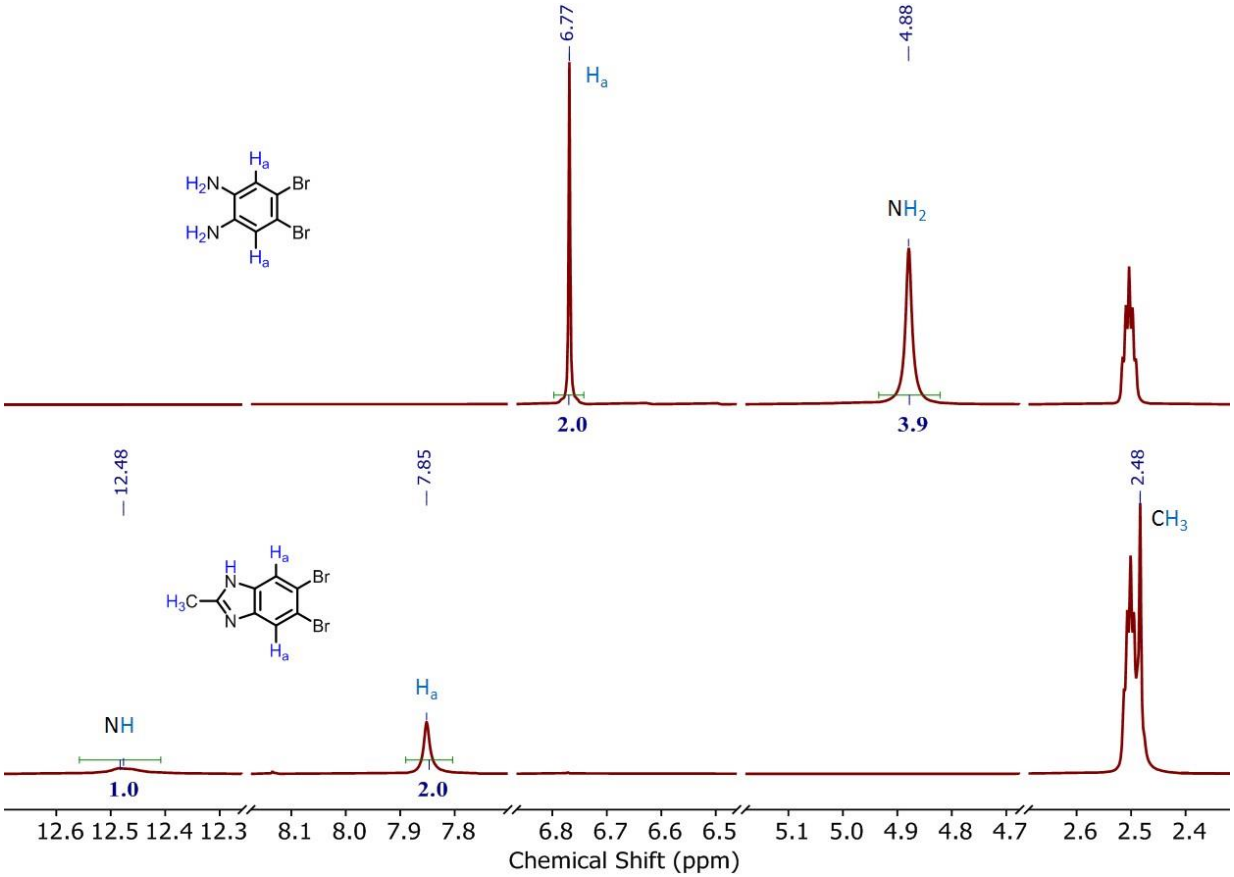

Figure 3.9 ^{1}H-NMR (300 MHz, DMSO-d_6) of **3-1-1** (bottom) and comparison with starting material (top). The peak at 2.50 ppm is due to the solvent residual peak.

3.2.2.2 Synthesis of 3-1-2

In contrast with **3-1-1**, which was a simple condensation reaction between a carboxylic acid and *o*-phenylenediamine, the condensation reaction between aldehydes needs to be carried out under oxidative conditions and often require bubbling air (oxygen) or using copper(II) acetate as an oxidant.[115-117] While these methods are efficient, the separation of the reduced copper species from

a coordinating imidazole or the experimental setup for bubbling air is unnecessarily challenging or cumbersome. Instead of these methods, we utilized a previously reported method that produces a stable bisulfite (**3-5** in Figure 3.8b).[118-121] The bisulfite can be easily formed from the appropriate aldehyde. Thus, as long as the desired aldehyde can be synthesized, then it is expected that the desired bisulfite can be utilized for this chemistry. This enables the researcher to easily introduce other aldehydes into the MOF-linker-synthesis manifold.

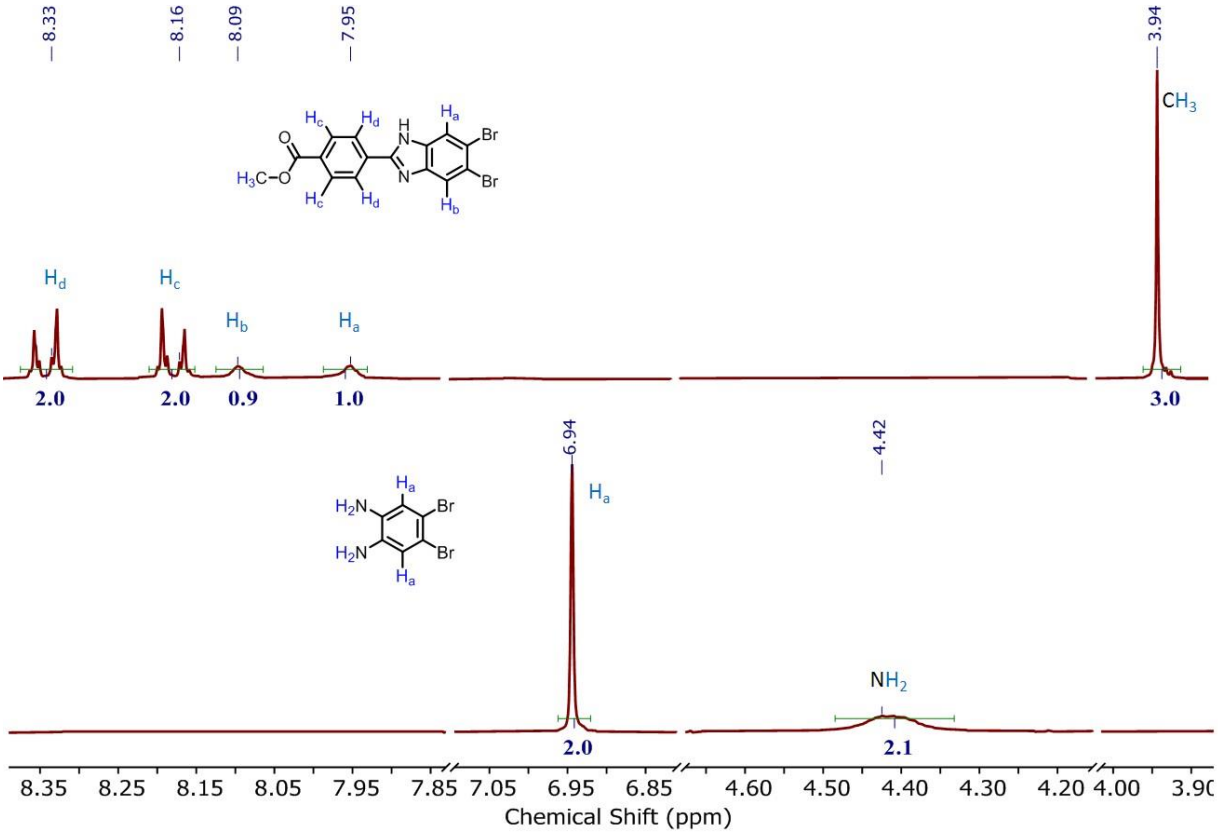

Figure 3.10 ^{1}H-NMR (300 MHz, acetone-d_6) of **3-1-2** (top) and comparison with the starting material (bottom).

Preparation of the bisulfite adduct (**3-5**) from methyl 4-formylbenzoate was done at room temperature in high yield (94%) via the reaction between an ethanolic solution of methyl-4-formylbenzoate and an aqueous solution of sodium metabisulfite (Figure 3.8b). The reaction forms an immediate precipitate that can be easily isolated by filtration; the product was

not characterized due to its limited solubility in common NMR solvents. With the **3-5** in hand, we synthesized **3-1-2** by reacting **3-5** and 4,5-dibromobenzene-1,2-diamine in DMF at 120 °C with stirring for 4 h. The product was precipitated via the addition of water to the cold solution. The product was filtered and washed with water and ethanol to produce a pale-yellow solid with a 71% yield. The resultant product was characterized by ^{1}H-NMR shown in Figure 3.10.

Figure 3.10 shows the stacked ^{1}H-NMR of the purified product **3-1-2** and starting material in deuterated acetone. It is clear from the comparison that the product of the reaction is not simply unreacted starting material. In acetone, H_a and H_b peaks are broad but resolved from those of H_c and H_d; the integration gives the expected integration of **3-1-2**. We further explored the ^{1}H-NMR of **3-1-2** in DMSO-d_6 that is shown in Figure 3.11 (bottom). This spectrum shows integration of the product peaks yields the 10 protons, but the aryl region is difficult to interpret. In the aryl region, we see three regions. For H_c and H_d protons, we expect an AB NMR spectrum of doublets. However, the less shielded protons at 8.13 ppm integrate to 3 rather than 2 and do not produce the expected AB spectrum. Meanwhile, the proton on the benzimidazole portion (H_a and H_b) integrates to one proton rather than two. This suggests that the two benzimidazole protons are chemically inequivalent, with one of the two protons coincidently overlapping with the 8.13 ppm peak of the AB spectrum for H_c and H_d. This observation is comparable to the ^{1}H-NMR spectrum of **3-1-2** in deuterated acetone (top spectrum in Figure 3.11), where two broad peaks associated with H_a and H_b at 7.95 and 8.09 ppm are observed, but the AB spectrum for H_c and H_d is reserved. To further explore this, we repeated the ^{1}H-NMR with a drop of D_2SO_4 to enable the rapid exchange of the N-H protons. As shown in the middle stack of the spectrum, H_a and H_b protons coalesce into a single sharp peak at 8.32 ppm downfield relative to the acid-free spectrum. Furthermore, the AB

spectrum of the benzoic acid component is restored. Therefore, these ^{1}H-NMR spectrum verify the formation of **3-1-2**. Thus, we turned our attention to the dinitrilation of these two compounds.

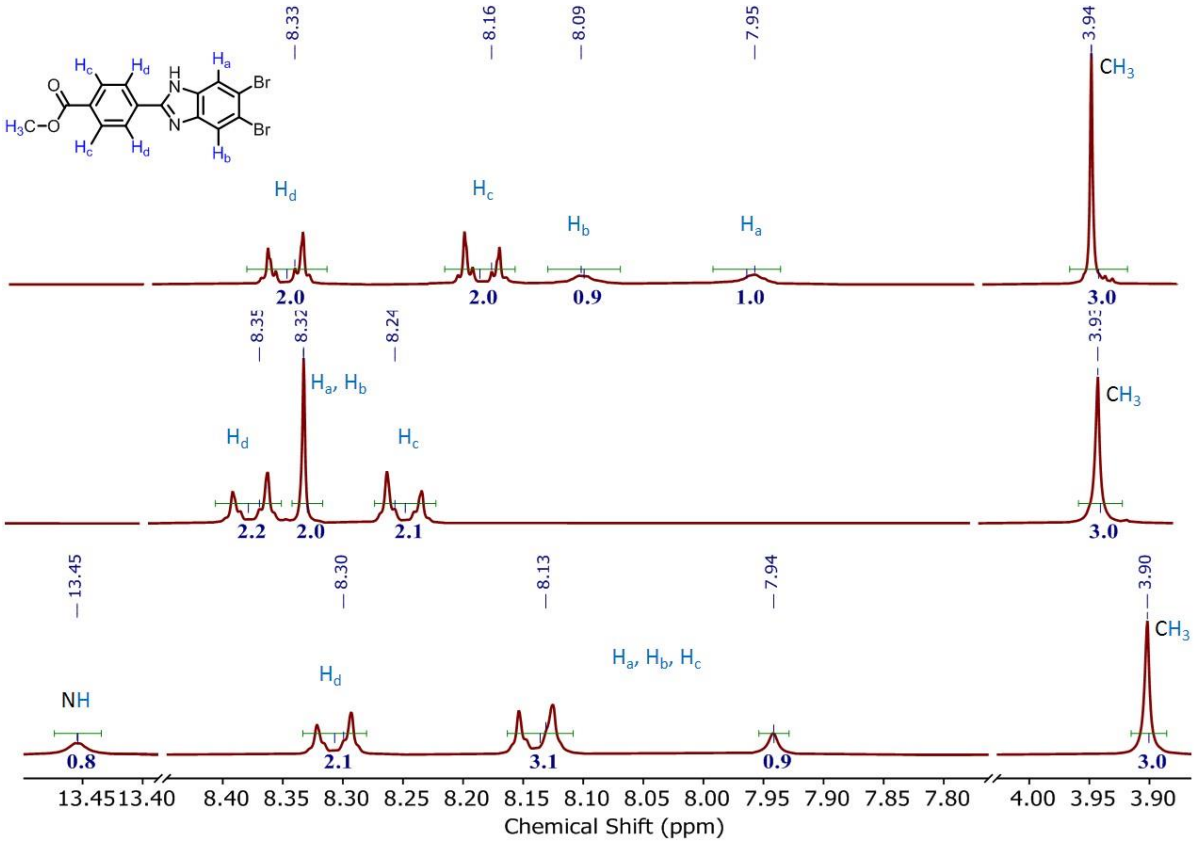

Figure 3.11 ^{1}H-NMR (300 MHz) of **3-1-2** in acetone-d_6 (top), DMSO-d_6+one drop D_2SO_4 (middle), and in DMSO-d_6 (bottom). H_c and H_b overlap at 8.13 ppm in the bottom spectrum.

3.2.2.3 Nitrilation reaction

For the synthesis of Pc with the method shown in Figure 3.7, we need a phthalonitrile derivative as our precursor (**3-3** in Figure 3.7). One of the most common methods to produce a phthalonitrile is via the Rosenmund-Von Braun reaction.[122, 123] Under the conventional reaction conditions, CuCN and a high boiling polar solvent such as DMF is usually used to convert dibromobenzene derivatives to phthalonitrile derivatives. Encouraged by Onal *et al.* work,[124] who reported on the synthesis of benzimadzophthanitriles from the dibromo-derivatives of this compound, we

investigated this reaction for the synthesis of **3-3-1** and **3-3-2** from **3-1-1** and **3-1-2**, respectively (Figure 3.12). We will discuss each of these reactions with further details accordingly.

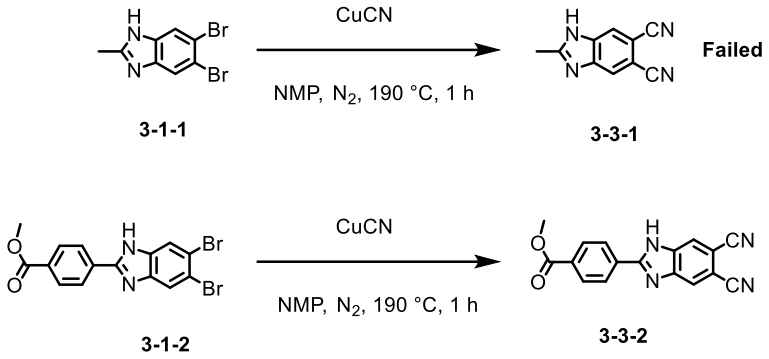

Figure 3.12 Nitrilation reaction on dibromobenzimidazole derivatives.

Onal *et al.* used microwave irradiation for converting dibromobenzimidazoles to benzimidazophthalonitries instead of direct heating,[124] which is conventionally employed in the Rosenmund-Von Braun reaction. They claimed that Rosenmund-Von Braun reaction fails under conventional conditions, as reported by others too,[123] but when microwave is used, the desired product is obtainable. Despite this report, we aimed to explore the dinitrilation reaction on **3-1-1** and **3-1-2** using conventional heating, but under other conditions similar to those reported by Onal *et al.* Unfortunately, the reaction for making **3-3-1** failed under these conditions. Following the reaction by TLC showed that the starting material was fully consumed, but no sign of product formation was observed in the ^{1}H-NMR. The ^{1}H-NMR indicated a complex mixture of materials formed.

Apart from the work by Onal *et al.*, which is the only report on the dinitrialtion of benzimidazole derivatives that are not substituted on the nitrogen atom, the literature is not rich when it comes to Rosenmund-Von Braun reaction on molecules bearing benzimidaloe. Pardo *et al.* reported that the synthesis of 1*H*-benzimidazole-5,6-dicarbonitrile (**B** in Figure 3.13) from 5,6-dibromo-1*H*-benzimidazole **A** fails.[123] Instead, the mono-nitrilated product,

5-bromo-1*H*-benzimidazole-6-carbonitrile, **C**, was isolated in 70% yield. No explanation is provided on why dinitrilation of **A** is not possible. Interestingly, the authors reported that dinitrilation was successful, with 57% yield, when *N*-substituted compound **D** is used instead of **A**.

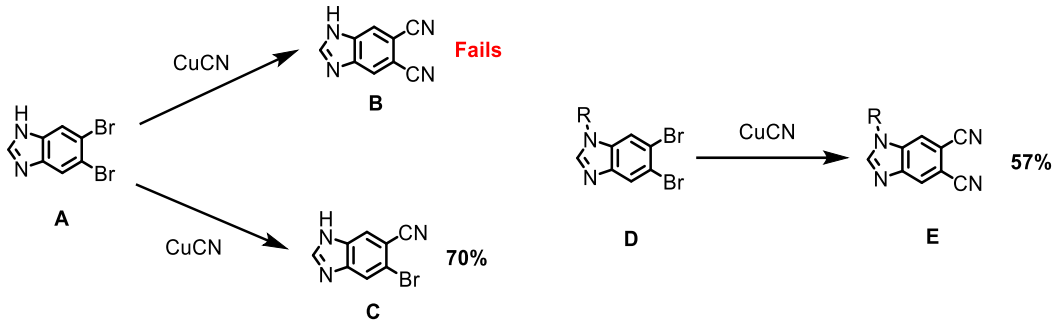

Figure 3.13 Some of the nitrilation reactions reported in reference 123 on dibromo benzimidazoles.

Interestingly, our initial reactions on the dinitrilation of **3-1-2** gave a small amount of **3-3-2** that was just enough for characterization by ^{1}H-NMR. ^{1}H-NMR (top spectrum in Figure 3.14) shows that the H_a protons peak were shifted downfield with respect to the parent material with considerably less shifting of H_b and H_c (as expected). This indicated that the extracted solid was the desired product **3-3-2**; however, the yield was negligible. We used the original workup procedure reported by Onal *et al.* to separate the product. This workup involves treating the crude product mixture with 16% ammonia solution for 3 h, filtering, and then extracting the solid with dichloromethane using Soxhlet overnight. Either the synthetic pathway or the workup was insufficient as only a few milligrams, just enough for ^{1}H-NMR analysis could be obtained. Attempts to improve the workup by using different solvents for the Soxhlet and extracting for longer times improved the yield to 13% (acetone for 15 h) and ultimately 25% (acetone for 48 h). The yield was deemed too low for the success of the project, but the ^{1}H-NMR proved that the extracted solid is **3-3-2**. Therefore, this synthesis shows that despite the negative

reports, it is possible to do dinitrilation with Rosenmund-Von Braun reaction on at least some benzimidazole derivatives with conventional heating, but the bottleneck might be the workup/extraction of the product. However, for our purpose of the synthesis of large quantities of Pc ligands, we needed higher yields and reproducible results from the dinitrilation reaction (synthesis of **3-3-1** failed while the maximum yield for **3-3-2** was 25% in 18 tries). Therefore, we shifted from pathway **A** to pathway **B** to see if the alternate pathway was more reliable with better yields.

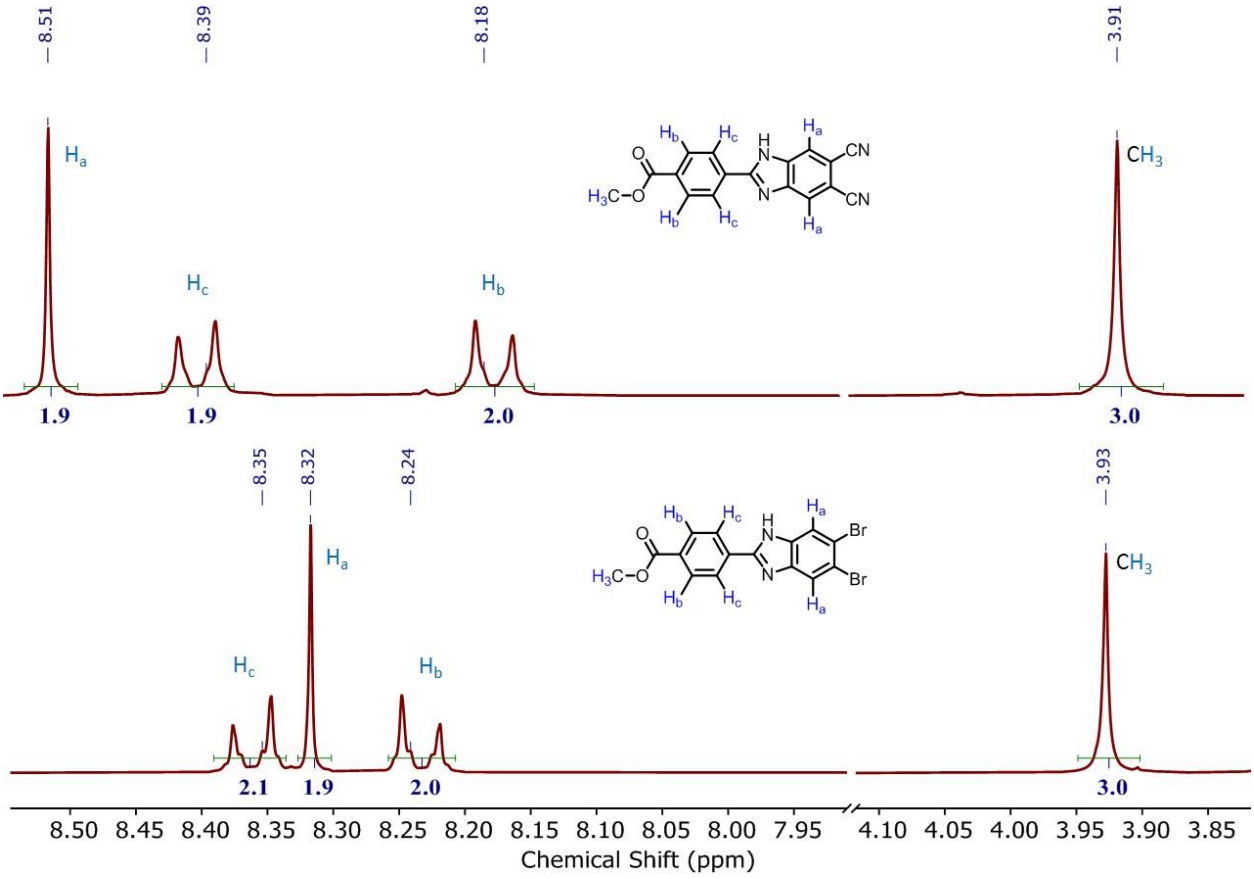

Figure 3.14 ^{1}H-NMR (300 MHz, DMSO-d_6) of **3-3-2** (top) synthesized using pathway **A**, and starting material **3-1-2** (bottom). One drop D_2SO_4 was added to the solvent.

3.2.3 Synthesis of benzimidazophthalonitriles using pathway B

As shown in Figure 3.15, the first step of pathway **B** is the dinitrilation of the parent 4,5-dibromobenzene-1,2-diamine compound to form **3-2**. Given the challenges with the dinitrilation step on dibromo benzimidazoles in pathway **A**, this approach puts the more challenging chemistry as the first step, and once **3-2** is in hand, then the existing chemistry, which was demonstrated to work for pathway **A**, can be applied.

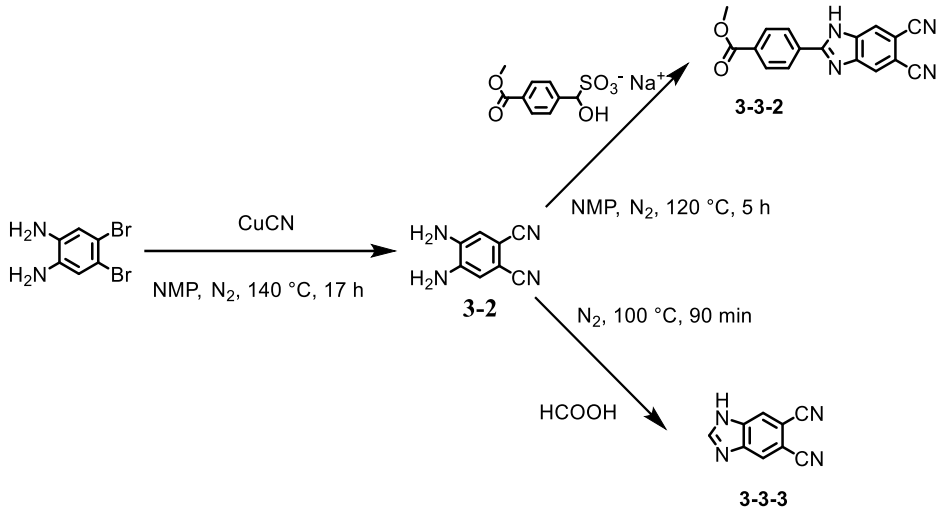

Figure 3.15 Alternative route for the synthesis of benzimidazophthalonitriles.

In our early attempts, Rosenmund-Von Braun reaction on 4,5-dibromobenzene-1,2-diamine was performed in DMF at 140 °C for 15-17 h based on a previously reported method.[125, 126] Workup of the crude product reported by Faust and co-workers requires washing the mixture with 9% ammonia solution to remove the copper ions.[125] The ammonia was necessary as it had to substitute any **3-2** that was acting as a ligand on the copper ions. The reaction for making **3-2** (Figure 3.15) was attempted several times with yields ranging from 4-41%, with the best yield (recrystallized) as high as 25%. This observation is not surprising based on the existing literature for the Rosenmund-Von Braun reaction on 4,5-dibromobenzene-1,2-diamine. One of the challenges that result in the low yield is the long and

tedious workups. The workup requires that the reaction product be poured into a 9% ammonia solution followed by filtering and washing the solid with ammonia until the filtrate is colorless. This is followed by washing the solid with acetone, which dissolves the product and causes additional losses. Given that this first step is key for the success of the project, finding a synthetic methodology that results in a consistent yield is critical.

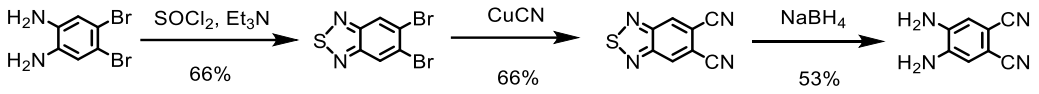

Figure 3.16 Dinitrilation of 4,5-dibromobenzene-1,2-diamine reported by Faust and co-workers in reference 127.

Faust and co-workers report a reliable and consistent 23% total yield over three steps for the dinitrilation of 4,5-dibromobenzene-1,2-diamine (Figure 3.16).[127] Alternatively, Youngblood reported a 55% yield from Rosenmund-Von Braun reaction.[128] In their procedure, the 4,5-diiodobenzene-1,2-diamine is used instead of 4,5-dibromobenzene-1,2-diamine. However, from our experience with the Rosenmund-Von Braun reaction, the limiting factor is the workup of the material rather than the actual chemical transformation (although we can't rule out the improvement of diiodo groups over dibromo groups). Youngblood used ethylenediaminetetraacetic acid trisodium salt (Na_3EDTA) to chelate the copper salts while bubbling oxygen into the reaction to oxidize any copper(I) back to copper(II). Given this, we opted to utilize Youngblood's synthetic pathway on the dibromo staring material. Using *N*-Methyl-2-pyrrolidone (NMP) rather than DMF as the reaction solvent (as in the Youngblood's report) and air (Youngblood used oxygen) to oxidize the copper(I) to copper(II) followed by chelation using Na_3EDTA, we could obtain yields ranging 53-79% (based on six tries). This procedure is consistently better than previous work on the Rosenumnd-Von Braun reaction.[125-127]

Figure 3.17 shows ^{1}H-NMR of **3-2** and a comparison with the starting material indicating the reaction was successful.

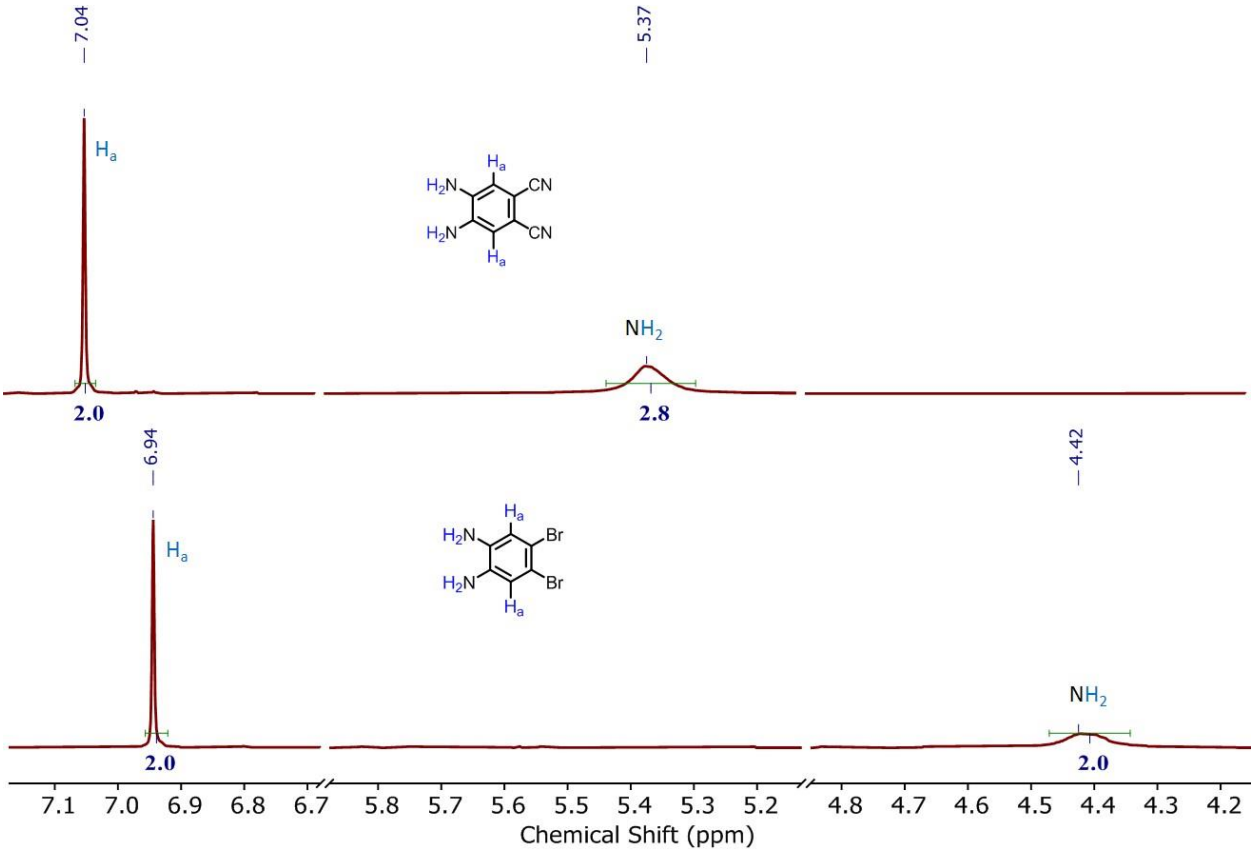

Figure 3.17 ^{1}H-NMR (300 MHz, acetone-d_6) of **3-2** (top) and comparison with starting material (down).

With **3-2** in hand, we were able to synthesize **3-3-2** using the existing chemistry described in section 3.2.2 for the synthesis of **3-1-2**. A workup procedure similar to that of **3-1-2** was performed on the crude product **3-3-2** to give a light-yellow solid. Over 10 tries, a yield of 55-79% was observed for this reaction (Figure 3.15 top). Figure 3.18 shows ^{1}H-NMR of **3-3-2** synthesized using the pathway **B** method. The ^{1}H-NMR spectrum in Figure 3.18 shows the same peaks with the corresponding integrations and chemical shifts as the spectrum obtained from **3-3-2** (Figure 3.14 top spectrum) that was synthesized with pathway **A**. These results show that the synthesis of **3-3-2** in pathway **B** was successful and with a good yield.

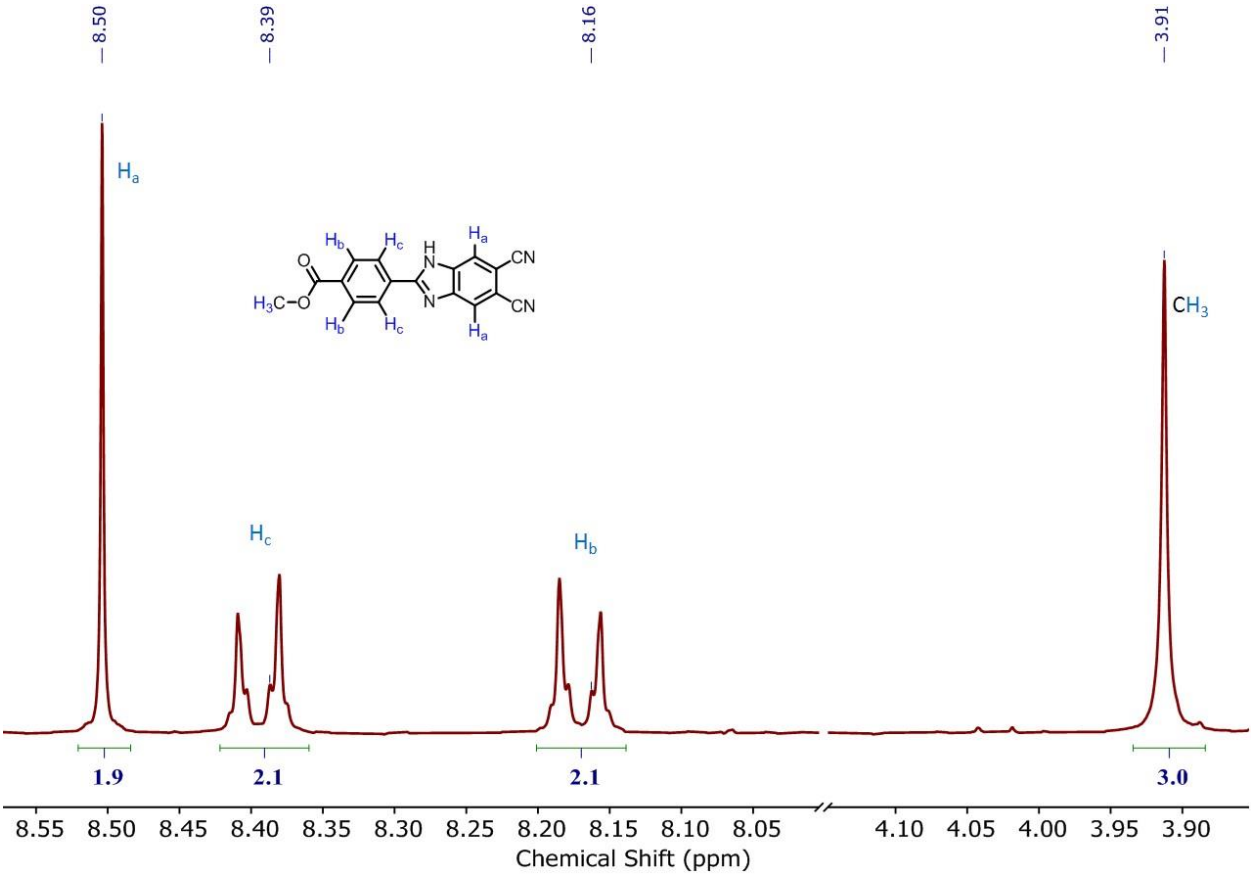

Figure 3.18 ^{1}H-NMR (300 MHz, DMSO-d_6) of **3-3-2** synthesized using pathway **B**. One drop D_2SO_4 was added to the solvent.

3-3-3 was synthesized by the reaction between **3-2** and formic acid that acts as both the reagent and solvent (Figure 3.15 bottom). To workup the crude product, the cold reaction mixture was poured into 0.8 M $NaHCO_3$ solution to neutralize the excess formic acid. This caused the product to precipitate. The resulted suspension was filtered and finally washed with water to give **3-3-3** as a beige solid in 51% yield. Figure 3.19 shows ^{1}H-NMR of **3-3-3**.

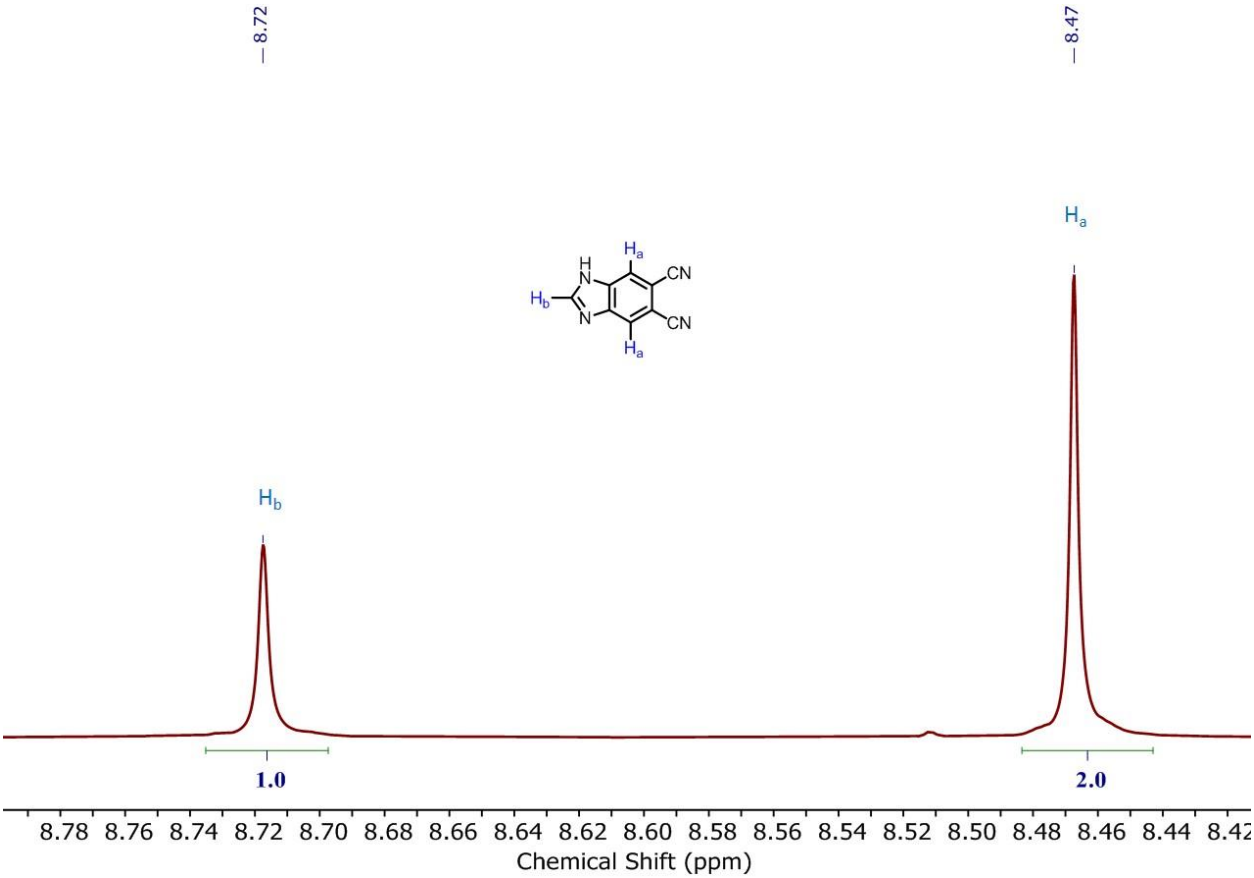

Figure 3.19 ^{1}H-NMR (300 MHz, DMSO-d_6) of **3-3-3**.

3.2.4 Pc synthesis and characterization

With the successful synthesis of **3-3-2** and **3-3-3** in modest yields, we turned our attention to the synthesis of the requisite metalated Pcs. High yields pave the way for the synthesis of **MPcH** and **NiPc2** ligands that belong to the imidazophthalocyanines family (Figure 3.20). However, due to the mentioned difficulties in the synthesis and purification of precursors (**3-2** and **3-3**), there are not many examples of imidazophthalocyanines synthesis.[123, 124, 128-134]

The synthetic pathway used in this work for **MPcH** is shown in Figure 3.20a and involves two steps. The first step is tetracyclization of **3-3-2** to form **MPc1**. The second step is the basic hydrolysis of **MPc1** followed by acidification of the carboxylate salt in the mixture to form carboxylic acid Pc (**MPcH**). Synthesis of **NiPc2**, on the other hand, involves only one step, which

is shown in Figure 3.20b. Here we first discuss the synthesis of **MPc1** and **MPcH** followed by **NiPc2**.

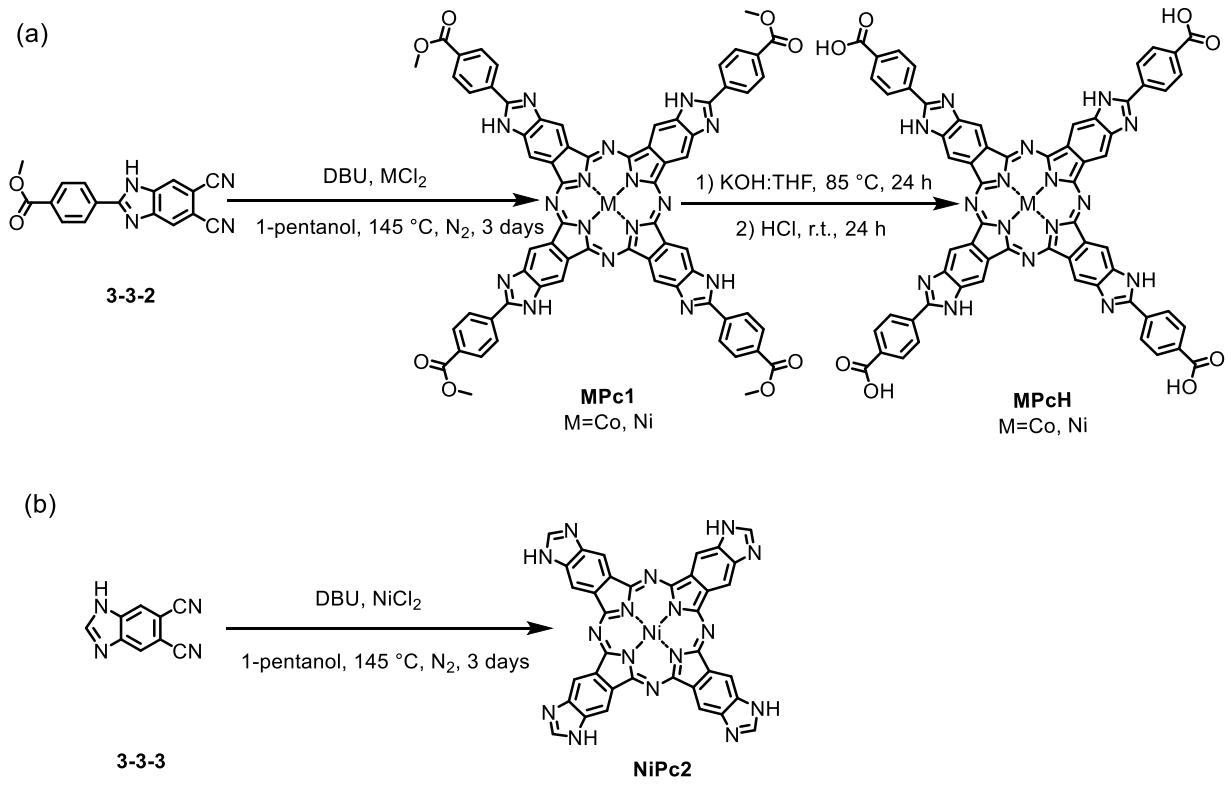

Figure 3.20 Synthesis of imidazophthalocyanine ligands with (a) O-donor in carboxylic acid (b) N-donor in imidazole bearing groups.

3.2.4.1 Synthesis of NiPc1

Our initial tries for the cyclization of **3-3-2** that were carried out in regular 1-pentanol at the presence of $Cu(CH_3COO)_2 \cdot xH_2O$ or $Cu(CH_3COO)_2$ and DBU failed (9 tries, no strong color, indicative of the formation of Pc was observed). Since the role of DBU is the formation of alkoxides in situ, we rationalized that the presence of water in the solvent or in the reagents was the cause of failures. Therefore, the rest of our efforts for the synthesis of Pcs was conducted using freshly dried starting materials (dried in a vacuum oven), anhydrous $NiCl_2$ and $CoCl_2$ (we didn't

use copper salts due to their propensity to be hygroscopic), fresh 1-pentanol, fresh DBU, and preheated glassware that was cooled under a nitrogen gas flow. As a result of these measures, a dark green mixture that is indicative of the formation of a Pc was observed. **NiPc1** formation was observed in the reaction vial after 14 h. To isolate the Pc, we developed a purification procedure for the product by using different organic solvents to remove impurities. This procedure was developed based on trial and error to find a solvent system that could dissolve the impurities. This made the separation of the insoluble product by centrifuging easy. In brief, the product was separated from the reaction mixture by adding DMF to the crude product mixture followed by sonicating the mixture, and then ethyl acetate was added to the solution to precipitate the green product; and then the precipitate was separated by centrifuging. This procedure was repeated until the decanted solution from the centrifuging step was colorless. Finally, the dark green product was washed with hexanes and then with 1M HCl solution (to dissolve any nickel-containing particles). Therefore, under the mentioned reaction conditions, and after purifying the sample by washing with organic solvents, 48-87% yield (10 tries) for **NiPc1** as a shiny black solid was achieved.

UV-Vis spectrum of Pcs is one of their most characteristic features.[124, 128, 129, 135-141] Because of their extended 18 electron π-conjugated system, Pcs have a high molar extinction coefficient (10^5 mol/L. cm) and show strong absorption in the UV (around 300-450 nm) and far-red region (600-750 nm) of the spectrum. These two regions are known as the B- and Q-bands, and the structure of the adsorption peak is telling about the Pc structure. The position of the Q-band depends on various factors such as the central metal in Pc, peripheral substituents, and solvent. The symmetry of the Pc molecule can affect the shape of the Q-band. For example, metal-free Pcs show a split Q-band, while the equivalent metalated Pc appears as a single peak. Peripheral substitution of the Pc macrocycle can also affect the splitting of the Q-band. For instance, if the

metalated Pc macrocycle is asymmetrically substituted, then even the metalated Q-band might also appear as a split peak. Furthermore, aggregation of Pc molecules causes broadening of the Q-band, while isolated Pc molecules result in a sharp Q-band. Aggregation of Pc molecules and the associated effects on the adsorption spectrum occurs from the electronic interactions between rings of Pc molecules, which causes perturbation of the electronic structure. Thus, a lot can be learned from the UV-Vis of Pcs.

UV-Vis spectrum of **NiPc1** measured in chloroform and concentrated sulfuric acid is shown in Figure 3.21. In chloroform (Figure 3.21a), broadening of the Q-band is evident. UV-Vis spectrum of the same compound dissolved in concentrated sulfuric acid (Figure 3.21b) shows a sharp and single Q-band peak. Comparing these two UV-Vis spectra, we can conclude that broadening of the Q-band in chloroform is a result of aggregation. Additionally, observation of a single peak in the Q-band region is indicative of a symmetric and metalated Pc which is expected from the synthesis of **NiPc1**.

Another feature of the acid-dissolved **NiPc1** is that the Q-band shifts to longer wavelength (lower energy). This is a result of the protonation of the *meso*-nitrogens of the porphyrazin ring, as well as the nitrogens of imidazoles. The shift of Q-band to lower energy has been previously reported for imidazophthalocyanins. The molar extinction coefficient for the Q-band calculated from spectrum in Figure 3.21 is 1.1×10^5 mol/L. cm, which is in good agreement with the typical values for Pcs. Therefore, from the UV-Vis investigation, and comparing the spectrum with the most similar Pc molecules in literature,[124] we conclude that the measured spectrum for **NiPc1** is consistent with what would be expected from a pure sample of **NiPc1**. With these results, we are confident that we have a pure material that can be hydrolyzed to make the MOF linker (**NiPcH**).

We will again discuss further characterization of **NiPc1** and other products in Figure 3.20 after discussing the **MPcH** synthesis.

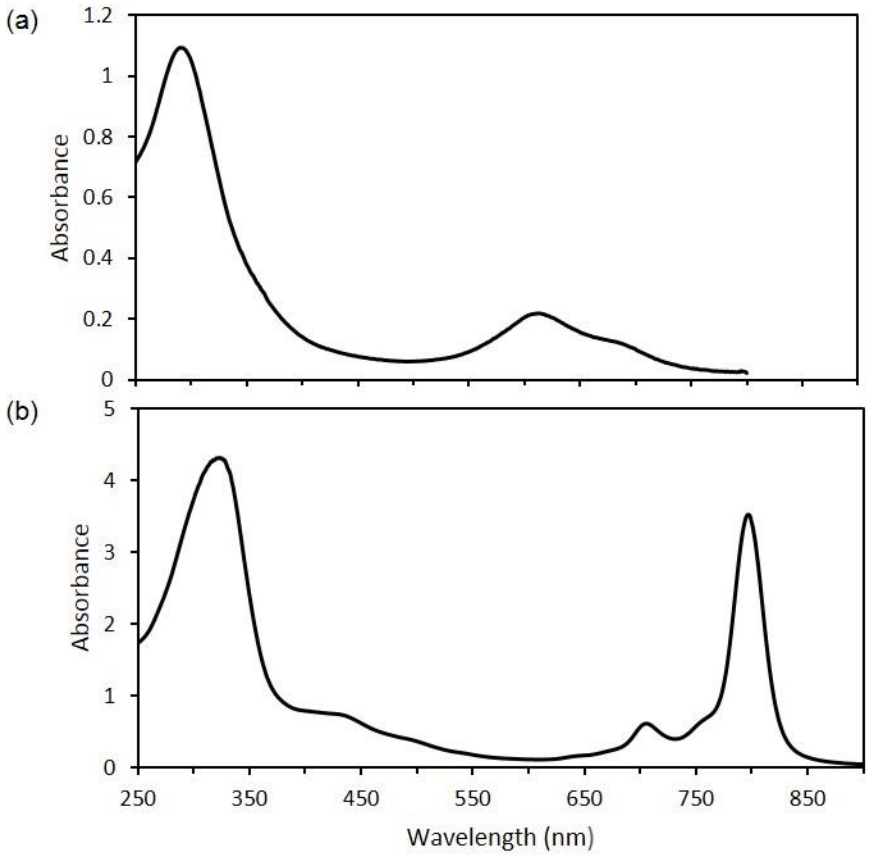

Figure 3.21 UV-Vis spectrum of **NiPc1** in (a) chloroform (b) H_2SO_4.

3.2.4.2 Synthesis of MPcH

Deprotection of **NiPc1** was performed under the mentioned reaction conditions in Figure 3.20. In brief, deprotection was performed in KOH:THF mixture followed by acidification by HCl to make **NiPcH**. We used our slightly modified washing protocol for **NiPc1** to separate and purify **NiPcH** from the reaction mixture. As such, we obtained **NiPcH** as a shiny black solid with 33-41% yield (8 tries).

Given the washing protocol we developed for the separation and purification of **MPc1** and **MPcH** is long and identical, subsequent synthesis of **MPcH** occurred with deprotection of the

crude **MPc1**. This synthesis was done by adding KOH:THF mixture to the reaction mixture from the first step (Figure 3.20a) and heating under reflux for 24 h followed by introducing excess HCl solution to the flask and stirring at room temperature for 24 h. As such, the overall yield for one-pot synthesis of **NiPcH** was 38-61% (three tries). Therefore, the one-pot method resulted in **NiPcH** with a higher yield (minimum 38%) with considerably less workup compared with the two-pot synthesis that resulted in a maximum 36% yield and significantly longer workup. To synthesis **CoPcH**, we used the one-pot synthesis procedure as that of **NiPcH** (but with $CoCl_2$ instead of $NiCl_2$) and the same purification protocol that resulted in **CoPcH** as a black solid with 26% yield (one try).

3.2.4.3 Synthesis of NiPc2

Synthesis of **NiPc2** involves only one step. This reaction goes through the same reaction conditions as that of **NiPc1** (Figure 3.20b), and the green color was observed after 22 h in the reaction flask that is an early indication of the formation of a Pc. During the wash procedure using our protocol, we noticed that **NiPc2** had lower solubility in DMF than other Pcs in this thesis; this led to a faster workup. In brief, DMF was added to the crude reaction mixture, followed by adding hexanes, centrifuging, and decanting. The dark green solid was washed with acetone and treated with 1 M HCl to dissolve the remaining nickel/nickel compound particles. However, we noticed that the solid was completely dissolved in 1 M HCl after 1 h of stirring to give a dark green solution. We rationalized that because **NiPc2** can protonate through the four imidazole nitrogens and it is a smaller molecule than **NiPc1**, the resulted charged molecule made **NiPc2** soluble dissolved in 1 M HCl while **NiPc1** was insoluble under the same conditions. The green solution was neutralized

with KOH solution to precipitate a green solid. Ultimately, **NiPc2** was obtained as a black solid with 73% yield.

3.2.4.4 FTIR analysis of NiPc1 and NiPcH

Perhaps unsurprising, despite all our efforts, we couldn't characterize **MPc1** and **MPcH** with ^{1}H-NMR. We tried to use both NMR 300 MHz and NMR 500 MHz, different solvents ($CDCl_3$, acetone-d_6, and DMSO-d_6), add a few drops of pyridine (to prevent aggregation), and adding drops of D_2SO_4, but none of these measures could help to acquire a sensible ^{1}H-NMR spectrum. This issue has been previously reported by Onal *et al.* for the structurally similar tetraimidazophthalocyaniens.[124] We attribute this to the aggregation and the low solubility of tetraimidazophthalocyanines.[141] This is likely one of the primary reasons why this class of Pcs have received considerably less attention in the literature. The only reports of ^{1}H-NMR for tetraimidazoPcs that have the closest similarity to **NiPc1** are for diamagnetic Zn, Mg, and free base tetraimidazoPcs with either propyl *N*-substituted imidazoles or pentyl substituted on the imidazole carbon.[123, 128, 131] In all these cases, it is the role of substituents and the central metal atom that increase the solubility, reduce the aggregation, and make observing the ^{1}H-NMR spectrum possible.

In order to obtain more details about the structure of the synthesized Pc, characterization of **NiPc1** was further carried out with attenuated total reflectance-Fourier transform infrared (ATR-FTIR) spectroscopy. We used FTIR primarily to identify if all of the methyl carboxylate ester groups in **NiPc1** are hydrolyzed to carboxylic acid groups in **NiPcH**. This characterization is important, because for the synthesis of PcMOFs, the Pc linker should have four carboxylic acids to form the desired MOF structure (similar to tetracarboxyl porphyrinic MOFs). Therefore, it is critical to develop a characteristic method to precisely identify a fully deprotected Pc before using

the synthesized material in MOF synthesis. ATR-FTIR spectrum of **NiPc1**, **NiPcH**, and a sample of partially deprotected (partially hydrolyzed to carboxylic acid) are shown in Figure 3.22. In the ATR-FTIR spectrum of **NiPc1** (the blue spectrum), we observed one band assigned to the C=O stretching at 1710 cm^{-1}, and two bands for the C-O stretching; one at 1269 cm^{-1} for the C-O of the carboxylate, and the other one at 1105 cm^{-1} for the C-O of the methoxy group. Additionally, stretching vibrations of sp^3 hybridized C-H from the methyl group of the ester are clearly showing in the 2850-2953 cm^{-1} region. Comparing the spectrum of **NiPc1** with **NiPcH** (green spectrum in Figure 3.22), the most obvious difference between these two are the absence of C-H bands in the 2850-2953 cm^{-1} region and the absence of the C-O band at 1269 and 1105 cm^{-1} in **NiPcH** spectrum. In a sample that is partially deprotected (partially hydrolyzed to acid, red spectrum in Figure 3.22), sp^3 C-H stretching in the 2850-2953 cm^{-1} region, and C-O stretching at 1269 cm^{-1} are still observed. Therefore, this sample (and any sample with these diagnostic peaks) is not appropriate to be used for MOF synthesis. Another feature that can be elucidated by comparing the ATR-FTIR spectra in Figure 3.22 is a slight shift of the C=O stretching from 1710 cm^{-1} in **NiPc1**, which contains an ester, to 1695 cm^{-1} in **NiPcH**, which contains a carboxylic acid, and a shift of the C-O stretching from 1269 cm^{-1} in **NiPc1** to 1223 cm^{-1} in **NiPcH**. This shift is expected for carboxylic acids compared with esters.

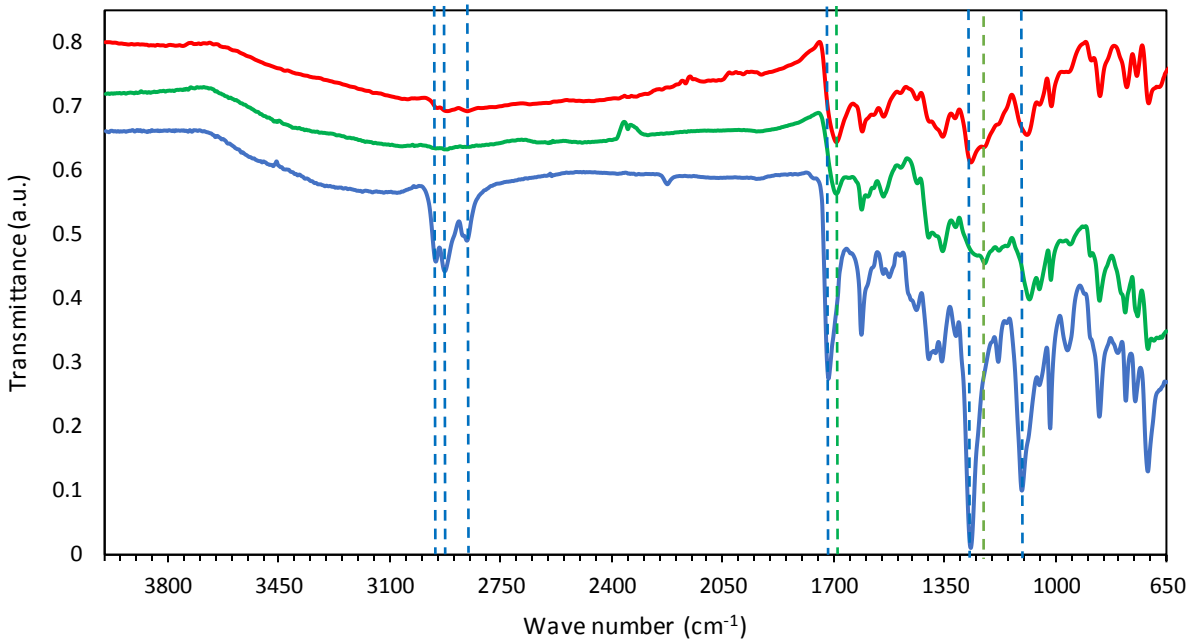

Figure 3.22 ATR-FTIR spectrum of **NiPc1** (blue), **NiPcH** (green), and partially hydrolyzed sample (red). The marked regions show 2850-2953, 1710, 1695, 1269, 1223, and 1105 cm^{-1}.

3.2.4.5 Mass spectrometry analysis of MPcH, and NiPc2

In this thesis, electrospray ionization mass spectrometry (ESI-MS) and laser desorption mass spectrometry (LD-MS) was performed on **MPc1**, **MPcH**, and **NiPc2**. Mass spectrum of **NiPcH** (Figure 3.23) was measured using laser desorption as ionization source (no matrix used) in positive mode. For **NiPcH** an exact mass of 1210.2 is expected (neutral species). As such, the signal at m/z = 1210.0 is due to the molecular ion $[M^{\bullet}]^{+}$. What is interesting in the mass spectrum shown in Figure 3.23 is that we were able to observe successive fragmentation of the carboxylic acid groups. The signals at 1166.0, 1123.0, 1077.9, and 1033.9 were correlated to the loss of one, two, three, and four carboxylic acids from **NiPcH** molecule, respectively (Table3.1).

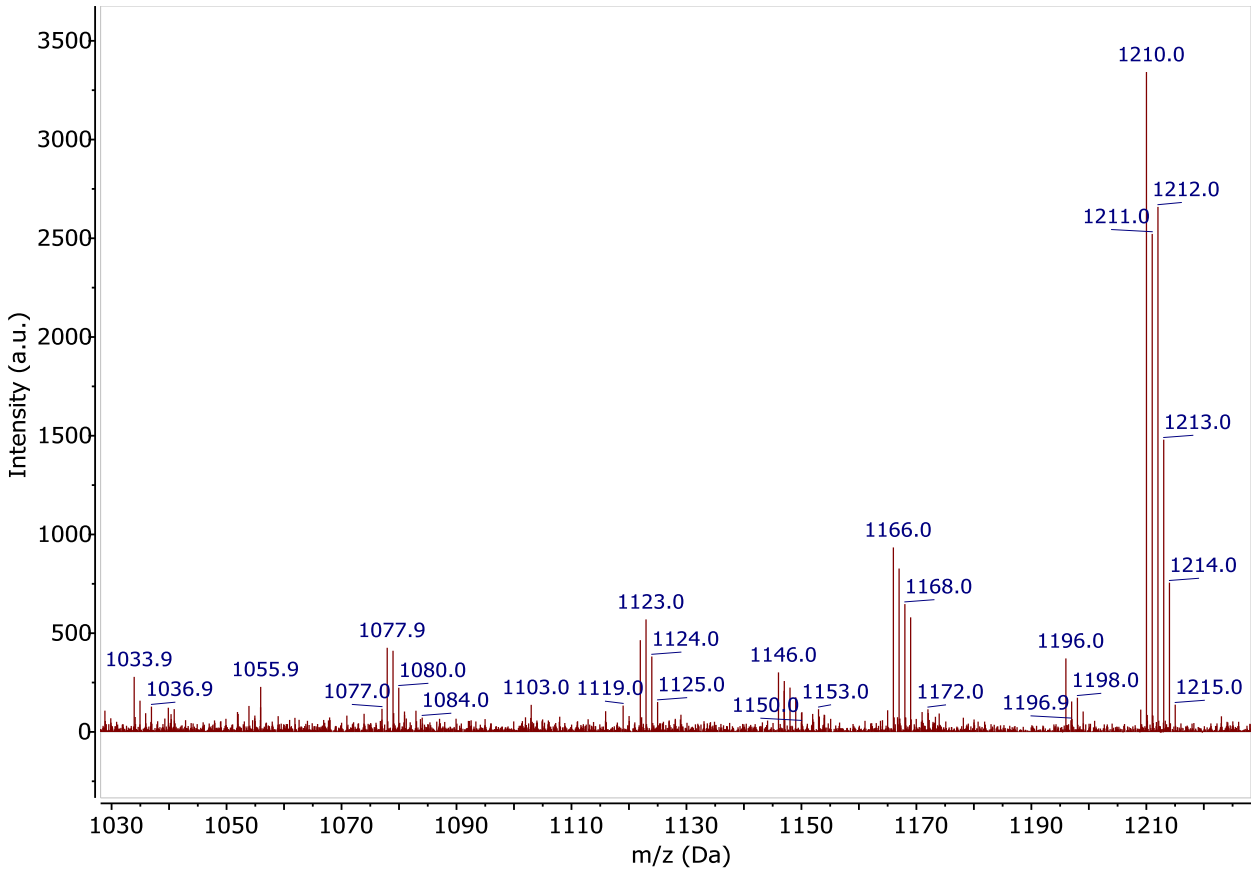

Figure 3.23 LD-MS spectrum of **NiPcH**. This spectrum shows the molecular ion signal at m/z = 1210.0 as well as signals for sequential loss of carboxylic acid groups from **NiPcH** at 1166.0, 1123.0, 1077.9, and 1033.9.

Table 3.1 Fragmentation pattern observed in LD-MS spectrum of **NiPcH**.

ion	Observed mass	Exact mass
$[M^{\bullet}]^{+}$	1210.0	1210.2
$[M^{\bullet}+H^{\bullet}-COOH^{\bullet}]^{+}$	1166.0	1166.2
$[M^{\bullet}+2H^{\bullet}-2COOH^{\bullet}]^{+}$	1123.0	1122.2
$[M^{\bullet}+3H^{\bullet}-3COOH^{\bullet}]^{+}$	1077.9	1078.2
$[M^{\bullet}+4H^{\bullet}-4COOH^{\bullet}]^{+}$	1033.9	1034.2

For the ESI-MS analysis on **NiPcH** (Figure 3.24), it was determined that negative ion mode would be the ideal method to ionize **NiPcH** since it could rapidly lose one proton from the ligand. However, it was necessary to set the skimmer voltage at higher than normal (-100 V while a typical analysis is done at -20 V) to get a signal. Indeed, when electrospray ionization was performed in negative mode, a predominant ion signal at m/z = 1209.2, consistent with the $[M\text{-}H^{+}]^{-}$ ion was observed. The signal at m/z = 1231.17 was correlated to $[M\text{-}2H^{+}\text{+}Na^{+}]^{-}$ (exact mass = 1231.17). Due to the high electrospray voltage, some fragmentation was also observed. As such, the signal at m/z = 1164.19 was correlated to $[M\text{-}H^{+}\text{-}COOH^{\bullet}]^{\bullet-}$ (exact mass = 1164.19).

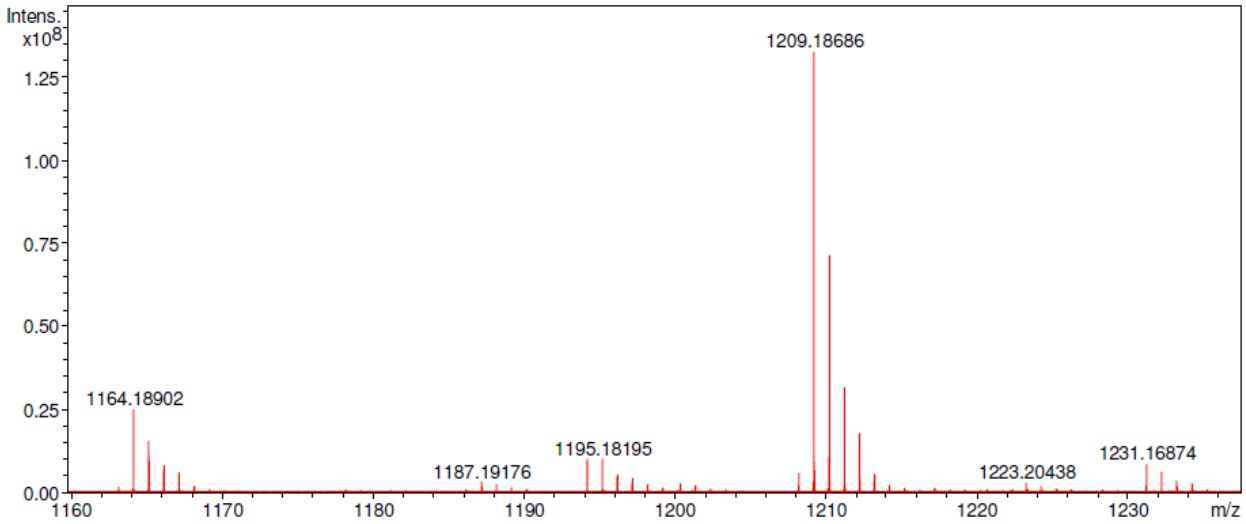

Figure 3.24 ESI-MS (in negative mode) spectrum of **NiPcH**. This spectrum shows the $[M\text{-}H^{+}]^{-}$ ion signal at m/z = 1209.19.

For **CoPcH**, an exact mass of 1211.2 is expected. Therefore, the signal at m/z = 1211.6 in the LD-MS spectrum in Figure 3.25 corresponds to the molecular ion $[M^{\bullet}]^{+}$. Similar to **NiPcH**, we can observe a fragmentation pattern for **CoPcH** that can be correlated to the successive loss of the carboxylic acid groups (Table3.2).

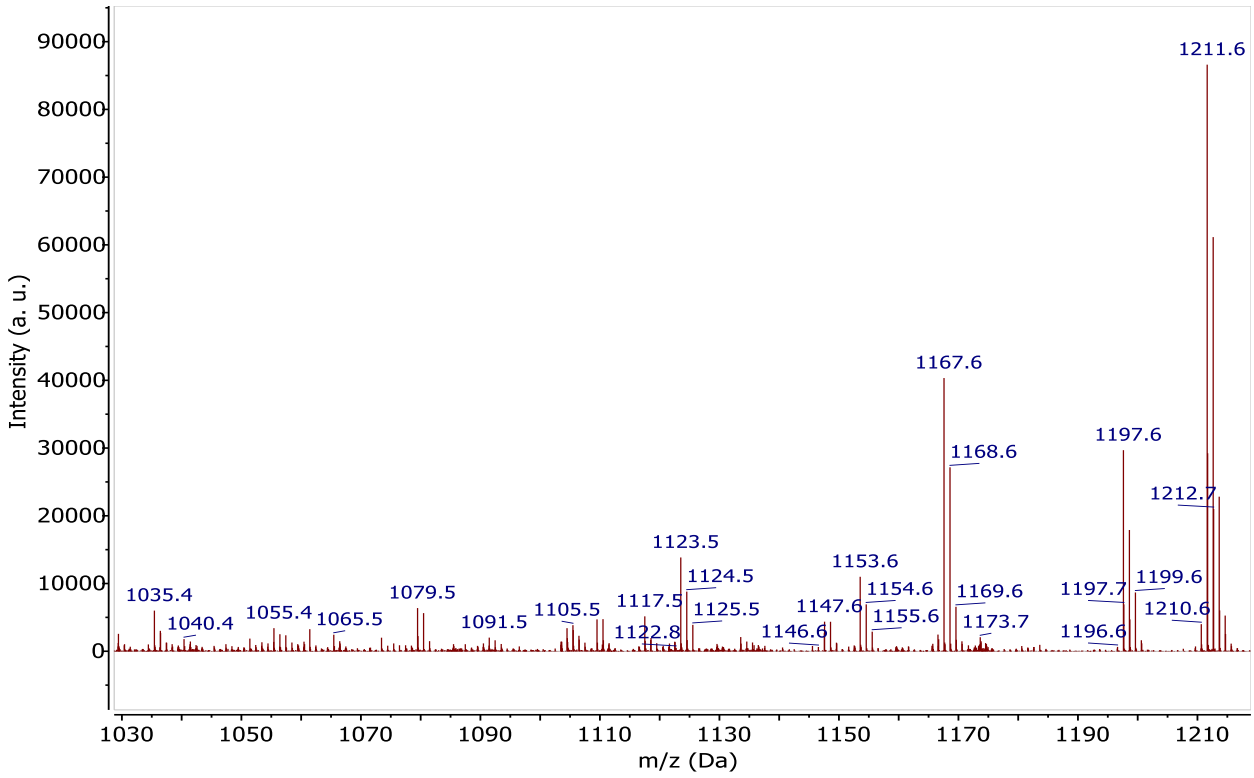

Figure 3.25 LD-MS spectrum of **CoPcH**. This spectrum shows the molecular ion signal at m/z = 1211.6 as well as signals for sequential loss of carboxylic acid groups from **CoPcH** at 1167.6, 1123.5, 1079.5, and 1035.4.

Table 3.2 Fragmentation pattern observed in LD-MS spectrum of **CoPcH**.

ion	**Observed mass**	**Exact mass**
$[M^{\bullet}]^{+}$	1211.6	1211.2
$[M^{\bullet}+H^{\bullet}-COOH^{\bullet}]^{+}$	1167.6	1167.2
$[M^{\bullet}+2H^{\bullet}-2COOH^{\bullet}]^{+}$	1123.5	1123.2
$[M^{\bullet}+3H^{\bullet}-3COOH^{\bullet}]^{+}$	1079.5	1079.2
$[M^{\bullet}+4H^{\bullet}-4COOH^{\bullet}]^{+}$	1035.4	1035.2

For **NiPc2**, an exact mass of 730.1 is expected. LD-MS spectrum of **NiPc2** in Figure 3.26 shows the molecular ion $[M^{\bullet}]^{+}$ signal as the predominant peak. Compared with **NiPcH**,

significantly less fragmentation was observed, which is expected from **NiPc2** owing to its smaller size and less labile bonds.

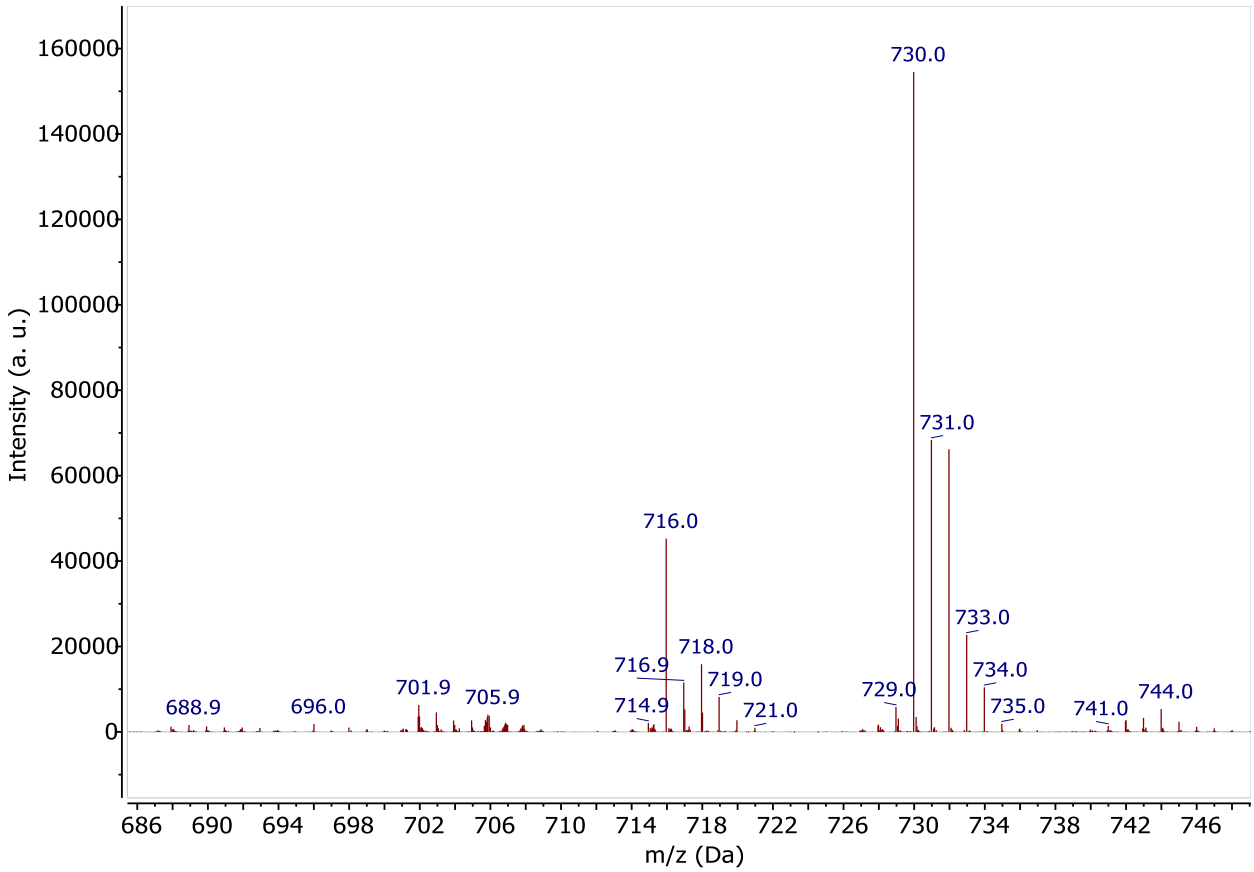

Figure 3.26 LD-MS spectrum of **NiPc2**. This spectrum shows the molecular ion signal at m/z = 730.0.

3.3 Conclusion

We synthesized tetraimidazophthalocyaniens that can be used as rigid linkers for MOFs synthesis. These linkers can have different metal cations coordinated in the cavity of the Pc molecule; therefore, different functionality can be introduced to the target MOF. We showed synthesis of two family of these Pc-based linkers. The first one is designed to have four imidazole groups as the coordinating groups to the metal ions that makes the MOF. This provides the opportunity for the synthesis of the first class of ZIFs that have imidazophthalocyanines as linker. The second family has four carboxylate groups in symmetrical fashion on the Pc core. With this linker the

carboxylic acid can coordinate to the metal ion. This provides opportunity for the synthesis of carboxylate based PcMOFs which are already lacking in the MOF field.

3.4 Experimental Details

3.4.1 General procedures, materials, and instrumentation

Reagents and solvents were purchased from commercial sources and used without Purification.

^{1}H-NMR spectra were recorded on a Bruker 300 MHz AVANCE III spectrometer using acetone-d_6, $CDCl_3$, DMSO-d_6, or DMSO-d_6 + 1 drop of D_2SO_4 as the NMR solvent. DMSO-d_6 was used as the lock solvent for the latter.

LD-MS was recorded on a Bruker ultraflexTOF/TOF mass spectrometer.

ESI-MS was recorded on a Bruker Apex-Qe 9.4T FTICR. The sample was dissolved in 65% methanol / 35% water with 0.5% ammonium hydroxide.

UV-Vis absorption spectra were recorded using a Cary 6000i spectrophotometer.

ATR-FTIR spectra were recorded using a Bruker Tensor 27 FT-IR equipped with a ZnSe MIRacle crystal.

3.4.2 Synthesis of 3-5

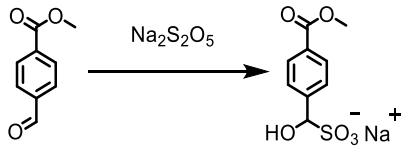

3-5

A 250 mL round bottom flask (RBF) was charged with 5.34 g methyl 4-formylbenzoate (32.5 mmol) and a magnetic stir bar. 100 mL 95% ethanol was added to the flask and stirred to completely dissolve the solid. In a separate beaker, 3.2 g sodium metabisulfite ($Na_2S_2O_5$) (17 mmol) was dissolved in 20 mL deionized water. Sodium metabisulfite solution was added dropwise to the stirring solution in the RBF. Upon addition of Sodium metabisulfite solution, the

Solution in the flask turns cloudy and a white precipitate gradually forms. Finally, 50 mL more ethanol was added to the white precipitate in the flask and it was stirred. The RBF was placed in a fridge. The RBF contents was suction filtered and was washed with 180 mL cold ethanol. The white solid was left on filter paper to dry. When dry, 8.23 g product **3-5** was obtained as a white powdery solid (30.7 mmol, yield = 94%).

3.4.3 Synthesis of 3-1-2

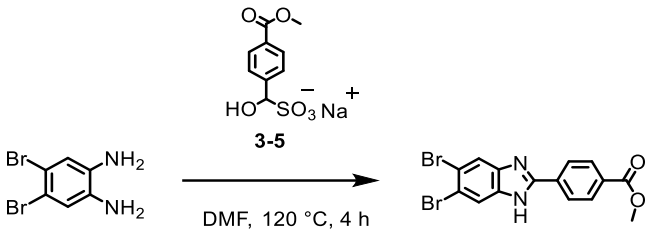

3-1-2

A 50 mL RBF was charged with 940 mg bisulfite adduct **3-5** (3.50 mmol), 832 mg 4,5-dibromobenzene-1,2-diamine (MW = 265.94 g/mol, 3.13 mmol), 10 mL DMF, and a magnetic stir bar. The RBF was capped with septa then heated in an oil bath at 120 °C for 4 h using a hot plate equipped with a temperature probe. The flask was removed from the oil bath and left to cool to room temperature. Once cooled, deionized water was added to the yellow mixture in the reaction RBF until it was filled. Using suction filter, the yellow mixture was isolated as a yellow solid on filter paper, which was washed with 50 mL of deionized water. The yellow solid was left to dry on the suction filter and further dried in a vacuum oven at 80 °C overnight. Once dry, 1.027 g yellow solid was obtained. The dry yellow solid was further purified by pouring 100 mL hot ethanol in a beaker containing the yellow solid then it was stirred with stirring rod. After being chilled, the mixture was suction filtered, and the obtained light-yellow solid was finally dried in a vacuum oven at 80 °C overnight. Once dried, 905 mg product **3-1-2** was obtained as a yellow solid

(2.21 mmol, yield = 71%). ^{1}H-NMR (300 MHz, acetone-d_6) δ 8.34 (d, 8.9 Hz, 2H), 8.17 (d, 8.9 Hz, 2H), 8.09 (s, 1H), 7.95 (s, 1H), 3.94 (s, 3H).

3.4.4 Synthesis of 3-1-1

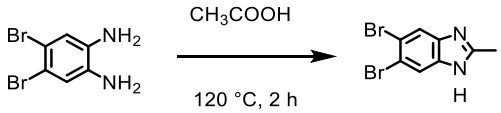

3-1-1

An 8 mL vial was charged with 427 mg 4,5-dibromobenzene-1,2-diamine (1.61 mmol), 2.5 mL glacial acetic acid (44 mmol), and a magnetic stir bar. The vial was sealed with a crimpable septa-containing cap. The vial was then heated in an oil bath at 120 °C using a hot plate equipped with a temperature probe. The reaction was followed by TLC (ethyl acetate: methanol 9:1). After 2 h, the vial was removed from the oil bath and it was left to cool down to room temperature. Then the vial content was poured into 50 mL dichloromethane then 100 mL $NaHCO_3$ solution (made by dissolving 15 g $NaHCO_3$ in 350 mL deionized water) was added to the mixture followed by stirring until foaming stopped. The mixture was poured into a separatory funnel and the product was extracted with dichloromethane. The combined organic layers were washed twice with water then it was dried over $MgSO_4$ followed by gravity filtering. Finally, the solvent was removed using rotary evaporator to obtain 360 mg product **3-1-1** as a yellow-orange powder (1.24 mmol, yield = 77%) compound. ^{1}H-NMR (300 MHz, DMSO-d_6) δ 12.48 (s, 1H), 7.85 (s, 2H), 2.48 (s, 3H).

3.4.5 Synthesis of 3-2

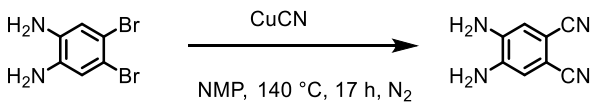

3-2

In a batch synthesis approach, eight 20 mL dry vials were all individually charged with 1.298 g 4,5-dibromobenzene-1,2-diamine (4.881 mmol), 1.817 g CuCN (20.29 mmol), 13 mL NMP (that was previously sparged with N_2 for 15 min), and a magnetic stir bar. The solution in these vials were stirred and subjected to sonication. The vial was sealed with a crimpable septa-containing cap, and subsequently sparged using a needle punctured through the septa with N_2; a second needle was pierced through the septa to vent the gas. Finally, these vials were heated in an oil bath at 140 °C for 17 h. The vials were removed from the oil bath and cooled to room temperature. Before opening the seals, as a precaution, the vials were vented with a syringe needle in the fume hood to help release any built-up pressure inside the vial. Contents of all vials were mixed in a 500 mL beaker and diluted with 120 mL of DMF. Two 1 L Erlenmeyer flasks each containing 60 g Na_3EDTA, and 300 mL deionized water, were heated while stirring on two hot plates until all solids dissolved. The diluted reaction solution was separated into two equal fractions which were decanted into the each of the 1 L Erlenmeyer flasks containing hot Na_3EDTA solution. The mixtures were heated while stirring vigorously on hot plates equipped with temperature probe with the solution temperature set on 95 °C. Meanwhile, air was bubbling into the solutions using an aquarium air pump (air flow was split to bubble in both flasks at the same time). After 2 h, 100 mL of hot deionized water was added to each flask and the heating/stirring /bubbling was continued, for another 2 h. After this, the hot plates were turned off and the reaction mixture left overnight in the fume hood. The solution component of both flasks was decanted into a large beaker. 100 mL ethyl acetate was added to the solid component in each 1 L Erlenmeyer flask and sonicated with manual stirring to dislodge the solid. The solid was then isolated with suction filtration. The filtrate was retained to potentially retrieve more product and added to the large beaker. The combined solution was extracted with ethyl acetate in seven batches using a 1 L

separatory funnel (3×50 mL ethyl acetate used for each batch). These combined organic layers were washed with 7×150 mL of deionized water and then with 5×90 mL of saturated NaCl solution, or until an aqueous fraction was colorless. The organic fraction was then dried over $MgSO_4$ and filtered to remove solid impurities. The organic phase was concentrated under reduced pressure with rotary evaporation. The resulting solid was further dried in a vacuum oven at 80 °C overnight to give 3.27 g product **3-2** as a beige powder (20.7 mmol, yield = 53%). ^{1}H-NMR (300 MHz, acetone-d_6) δ 7.04 (s, 2H), 5.37 (s, 4H).

3.4.6 Synthesis and workup of 3-3-2

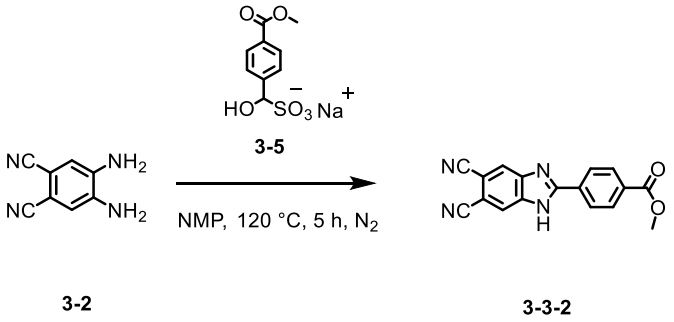

Four dry 20 mL vials each were charged with 914 mg **3-2** (5.78 mmol), 1.76 g bisulfite adduct **3-5** (6.56 mmol), 11.5 mL NMP, and a magnetic stir bar. The vials were sealed with a crimpable septa-containing cap, and subsequently sparged using a needle punctured through the septa with N_2; a second needle was pierced through the septa to vent the gas. The vials were heated in an oil bath at 120 °C using a hot plate equipped with temperature probe. The reaction was monitored by TLC (hexanes: ethyl acetate 3:7). The vials were removed from the oil bath after 5 h and left to cool to room temperature. Before opening the seals, the vials were vented carefully with a syringe needle in the fume hood. The vial content (light brown solution containing yellow precipitate) was emptied into a 500 mL beaker then 300 mL deionized water was added to the mixture with stirring and finally the mixture was centrifuged. The yellow solid collected from the centrifuge tubes were

suction filtered and washed with portions of 200 mL ethanol: water (1:1). The yellow solid left on the suction filter to dry, then placed in vacuum oven at 80 °C overnight to give 4.12 g product **3-3-2** as a light-yellow powder (13.6 mmol, yield = 59%). ^{1}H-NMR (300 MHz, DMSO-d_6) δ 8.50 (s, 2H), 8.39 (d, 8.8 Hz, 2H), 8.17 (d, 8.8 Hz, 2H), 3.91 (s, 3H).

3.4.7 Synthesis of 3-3-3

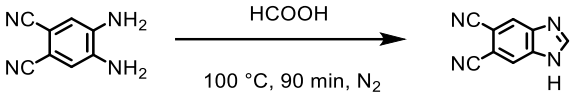

3-2 **3-3-3**

A dry 8 mL vial was charged with 255 mg **3-2** (1.61 mmol), 3.2 mL formic acid (85 mmol), and a magnetic stir bar. The solution in this vial was stirred and subjected to sonication, The vial was sealed with a crimpable septa-containing cap, and subsequently sparged using a needle punctured through the septa with N_2; a second needle was pierced through the septa to vent the gas. The vial was then heated in an oil bath at 100 °C using a hot plate equipped with a temperature probe. The reaction was followed by TLC (hexanes: ethyl acetate 3:7). After 90 minutes, the vial was removed from the oil bath and it was left to cool down to room temperature. Before opening the seal, the vial was vented carefully with a syringe needle in the fume hood. The vials contents were decanted into 150 mL $NaHCO_3$ solution (made by dissolving 10 g $NaHCO_3$ in 150 mL deionized water). The resulted mixture was suction filtered. The solid on the filter paper was dried further in a vacuum oven at 80 °C overnight to obtain 137 mg product **3-3-3** as a beige powder (0.815 mmol, yield = 51%). ^{1}H-NMR (300 MHz, DMSO-d_6) δ 8.72 (s, 1H), 8.47 (s, 2H).

3.4.8 Synthesis of NiPc1

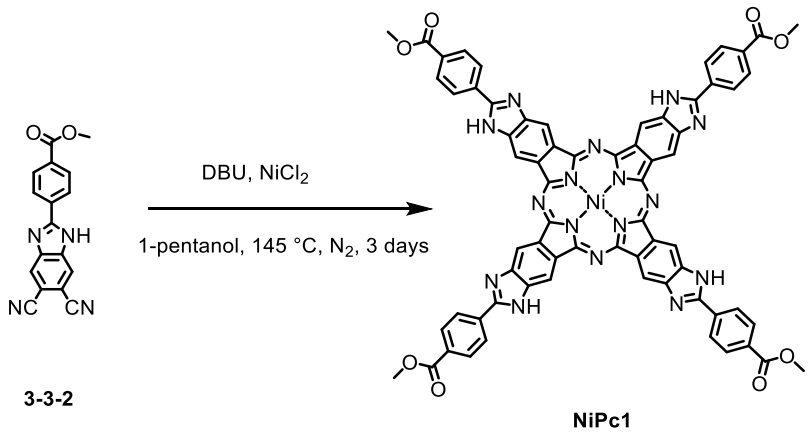

A dry 20 mL vial was charged with 660 mg **3-3-2** (2.18 mmol), 160 mg $NiCl_2$ (1.23 mmol), 11 mL 1-Pentanol, and a magnetic stir bar. The solution in this vial was stirred and subjected to sonication. The vial was sealed with a crimpable septa-containing cap, and subsequently sparged using a needle punctured through the septa with N_2; a second needle was pierced through the septa to vent the gas. The vial was then heated in an oil bath using a hot plate equipped with a temperature probe for 10 min at 145 °C, then the vial was carefully vented with a syringe needle in the fume hood to release the pressure. 1090 µL of DBU (7.3 mmol) measured by a micropipette was injected into the vial using a syringe and needle. After heating the vial at 145 °C for 66 h, the vial was removed from the oil bath and it was left to cool down to room temperature. The vial was vented with a syringe needle before opening the seal, and its contents were emptied into a centrifuge tube and 15 mL of DMF was added. The centrifuge tube was sonicated then 8 mL of ethyl acetate was added to the solution to precipitate out phthalocyanines as a green solid. This green solid was then isolated from the mixture by centrifugation. The addition of DMF, sonication, adding ethyl acetate, and centrifugation was repeated until the decanted solution was colorless or was very light brown in color. Next, the solid was washed with 3×30 mL hexanes, centrifuged, and decanted, followed by the addition of 35 mL 1 M HCl to the green solid, followed by stirring the mixture overnight at

room temperature to dissolve any remaining nickel particles. The next day, this mixture was centrifuged, and solution was decanted. The remaining solid was washed three times with deionized water and centrifuged. Then water was decanted and the solid was dried in a vacuum oven at 80 °C overnight to obtain 330 mg **NiPc1** as a dark solid (0.260 mmol, yield = 48%).

3.4.9 Synthesis of NiPcH from NiPc1

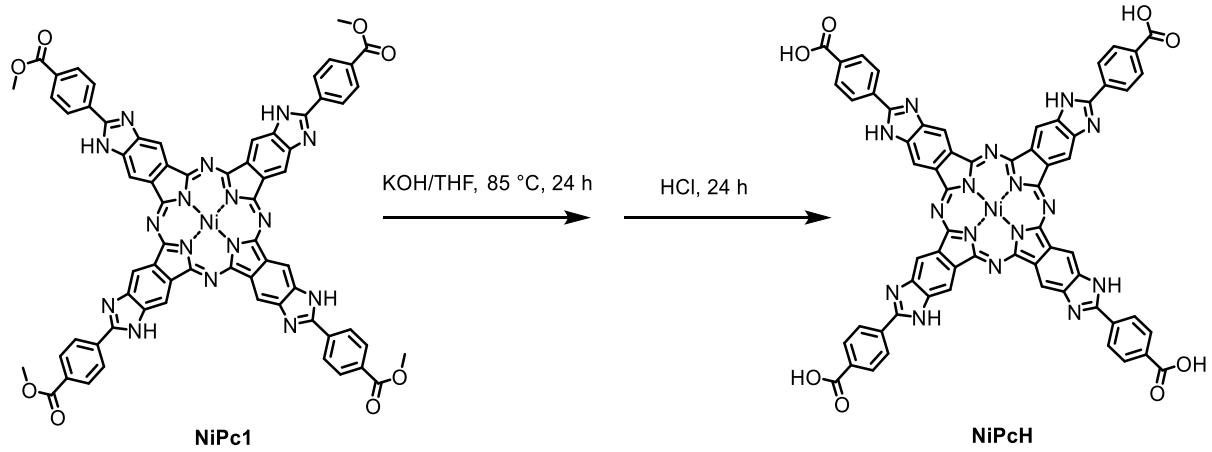

A 100 mL RBF was charged with 330 mg **NiPc1** (0.260 mmol), 25 mL THF, 25 mL 2 M KOH, and a magnetic stir bar. Then the RBF was heated in an oil bath with refluxing at 85 °C for 24 h. After cooling down to room temperature, 30 mL DMF was added to the brown mixture in the RBF followed by stirring the mixture and adding 15 mL ethyl acetate. The mixture was centrifuged and decanted, then the solid was transferred into a 100 mL RBF. 75 mL of 1 M HCl was added to the solid in the RBF and it was stirred at room temperature overnight. The next day, the mixture was centrifuged and decanted before adding 15 mL DMF to the solid in the centrifuge tube. The centrifuge tube was sonicated, then 8 mL ethyl acetate was slowly added to precipitate the phthalocyanine as a green solid. The procedure of adding DMF and ethyl acetate, followed by centrifugation and decanting was repeated until the decanted solution was colorless. The solid was washed three times with deionized water and centrifuged. The water was then decanted and the

solid was dried in a vacuum oven at 80 °C overnight to obtain 130 mg product **NiPcH** as a dark grainy solid (0.107 mmol, yield = 41%).

3.4.10 One-pot synthesis of NiPcH from 3-3-2

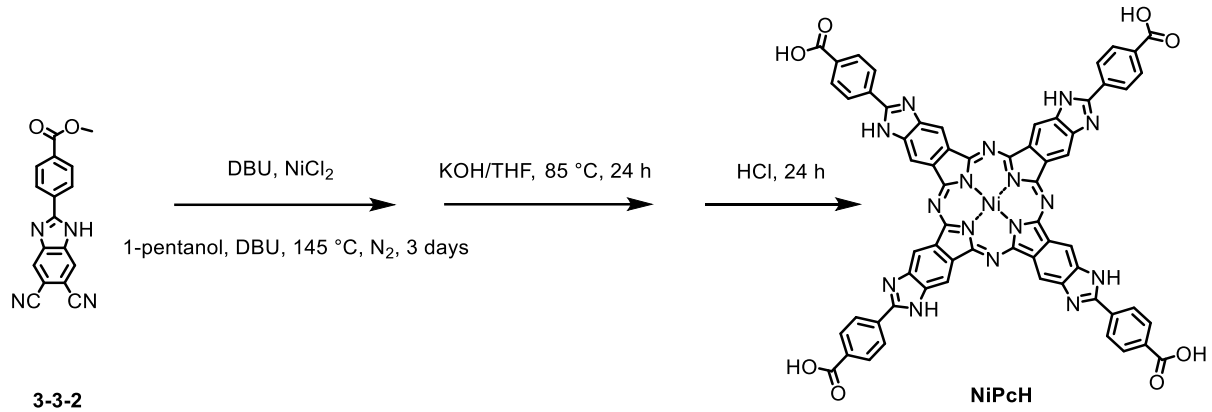

Five 20 mL dry vials each were charged with 740 mg **3-3-2** (2.45 mmol), 179 mg $NiCl_2$ (1.38 mmol), 12.2 mL 1-Pentanol, and a magnetic stir bar. The solution in these vials were stirred and subjected to sonication. The vials were sealed with a crimpable septa-containing cap, and subsequently sparged using a needle punctured through the septa with N_2; a second needle was pierced through the septa to vent the gas. The vials were heated in an oil bath using a hot plate equipped with temperature probe for 10 min at 145 °C, then the vials were vented carefully with a syringe needle in the fume hood to release the pressure. 1225 µL of DBU (8.207 mmol) was measured by micropipette and injected into each vial using a syringe and needle. Heating continued for 66 h at 145 °C. The vials were removed from the oil bath and left to cool to room temperature, then vented with a syringe needle before opening the seal. All five vials content were transferred into a 500 mL RBF. 60 mL THF and 130 mL 2 M KOH was added to the RBF. The mixture was heated in an oil bath under reflux at 85 °C for 24 h. After this, the condenser was removed, heating continued for another 1 h to evaporate THF, and the reaction flask was left stirring overnight at a reduced temperature of 40 °C. The resulting brown mixture was transferred into a 1 L Erlenmeyer

flask, then 300 mL 1 M HCl added to the flask and stirred at room temperature for 24 h. The mixture was then centrifuged to separate the crude phthalocyanine product. Centrifuge tubes containing dark brown solution were decanted, and the solids were collected and emptied into a single centrifuge tube. The collected solid was washed with a few solvents followed by centrifuging with the mentioned order: three times with deionized water. Methanol: water 4:1. Methanol: water 3:1. Many times methanol: water 1:1. The solid was dried in vacuum oven at 80 °C overnight. Dry solid was washed with acetone and centrifuged. The collected solid was dried in a vacuum oven at 80 °C overnight to give 2.25 g product **NiPcH** as a dark grainy solid (1.86 mmol, yield = 61%).

3.4.11 One-pot synthesis of NiPcH from 3-3-2 (smaller scale, modified workup)

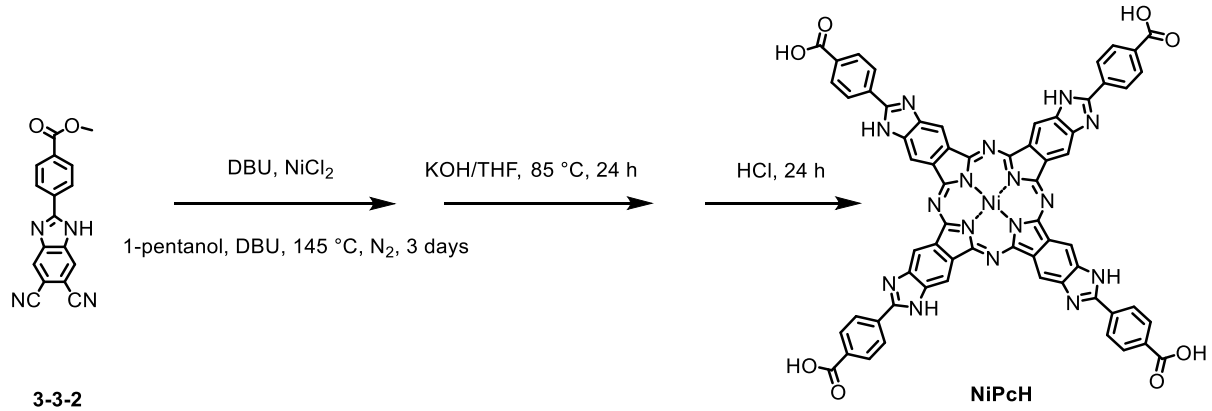

A dry 20 mL vial was charged with 740 mg **3-3-2** (2.45 mmol), 179 mg $NiCl_2$ (1.38 mmol), 12.2 mL 1-Pentanol, and a magnetic stir bar. The solution in this vial was stirred and subjected to sonicationThe vial was sealed with a crimpable septa-containing cap, and subsequently sparged using a needle punctured through the septa with N_2; a second needle was pierced through the septa to vent the gas. The vial was heated in an oil bath using a hot plate equipped with a temperature probe for 10 min at 145 °C, then the vial was vented carefully with a syringe needle in the fume hood to release the pressure. 1225 µL of DBU (8.207 mmol) measured by micropipette was

injected into the vial using a syringe and needle. After heating at 145 °C for 66 h, the vial was removed from the oil bath and it was left to cool to room temperature. The vial was then vented with a syringe needle before opening the seal. The vial contents were transferred into a 100 mL RBF. Then 12 mL THF and 26 mL 2 M KOH was added to the RBF. The RBF was then heated in an oil bath under reflux (at 85 °C) for 24 h. The condenser was removed after 24 h with continued heating for 1 h to evaporate THF. The brown mixture was transferred into a 250 mL RBF, followed by subsequent addition of 75 mL of 1 M HCl. The mixture was then stirred at room temperature for 24 h. The brown mixture was then centrifuged to separate crude product. The dark brown solution was decanted, followed by addition of 15 mL of DMF to the isolated crude solid. The centrifuge tube was sonicated, then 8 mL ethyl acetate was slowly added to the solution to precipitate the product as a green solid, which was isolated by centrifugation. The process of adding DMF, sonicating, adding ethyl acetate, and centrifuging was repeated many times until the decanted solution was colorless or very light brown in color. Finally, the solid was washed three times with deionized water, centrifuged, and decanted. The solid was dried in a vacuum oven at 80 °C overnight to obtain 285 mg product **NiPcH** as a dark grainy solid (0.235 mmol, yield = 38%).

3.4.12 One-pot Synthesis of CoPcH from 3-3-2

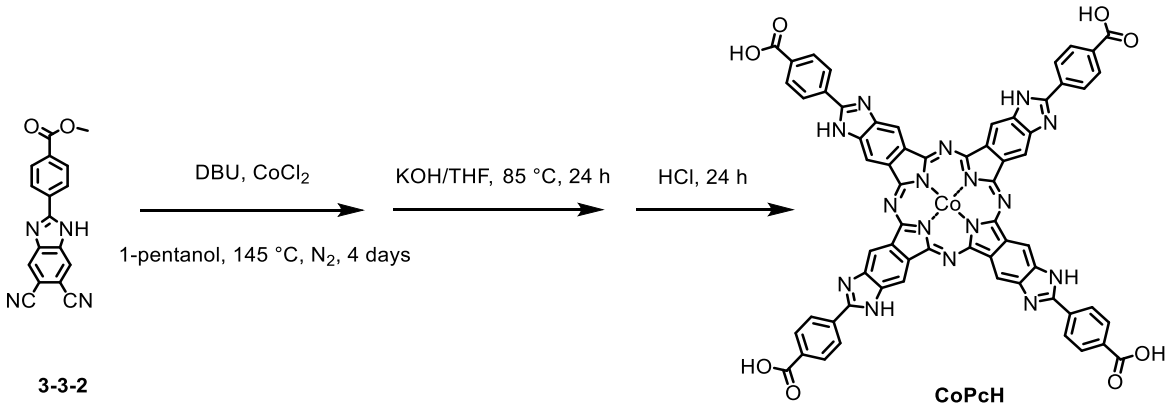

A dry 20 mL microwave vial was charged with 740 mg **3-3-2** (2.45 mmol), 179 mg $CoCl_2$ (1.38 mmol), 12.2 mL 1-Pentanol, and a magnetic stir bar. The solution in this vial was stirred and subjected to sonication, followed by N_2 sparging, before being sealed and finally the vial was flushed and filled with N_2 The vial was heated in an oil bath using a hot plate equipped with a temperature probe for 10 min at 145 °C, then the vial was vented carefully with a syringe needle in the fume hood to release the pressure. 1.3 mL DBU (8.7 mmol) was added via syringe into the vial using a syringe and needle. After heating the vial at 145 °C for 4 days, the vial was removed from the oil bath, and cooled to room temperature. Pressure built during the reaction was vented with a syringe needle before opening the seal. The vial content was transferred into a 100 mL RBF, after which 12 mL THF and 26 mL 2 M KOH was added to the flask. The RBF was heated in an oil bath under reflux at 85 °C for 24 h. After 24 h the condenser was removed, but heating was continued for another 3 h to evaporate THF. The brown mixture was transferred into a 250 mL RBF, then 75 mL 1 M HCl was added to the flask and it was stirred at room temperature for 24 h. The brown mixture was then centrifuged to separate the crude product. Dark brown solution was decanted, followed by addition of 15 mL DMF to the isolated solid. The centrifuge tube was sonicated, then 8 mL ethyl acetate was slowly added to the solution to precipitate a green solid, which was isolated by centrifugation. The process of adding DMF, sonicating, adding ethyl acetate, and centrifuging was repeated until the decanted solution was colorless or very light brown in color. Finally, the solid was washed three times with water, centrifuged, and decanted. The solid was dried in a vacuum oven at 80 °C overnight to give 196 mg product **CoPcH** as a dark grainy solid,) of dark grainy solid (0.162 mmol, yield = 26%).

3.4.13 Synthesis of NiPc2

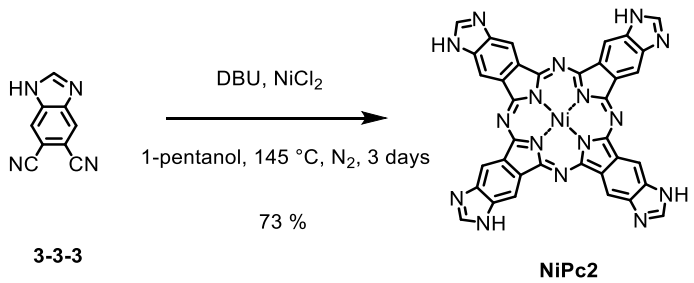

An 8 mL dry vial was charged with 110 mg **3-3-3** (0.654 mmol), 49 mg $NiCl_2$ (0.38 mmol), 3.3 mL 1-Pentanol, and a magnetic stir bar. The solution in this vial was stirred and subjected to sonication, The vial was sealed with a crimpable septa-containing cap, and subsequently sparged using a needle punctured through the septa with N_2; a second needle was pierced through the septa to vent the gas. The vial was heated in an oil bath at 145 °C using a hot plate equipped with temperature probe for 10 min. The vial was carefully vented with a syringe needle in the fume hood to release the pressure. 331 μL DBU (2.22 mmol) measured by micropipette was injected into the vial using a syringe and needle. After heating the vial at 145 °C for 3 days, the vial was removed from the oil bath and cooled down to room temperature. The vessel was vented with a syringe needle before opening the seal. The vial contents were emptied into a centrifuge tube, followed by a subsequent addition of 15 mL of DMF. The centrifuge tube was sonicated, then 8 mL hexanes was slowly added to the solution to precipitate a green solid, which was isolated by centrifugation. The solid was further washed with 2×15 mL acetone followed by centrifuging and decanting. Then 30 mL 1 M HCl was added to the solid in the centrifuge tube followed by stirring for 1 h. The resulting green solution was emptied into an RBF and neutralized with 2 M KOH until pH was neutral as indicated by litmus paper. This precipitate was washed two times with 2×30 mL deionized water, followed by centrifugation and decanting. Then the solid was dried in a vacuum

oven at 80 ℃ overnight to obtain 86.9 mg product **NiPc2** as a dark grainy solid (0.119 mmol, yield = 73%).

4 Synthesis of phthalocyanine-based MOFs

4.1 Introduction

In Chapter 3, we demonstrated that two Pc ligands can be synthesized with the necessary coordination chemistry installed to allow for the formation of porous materials. With these ligands in hand, we can now attempt the daunting task of synthesizing and characterizing MOFs formed from these ligands.

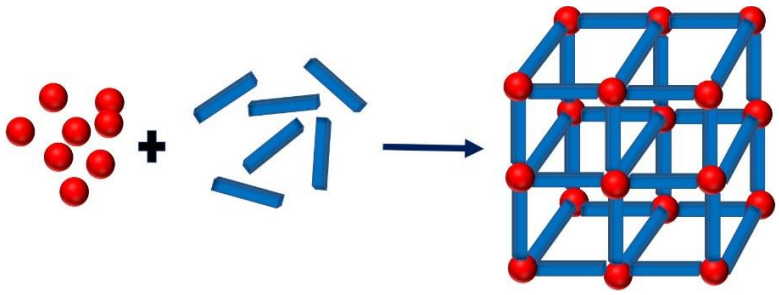

Figure 4.1 Schematic representation of MOF formation from nodes (red balls) and ligands (blue bars).

In the simplest way (Figure 4.1), MOFs are prepared by combining metal ions (nodes) and organic ligands (linkers) at elevated temperatures until the process of nucleation and crystal growth occurs resulting in a 3-D crystalline and porous material. Often, the marks for a successful synthetic procedure are the reproducible diffraction pattern and gas adsorption properties. Furthermore, an ideal synthetic procedure would be flexible enough that slight changes in reaction conditions do not drastically affect the results. Anecdotally, there are several procedures that struggle outside of the originating lab; this is likely due to changes in reaction conditions that are not included (or known) in the original procedure (i.e., reaction container size, oven heating method, water content in the solvent, *etc.*). While the process of synthesizing new MOFs may seem simple, the reality is that determining the reaction conditions can be a challenging endeavor. It is true that the ligand charge and the node charge will often balance one another (i.e., leave no cations

or anions in the pore). However, this does not mean that simply mixing the node and ligand in this ratio is sufficient to make the desired MOF. The synthesis of MOFs requires the careful balance of kinetics to allow the formation of a crystalline product of a single phase. If the metal-ligand bonds form quickly and irreversibly, then it is more likely that an amorphous phase which may still be of interest forms.[142, 143] With this in mind, the synthesis of MOFs requires that the formed M-L bonds can also be broken so that the chemistry can make and break bonds until the thermodynamic product (ideally a porous MOF) can form. To accomplish this, MOF chemists tune reaction conditions such as solvent choice, metal:ligand ratio, addition of additives, temperature, concentration of the reaction, and workup conditions, to try to synthesize MOFs. The challenge is that for every new ligand and/or metal that is being attempted, the conditions may be drastically different. For example, the addition of small amounts of acid (1-2 drops in 10-20 mL of solvent) can help optimize the kinetics of crystal growth but large amounts of acids (1 mL in 10-20 mL of solvent) would be viewed as detrimental. For Cu/Zn MOFs (and likely others), this statement would be true. However, for a Zr-MOF like UiO-66, large amounts of acid are necessary and often lead to rapid formation of a single phase of the desired MOF.[144]

Just as NMR and mass spectrometry are used as a guide for the synthesis of small molecules, X-ray diffraction and gas adsorption isotherms are used to guide the successful synthesis of porous materials. Only once a reproducible gas adsorption isotherm with a consistent diffraction pattern, which may be amorphous, is formed, we can assume that a procedure is successful. With this in mind, the following sections of the introduction will briefly introduce MOFs synthesis and some background information on the factors that are often considered in the synthesis of MOFs and the roles they play. Lastly, we will cover the basic characterization methods that help guide the synthetic approach towards MOF synthesis.

4.1.1 Synthesis

MOF synthesis methods can be classified as conventional and unconventional.[43] The conventional method places the reagents in a sealed vial/Teflon reactor vessel with a polar high boiling solvent. The vessel is then heated at elevated temperatures for anywhere between hours to days. Unconventional methods have been developed to reduce the amount of organic solvent used in the synthesis or to completely replace it. In some cases, these unconventional methods also shorten the synthesis time. Some common unconventional synthesis procedures include microwave heating,[145] electrochemical synthesis,[146] mechanochemical synthesis,[147] and ultrasonic synthesis.[148] Given that the work herein has focused on conventional methods, the remaining discussion will focus on conventional MOF synthesis.

There are many factors that affect the synthesis of MOFs such as temperature, reactant solubility, pH, concentrations of metal salt, ligand, and modulator, metal-ligand ratios, and even the counterions associated with the precursor metal salt.[43, 149] The following sections address some of these parameters.

4.1.1.1 Solvent

The prototypical solvent that is used in the large majority of MOF syntheses is DMF, while other solvents like *N*,*N*-diethylformamide (DEF), *N*,*N*-dimethylacetamide (DMA), and dimethyl sulfoxide (DMSO) have also been used.[150-153] These solvents are chosen because most starting materials are soluble in them, and they are relatively stable solvents at elevated temperatures. For the focus of incorporating Pc linkers into MOFs, this work primarily utilizes DMF. DMF is a high boiling point (153 °C) and highly polar solvent. This means that it should have the ability to dissolve most ligands and node precursors while also offering a wide temperature range to explore the parameter space of MOF synthesis. In the case of DMF and DEF,

the solvent slowly breaks down at elevated temperature. While this may seem detrimental, it is critical in the synthesis of MOFs by serving an additional purpose. As shown in Equation 4.1, the formation of a MOF from an acid ligand precursor (H_mL) and a Lewis-acidic metal precursor (MX_n) produces an acid (HX) as a product. This acid can break the node-ligand bonds in the MOF leading to a dynamic equilibrium. As the DMF is heated, it decomposes to dimethylamine, a base, and formic acid (Equation 4.2). The dimethylamine can subsequently react with the produced acid from the MOF synthesis and shift the equilibrium to favour MOF formation as a function of how fast DMF is decomposed. Modulating the rate of DMF decomposition allows us to control the rate of crystal formation, and in turn the quality and size of the formed crystals. Thus, controlling the rate of decomposition of DMF favours product formation and leads to crystalline, porous structures.

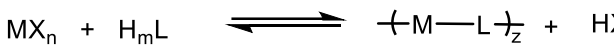

Equation 4.1

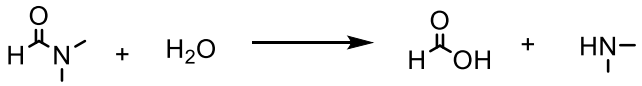

Equation 4.2

4.1.1.2 Temperature

The range of temperature used in MOF syntheses is typically 80-150 °C. Over this temperature range, nucleation and crystal growth rates can be controlled.[153] To achieve high crystallinity, dissociation/association rates in the MOF formation need to be properly balanced. In addition, by slowly cooling the reaction mixture, the critical nucleation concentration can be exceeded, and crystal growth takes place. The structure of synthesized MOFs can also be altered by varying the temperature of the reaction medium. As such, temperature can be manipulated for kinetic and thermodynamic control of the formation of MOFs. For example, Oliveira *et al.* made MOFs with same empirical formula but different structures by controlling the temperature.[154] They used

butanedioic acid and Tm^{3+} at two different temperatures (100 °C and 180 °C) and showed that because ligand flexibility causes different conformations, different coordination modes of the ligand at different temperatures provides opportunity to form two different MOF structures.

4.1.1.3 Modulator

In MOF syntheses, when many nucleation sites are formed and grow rapidly, this leads to the formation of smaller crystals. Therefore, controlling the rate of nucleation *vs.* crystal growth is vital for the formation of larger MOF crystals. A modulator is a non-structural, monotopic ligand (such as benzoic acid and acetic acid) which is added to the reaction mixture.[155] Modulators coordinate to the metal node and compete with the organic ligands, in turn, allowing MOF crystal size and morphology to be controlled. For example, Kitagawa and co-workers synthesized HKUST-1 with different crystal sizes ranging from nanometer to micrometer by using different concentrations of *n*-dodecanoic acid as modulator.[156] This study showed that the synthesized MOF has improved crystallinity (sharper PXRD peaks) and nitrogen adsorption (compared with non-modulated synthesis). In another study, Kitagawa *et al.* showed that morphology design of HKUST-1 is also feasible by controlling the modulator concentration. They showed that increase in *n*-dodecanoic acid concentration changes the HKUST-1 morphology from octahedron to cuboctahedron and then to cube.[157] Use of modulators in the synthesis of Zr-based MOFs have also been investigated.[144, 158-164] For example, Behrens and co-workers showed that increasing the amount of modulator (benzoic acid or acetic acid with respect to $ZrCl_4$) in the reaction mixture improves crystal size, crystallinity, and surface area of UiO-66 and UiO-67.[161] In the case of UiO-67, when 30 equivalent of benzoic acid (with respect to $ZrCl_4$) were used, the authors could even obtain octahedral single crystals (Figure 4.2) and reported increase of the specific surface

area from 270 m^2/g for the non-modulated synthesized UiO-67 to 3000 m^2/g for the 30 equivalent benzoic acid modulator.

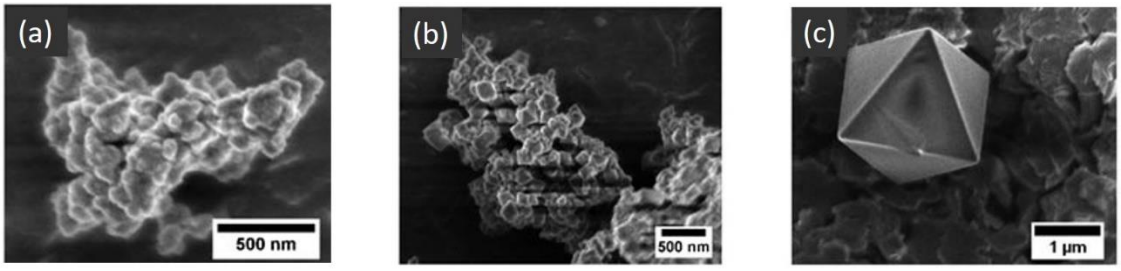

Figure 4.2 SEM image of UiO-67 showing change in crystal sizes and morphology by change in the amount of benzoic acid modulator with respect to $ZrCl_4$. (a) 0 equivalent (b) 3 equivalent (c) 30 equivalent. Reprinted with permission from reference 161 Copyright (2011) Wiley.

The examples discussed above show that the synthesis of MOFs can be very sensitive to the reaction parameters. Often there is a complex relationship between these parameters. As such, for the discovery of most MOFs, systematic exploring of the mentioned parameters is necessary. In saying this, with enough work; synthetic procedures that are tolerant to moderate changes in reaction conditions can be discovered.[144]

4.1.2 Activation

Activation is a term used to describe the removal of impurities residing inside the pores of a MOF such as residual solvent molecules and node/linker precursors which are trapped in the pores of the framework.[165] To utilize MOFs for a targeted application, it is critical to find the appropriate conditions to remove these undesirable guest molecules while leaving the structure intact. In many ways, determining the optimum parameters for the activation of a MOF can be as challenging to determine as the synthetic conditions of the MOF. This is especially true for larger pore MOFs, which are generally more sensitive to collapse. The section which follows discusses the most common activation techniques currently used.

4.1.2.1 Vacuum Drying

Traditional activation requires heating the as-synthesized MOF under vacuum to make the pores of a MOF free from trapped solvent molecules. Unfortunately, in many instances, vacuum drying cause channel collapse or blockage that result in partial or even full loss of porosity.[165] This happens because liquid- to gas-phase transformation of solvent molecules trapped in the pores generates intense capillary action that eventually cause the framework's collapse. This phenomenon is more pronounced when the trapped solvent has high surface tension (and high boiling point). Therefore, gentler techniques have been developed to mitigate this problem.

4.1.2.2 Solvent Exchange

Solvent exchange is used to solve the pore collapse problem encountered with vacuum drying.[165] In this method the MOF sample is first washed with the reaction solvent (often DMF) to remove impurities such as node precursors and non-coordinated species. Then the sample is soaked in a solvent with lower surface tension (e.g., acetone, dichloromethane, methanol) than the reaction solvent. This process is repeated several times to fully exchange the reaction solvent for the new solvent. Solvent exchange is often performed overnight to ensure complete exchange. Finally, since the pores are filled with a low boiling point and low surface tension solvent, vacuum drying can be applied to activate the MOF with reduced risk to the framework. Although this procedure has become popular for MOF activation, direct transition of the solvent from liquid to gas phase can still impose capillary action and cause the partial or full collapse of the framework. For such situations, even milder activation procedures have been developed to activate MOFs that have rather delicate structure and are more prone to structural collapse.

4.1.2.3 Supercritical Processing

Activation by supercritical CO_2 ($scCO_2$) is developed to address the encountered issue with the conventional solvent exchange process.[155, 165, 166] The success of this method is based on eliminating the liquid to gas phase transition that happens in solvent exchange and vacuum drying methods. When drying MOFs while using $scCO_2$, the MOF reaction solvent is first exchanged with a solvent such as ethanol (or other solvents that are compatible with the instrumentation and miscible in liquid CO_2). The sample is subsequently placed in a chamber in which the solvent is exchanged with liquid CO_2. Next, the temperature is increased until the pressure and temperature are in the region of supercritical CO_2 (critical point of CO_2 is 73 atm at 31 °C); at this stage, the framework is filled with $scCO_2$. Finally, the chamber is slowly vented to leave behind the activated sample. In this process, liquid to gas phase transformation which happen in conventional liquid-liquid solvent exchange activation processes is completely avoided. Along with the benefit of reduced structural damage through capillary action, $scCO_2$ activation usually produces MOFs with higher surface area, when compared with an identical sample activated by conventional solvent exchange methods.[166]

4.1.3 Characterization

4.1.3.1 X-ray Diffraction

The product of the self assembly between node and linker is often an ordered and crystalline material. Therefore, X-ray diffraction (XRD) is an ideal tool to elucidate the MOF structure and monitor the crystallinity and structure and how they may change in response to changing reaction conditions. For new MOFs, or any material whose structure needs to be determined, single crystal XRD is the best method. In this method, the atomic connectivity of a material can be known. For MOFs, this means that we can easily determine the pore size, shape, aperture, and other structural

information for guiding us to understand the applications of a novel material.[155] The challenge with single crystal XRD is that you have to grow a crystal, ideally a single domain, that is sufficiently large enough. Typically, for MOFs, a crystal should be approximately 1 mm or larger. While some MOFs naturally grow large single crystals, other MOFs have taken years to determine the optimal reaction conditions to grow sufficiently large crystals. For example, UiO-66 was first reported in 2008, but the single crystal XRD structure was not reported until 2014.[167] Alternatively, X-ray diffraction analysis can be performed on multicrystalline powder samples using PXRD.[168] Depending on the quality of the powder diffraction pattern (diffractogram), either 3-D connectivity can be determined or the powder diffractogram can be used to fingerprint a material; the former method was used for UiO-66. The latter method can be used to examine the crystallinity of the material to guide chemists towards the ideal reaction conditions. Examining the breadth of the peak can yield information about the average particle size, or even the mosaicity of the crystal.[169] The relative intensities can yield information about phase purity or preferred orientation of the crystallites. If the synthesized MOF already exists, or if the proposed structure of the MOF can be simulated, then the peak position and intensities, to some degree, of the synthesized MOF can be compared with that of the simulated PXRD pattern for that MOF.[155] As mentioned in the previous sections, activation of MOFs is a challenging step of the synthesis because it might cause loss of crystallinity or cause collapse of the framework, as such comparing PXRD pattern of the MOF sample pre- and post- activation can be employed as a helpful characterization tool to monitor the crystallinity after activation. In a similar fashion, chemical stability of the MOF in applications that involves exposure of the MOF to the environments that might alter the MOF structure (such as water, acidic and basic conditions) can be examined through PXRD analysis.

4.1.3.2 Nitrogen Gas Adsorption Isotherms

One of the key features of MOFs is the porous structure that they produce. With that in mind, one of the key properties that identify a MOF is the gas adsorption properties, and the associated information that can be gleaned from them. While gas adsorption can be done with several different gases or vapours, the most common characterization methodology is nitrogen gas adsorption at 77 K.[155, 170, 171] For this experiment, activated MOF is gradually exposed to an increasing volume of nitrogen gas and the amount of nitrogen uptake by MOF is calculated. From the obtained gas adsorption isotherm, the surface area, pore width, pore volume, and information about the pore aperture can be determined; these obtained metrics are invaluable for the comparison of MOFs.

Gas adsorption isotherms are a critical metric in the design of new MOFs. For example, when the synthesis of new MOFs is being explored, similar PXRD patterns may be observed; however, this does not mean that amorphous impurities are not present. By comparing the surface areas obtained from different reactions, or the pore size distributions with the expected pore information found from single crystal XRD, we can determine if there are structural defects, species trapped inside the pores such as incomplete solvent removal, and partial collapse of the framework. All of these affect the gas adsorption isotherm and the calculated surface area, as well as the pore size distribution calculated from the isotherm, to be different among the samples obtained from different reactions, and different from the expected values.

In this chapter, we take **NiPcH** linker that we designed in Chapter 3, and we explore how PcMOFs can be constructed with them. Using PXRD and gas adsorption as our metric for the quality of the material, we set out to explore MOFs with **NiPcH** linker and Zr-based nodes.

4.2 Results and discussion

As stated in Chapter 1 and Chapter 3, H_4TCPP and its derivatives are among the most widely used porphyrinic linkers employed in MOF synthesis. In Chapter 3 we synthesized two tetracarboxyl phthalocyanine linkers (**NiPcH** and **CoPcH**) as well as one Pc ligand with only the imidazole groups as coordination sites (**NiPc2)**. However, due to the low solubility of **NiPc2**, this ligand was not explored in MOF synthesis. **NiPcH** and **CoPcH** are geometrically and chemically similar to the H_4TCPP linkers (π-conjugated, planar, and with four carboxylic acid groups). Therefore, we would expect these linkers to act in a similar way and produce similar MOF structures to their porphyrin counterparts. As such, we explored the synthesis of PcMOFs with different node precursors, under various conditions with **NiPcH** linker. The aim was to explore the reaction space associated with this linker to determine if, and how these MOFs can be formed. Therefore, the synthesis of PcMOFs was explored with Zr^{4+} salts to examine zirconium cluster-based MOFs.

Considering the hard Lewis-base character of carboxylate ligands and the hard Lewis-acid character of high-valent metal cations such as Zr^{4+}, the field of Zr-based porphyrinic MOFs is rich with a large diversity of MOF structures. Some examples of these porphyrinic MOFs are discussed in Chapter 1. Considering all these examples, we embarked on the synthesis of PcMOFs with potentially similar structure to their porphyrinic analogues. For this purpose, we used **NiPcH** as linker in our synthesis.

In this thesis, we use the **Pc*M*MOF*n*** as the generic notation for these PcMOFs. In this notation, ***M*** is the metal ion used as the inorganic building block, and ***n*** is a code that refers to the synthesis condition for a given ***M***. For example, **PcZrMOF16** and **PcZrMOF17** differ on the synthesis conditions that can be found in the according table (Table 4.2 in this example). Since all the MOF syntheses were performed with **NiPcH**, **Pc*M*MOF*n*** refers to the **NiPc*M*MOF*n***.

4.2.1 Synthesis of Zirconium cluster-containing Pc MOFs (PcZrMOFs)

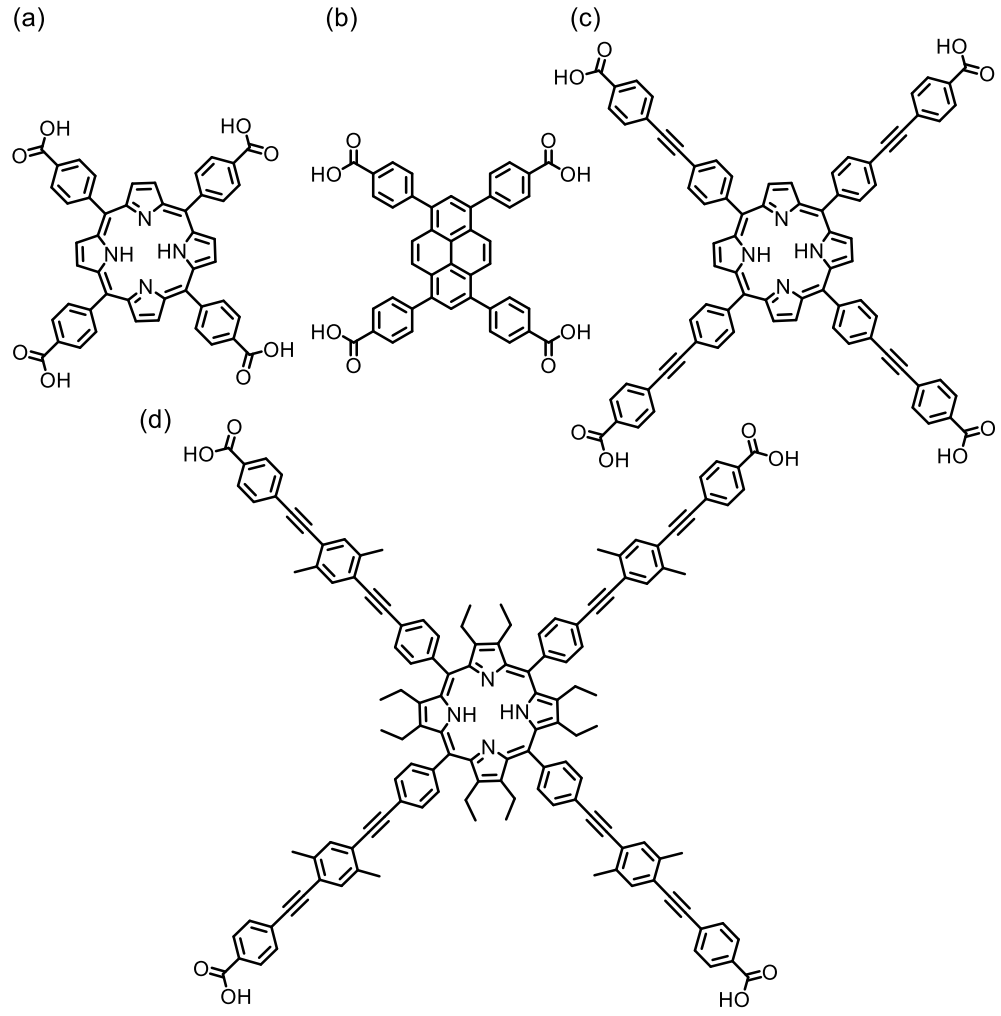

Figure 4.3 (a) H_4TCPP linker used to make PCN-222 in reference 42. (b) H_4TBAPy linker used to make NU-1000 in reference 172. (c) H_4Por-PTP linker used to make NU-1104 in reference 57. (d) H_4TCP-3 linker used in the synthesis of PCN-230 in reference 38.

The reaction space for the formation of zirconium-containing MOFs is extremely large. To help narrow down where to start, we started with the synthetic procedure of some Zr-based MOFs that utilizes tetratopic linkers like the Pc linker (Figure 4.3 and Table 4.1); we rationalized that our linker would potentially generate topologically similar MOFs. We began by utilizing the synthetic conditions for PCN-222.[42] We subsequently explored the synthesis of NU-1000 which

procedurally is very similar to that of PCN-222,[172] then we investigated synthesis conditions of NU-1104 which is prepared similarly to NU-1000.[57] For all these MOFs, benzoic acid is used as a modulator. Finally, we explored the synthesis conditions of PCN-230 which uses acetic acid as modulator.[38]

Table 4.1 Reaction conditions for the synthesis of some Zr-based MOFs with tetratopic carboxylate ligands.

	Mod[a]:Zr:L Mole ratio	**Zr source**	**[Mod., Zr, L[b]] (mM)**	**Solvent**	**Temp. (°C)**	**Time (h)**	**SSA[c] (m^2/g)**	**Ref.**
PCN-222	388:5.1:1	$ZrCl_4$	2763, 38, 7.4	DEF	120	48	2283	42
NU-1000	381:5.2:1	$ZrOCl_2 \cdot 8H_2O$	2763, 38, 7.3	DMF	100	16	2315	172
NU-1104	490:5.0:1	$ZrOCl_2 \cdot 8H_2O$	613, 6.3, 1.3	DMF	120	48	6231	57
PCN-230	674[d]:6.2:1	$ZrCl_4$	2912, 27, 4.3	DMF	120	24	4455	38

[a] modulator
[b] ligand
[c] specific surface area
[d] acetic acid is used as modulator

As a starting point for the synthesis of PcZrMOFs, we explored the synthetic conditions used to make PCN-222. Briefly, PCN-222 is made using $ZrCl_4$, H_4TCPP, and benzoic acid, mixed in DEF in a screw-top glass vial. The vial is sonicated to dissolve the solids and then heated in an oven at 120 °C for 48 h. Details of this procedure are presented in Table 4.1. Using this procedure with our linker instead of H_4TCPP, resulted in a product which was not porous (**PcZrMOF8** in Table A1.1 in the Appendix 1). Moving forward from these initial results, we opted to change the parameters to see if this procedure would be better optimized through controlled variations. With this in mind, we kept the mole ratios of benzoic acid, zirconium salt, and the ligand as per the original PCN-222 procedure. We explored the role of two different zirconium starting materials ($ZrCl_4$, and $ZrOCl_2 \cdot 8H_2O$), two different solvents (DMF and DEF), different concentration,

different temperature (90-140 °C), and different reaction time (48-72 h). As shown in Appendix 1 all the reaction conditions led to materials that showed no evidence of notable porosity.

Table 4.2 PcZrMOF synthesis conditions. DMF is used as solvent. $ZrCl_4$ used as Zr source unless otherwise indicated.

	SSA[a] (m^2/g)	BA[b]:Zr:NiPcH mole ratio	[HCl] (mM)	[NiPcH] (mM)	Temp. (°C)	Time (h)
PcZrMOF16[c]	127	381:5.2:1	-	1.8	100	16
PcZrMOF17	402	508:5.2:1	-	1.2	120	48
PcZrMOF18	180	508:5.2:1	777	1.2	120	48
PcZrMOF19	345	508:5.2:1	233	1.2	120	48
PcZrMOF20	445	508:5.2:1	-	1.2	120	72
PcZrMOF21	486	508:5.2:1	19	1.2	120	72
PcZrMOF22	795	508:5.2:1	39	1.2	120	72
PcZrMOF23	673	508:5.2:1	39	1.2	120	120
PcZrMOF24	542	508:5.2:1	39	0.40	120	72
PcZrMOF25	715	254:5.2:1	39	1.2	120	72
PcZrMOF26	615	00:5.2:1	39	1.2	120	72
PcZrMOF27	117	508:3.0:1	39	1.2	120	72
PcZrMOF28	1100	508:10.3:1	39	1.2	120	72
PcZrMOF29	811	1267:10.3:1	39	1.2	120	72
PcZrMOF30	622	508:10.3:1	87	1.2	120	72
PcZrMOF31[d]	1221	508:10.3:1	39	1.2	120	72

[a] specific surface area
[b] benzoic acid
[c] $ZrOCl_2 \cdot 8H_2O$ used
[d] sonicated for one hour

Since PCN-222 synthesis procedure didn't produce porous material with our linker, we explored a synthetic procedure that forms NU-1000. NU-1000 and PCN-222 have identical structures, but the linkers are different (Figure 4.3a *vs.* b), and the synthesis procedure is slightly different. Briefly, the synthesis of NU-1000 is as follows. $ZrOCl_2 \cdot 8H_2O$ and benzoic acid are mixed in DMF in a screw-top glass vial then the vial is sonicated to dissolve the solids. The vial is then placed in an oven at 80 °C for one hour. After cooling down to room temperature, H_4TBAPy (Figure 4.3 b) is added to the solution followed by sonicating the mixture for 10 min, finally the vial is placed in an oven at 100 °C for 16 h. Details of this procedure are presented in Table 4.1. Synthesis of PcZrMOF with this procedure and same mole ratio but using our linker instead of

H_4TBAPy and diluting the mixture produced a porous material (**PcZrMOF16** in Table 4.2), but the surface area was lower than expected (127 m^2/g) in comparison with what was observed for NU-1000, which uses the shorter H_4TBAPy linker (2300 m^2/g).

With the observation that the procedure for NU-1000 led to our first successful gas adsorption data, we used this as a starting point to improve our results. Looking at NU-1102 and NU-1104 synthesis procedures that use extended porphyrinic ligands, we started to explore the reaction space around these reaction conditions.[57] Briefly, the synthetic procedure for the synthesis of NU-1104 is as follows. $ZrOCl_2 \cdot 8H_2O$ and benzoic acid are mixed in DMF in a screw-top glass vial then the vial is sonicated to dissolve the solids. The vial is placed in an oven at 80 °C for one hour. After cooling down to room temperature H_4Por-PTP (Figure 4.3c) is added to the solution followed by sonicating the mixture for 10 min, finally the vial is placed in an oven at 120 °C for 48 h. Details of this procedure are presented in Table 4.1. In a similar procedure, with the same mole ratios, we used our linker and $ZrCl_4$. As shown in row 2 of Table 4.2 this procedure resulted in a surface area of almost 400 m^2/g (**PcZrMOF17**). With our newfound success, we continued to explore the reaction parameters to determine if we can increase the surface area. Doing the same reaction under acidic conditions (e.g., by adding concentrated HCl) caused a reduction in surface area (**PcZrMOF18**). However, as the concentration of acid was decreased from 777 mM to 233 mM and subsequently down to 39 mM, albeit with increased reaction time, we observed an increase in the surface area to nearly 800 m^2/g (**PcZrMOF22**). Further decreasing the HCl concentration to 19 mM decreased the surface area, indicating that there is an optimal amount of acid necessary to optimize the reaction conditions.

To explore the role of reaction time, we examined the initial reaction (**PcZrMOF16**) under different reaction times. As shown in Table 4.2 by comparing **PcZrMOF17** and **PcZrMOF20**,

the surface area was slightly increased when the time was increased from 48 to 72 h. However, comparing **PcZrMOF23** and **PcZrMOF22**, where 39 mM of HCl was used and the reaction was changed from 72 to 120 h, the surface area decreased. This suggests that there is an optimal reaction time around 72 h.

Based on the surface areas of other Zr-based MOFs (around 2300 m^2/g for PCN-222 and NU-1000, and 6230 m^2/g for NU-1104) that have tetratopic carboxylic acid-based linkers with geometrical structures similar to **NiPcH**, we expect a much higher surface area than what we obtained thus far. With that in mind, we continued to investigate the effect of changing the synthesis parameters. While keeping other parameters constant and similar to the synthetic conditions of **PcZrMOF22**, which thus far resulted in the highest surface area, we changed one parameter at a time to see how the surface area change. Several attempts were made by decreasing the reagents concentration (**PcZrMOF24**), decreasing the amount of benzoic aid (**PcZrMOF25** and **PcZrMOF26**), and decreasing the amount of Zr salt (**PcZrMOF27**). However, all these changes resulted products with lower surface areas than the original **PcZrMOF22**. However, the effect of decreasing the amount of Zr salt (relative to other reagents in the reaction mixture) was the most severe one (**PcZrMOF27**). This indicated that the reaction is extremely sensitive to the amount of zirconium salt used.

In observing the importance of zirconium salt stoichiometry in the reaction conditions; we turned our attention to exploring the optimal zirconium mole ratio. By doubling the amount of zirconium (**PcZrMOF28**), a surface area of 1100 m^2/g was observed. Attempts to re-optimize these reaction conditions by increasing the amount of benzoic acid by 2.5 times, decreased the surface area to almost 800 m^2/g (**PcZrMOF29**). Doubling the HCl concentration to match the increase in zirconium resulted in a decrease in surface area by almost half (**PcZrMOF30**). This

suggests that the role of acid/benzoic acid is likely in proportion to the amount of linker and not to the amount of zirconium.

One of the challenges with Pcs is that they aggregate in solution. While forming a MOF with Pcs prevents aggregation, the act of forming the MOF requires that these aggregates are broken up. To that end, we examined the role of increasing the sonication time on the reaction conditions. Rather than the standard 10 minutes used up until now, we sonicated the reaction for 60 minutes. The resultant surface area for the reaction increased to almost 1200 m^2/g (**PcZrMOF31**), while only a modest change, it clearly delineates the need to reduce aggregation as much as possible.

We also investigated reaction conditions based on other porphyrinic MOFs with zirconium based SBU procedures. One of these conditions was based on the procedure for preparing PCN-230. Briefly, preparation of PCN-230 is as follows. $ZrCl_4$, H_4TCP-3 (Figure 4.3d), acetic acid (as a modulator), and DMF are mixed in a vial and dissolved with the aid of sonication. The resultant mixture is heated at 120 °C for 24 h. Details of this procedure are presented in Table 4.1. This procedure with our **NiPcH** linker resulted **PcZrMOF35** (Table 4.3). After activating with supercritical carbon dioxide, the surface area of the product was almost 700 m^2/g. When we kept the mole ratio as that of **PcZrMOF35**, but changed other parameters indicated in Table 4.3. The result was a product (**PcZrMOF34**) with a slightly higher surface area of almost 750 m^2/g. We also used L-proline as a modulator (**PcZrMOF36**), which other researchers have had great success with.[158, 160] Alternatively, pyridine was added to the reaction mixture to prevent aggregation of **NiPcH** and improve the solubility of the ligand (**PcZrMOF37**). We also tried an alternative procedure to PCN-222 that involves different mole ratios than the original PCN-222 synthesis (**PcZrMOF38**).[42] Other research groups have had success with using DMSO as a solvent/co-

solvent in MOF synthesis (e.g., ZIF-8, ZIF-67, HKUST-1).[150-152] With that in mind, we tested the solubility of **NiPcH** in DMSO and noticed that **NiPcH** stays in solution even after being exposed to prolonged heating in the oven (under similar MOF synthesis conditions) while **NiPcH** dissolved in DMF tends to aggregate under similar conditions. With this success, we utilized DMSO as a co-solvent with DMF in **PcZrMOF** synthesis (**PcZrMOF32** and **PcZrMOF33**). In every example in Table 4.3, none of these measures gave surface area higher than 763 m^2/g.

Table 4.3 PcZrMOF synthesis conditions. DMF is used as solvent and $ZrCl_4$ as Zr source unless otherwise indicated. BA stands for benzoic acid, AA stands for acetic acid, and Pyr for pyridine.

	SSA[a] (m^2/g)	**Mod[b]:Zr: NiPcH mole ratio**	**[HCl] (mM)**	**Other conditions**	**[NiPcH] (mM)**	**Temp. (°C)**	**Time (h)**
PcZrMOF32	638[sc]	508:10.3:1	23	Mod. = BA 65% DMSO, 35% DMF, $ZrOCl_2 \cdot 8H_2O$	1.2	120	72
PcZrMOF33	632[sc]	508:10.3:1	39	Mod. = BA 75% DMSO, 25% DMF $ZrOCl_2 \cdot 8H_2O$	1.2	120	72
PcZrMOF34	763	724:6.4:1	-	Mod. = AA 2% water, 1 h sonication	1.2	150	72
PcZrMOF35	709[sc]	724:6.4:1	-	Mod. = AA	4.1	120	24
PcZrMOF36	334	5.0:3.0:1	93	Mod. = L-proline	4.3	120	48
PcZrMOF37	616	508:5.2:1	-	Mod. = BA Pyr.[c]:NiPcH mole ratio 2.2:1	1.2	120	48
PcZrMOF38	435	536:7.8:1	125	Mod. = BA	5.2	120	24
PcZrMOF39	429	1267:10.3:1	87	Mod. = BA	1.2	120	72
PcZrMOF40	644	264:10.3:1	93	Mod. = BA	5.8	120	64
PcZrMOF41	467	381:5.2:1	117	Mod. = BA $ZrOCl_2 \cdot 8H_2O$	7.3	150	21

[a] specific surface area
[b] modulator
sc = activated by supercritical CO_2

To get a better understanding of the materials that were being made, we examined the gas adsorption properties of the MOFs in more detail. While Table 4.2 and Table 4.3 contain the experimentally determined surface area, there is considerably more that can be learned from the isotherm data. The nitrogen gas adsorption isotherms for **PcZrMOF28**, **PcZrMOF31**, **PcZrMOF40**, and **PcZrMOF41** are shown in Figure 4.4. The shape of these isotherms (reaching almost plateau in the low-pressure region but close to $P/P^0 = 0.1$) suggests the synthesized material is microporous but it also contains larger micropores. As such, pore size distribution (PSD) calculated from these isotherms (using density functional theory (DFT) fitted with the Tarazona model) show the presence of two kinds of pores. Figure 4.5 shows the PSD obtained from the isotherms of the initial success (**PcZrMOF16**, SSA = 127 m^2/g) as well as the PSD for MOFs with intermediate surface areas (**PcZrMOF21**, **PcZrMOF22**, **PcZrMOF23**, and **PcZrMOF36**), and the highest surface area material (**PcZrMOF31**, SSA = 1221 m^2/g). (PSD obtained from the isotherms of the rest of the PcZrMOFs are in Appendix 2). As it can be seen, in all these MOF samples, there are pores of two sizes with the majority centered around 10 and 20 Å. We observe that although pore sizes are almost in the same range, both the small and the large pores are clogged in **PcZrMOF16**. If we look at the intermediate values, we observe that pores are less clogged compared with the low surface area material, but these pores are still clogged compared with the higher surface area materials. This indicates that although isotherms for these PcZrMOFs show different nitrogen uptakes and the MOFs have varying surface areas, the pore sizes are all very similar but it's the clogged pores that cause the difference between calculated surface areas. This observation indicates that PcZrMOF samples that we synthesised probably share same structures.

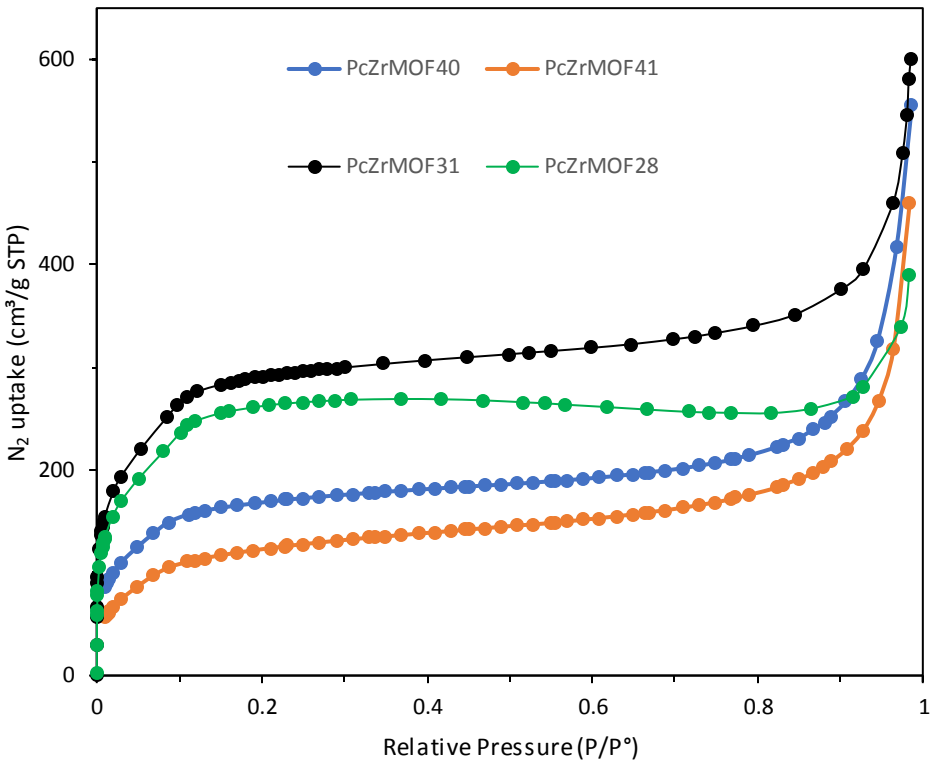

Figure 4.4 N_2 gas adsorption isotherms, measured at 77 K, for some of the PcZrMOF samples.

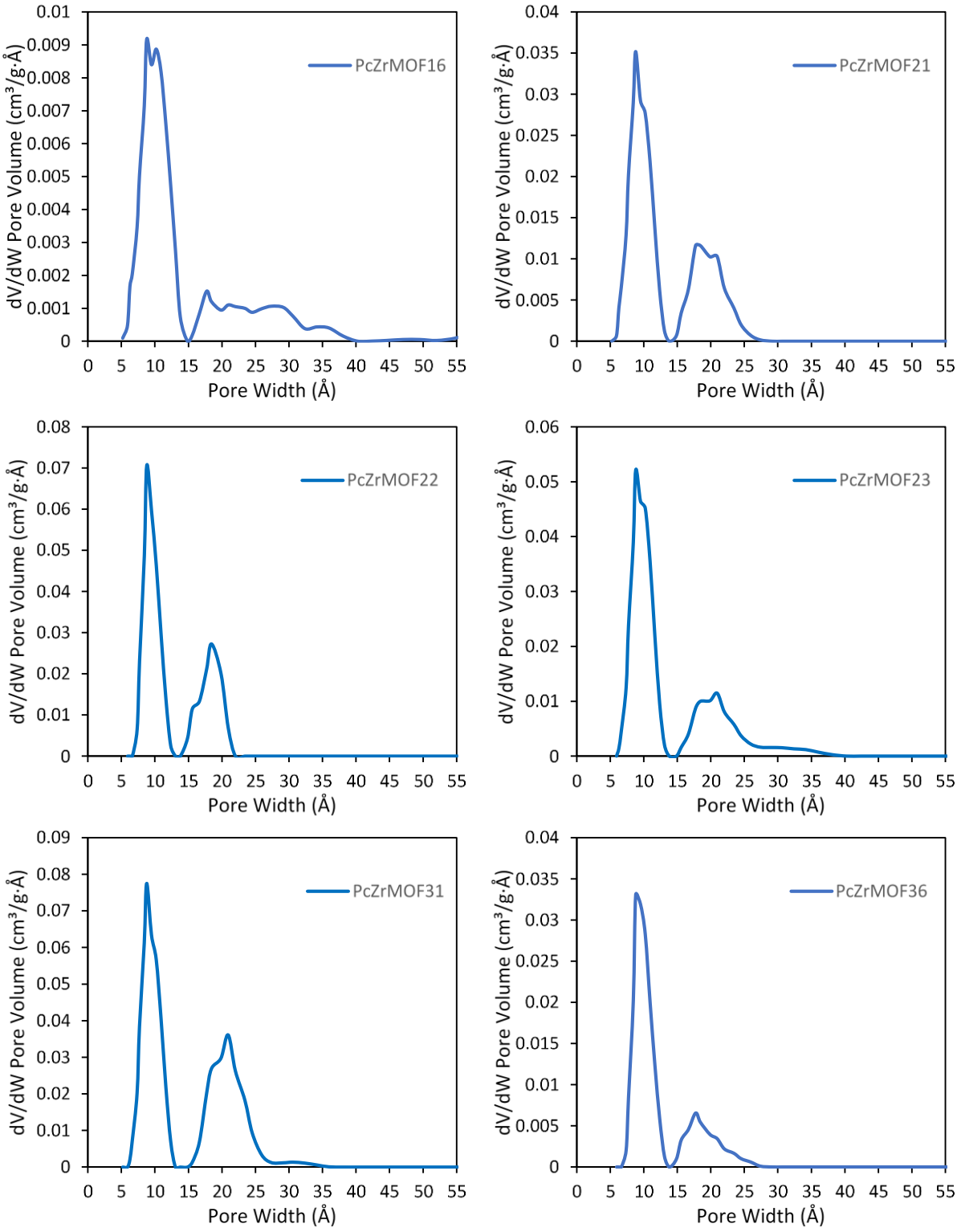

Figure 4.5 DFT Pore size distribution calculated for some of the PcZrMOFs.

With all the different observed surface areas, but relatively similar pore size distributions, we turned our attention to PXRD to look at the structural features of these MOFs. Comparison between PXRDs of PcZrMOFs (Figure 4.6) obtained from different synthesis methods show that all these PcZrMOF samples share similar features. This indicates that different reaction conditions resulted a MOF with same structure, even though they have different surface areas. Thus, the surface area problems are likely due to the presence of impurities (internal to the MOF or external to the crystal), but not due to the formation of different MOFs/non-porous coordination polymers.

In order to investigate the effect of activation procedure (solvent exchange followed by thermal activation) on the MOF, PXRD of **PcZrMOF31** before and after thermal activation was measured (Figure 4.7). This comparison shows that the activation does not affect the crystallinity and the PcZrMOF structure remains intact during the activation process. This suggests that the materials we are making are stable to thermal activation.

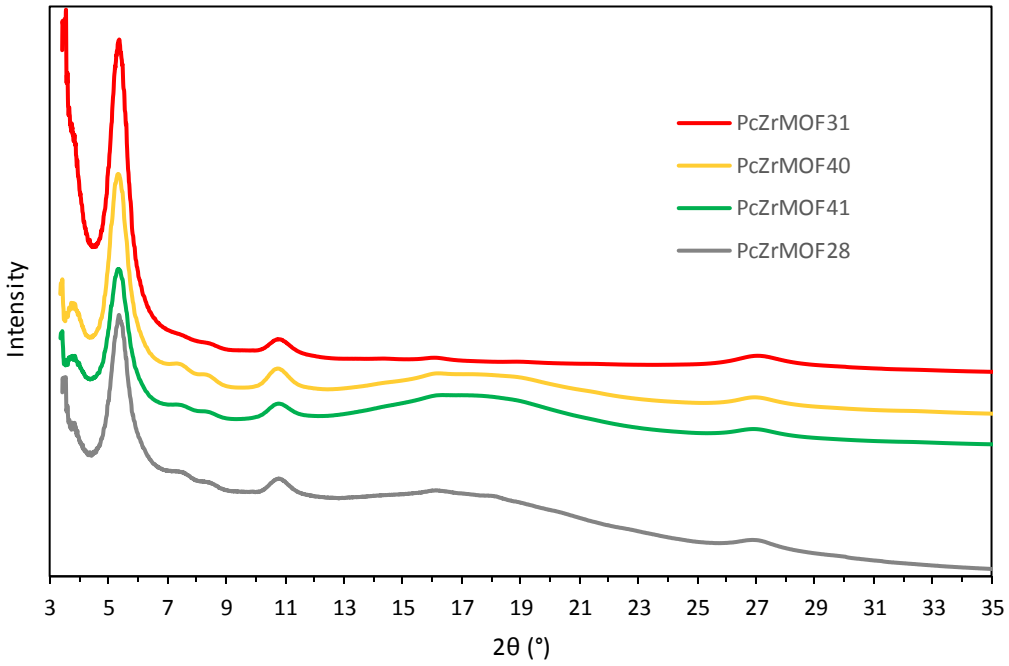

Figure 4.6 PXRD of some of the activated PcZrMOFs that have different surface areas.

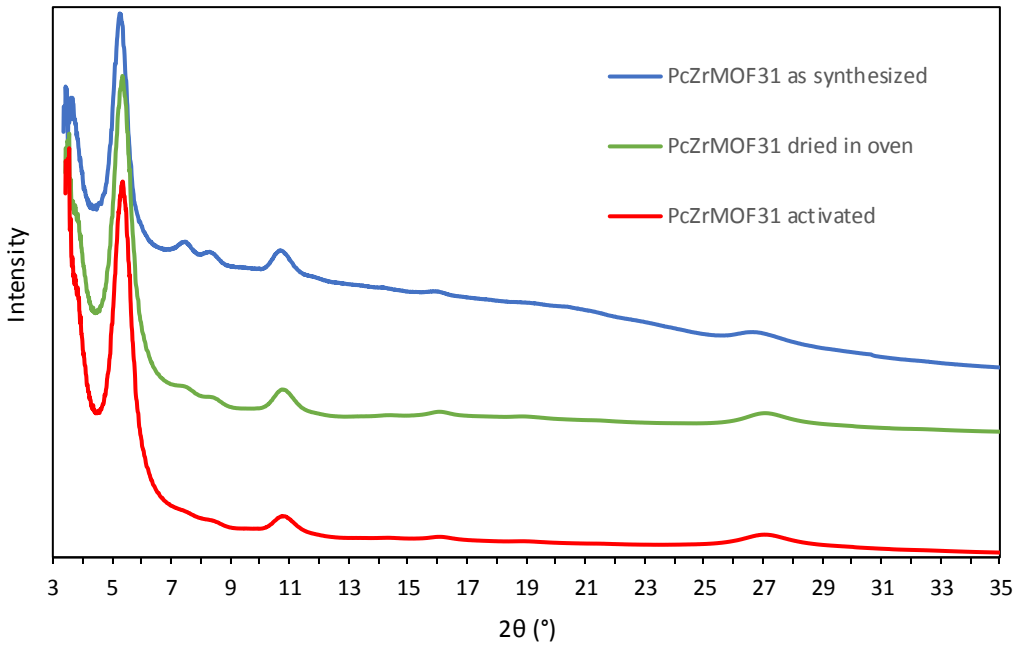

Figure 4.7 PXRD of **PcZrMOF31**.

To further probe the nature of the X-ray diffraction pattern, we examined the PXRD of **NiPcH** (i.e., the free linker). We examined the as-synthesized linker as well as the linker after exposing the linker to the MOF reaction conditions, but in the absence of zirconium. Figure 4.8 compares **PcZrMOF40** and the PXRD of the control experiment. At first glance, it can be seen that the more intense peaks in the diffractogram are only present in the MOF and thus represent the MOF and not the linker. Upon closer investigation, there exists a Bragg diffraction around 27° in 2θ in the diffractogram of both MOF and linker sample. This indicates that **NiPcH** is present in the PcZrMOF sample. Diffraction at this angle correlates to d-spacing of 3.3 Å. This distance is within the acceptable range for stacking of Pcs. For example, similar distances were reported in 2-D PcMOFs.[81-83, 86-90, 92] Therebefore, the MOF sample might be contaminated with stacked aggregated **NiPcH** impurity.

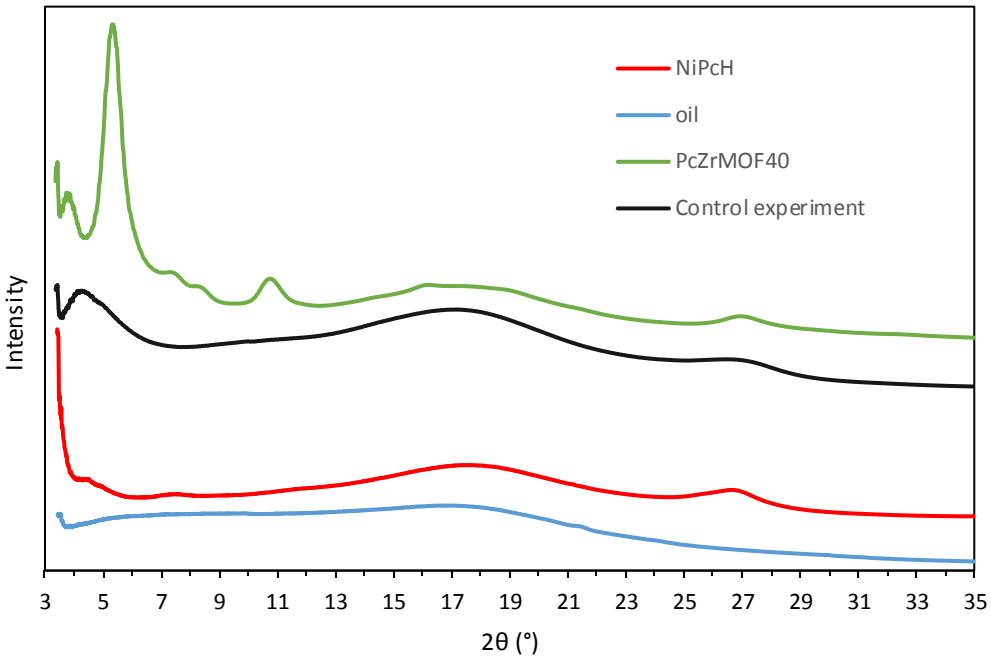

Figure 4.8 PXRD of **PcZrMOF40** and comparison with control experiment, ligand, Paratone oil, and **NiPcH**.

The fact that PXRD of PcZrMOF samples obtained from different reaction conditions share similar features is an encouraging result and may suggest that **NiPcH** is more likely to make phase-pure MOF than its porphyrin counterpart. For example, PCN-221,[173] PCN-222,[42] PCN-223,[174] PCN-224,[175] PCN-225,[176] and MOF-525[39] are made of the same starting materials (H_4TCPP linker and Zr node) under very similar reaction conditions (with varying ratios of modulator:metal:ligand, and different reaction times). However, despite all our attempts to make the target MOF, we only see one phase. In the mentioned examples of PCN-22x (where x = 1, 2, 3, 4, 5) and MOF-525, the structural differences that lead to the different topologies is due to the rotation of the benzoate in $TCPP^{4-}$ relative to the $TCPP^{4-}$ core (Figure 1.20 in Chapter1). This feature enables multiple structures to be formed based on the synthetic conditions. In the case of **NiPcH**, despite several different reaction conditions that we attempted, the PXRD and gas adsorption data suggests that only one phase.

Given that the pore size distribution and the X-ray diffraction patterns illustrate that the structure of the MOF is unchanged, it is worth comparing our data to the available MOF structures in the literature. It has been shown in literature that when the tetratopic carboxylate-based pyrene and porphyrin ligands are extended, the resultant MOFs have a cubic network (PCN-228 to PCN-230,[38] and NU-1101 to NU-1104,[57]). In these extended ligands, the benzoate is free to stay in the plane of the core porphyrin (ligand in NU-1102 is shown in Figure 4.9 as an example) as it is opposed to $TCPP^{4-}$ where the benzoate is under torsion stress if is in the plane of porphyrin, as a result, with 12-connected Zr_6 SBU, formation of cubic network is more favorable with these extended ligands, and the mentioned MOFs are obtained as the only products. This is in contrast to $TCPP^{4-}$ that requires energetically demanding conformation in the cubic network. Similarly, **NiPcH** can make cubic framework isostructural with NU-1102.

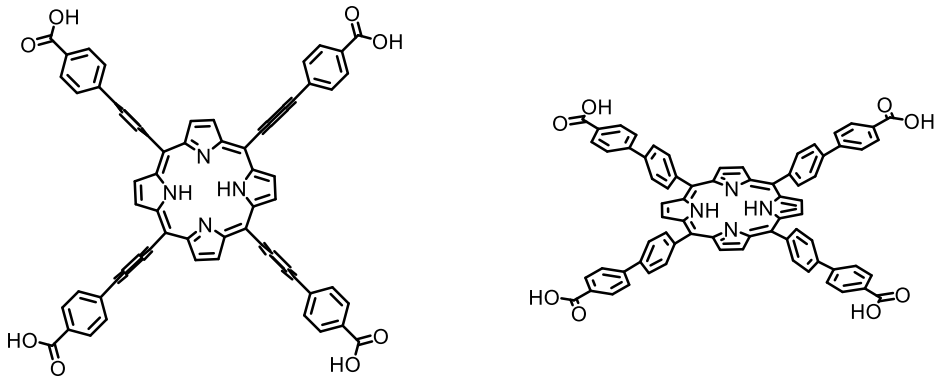

Figure 4.9 The linker used in the synthesis of NU-1102 in reference 57 shown from two different perspectives. This figure shows how the benzoate is free to stay in the plane of core porphyrin.

4.3 Conclusion

The synthesis of PcMOFs was explored using **NiPcH** as linker and two Zr^{4+} salts. We explored the synthesis of PcMOFs under various conditions. The aim was to explore the reaction space associated with **NiPcH** to determine if, and how, PcMOFs can be formed. These conditions include

temperature, different ligand and node precursor concentration and ratios, reaction time, use of different modulators and the modulator concentration, use of varying concentrations of hydrochloric acid as additive, use of different solvents and solvents mixture, and sonication of the reaction mixture. With **NiPcH** linker, PXRD and N_2 gas adsorption of the synthesized MOF samples were evaluated as our metric for the quality of the material. As such, the highest BET surface area for PcMOF was 1220 m^2/g. PSD and PXRD analysis show that the synthesized materials that were obtained under different reaction conditions share similar features in terms of pore size distribution and diffraction pattern. This finding suggests that when a porous material was obtained, the synthesis procedure could produce the same material (phase) although they have different surface areas. Therefore, increasing the surface area of PcMOF synthesized from **NiPcH** and Zr nodes requires removal of the unreacted starting materials to free the pores of the material.

4.4 Experimental Details

4.4.1 General procedures, materials, and instrumentation

Reagents and solvents were purchased from commercial sources and used without Purification.

Nitrogen gas adsorption isotherm measurements were performed at 77 K on a Micromeritics TriStar II surface area and porosity analyzer. All the samples were activated before colleting isotherm data on Micromeritics Smart VacPrep instrument.

PXRD patterns were obtained using a Rigaku XtaLAB Synergy-S X-ray diffractometer equipped with a 4-circle Kappa goniometer, dual PhotonJet sources (Cu and Mo), a HyPix-6000HE Hybrid Photon Counting detector, and an Oxford Cryosystems 800 Series Cryostream. Our measurements were performed at room temperature with Cu Kα (1.54178 Å) as the radiation source.

4.4.2 Synthesis of PcZrMOFs

A general synthesis procedure is described below. Synthetic procedure for **PcZrMOF31** is provided as an example. Details for the synthesis of other PcZrMOFs is provided in Table 4.4. In all the experiments (unless otherwise indicated in the other conditions column in Table 4.4) **NiPcH** (35.2 mg, 0.0290 mmol) was used as ligand, benzoic acid as modulator, DMF as solvent, and the synthesis was done in a 50 mL screw-top glass jar. Synthesis of PcZrMOFs that don't fit into the mentioned categories are described separately.

$ZrCl_4$ should be stored is a glovebox or desiccator. When we repeated the **PcZrMOF29** synthesis with an old $ZrCl_4$ sample, the product had a very low surface area of 125 m^2/g.

4.4.2.1 General synthesis procedure of PcZrMOFs

Zr^{4+} salt, modulator, and solvent were added to a screw-top vessel. The mixture was then sonicated for 10 min to give a clear colorless solution. The sealed vessel was placed in an oven at 80 °C for 1 h. Once removed from the oven, the vessel was left to cool down to room temperature, then **NiPcH** was added to the solution followed by adding concentrated HCl (if indicated). The mixture was then sonicated for 10 min (60 min for **PcZrMOF31**). The vessel was placed in an oven. The vessel containing the solution and the precipitate was removed from the oven and was set aside to cool to room temperature, then the wash procedure was done followed by the mentioned activation method (see below for the wash and activation procedures).

Example: Synthesis of PcZrMOF31: 70.0 mg $ZrCl_4$ (0.300 mmol), 1.800 g benzoic acid (14.74 mmol), and 24.0 mL DMF were added to a 50 mL screw-top glass jar. The resulting mixture was sonicated for 10 min to give a clear colorless solution, and this solution was heated in an oven at 80 °C for 1 h. Once removed from the oven, the jar was left to cool down to room temperature. Subsequently, 35.2 mg **NiPcH** (0.0290 mmol) was added to the solution, followed by 80 μL

concentrated HCl. The mixture was then sonicated for 1 h. This mixture was then placed in an oven at 120 °C for 72 h. Once completed, the resulting light green solution and green precipitate was removed from the oven and allowed to cool to room temperature, then the wash procedure was done followed by the thermal activation (see below) to give 32.2 mg of a dark solid with a measured BET surface area of 1221 m^2/g was obtained.

Table 4.4 Synthesis conditions of PcZrMOFs. For the synthesis of all the PcZrMOFs, 35.2 mg **NiPcH** was used except for those mentioned in the other conditions column. The reaction was done in 50 mL screw-top glass jar and $ZrCl_4$ was used as Zr source unless otherwise indicated.

	Zr salt (mg)	**BA[a] (mg)**	**HCl (µL)**	**DMF (mL)**	**Other conditions**	**Temp. (°C)**	**Time (h)**	**Mass of MOF (mg)**
PcZrMOF1	35	1350	-	4.0	15 mL vial	140	120	22.5
PcZrMOF2	35	1350	-	-	4 mL DEF 15 mL vial	140	72	21.0
PcZrMOF3	48	1350	-	-	4 mL DEF 15 mL vial $ZrOCl_2•8H_2O$	140	72	19.9
PcZrMOF4	35	1350	-	-	4 mL DEF 15 mL vial	120	72	20.4
PcZrMOF5	35	1350	-	4.0	15 mL vial	120	72	27.3
PcZrMOF6	48	1350	-	-	4 mL DEF 15 mL vial $ZrOCl_2•8H_2O$	120	72	18.1
PcZrMOF7	48	1350	-	4.0	15 mL vial $ZrOCl_2•8H_2O$	120	72	29.8
PcZrMOF8	22	845	-		22 mg **NiPcH** 2.5 mL DEF 7 mL vial	120	48	16.0
PcZrMOF9	48	1350	-	4.0	15 mL vial $ZrOCl_2•8H_2O$	110	48	19.0
PcZrMOF10	35	1350	-	4.0	15 mL vial	90	72	24.1
PcZrMOF11	35	1350	-	8.0	15 mL vial	140	72	34.0
PcZrMOF12	35	1350	-	8.0	15 mL vial	120	120	27.9
PcZrMOF13	35	1350	-	8.0	15 mL vial	120	72	29.3
PcZrMOF14	35	1350	-	16.0		140	120	41.0
PcZrMOF15	35	1350	-	16.0		140	72	42.0
PcZrMOF16	49	1350	-	16.0	$ZrOCl_2•8H_2O$	100	16	34.8
PcZrMOF17	35	1800	-	24.0	$ZrOCl_2•8H_2O$	120	48	30.1
PcZrMOF18	35	1800	1600	24.0	$ZrOCl_2•8H_2O$	120	48	26.2
PcZrMOF19	35	1800	480	24.0	$ZrOCl_2•8H_2O$	120	48	29.7
PcZrMOF20	35	1800	-	24.0		120	72	21.9
PcZrMOF21	35	1800	40	24.0		120	72	24.4
PcZrMOF22	35	1800	80	24.0		120	72	18.4

	Zr salt (mg)	BA[a] (mg)	HCl (µL)	DMF (mL)	Other conditions	Temp. (°C)	Time (h)	Mass of MOF (mg)
PcZrMOF23	35	1800	80	24.0		120	120	25.0
PcZrMOF24	35	1800	240	72.0	250 mL jar	120	72	27.0
PcZrMOF25	35	900	80	24.0		120	72	29.0
PcZrMOF26	35	-	80	24.0		120	72	17.0
PcZrMOF27	20	1800	80	24.0		120	72	21.0
PcZrMOF28	70	1800	80	24.0		120	72	16.0
PcZrMOF29	70	4488	80	24.0		120	72	20.2
PcZrMOF30	70	1800	180	24.0		120	72	21.0
PcZrMOF31	70	1800	80	24.0	60 min sonic.	120	72	32.2
PcZrMOF32	39	720	20	3.5	6.5 mL DMSO 14 mg **NiPcH** 25 mL jar $ZrOCl_2•8H_2O$	120	72	35.4
PcZrMOF33	97	1800	80	6.0	18 mL DMSO $ZrOCl_2•8H_2O$	120	72	18.0
PcZrMOF34	44	-	-	22.8	1.2 ml acetic acid 10 drops water 1 h sonic.	150	72	44.3
PcZrMOF35	43	-	-	5.8	1.2 mL acetic acid 15 mL vial	120	24	20.6
PcZrMOF36	20	-	80	10.0	167 mg L- proline	120	48	30.0
PcZrMOF37	35	1800	-	24.0	Pyridine added	120	48	26.6
PcZrMOF38	53	1898	60	5.6	Heated in Oil bath	120	24	16.2
PcZrMOF39	70	4488	180	24.0		120	72	17.0
PcZrMOF40	70	935	40	5.0	15 mL vial	120	64	28.1
PcZrMOF41	48	1350	40	4.0	15 mL vial $ZrOCl_2•8H_2O$	150	21	21.3
PcZrMOF42[b]	35	4488	80	24.0		120	72	15.3
PcZrMOF43[b]	35	4488	140	24.0		120	72	16.3
PcZrMOF44[b]	70	4488	40	24.0		120	72	16.7
PcZrMOF45[b]	35	1800	180	24.0		120	72	19.1
PcZrMOF46[b]	70	1800	80	24.0		120	48	21.1
PcZrMOF47[b]	97	1800	80	24.0	$ZrOCl_2•8H_2O$	120	72	44.0
PcZrMOF48[b]	35	-	80	24.0		120	72	45.1
PcZrMOF49[b]	35	-	-	23.0	1 mL acetic acid	120	24	39.0

[a] benzoic acid

[b] ligand was not fully deprotected. The product was non-porous

4.4.2.2 Synthesis procedure for other PcZrMOFs that don't fit into the described method above

Synthesis of PcZrMOF32: 38.8 mg $ZrOCl_2•8H_2O$ (0.120 mmol), 0.720 g benzoic acid (5.90 mmol), 6.5 mL DMSO, and 3.5 mL DMF added into a 25 mL screw-top glass jar followed by sonication for 10 min. The jar was then placed in an oven at 80 °C for 1 h. After cooling down to room temperature, 14.0 mg **NiPcH** (0.0116 mmol) was added to the solution followed by adding

20 μL concentrated HCl. Then the jar was sonicated for 45 min. The jar containing a dark green solution was placed in an oven at 120 °C for 72 h. The jar containing a dark green solid suspended in the solution was removed from the oven and was set aside to cool to room temperature, then the wash procedure was done followed by $scCO_2$ procedure (see below) to give 35.4 mg of a dark solid with a measured BET surface area of 638 m^2/g.

Synthesis of PcZrMOF33: 35.2 mg **NiPcH** (0.0290 mmol), 2.5 mL DMF, and 7.5 mL DMSO were added into a 15 mL vial, then 80 μL concentrated HCl was added into the vial. The vial was sonicated for 1 h. In a separate 50 mL jar, 97.0 mg $ZrOCl_2 \cdot 8H_2O$ (0.301 mmol), 1.800 g benzoic acid (14.74 mmol), 10.5 mL DMSO, and 3.5 mL were mixed followed by sonication for 10 min. The jar was placed in an oven at 80 °C for 1 h, after which the contents of the first vial was transferred into the second jar (while the solution was still warm). The jar was then placed in an oven at 120 °C for 72 h. The jar containing a dark green solid suspended in the solution was removed from the oven and was set aside to cool to room temperature, then the wash procedure was done followed by $scCO_2$ procedure (see below) to give 18.0 mg of a dark solid with a measured BET surface area of 632 m^2/g.

Synthesis of PcZrMOF34: 43.5 mg $ZrCl_4$ (0.187 mmol), 22.8 mL DMF, 35.2 mg **NiPcH** (0.0290 mmol), 1.2 mL acetic acid (21 mmol), and 500 μL water were added to a 50 mL screw-top glass jar, the mixture was sonicated for 1 h, then the jar was placed in an oven at 150 °C for 72 h. The jar containing a clear colorless solution and a dark green precipitate was removed from the oven and was set aside to cool to room temperature, then the wash procedure was done followed by thermal activation (see below) to give 44.3 mg of a dark solid with BET surface area of 763 m^2/g.

Synthesis of PcZrMOF35: 43.5 mg (0.187 mmol) $ZrCl_4$, 5.8 mL DMF, 35.2 mg (0.0290 mmol) **NiPcH**, and 1.2 mL (21 mmol) acetic acid, was added to a 15 mL screw-top glass vial, the mixture was sonicated for 10 min, then the vial was placed in an oven at 120 °C for 24 h. The vial containing a clear colorless solution and a dark green precipitate was removed from the oven and was set aside to cool to room temperature, then the wash procedure was done followed by $scCO_2$ procedure (see below) to give 20.6 mg dark solid with a measured BET surface area of 709 m^2/g.

Synthesis of PcZrMOF36: (modified procedure reported by Gutov *et. al* [160]) 20.3 mg $ZrCl_4$ (0.0871 mmol), 50.0 mg L-proline (0.434 mmol), and 10.0 mL DMF were added to a 50 mL screw-top glass jar, then 80 µL concentrated HCl was added to the jar. The jar was sonicated for 5 min then 35.2 mg **NiPcH** (0.0290 mmol) was added to the solution followed by 5 min sonication, then 10.0 mL DMF was added to the jar then the solution was sonicated for another 5 min before placing the jar in 120 °C oven for 48 h. The jar containing a light green solution and a green precipitate was removed from the oven and was left to cool to room temperature, then the wash procedure was done followed by the thermal activation (see below) to give 30.0 mg of a dark solid with a measured BET surface area of 334 m^2/g.

Synthesis of PcZrMOF37: 20 µL pyridine (12 mg, 0.15 mmol) was added to 45.0 mL DMF, then 19.0 mL of this solution (containing 5.0 mg, 0.063 mmol pyridine) was transferred into a 50 mL screw-top glass jar. 35.2 mg **NiPcH** (0.0290 mmol) was added to the jar followed by sonicating for 10 min, then the jar was placed in an oven at 80 °C for 1 h. In a second 50 mL screw-top glass jar, 35.0 mg $ZrCl_4$ (0.150 mmol), 1.800 g benzoic acid (14.74 mmol), and 5.0 mL DMF were added, then the jar was placed in 80 °C oven for 1 h. While the solution in both jars was hot, the contents of the first jar was emptied to the second one, then the second jar was placed in 120 °C oven for 48 h. The jar containing a light yellow-brown solution and a dark green precipitate was

removed from the oven and was left to cool to room temperature, then the wash procedure was done followed by thermal activation (see below) to give 26.6 mg of a dark solid with a measured BET surface area of 616 m^2/g.

Synthesis of PcZrMOF38: 52.7 mg $ZrCl_4$ (0.226 mmol), 1.898 g benzoic acid (15.54 mmol), 5.6 mL DMF, 35.2 mg **NiPcH** (0.0290 mmol), and a magnetic stir bar were added to a 20 mL microwave vial followed by adding 60 µL concentrated HCl. The vial was sealed (cap and crimp) then sonicated for 10 min before heating in an oil bath at 120 °C using a hot plate equipped with a temperature probe. The vial was removed from the oil bath after 24 h and was left to cool to room temperature, then the wash procedure was done followed by the thermal activation (see below) to give 16.2 mg of a dark solid with a measured BET surface area of 435 m^2/g.

4.4.2.3 Wash procedure for all PcMOFs

The steps with the following order were performed as the wash procedure.

(**I**). Once the reaction vial was cooled, the contents of the vial were emptied into a centrifuge tube and centrifuged at 5500-7500 rpm for 5-15 min (i.e., until the particles settled at the bottom). The mother liquor was carefully decanted.

(**II**). 15 mL of DMF was added to the centrifuge tube, the centrifuge tube was shaken well and subsequently centrifuged at 5500-7500 rpm for 5-15 min. This procedure was repeated a total of three times.

(**III**). 15 mL of fresh DMF was added to the centrifuge tube followed by shaking the centrifuge tube vigorously. The capped centrifuge tube was left overnight. The following morning, the centrifuge tube was centrifuged at 5500-7500 rpm for 5-15 min, and the solution was subsequently decanted.

(**IV**). 15 mL of acetone was added to the centrifuge tube. The centrifuge tube was shaken well and once again centrifuged at 5500-7500 rpm for 5-15 min and subsequently decanted. The procedure of adding acetone, shaking, centrifuging, and decanting was repeated a total of three times.

(**V**). 15 mL of fresh acetone was added to the centrifuge tube followed by shaking and the centrifuge tube was left capped overnight. The next morning the centrifuge tube was centrifuged, and the solvent was decanted.

Note: For **PcZrMOF16**, an alternative wash procedure was used which is similar to established protocol for NU-1000).[172] The first three steps are identical to the previous steps (**I-III**) discussed above. After this step, the solid in the centrifuge tube was transferred into a 15 mL vial with 7 mL DMF. Subsequently, 270 μL of 8 M HCl aqueous solution was added into the vial followed by shaking. The vial was placed in an oven at 100 °C for 12 h. Then steps **I** to **V** were performed on the sample.

4.4.3 Activation of PcMOFs

4.4.3.1 Thermal activation procedure

After the wash procedure, the centrifuge tube was placed in a vacuum oven at 80 °C overnight. The dried MOF sample was transferred into a sample holder for a Micromeritics gas adsorption instrument. The sample in the sample holder was activated on Micromeritics Smart VacPrep instrument. For this purpose, the sample tube was first heated to 90 °C (5 °C/min) while slowly evacuating (5 mmHg/s), then it was held for 30 min at this temperature and low pressure. Then, the sample tube was heated to 120 °C (5 °C /min) and maintained at this temperature for 10 h. Finally, the sample tube was cooled down to room temperature then it was backfilled with nitrogen gas.

4.4.3.2 Supercritical CO_2 activation procedure

After the wash procedure, the solid was transferred into a critical point drier sample holder. Anhydrous ethanol was carefully added to the sample holder to fully cover the solid and fill the sample holder. The sample holder was then covered by a watch glass and was left overnight to ensure the pores of the MOF were properly exchanged for ethanol since the instrument cannot be used with acetone, or other incompatible solvents, in the pores. The solution was carefully replaced with fresh anhydrous ethanol three times a day for three days. Afterwards, ethanol was removed leaving only the bare minimum ethanol necessary to cover the material. The sample holder was loaded into the activation chamber of a Tousimis™ Samdri® PVT-30 critical point drier instrument. The chamber was slowly filled with liquid CO_2 during which the temperature was maintained between 0-10 °C to avoid solidifying CO_2 or forming scCO_2. The chamber was exchanged with liquid CO_2 to exchange ethanol with liquid CO_2 during which the flow of CO_2 inlet and outlet was adjusted to maintain the level of liquid CO_2 constant inside the chamber. The process of liquid exchange was repeated every 2 h. Once the solvent was exchanged 3x to remove as much ethanol as possible, the instrument was heated to 40 °C while maintaining a pressure around 1400 psi (±100 psi). At this stage, all the remaining liquid CO_2 becomes a supercritical fluid (CO_2 critical point is 31 °C at 1073 psi). The chamber was maintained in super critical conditions for 1 h. Subsequently, the supercritical fluid was slowly exhausted at a flow rate of 1 cm^3/min to slowly release CO_2 from the chamber. Once completed, the sample was removed from the chamber, and it was degassed under vacuum at room temperature for 1 h to ensure no CO_2 remained in the pores.

5 Future work

While working on projects during my PhD program, both when I was working in the lab and when I was writing my thesis, I came up with ideas for improving the results I obtained. However, due to the pandemic, and the reality that no good project is ever complete, I simply didn't have enough time to put those ideas into practice. In this chapter I will talk about these ideas.

5.1 A new macrocyclic linker

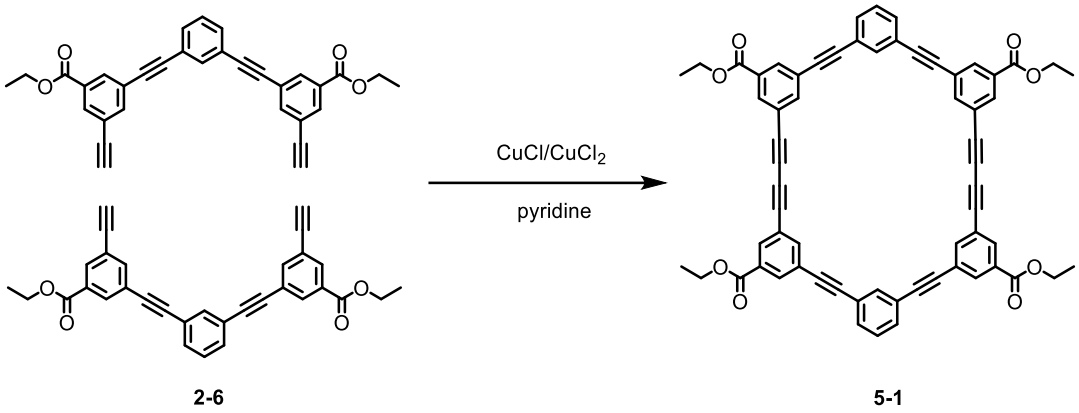

Figure 5.1 Cyclization of compound **2-6** for making a new tetratopic linker precursor **5-1**.

In Chapter 2 we synthesized two halves of the desired macrocyclic linker **2-7** (compounds **2-6** and **2-3**) and we showed that it is possible to synthesize the macrocycle compound **2-6-1**. This synthesis required 8 steps in 6 pots. Here I'm going to introduce the possibility of synthesis of a new linker (**5-1**) that has not been explored in MOF synthesis yet. Cyclization between two molecules of compound **2-6** that was synthesized in Chapter 2 can result in a new macrocyclic compound that might be of interest as a tetratopic linker (Figure 5.1). Synthesis of compound **2-6** can be achieved in 3 steps and 2 pots with overall yield of 52%; therefore, synthesis of **5-1** by coupling two **2-6** molecules would be a faster approach than the synthesis of compound **2-7**. The chemistry under which this type of coupling and cyclization occurs is already known and is reported for

macrocycles similar to compound **5-1**.[177, 178] Therefore, compound **5-1** can be made in as little as 4 steps and 3 pots with potentially good yield.

5.2 Addressing Pc linker solubility issue

In Chapter 3, we discussed the synthesis of **NiPcH**, **CoPcH**, and **NiPc2**. However, low solubility of these compounds made characterization as well as the MOF synthesis procedure difficult. Here I will briefly discuss some of the solutions that can potentially resolve the mentioned issues.

Substitution on Pc is one the straightforward methods that can be done to increase their solubility. In order to do so, we can substitute N-H proton of **3-3-2** with an alkyl group first to make **5-2** (Figure 5.2),[128, 132] then perform the tetracyclization to make the desired Pc (**5-5**) that will potentially have higher solubility than unsubstituted **MPcH**.

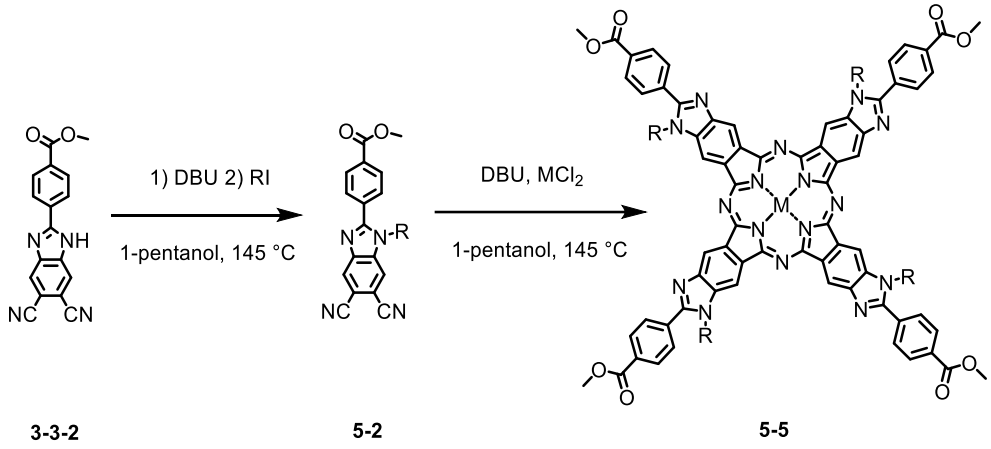

Figure 5.2 Substitution of R group on N-H of imidazole for the synthesises of Pc linkers with higher solubility.

The second approach for making the **MPcH** and **MPc2** with higher solubility is to have other metal ions (instead of Ni^{2+} and Co^{2+}) coordinated inside the cavity of Pc. Onal and co-workers reported that in their synthesized imidazophthalocyanine, when the Pc cavity is coordinated to Cu^{2+}, the molecule had higher solubility and less aggregation than the Pc molecule

with Ni^{2+} coordinated in the cavity.[124] Therefore, it is worthwhile to synthesize **CuPcH** and **CuPc2** for their higher solubility.

When M^{3+} and M^{4+} such as Al^{3+} and Si^{4+} are coordinated at the center of Pc, there would be axial ligands (X in Figure 5.3) on M or axial ligands can be substituted on M so that the steric hinderance between Pc molecules can prevent aggregation; therefore, the resultant MPc can have higher solubility (Figure 5.3).[179-181]. As such, synthesis of $MPcHX_n$ (i.e., where M = Al, n = 1 or M= Si, n = 2) can address solubility issue of our phthalocyanine linker.

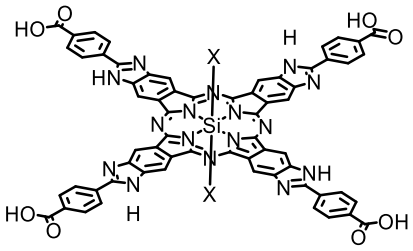

Figure 5.3 Axial substitution of X on the central metal of the Pc core to reduce aggregation and increase solubility.

5.3 Pc linker purification

For the synthesis of a good quality MOF crystals, we need to have a linker that is as pure as possible. The purification method that I used for the synthesis of **NiPcH**, **CoPcH**, and **NiPc2** was washing the product with multiple organic solvent. Although the wash protocol that I developed could remove most of the soluble impurities (which was visually inspected), there could be insoluble impurities remaining mixed with the product. There are two other methods for purification of Pcs that could potentially give a higher quality Pc. The first method is, dissolving the Pc linker in concentrated sulfuric acid and then crashing out the Pc in ice-cold water followed by washing with water.[182] The second method is sublimation of the Pc linker.[183, 184]

5.4 PcMOF synthesis

With a Pc linker that is pure and has improved solubility, synthesis of PcMOF would be potentially feasible. In addition to these, I have a few more ideas that can be employed for the synthesis of PcMOFs.

The solvent in which I synthesized the Pc linkers is 1-pentanol. In this solvent, and under the Pc synthesis conditions, Pc was fairly soluble (no significant amount of precipitate was observed) therefore, it might be worthwhile to explore PcMOF synthesis in 1-pentanol in the presence of TEA (to promote deprotonation of the linker) or in a mixture of 1-pentanol and DMF.

One of the unconventional MOF synthesis methods is mechanochemical synthesis. If solubility is a pertinent issue in synthesis, then mechanochemical synthesis might be a solution because this method doesn't need a solvent.

Linker exchange is another MOF synthesis method that is developed for MOFs that can not be synthesized otherwise.[185, 186] In this method, linker of an already existing MOF is exchanged in solution with a new linker that is dissolved in the reaction solvent. In our case, NU-1102 is a good candidate in which it might be possible to exchange the porphyrin linker with our Pc linker.

5.5 Conclusion

We have introduced a new linker to the field of MOFs. This means that there are lots of other venues can be exploited for the synthesis of new porous material. Here I talked about some of the options that can be explored in the future, but there are a lot more that future researcher can embark on exploring.

Appendix 1

Our Initial attempts for the synthesis of PcZrMOFs didn't produce a porous material. Reaction conditions under which these non-porous materials were obtained are shown in Table A.1.1

Table A 1.1 PcZrMOFs synthesis conditions that led to non-porous products. DMF was used as solvent and $ZrCl_4$ as Zr source unless otherwise indicated.

	SSA[a] (m^2/g)	**BA[b]:Zr:NiPcH mole ratio**	**[HCl] (mM)**	**Other conditions**	**[NiPcH] (mM)**	**Temp. (°C)**	**Time (h)**
PcZrMOF1	-	381:5.2:1	-		7.3	140	120
PcZrMOF2	-	381:5.2:1	-	DEF	7.3	140	72
PcZrMOF3	-	381:5.2:1	-	DEF, $ZrOCl_2 \cdot 8H_2O$	7.3	140	72
PcZrMOF4	-	381:5.2:1	-	DEF	7.3	120	72
PcZrMOF5	-	381:5.2:1	-		7.3	120	72
PcZrMOF6	-	381:5.2:1	-	DEF, $ZrOCl_2 \cdot 8H_2O$	7.3	120	72
PcZrMOF7	-	381:5.2:1	-	$ZrOCl_2 \cdot 8H_2O$	7.3	120	72
PcZrMOF8	-	381:5.2:1	-	DEF	7.3	120	48
PcZrMOF9	-	381:5.2:1	-	$ZrOCl_2 \cdot 8H_2O$	7.3	110	48
PcZrMOF10	-	381:5.2:1	-		7.3	90	72
PcZrMOF11	-	381:5.2:1	-		3.6	140	72
PcZrMOF12	-	381:5.2:1	-		3.6	120	120
PcZrMOF13	-	381:5.2:1	-		3.6	120	72
PcZrMOF14	-	381:5.2:1	-		1.8	140	120
PcZrMOF15	-	381:5.2:1	-		1.8	140	72

[a] specific surface area

[b] benzoic acid

Appendix 2

Pore size distribution that was calculated for some of the PcZrMOF samples were discussed in Chapter 4. In this appendix, PSD of other PcZrMOF samples is shown in Figure A2.1.

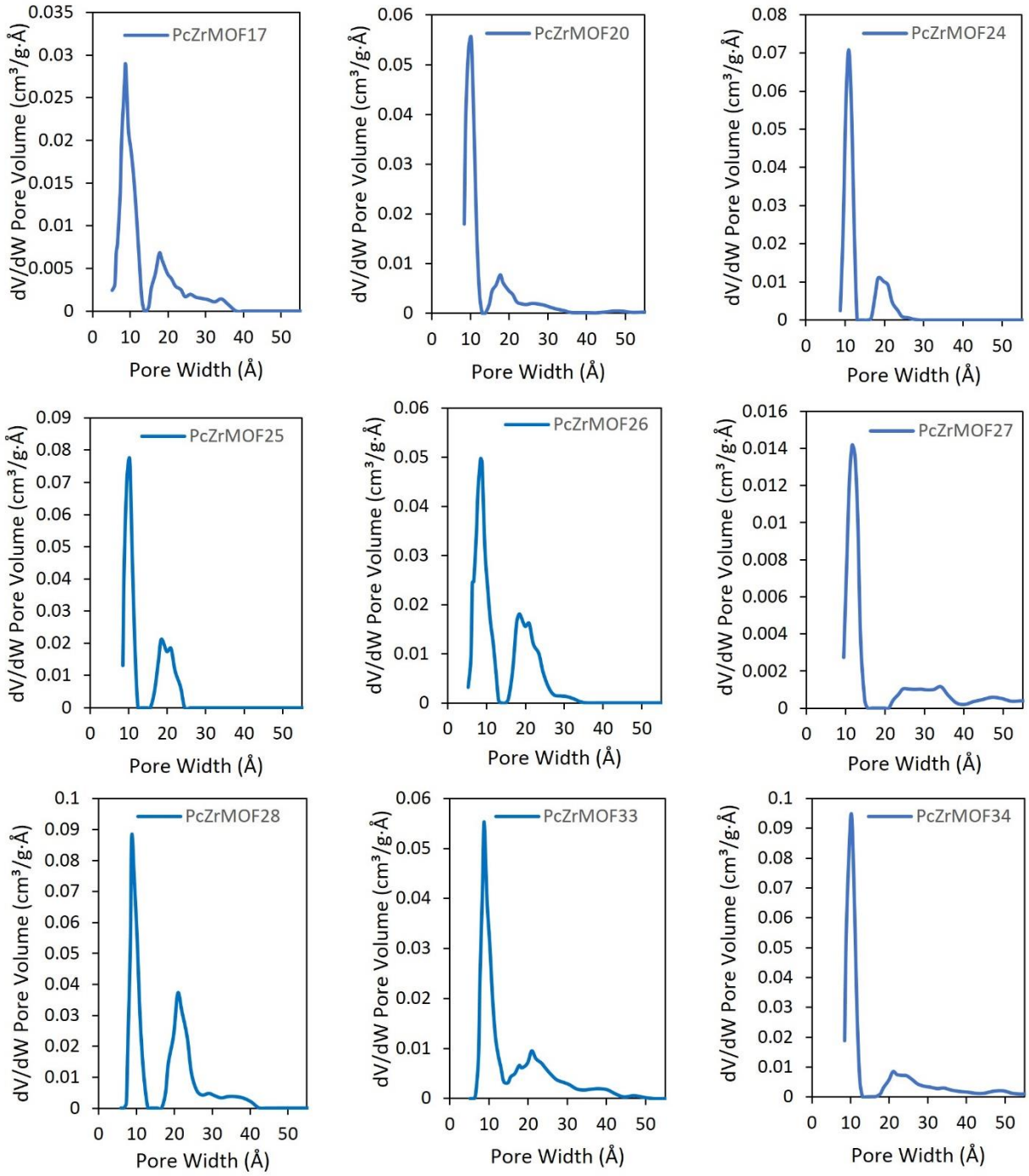

Figure A 2.1 DFT pore size distribution calculated for some of the PcZrMOFs.

References

1. Schaefer, D. W., Engineered Porous Materials. *MRS Bulletin* **1994,** *19* (4), 14-19.
2. Makal, T. A.; Li, J.-R.; Lu, W.; Zhou, H.-C., Methane storage in advanced porous materials. *Chemical Society Reviews* **2012,** *41* (23), 7761-7779.
3. Adebajo, M. O.; Frost, R. L.; Kloprogge, J. T.; Carmody, O.; Kokot, S., Porous materials for oil spill cleanup: A review of synthesis and absorbing properties. *Journal of Porous Materials* **2003,** *10* (3), 159-170.
4. Parlett, C. M. A.; Wilson, K.; Lee, A. F., Hierarchical porous materials: catalytic applications. *Chemical Society Reviews* **2013,** *42* (9), 3876-3893.
5. Valdés, M. G.; Pérez-Cordoves, A. I.; Díaz-García, M. E., Zeolites and zeolite-based materials in analytical chemistry. *TRAC Trends in Analytical Chemistry* **2006,** *25* (1), 24-30.
6. Guan, H.-Y.; LeBlanc, R. J.; Xie, S.-Y.; Yue, Y., Recent progress in the syntheses of mesoporous metal-organic framework materials. *Coordination Chemistry Reviews* **2018,** *369*, 76-90.
7. Weckhuysen, B. M.; Yu, J., Recent advances in zeolite chemistry and catalysis. *Chemical Society Reviews* **2015,** *44* (20), 7022-7024.
8. Ma, Y.; Tong, W.; Zhou, H.; Suib, S. L., A review of zeolite-like porous materials. *Microporous and Mesoporous Materials* **2000,** *37* (1), 243-252.
9. Li, Y.; Yu, J., Emerging applications of zeolites in catalysis, separation and host–guest assembly. *Nature Reviews Materials* **2021**.
10. Barrer, R. M., 435. Syntheses and reactions of mordenite. *Journal of the Chemical Society (Resumed)* **1948,** (0), 2158-2163.
11. Flanigen, E. M.; Bennett, J. M.; Grose, R. W.; Cohen, J. P.; Patton, R. L.; Kirchner, R. M.; Smith, J. V., Silicalite, a new hydrophobic crystalline silica molecular sieve. *Nature* **1978,** *271* (5645), 512-516.
12. Dusselier, M.; Davis, M. E., Small-pore zeolites: Synthesis and catalysis. *Chemical Reviews* **2018,** *118* (11), 5265-5329.
13. Narayanan, S.; Tamizhdurai, P.; Mangesh, V. L.; Ragupathi, C.; Santhana krishnan, P.; Ramesh, A., Recent advances in the synthesis and applications of mordenite zeolite – review. *RSC Advances* **2021,** *11* (1), 250-267.
14. Shamzhy, M.; Opanasenko, M.; Concepción, P.; Martínez, A., New trends in tailoring active sites in zeolite-based catalysts. *Chemical Society Reviews* **2019,** *48* (4), 1095-1149.
15. Brühwiler, D.; Calzaferri, G., Selective functionalization of the external surface of zeolite L. *Comptes Rendus Chimie* **2005,** *8* (3), 391-398.
16. Estevez, R.; Iglesias, I.; Luna, D.; Bautista, F. M., Sulfonic acid functionalization of different zeolites and their use as catalysts in the microwave-assisted etherification of glycerol with tert-butyl alcohol. *Molecules (Basel, Switzerland)* **2017,** *22* (12), 2206.
17. Vyas, R.; Kumar, S.; Kumar, S., Determination of micropore volume and surface area of zeolite molecular sieves by D-R and D-A equations: A comparative study. *Indian Journal of Chemical Technology* **2004,** *11*.
18. Bai, Y.; Dou, Y.; Xie, L.-H.; Rutledge, W.; Li, J.-R.; Zhou, H.-C., Zr-based metal-organic frameworks: design, synthesis, structure, and applications. *Chemical Society Reviews* **2016,** *45* (8), 2327-2367.

19. Lu, W.; Wei, Z.; Gu, Z.-Y.; Liu, T.-F.; Park, J.; Park, J.; Tian, J.; Zhang, M.; Zhang, Q.; Gentle III, T.; Bosch, M.; Zhou, H.-C., Tuning the structure and function of metal-organic frameworks via linker design. *Chemical Society Reviews* **2014,** *43* (16), 5561-5593.
20. Wang, K.; Feng, D.; Liu, T.-F.; Su, J.; Yuan, S.; Chen, Y.-P.; Bosch, M.; Zou, X.; Zhou, H.-C., A series of highly stable mesoporous metalloporphyrin Fe-MOFs. *Journal of the American Chemical Society* **2014,** *136* (40), 13983-13986.
21. Zhou, H.-C.; Long, J. R.; Yaghi, O. M., Introduction to metal-organic frameworks. *Chemical Reviews* **2012,** *112* (2), 673-674.
22. Furukawa, H.; Cordova, K. E.; O'Keeffe, M.; Yaghi, O. M., The chemistry and applications of metal-organic frameworks. *Science* **2013,** *341* (6149), 1230444.
23. Li, H.; Eddaoudi, M.; O'Keeffe, M.; Yaghi, O. M., Design and synthesis of an exceptionally stable and highly porous metal-organic framework. *Nature* **1999,** *402* (6759), 276-279.
24. Natarajan, S.; Mahata, P., Non-carboxylate based metal-organic frameworks (MOFs) and related aspects. *Current Opinion in Solid State and Materials Science* **2009,** *13* (3), 46-53.
25. Ghasempour, H.; Wang, K.-Y.; Powell, J. A.; ZareKarizi, F.; Lv, X.-L.; Morsali, A.; Zhou, H.-C., Metal-organic frameworks based on multicarboxylate linkers. *Coordination Chemistry Reviews* **2021,** *426*, 213542.
26. Ali Akbar Razavi, S.; Morsali, A., Linker functionalized metal-organic frameworks. *Coordination Chemistry Reviews* **2019,** *399*, 213023.
27. Couck, S.; Denayer, J. F. M.; Baron, G. V.; Rémy, T.; Gascon, J.; Kapteijn, F., An amine-functionalized MIL-53 metal−organic framework with large separation power for CO_2 and CH_4. *Journal of the American Chemical Society* **2009,** *131* (18), 6326-6327.
28. Yee, K.-K.; Reimer, N.; Liu, J.; Cheng, S.-Y.; Yiu, S.-M.; Weber, J.; Stock, N.; Xu, Z., Effective mercury sorption by thiol-laced metal-organic frameworks: in strong acid and the vapor Phase. *Journal of the American Chemical Society* **2013,** *135* (21), 7795-7798.
29. Griffin, S. L.; Champness, N. R., A periodic table of metal-organic frameworks. *Coordination Chemistry Reviews* **2020,** *414*, 213295.
30. Britt, D.; Furukawa, H.; Wang, B.; Glover, T. G.; Yaghi, O. M.; Halpern, J., Highly efficient separation of carbon dioxide by a metal-organic framework replete with open metal sites. *Proceedings of the National Academy of Sciences of the United States of America* **2009,** *106* (49), 20637-20640.
31. Ding, M.; Cai, X.; Jiang, H.-L., Improving MOF stability: approaches and applications. *Chemical Science* **2019,** *10* (44), 10209-10230.
32. Cavka, J. H.; Jakobsen, S.; Olsbye, U.; Guillou, N.; Lamberti, C.; Bordiga, S.; Lillerud, K. P., A new zirconium inorganic building brick forming metal organic frameworks with exceptional stability. *Journal of the American Chemical Society* **2008,** *130* (42), 13850-13851.
33. Winarta, J.; Shan, B.; McIntyre, S. M.; Ye, L.; Wang, C.; Liu, J.; Mu, B., A decade of UiO-66 research: A historic review of dynamic structure, synthesis mechanisms, and characterization techniques of an archetypal metal-organic framework. *Crystal Growth & Design* **2020,** *20* (2), 1347-1362.
34. Xiao, T.; Liu, D., The most advanced synthesis and a wide range of applications of MOF-74 and its derivatives. *Microporous and Mesoporous Materials* **2019,** *283*, 88-103.
35. Kökçam-Demir, Ü.; Goldman, A.; Esrafili, L.; Gharib, M.; Morsali, A.; Weingart, O.; Janiak, C., Coordinatively unsaturated metal sites (open metal sites) in metal-organic frameworks: design and applications. *Chemical Society Reviews* **2020,** *49* (9), 2751-2798.

36. Isaeva, V. I.; Kustov, L. M., The application of metal-organic frameworks in catalysis (Review). *Petroleum Chemistry* **2010,** *50* (3), 167-180.
37. Yaghi, O. M.; O'Keeffe, M.; Ockwig, N. W.; Chae, H. K.; Eddaoudi, M.; Kim, J., Reticular synthesis and the design of new materials. *Nature* **2003,** *423* (6941), 705-714.
38. Liu, T.-F.; Feng, D.; Chen, Y.-P.; Zou, L.; Bosch, M.; Yuan, S.; Wei, Z.; Fordham, S.; Wang, K.; Zhou, H.-C., Topology-guided design and syntheses of highly stable mesoporous porphyrinic zirconium metal-organic frameworks with high surface area. *Journal of the American Chemical Society* **2015,** *137* (1), 413-419.
39. Morris, W.; Volosskiy, B.; Demir, S.; Gándara, F.; McGrier, P. L.; Furukawa, H.; Cascio, D.; Stoddart, J. F.; Yaghi, O. M., Synthesis, structure, and metalation of two new highly porous zirconium metal-organic frameworks. *Inorganic Chemistry* **2012,** *51* (12), 6443-6445.
40. Eddaoudi, M.; Moler, D. B.; Li, H.; Chen, B.; Reineke, T. M.; O'Keeffe, M.; Yaghi, O. M., Modular chemistry: Secondary building units as a basis for the design of highly porous and robust metal−organic carboxylate frameworks. *Accounts of Chemical Research* **2001,** *34* (4), 319-330.
41. Fang, Q.-R.; Makal, T. A.; Young, M. D.; Zhou, H.-C., Recent advances in the study of mesoporous metal-organic frameworks. *Comments on Inorganic Chemistry* **2010,** *31* (5-6), 165-195.
42. Feng, D.; Gu, Z.-Y.; Li, J.-R.; Jiang, H.-L.; Wei, Z.; Zhou, H.-C., Zirconium-metalloporphyrin PCN-222: Mesoporous metal-organic frameworks with ultrahigh stability as biomimetic catalysts. *Angewandte Chemie International Edition* **2012,** *51* (41), 10307-10310.
43. Stock, N.; Biswas, S., Synthesis of metal-organic frameworks (MOFs): Routes to various MOF topologies, morphologies, and composites. *Chemical Reviews* **2012,** *112* (2), 933-969.
44. Schweighauser, L.; Harano, K.; Nakamura, E., Experimental study on interconversion between cubic MOF-5 and square MOF-2 arrays. *Inorganic Chemistry Communications* **2017,** *84*, 1-4.
45. Chui, S. S.-Y.; Lo, S. M.-F.; Charmant, J. P. H.; Orpen, A. G.; Williams, I. D., A Chemically Functionalizable Nanoporous Material. *Science* **1999,** *283* (5405), 1148-1150.
46. Xuan, W.; Zhu, C.; Liu, Y.; Cui, Y., Mesoporous metal-organic framework materials. *Chemical Society Reviews* **2012,** *41* (5), 1677-1695.
47. Eddaoudi, M.; Kim, J.; Rosi, N.; Vodak, D.; Wachter, J.; O'Keeffe, M.; Yaghi, O. M., Systematic design of pore size and functionality in isoreticular MOFs and their application in methane storage. *Science* **2002,** *295* (5554), 469-472.
48. Mai, Z.; Liu, D., Synthesis and applications of isoreticular metal-organic frameworks IRMOFs-n (n = 1, 3, 6, 8). *Crystal Growth & Design* **2019,** *19* (12), 7439-7462.
49. Furukawa, H.; Ko, N.; Go, Y. B.; Aratani, N.; Choi, S. B.; Choi, E.; Yazaydin, A. Ö.; Snurr, R. Q.; O'Keeffe, M.; Kim, J.; Yaghi, O. M., Ultrahigh porosity in metal-organic frameworks. *Science* **2010,** *329* (5990), 424-428.
50. Hönicke, I. M.; Senkovska, I.; Bon, V.; Baburin, I. A.; Bönisch, N.; Raschke, S.; Evans, J. D.; Kaskel, S., Balancing mechanicalstability and ultrahigh porosity in crystalline framework materials. *Angewandte Chemie International Edition* **2018,** *57* (42), 13780-13783.
51. Furukawa, H.; Müller, U.; Yaghi, O. M., "Heterogeneity within order" in metal-organic frameworks. *Angewandte Chemie International Edition* **2015,** *54* (11), 3417-3430.
52. Thomas, A., Much ado about nothing – a decade of porous materials research. *Nature Communications* **2020,** *11* (1), 4985.

53. Liu, D.; Zou, D.; Zhu, H.; Zhang, J., Mesoporous metal-organic frameworks: Synthetic strategies and emerging applications. *Small* **2018,** *14* (37), 1801454.
54. Deng, H.; Grunder, S.; Cordova, K. E.; Valente, C.; Furukawa, H.; Hmadeh, M.; Gándara, F.; Whalley, A. C.; Liu, Z.; Asahina, S.; Kazumori, H.; O'Keeffe, M.; Terasaki, O.; Stoddart, J. F.; Yaghi, O. M., Large-pore apertures in a series of metal-organic frameworks. *Science* **2012,** *336* (6084), 1018-1023.
55. Mondloch, J. E.; Bury, W.; Fairen-Jimenez, D.; Kwon, S.; DeMarco, E. J.; Weston, M. H.; Sarjeant, A. A.; Nguyen, S. T.; Stair, P. C.; Snurr, R. Q.; Farha, O. K.; Hupp, J. T., Vapor-phase metalation by atomic layer deposition in a metal-organic framework. *Journal of the American Chemical Society* **2013,** *135* (28), 10294-10297.
56. Li, P.; Chen, Q.; Wang, T. C.; Vermeulen, N. A.; Mehdi, B. L.; Dohnalkova, A.; Browning, N. D.; Shen, D.; Anderson, R.; Gómez-Gualdrón, D. A.; Cetin, F. M.; Jagiello, J.; Asiri, A. M.; Stoddart, J. F.; Farha, O. K., Hierarchically engineered mesoporous metal-organic frameworks toward cell-free immobilized enzyme systems. *Chem* **2018,** *4* (5), 1022-1034.
57. Wang, T. C.; Bury, W.; Gómez-Gualdrón, D. A.; Vermeulen, N. A.; Mondloch, J. E.; Deria, P.; Zhang, K.; Moghadam, P. Z.; Sarjeant, A. A.; Snurr, R. Q.; Stoddart, J. F.; Hupp, J. T.; Farha, O. K., Ultrahigh surface area zirconium MOFs and insights into the applicability of the BET theory. *Journal of the American Chemical Society* **2015,** *137* (10), 3585-3591.
58. Maldonado, R. R.; Zhang, X.; Hanna, S.; Gong, X.; Gianneschi, N. C.; Hupp, J. T.; Farha, O. K., Squeezing the box: isoreticular contraction of pyrene-based linker in a Zr-based metal-organic framework for Xe/Kr separation. *Dalton Transactions* **2020,** *49* (20), 6553-6556.
59. Gutov, O. V.; Bury, W.; Gomez-Gualdron, D. A.; Krungleviciute, V.; Fairen-Jimenez, D.; Mondloch, J. E.; Sarjeant, A. A.; Al-Juaid, S. S.; Snurr, R. Q.; Hupp, J. T.; Yildirim, T.; Farha, O. K., Water-stable zirconium-based metal-organic framework material with high-surface area and gas-storage capacities. *Chemistry – A European Journal* **2014,** *20* (39), 12389-12393.
60. Chen, T.-H.; Popov, I.; Chuang, Y.-C.; Chen, Y.-S.; Miljanić, O. Š., A mesoporous metal-organic framework based on a shape-persistent macrocycle. *Chemical Communications* **2015,** *51* (29), 6340-6342.
61. Chen, T.-H.; Popov, I.; Miljanić, O. Š., A zirconium macrocyclic metal-organic framework with predesigned shape-persistent apertures. *Chemistry – A European Journal* **2017,** *23* (2), 286-290.
62. Zhang, X.; Wasson, M. C.; Shayan, M.; Berdichevsky, E. K.; Ricardo-Noordberg, J.; Singh, Z.; Papazyan, E. K.; Castro, A. J.; Marino, P.; Ajoyan, Z.; Chen, Z.; Islamoglu, T.; Howarth, A. J.; Liu, Y.; Majewski, M. B.; Katz, M. J.; Mondloch, J. E.; Farha, O. K., A historical perspective on porphyrin-based metal-organic frameworks and their applications. *Coordination Chemistry Reviews* **2021,** *429*, 213615.
63. De, S.; Devic, T.; Fateeva, A., Porphyrin and phthalocyanine-based metal organic frameworks beyond metal-carboxylates. *Dalton Transactions* **2021,** *50* (4), 1166-1188.
64. Huh, S.; Kim, S.-J.; Kim, Y., Porphyrinic metal-organic frameworks from custom-designed porphyrins. *CrystEngComm* **2016,** *18* (3), 345-368.
65. Pereira, C. F.; Simões, M. M. Q.; Tomé, J. P. C.; Almeida Paz, F. A., Porphyrin-based metal-organic frameworks as heterogeneous catalysts in oxidation reactions. *Molecules (Basel, Switzerland)* **2016,** *21* (10), 1348.
66. Younis, S. A.; Lim, D.-K.; Kim, K.-H.; Deep, A., Metalloporphyrinic metal-organic frameworks: Controlled synthesis for catalytic applications in environmental and biological media. *Advances in Colloid and Interface Science* **2020,** *277*, 102108.

67. Abrahams, B. F.; Hoskins, B. F.; Michail, D. M.; Robson, R., Assembly of porphyrin building blocks into network structures with large channels. *Nature* **1994,** *369* (6483), 727-729.
68. Lin, K. J., SMTP-1: The first functionalized metallo-porphyrin molecular sieves with large channels. *Angewandte Chemie - International Edition* **1999,** *38* (18), 2730-2732.
69. Hagrman, D.; Hagrman, P. J.; Zubieta, J., Solid-state coordination chemistry: The self-assembly of microporous organic-inorganic hybrid framework constructed from tetrapyridylprophyrin and bimetallic oxide chains or oxide cluster. *Angewandte Chemie - International Edition* **1999,** *38* (21), 3165-3168.
70. Fateeva, A.; Chater, P. A.; Ireland, C. P.; Tahir, A. A.; Khimyak, Y. Z.; Wiper, P. V.; Darwent, J. R.; Rosseinsky, M. J., A water-stable porphyrin-based metal-organic framework active for visible-light photocatalysis. *Angewandte Chemie International Edition* **2012,** *51* (30), 7440-7444.
71. Yu, K.; Won, D.-I.; Lee, W. I.; Ahn, W.-S., Porphyrinic zirconium metal-organic frameworks: Synthesis and applications for adsorption/catalysis. *Korean Journal of Chemical Engineering* **2021,** *38* (4), 653-673.
72. Lin, Q.; Bu, X.; Kong, A.; Mao, C.; Zhao, X.; Bu, F.; Feng, P., New heterometallic zirconium metalloporphyrin frameworks and their heteroatom-activated high-surface-area carbon derivatives. *Journal of the American Chemical Society* **2015,** *137* (6), 2235-2238.
73. de la Torre, G.; Claessens, C. G.; Torres, T., Phthalocyanines: old dyes, new materials. Putting color in nanotechnology. *Chemical Communications* **2007,** (20), 2000-2015.
74. Aykanat, A.; Meng, Z.; Benedetto, G.; Mirica, K. A., Molecular engineering of multifunctional metallophthalocyanine-containing framework materials. *Chemistry of Materials* **2020,** *32* (13), 5372-5409.
75. Kluson, P.; Drobek, M.; Kalaji, A.; Karaskova, M.; Rakusan, J., Preparation, chemical modification and absorption properties of various phthalocyanines. *Research on Chemical Intermediates* **2009,** *35* (1), 103-116.
76. Claessens, C. G.; Hahn, U.; Torres, T., Phthalocyanines: From outstanding electronic properties to emerging applications. *The Chemical Record* **2008,** *8* (2), 75-97.
77. Lü, C.-X.; Zhan, G.-P.; Chen, K.; Liu, Z.-K.; Wu, C.-D., Anchoring Zn-phthalocyanines in the pore matrices of UiO-67 to improve highly the photocatalytic oxidation efficiency. *Applied Catalysis B: Environmental* **2020,** *279*, 119350.
78. Qiao, G.-Y.; Yuan, S.; Pang, J.; Rao, H.; Lollar, C. T.; Dang, D.; Qin, J.-S.; Zhou, H.-C.; Yu, J., Functionalization of zirconium-based metal-organic layers with tailored pore environments for heterogeneous catalysis. *Angewandte Chemie International Edition* **2020,** *59* (41), 18224-18228.
79. Peng, J.; Wei, L.; Liu, Y.; Zhuge, W.; Huang, Q.; Huang, W.; Xiang, G.; Zhang, C., Novel porous iron phthalocyanine based metal-organic framework electrochemical sensor for sensitive vanillin detection. *RSC Advances* **2020,** *10* (60), 36828-36835.
80. Nagatomi, H.; Yanai, N.; Yamada, T.; Shiraishi, K.; Kimizuka, N., Synthesis and electric properties of a two-dimensional metal-organic framework based on phthalocyanine. *Chemistry – A European Journal* **2018,** *24* (8), 1806-1810.
81. Jia, H.; Yao, Y.; Zhao, J.; Gao, Y.; Luo, Z.; Du, P., A novel two-dimensional nickel phthalocyanine-based metal-organic framework for highly efficient water oxidation catalysis. *Journal of Materials Chemistry A* **2018,** *6* (3), 1188-1195.
82. Zhong, H.; Ly, K. H.; Wang, M.; Krupskaya, Y.; Han, X.; Zhang, J.; Zhang, J.; Kataev, V.; Büchner, B.; Weidinger, I. M.; Kaskel, S.; Liu, P.; Chen, M.; Dong, R.; Feng, X., A

phthalocyanine-based layered two-dimensional conjugated metal-organic framework as a highly efficient electrocatalyst for the oxygen reduction reaction. *Angewandte Chemie International Edition* **2019,** *58* (31), 10677-10682.
83. Yang, C.; Dong, R.; Wang, M.; Petkov, P. S.; Zhang, Z.; Wang, M.; Han, P.; Ballabio, M.; Bräuninger, S. A.; Liao, Z.; Zhang, J.; Schwotzer, F.; Zschech, E.; Klauss, H.-H.; Cánovas, E.; Kaskel, S.; Bonn, M.; Zhou, S.; Heine, T.; Feng, X., A semiconducting layered metal-organic framework magnet. *Nature Communications* **2019,** *10* (1), 3260.
84. Wang, F.; Liu, Z.; Yang, C.; Zhong, H.; Nam, G.; Zhang, P.; Dong, R.; Wu, Y.; Cho, J.; Zhang, J.; Feng, X., Fully conjugated phthalocyanine copper metal-organic frameworks for sodium–iodine batteries with long-time-cycling durability. *Advanced Materials* **2020,** *32* (4), 1905361.
85. Meng, Z.; Aykanat, A.; Mirica, K. A., Welding metallophthalocyanines into bimetallic molecular meshes for ultrasensitive, low-power chemiresistive detection of gases. *Journal of the American Chemical Society* **2019,** *141* (5), 2046-2053.
86. Zhong, H.; Ghorbani-Asl, M.; Ly, K. H.; Zhang, J.; Ge, J.; Wang, M.; Liao, Z.; Makarov, D.; Zschech, E.; Brunner, E.; Weidinger, I. M.; Zhang, J.; Krasheninnikov, A. V.; Kaskel, S.; Dong, R.; Feng, X., Synergistic electroreduction of carbon dioxide to carbon monoxide on bimetallic layered conjugated metal-organic frameworks. *Nature Communications* **2020,** *11* (1), 1409.
87. Wang, M.; Shi, H.; Zhang, P.; Liao, Z.; Wang, M.; Zhong, H.; Schwotzer, F.; Nia, A. S.; Zschech, E.; Zhou, S.; Kaskel, S.; Dong, R.; Feng, X., Phthalocyanine-based 2D conjugated metal-organic framework nanosheets for high-performance micro-supercapacitors. *Advanced Functional Materials* **2020,** *30* (30), 2002664.
88. Meng, Z.; Luo, J.; Li, W.; Mirica, K. A., Hierarchical tuning of the performance of electrochemical carbon dioxide reduction using conductive two-dimensional metallophthalocyanine based metal-organic frameworks. *Journal of the American Chemical Society* **2020,** *142* (52), 21656-21669.
89. Yi, J.-D.; Si, D.-H.; Xie, R.; Yin, Q.; Zhang, M.-D.; Wu, Q.; Chai, G.-L.; Huang, Y.-B.; Cao, R., Conductive two-dimensional phthalocyanine-based metal-organic framework nanosheets for efficient electroreduction of CO_2. *Angewandte Chemie International Edition* **2021,** *60* (31), 17108-17114.
90. Zhang, M.-D.; Si, D.-H.; Yi, J.-D.; Yin, Q.; Huang, Y.-B.; Cao, R., Conductive phthalocyanine-based metal-organic framework as a highly efficient electrocatalyst for carbon dioxide reduction reaction. *Science China Chemistry* **2021,** *64* (8), 1332-1339.
91. Lu, S.; Jia, H.; Hummel, M.; Wu, Y.; Wang, K.; Qi, X.; Gu, Z., Two-dimensional conductive phthalocyanine-based metal-organic frameworks for electrochemical nitrite sensing. *RSC Advances* **2021,** *11* (8), 4472-4477.
92. Wang, M.; Zhang, Z.; Zhong, H.; Huang, X.; Li, W.; Hambsch, M.; Zhang, P.; Wang, Z.; St. Petkov, P.; Heine, T.; Mannsfeld, S. C. B.; Feng, X.; Dong, R., Surface-modified phthalocyanine-based two-dimensional conjugated metal-organic framework films for polarity-selective chemiresistive sensing. *Angewandte Chemie International Edition* **2021,** *60* (34), 18666-18672.
93. Matheu, R.; Gutierrez-Puebla, E.; Monge, M. Á.; Diercks, C. S.; Kang, J.; Prévot, M. S.; Pei, X.; Hanikel, N.; Zhang, B.; Yang, P.; Yaghi, O. M., Three-dimensional phthalocyanine metal-catecholates for high electrochemical carbon dioxide reduction. *Journal of the American Chemical Society* **2019,** *141* (43), 17081-17085.

94. Höger, S., Shape-persistent macrocycles: From molecules to materials. *Chemistry – A European Journal* **2004,** *10* (6), 1320-1329.
95. Hu, X.; Yu, C.; D. Okochi, K.; Jin, Y.; Liu, Z.; Zhang, W., Phenylene vinylene macrocycles as artificial transmembrane transporters. *Chemical Communications* **2016,** *52* (34), 5848-5851.
96. Zhang, W.; Moore, J. S., Arylene ethynylene macrocycles prepared by precipitation-driven alkyne metathesis. *Journal of the American Chemical Society* **2004,** *126* (40), 12796-12796.
97. Zhang, J.; Moore, J. S., Nanoarchitectures. 6. Liquid crystals based on shape-persistent macrocyclic mesogens. *Journal of the American Chemical Society* **1994,** *116* (6), 2655-2656.
98. Traber, B.; Oeser, T.; Gleiter, R., Donor–acceptor-substituted phenylacetylene macrocycles with threefold symmetry. *European Journal of Organic Chemistry* **2005,** *2005* (7), 1283-1292.
99. Cantin, K.; Rondeau-Gagné, S.; Néabo, J. R.; Daigle, M.; Morin, J.-F., H-Bonding-driven gel formation of a phenylacetylene macrocycle. *Organic & Biomolecular Chemistry* **2011,** *9* (12), 4440-4443.
100. Zhou, X.; Liu, G.; Yamato, K.; Shen, Y.; Cheng, R.; Wei, X.; Bai, W.; Gao, Y.; Li, H.; Liu, Y.; Liu, F.; Czajkowsky, D. M.; Wang, J.; Dabney, M. J.; Cai, Z.; Hu, J.; Bright, F. V.; He, L.; Zeng, X. C.; Shao, Z.; Gong, B., Self-assembling subnanometer pores with unusual mass-transport properties. *Nature Communications* **2012,** *3* (1), 949.
101. Li, J.; Zhou, W.; Yang, J.; Lang, X.; Huang, P., One-dimensional self-assembly of phenylacetylene macrocycles: Effect of peripheral substituents. *Journal of Colloid and Interface Science* **2013,** *395*, 99-103.
102. Yamasaki, R.; Shigeto, A.; Saito, S., Preparation of shape-persistent macrocycles with a single pyridine unit by double cross-coupling reactions of aryl bromides and alkynes. *The Journal of Organic Chemistry* **2011,** *76* (24), 10299-10305.
103. Zhong, Y.; Wang, Q.; Yang, Y.; Lu, Z.; He, L.; Gong, B., Hexakis(*m*-phenylene ethynylene) macrocycles with multiple H-Bonding side chains and modified cavities: Altered stacking strength and persistent tubular assembly. *Organic Letters* **2016,** *18* (9), 2094-2097.
104. Mindyuk, O. Y.; Stetzer, M. R.; Heiney, P. A.; Nelson, J. C.; Moore, J. S., High resolution X-ray diffraction study of a tubular liquid crystal. *Advanced Materials* **1998,** *10* (16), 1363-1366.
105. Zhang, J.; Pesak, D. J.; Ludwick, J. L.; Moore, J. S., Geometrically-controlled and site-specifically-functionalized phenylacetylene macrocycles. *Journal of the American Chemical Society* **1994,** *116* (10), 4227-4239.
106. Popov, I.; Chen, T.-H.; Belyakov, S.; Daugulis, O.; Wheeler, S. E.; Miljanić, O. Š., Macrocycle embrace: Encapsulation of fluoroarenes by *m*-phenylene ethynylene host. *Chemistry – A European Journal* **2015,** *21* (7), 2750-2754.
107. Chinchilla, R.; Nájera, C., The Sonogashira reaction: A booming methodology in synthetic organic chemistry. *Chemical Reviews* **2007,** *107* (3), 874-922.
108. Sakamoto, K.; Ohno-Okumura, E., Syntheses and functional properties of phthalocyanines. *Materials* **2009,** *2* (3), 1127-1179.
109. Nemykin, V. N.; Lukyanets, E. A., Synthesis of substituted phthalocyanines. *ARKIVOC* **2010,** *2010* (1), 136-208.
110. Wöhrle, D.; Schnurpfeil, G.; Knothe, G., Efficient synthesis of phthalocyanines and related macrocyclic compounds in the presence of organic bases. *Dyes and Pigments* **1992,** *18* (2), 91-102.

111. Oliver, S. W.; Smith, T. D., Oligomeric cyclization of dinitriles in the synthesis of phthalocyanines and related compounds: the role of the alkoxide anion. *Journal of the Chemical Society, Perkin Transactions 2* **1987,** (11), 1579-1582.
112. Christie, R. M.; Deans, D. D., An investigation into the mechanism of the phthalonitrile route to copper phthalocyanines using differential scanning calorimetry. *Journal of the Chemical Society, Perkin Transactions 2* **1989,** (2), 193-198.
113. Zou, D.; Liu, D.; Zhang, J., From zeolitic imidazolate framework-8 to metal-organic frameworks (MOFs): Representative substance for the general study of pioneering MOF applications. *Energy & Environmental Materials* **2018,** *1* (4), 209-220.
114. Chen, B.; Yang, Z.; Zhu, Y.; Xia, Y., Zeolitic imidazolate framework materials: recent progress in synthesis and applications. *Journal of Materials Chemistry A* **2014,** *2* (40), 16811-16831.
115. Ravi, O.; Shaikh, A.; Upare, A.; Singarapu, K. K.; Bathula, S. R., Benzimidazoles from aryl alkyl ketones and 2-amino anilines by an iodine catalyzed oxidative C(CO)–C(alkyl) bond cleavage. *The Journal of Organic Chemistry* **2017,** *82* (8), 4422-4428.
116. Alaqeel, S. I., Synthetic approaches to benzimidazoles from *o*-phenylenediamine: A literature review. *Journal of Saudi Chemical Society* **2017,** *21* (2), 229-237.
117. Lin, S.; Yang, L., A simple and efficient procedure for the synthesis of benzimidazoles using air as the oxidant. *Tetrahedron Letters* **2005,** *46* (25), 4315-4319.
118. Ridley, H. F.; Spickett, R. G. W.; Timmis, G. M., A new synthesis of benzimidazoles and aza-analogs. *Journal of Heterocyclic Chemistry* **1965,** *2* (4), 453-456.
119. Betti, M.; Genesio, E.; Marconi, G.; Sanna Coccone, S.; Wiedenau, P., A scalable route to the SMO receptor antagonist SEN826: Benzimidazole synthesis via enhanced in situ formation of the bisulfite–aldehyde complex. *Organic Process Research & Development* **2014,** *18* (6), 699-708.
120. Göker, H.; Kuş, C.; Boykin, D. W.; Yildiz, S.; Altanlar, N., Synthesis of some new 2-substituted-phenyl-1H-benzimidazole-5-carbonitriles and their potent activity against candida species. *Bioorganic & Medicinal Chemistry* **2002,** *10* (8), 2589-2596.
121. Göker, H.; Alp, M.; Ateş-Alagöz, Z.; Yıldız, S., Synthesis and potent antifungal activity against Candida species of some novel 1H-benzimidazoles. *Journal of Heterocyclic Chemistry* **2009,** *46* (5), 936-948.
122. Zanon, J.; Klapars, A.; Buchwald, S. L., Copper-catalyzed domino halide exchange-cyanation of aryl bromides. *Journal of the American Chemical Society* **2003,** *125* (10), 2890-2891.
123. PARDO, C.; YUSTE, M.; ELGUERO, J., Tetraimidazophthalocyanines. *Journal of Porphyrins and Phthalocyanines* **2000,** *04* (05), 505-509.
124. Önal, E.; Dumoulin, F.; Hirel, C., Tetraimidazophthalocyanines: influence of protonation and aggregation on spectroscopic observations. *Journal of Porphyrins and Phthalocyanines* **2009,** *13* (06), 702-711.
125. Mitzel, F.; FitzGerald, S.; Beeby, A.; Faust, R., Acetylenic quinoxalinoporphyrazines as photosensitisers for photodynamic therapy. *Chemistry – A European Journal* **2003,** *9* (5), 1233-1241.
126. Mitzel, F.; FitzGerald, S.; Beeby, A.; Faust, R., Octaalkynyltetra[6,7]quinoxalinoporphyrazines: a new class of photosensitisers with potential for photodynamic therapy. *Chemical Communications* **2001,** (24), 2596-2597.
127. Burmester, C.; Faust, R., A reliable route to 1,2-diamino-4,5-phthalodinitrile. *Synthesis* **2008,** *2008* (08), 1179-1181.

128. Youngblood, W. J., Synthesis of a new trans-A2B2 Phthalocyanine motif as a building block for rodlike phthalocyanine polymers. *The Journal of Organic Chemistry* **2006,** *71* (9), 3345-3356.
129. Maizlish, V. E.; Shaposhnikov, G. P.; Balakireva, O. V.; Zharnikova, M. A.; Abramov, I. G.; Ivanovskii, S. A.; Smirnov, A. V., Metal complexes of phthalocyanine structural analogs with oxygen- or nitrogen-containing heterorings. Synthesis and properties. *Russian Journal of General Chemistry* **2004,** *74* (5), 787-790.
130. Balakirev, A. E.; Kudrik, E. V.; Shaposhnikov, G. P., Synthesis and properties of copper(II) tetra(2-alkyl-4,5-benzimidazolo)- and tetra(2,2'-Dimethyl-4,5-benzodiazepino)porphyrazines. *Russian Journal of General Chemistry* **2002,** *72* (10), 1616-1619.
131. Topal, S. Z.; Önal, E.; Gürek, A. G.; Hirel, C., pH-induced "off-on-off" type molecular switch behaviors of zinc and free tetraimidazophthalocyanines. *Dalton Transactions* **2013,** *42* (32), 11528-11536.
132. Padmaja, K.; Youngblood, W. J.; Wei, L.; Bocian, D. F.; Lindsey, J. S., Triple-decker sandwich compounds bearing compact triallyl tripods for molecular information storage applications. *Inorganic Chemistry* **2006,** *45* (14), 5479-5492.
133. Galanin, N. E.; Kudrik, E. V.; Shaposhnikov, G. P., Synthesis and spectral characteristics of phthalocyanines of unsymmetrical structure containing fragments of 3,6-didecyloxyphthalonitrile and 2-methyl-5,6-dicyanobenzimidazole. *Russian Journal of Organic Chemistry* **2008,** *44* (2), 225-230.
134. Schönamsgruber, J.; Maid, H.; Bauer, W.; Hirsch, A., Fused perylene-phthalocyanine macrocycles: a new family of NIR-dyes with pronounced basicity. *Chemistry* **2014,** *20* (51), 16969-79.
135. Dede, G.; Bayrak, R.; Er, M.; Özkaya, A. R.; Değirmencioğlu, İ., DBU-catalyzed condensation of metal free and metallophthalocyanines containing thiazole and azine moieties: Synthesis, characterization and electrochemical properties. *Journal of Organometallic Chemistry* **2013,** *740*, 70-77.
136. Cong, F.; Wei, Z.; Huang, Z.; Yu, F.; Liu, H.; Cui, J.; Yu, H.; Chu, X.; Du, X.; Xing, K.; Lai, J., Characteristic absorption band split of symmetrically tetra-octyloxy metal phthalocyanines. *Dyes and Pigments* **2015,** *120*, 1-7.
137. Ogunbayo, T. B.; Nyokong, T., Photophysical and photochemical properties of Ni(II), Pd(II) and Pt(II) aryloxo and alkylthio derivatised phthalocyanine. *Journal of Molecular Structure* **2010,** *973* (1), 96-103.
138. Kimura, M.; Sakaguchi, A.; Ohta, K.; Hanabusa, K.; Shirai, H.; Kobayashi, N., Selective ligation to sterically isolated metallophthalocyanines. *Inorganic Chemistry* **2003,** *42* (9), 2821-2823.
139. Bayo, K.; Mossoyan, J. C.; Ouedraogo, G. V., Preparation and analysis by UV-Vis of zinc phthalocyanine complexes. *Spectrochimica Acta Part A: Molecular and Biomolecular Spectroscopy* **2004,** *60* (3), 653-657.
140. Yüksel, F.; Gül Gürek, A.; Lebrun, C.; Ahsen, V., Synthesis and solvent effects on the spectroscopic properties of octatosylamido phthalocyanines. *New Journal of Chemistry* **2005,** *29* (5), 726-732.
141. Snow, A. W., 109 - Phthalocyanine aggregation. In *The Porphyrin Handbook*, Kadish, K. M.; Smith, K. M.; Guilard, R., Eds. Academic Press: Amsterdam, 2003; pp 129-176.
142. Bennett, T. D.; Cheetham, A. K., Amorphous metal-organic frameworks. *Accounts of Chemical Research* **2014,** *47* (5), 1555-1562.

143. Hou, J.; Sapnik, A. F.; Bennett, T. D., Metal-organic framework gels and monoliths. *Chemical Science* **2020,** *11* (2), 310-323.
144. Katz, M. J.; Brown, Z. J.; Colón, Y. J.; Siu, P. W.; Scheidt, K. A.; Snurr, R. Q.; Hupp, J. T.; Farha, O. K., A facile synthesis of UiO-66, UiO-67 and their derivatives. *Chemical Communications* **2013,** *49* (82), 9449-9451.
145. Klinowski, J.; Almeida Paz, F. A.; Silva, P.; Rocha, J., Microwave-assisted synthesis of metal-organic frameworks. *Dalton Transactions* **2011,** *40* (2), 321-330.
146. Ameloot, R.; Stappers, L.; Fransaer, J.; Alaerts, L.; Sels, B. F.; De Vos, D. E., Patterned growth of metal-organic framework coatings by electrochemical synthesis. *Chemistry of Materials* **2009,** *21* (13), 2580-2582.
147. Friščić, T., New opportunities for materials synthesis using mechanochemistry. *Journal of Materials Chemistry* **2010,** *20* (36), 7599-7605.
148. Vaitsis, C.; Sourkouni, G.; Argirusis, C., Metal organic frameworks (MOFs) and ultrasound: A review. *Ultrasonics Sonochemistry* **2019,** *52*, 106-119.
149. He, H.; Hashemi, L.; Hu, M.-L.; Morsali, A., The role of the counter-ion in metal-organic frameworks' chemistry and applications. *Coordination Chemistry Reviews* **2018,** *376*, 319-347.
150. Doan, H. V.; Fang, Y.; Yao, B.; Dong, Z.; White, T. J.; Sartbaeva, A.; Hintermair, U.; Ting, V. P., Controlled formation of hierarchical metal-organic frameworks using CO_2-expanded solvent systems. *ACS Sustainable Chemistry & Engineering* **2017,** *5* (9), 7887-7893.
151. Ameloot, R.; Gobechiya, E.; Uji-i, H.; Martens, J. A.; Hofkens, J.; Alaerts, L.; Sels, B. F.; De Vos, D. E., Direct patterning of oriented metal-organic framework crystals via control over crystallization kinetics in clear precursor solutions. *Advanced Materials* **2010,** *22* (24), 2685-2688.
152. Feng, X.; Wu, T.; Carreon, M. A., Synthesis of ZIF-67 and ZIF-8 crystals using DMSO (Dimethyl Sulfoxide) as solvent and kinetic transformation studies. *Journal of Crystal Growth* **2016,** *455*, 152-156.
153. Seetharaj, R.; Vandana, P. V.; Arya, P.; Mathew, S., Dependence of solvents, pH, molar ratio and temperature in tuning metal organic framework architecture. *Arabian Journal of Chemistry* **2019,** *12* (3), 295-315.
154. de Oliveira, C. A. F.; da Silva, F. F.; Malvestiti, I.; Malta, V. R. d. S.; Dutra, J. D. L.; da Costa, N. B.; Freire, R. O.; Júnior, S. A., Effect of temperature on formation of two new lanthanide metal-organic frameworks: Synthesis, characterization and theoretical studies of Tm(III)-succinate. *Journal of Solid State Chemistry* **2013,** *197*, 7-13.
155. Howarth, A. J.; Peters, A. W.; Vermeulen, N. A.; Wang, T. C.; Hupp, J. T.; Farha, O. K., Best practices for the synthesis, activation, and characterization of metal-organic frameworks. *Chemistry of Materials* **2017,** *29* (1), 26-39.
156. Diring, S.; Furukawa, S.; Takashima, Y.; Tsuruoka, T.; Kitagawa, S., Controlled multiscale synthesis of porous coordination polymer in nano/micro regimes. *Chemistry of Materials* **2010,** *22* (16), 4531-4538.
157. Umemura, A.; Diring, S.; Furukawa, S.; Uehara, H.; Tsuruoka, T.; Kitagawa, S., Morphology design of porous coordination polymer crystals by coordination modulation. *Journal of the American Chemical Society* **2011,** *133* (39), 15506-15513.
158. Marshall, R. J.; Hobday, C. L.; Murphie, C. F.; Griffin, S. L.; Morrison, C. A.; Moggach, S. A.; Forgan, R. S., Amino acids as highly efficient modulators for single crystals of zirconium and hafnium metal-organic frameworks. *Journal of Materials Chemistry A* **2016,** *4* (18), 6955-6963.

159. Ragon, F.; Horcajada, P.; Chevreau, H.; Hwang, Y. K.; Lee, U. H.; Miller, S. R.; Devic, T.; Chang, J.-S.; Serre, C., In situ energy-dispersive X-ray diffraction for the synthesis optimization and scale-up of the porous zirconium terephthalate UiO-66. *Inorganic Chemistry* **2014,** *53* (5), 2491-2500.
160. Gutov, O. V.; Molina, S.; Escudero-Adán, E. C.; Shafir, A., Modulation by amino acids: Toward superior control in the synthesis of zirconium metal-organic frameworks. *Chemistry – A European Journal* **2016,** *22* (38), 13582-13587.
161. Schaate, A.; Roy, P.; Godt, A.; Lippke, J.; Waltz, F.; Wiebcke, M.; Behrens, P., Modulated synthesis of Zr-based metal-organic frameworks: From nano to single crystals. *Chemistry – A European Journal* **2011,** *17* (24), 6643-6651.
162. Ma, J.; Wong-Foy, A. G.; Matzger, A. J., The role of modulators in controlling layer spacings in a tritopic linker based zirconium 2D microporous coordination polymer. *Inorganic Chemistry* **2015,** *54* (10), 4591-4593.
163. Lyu, J.; Gong, X.; Lee, S.-J.; Gnanasekaran, K.; Zhang, X.; Wasson, M. C.; Wang, X.; Bai, P.; Guo, X.; Gianneschi, N. C.; Farha, O. K., Phase transitions in metal-organic frameworks directly monitored through in situ variable temperature liquid-cell transmission electron microscopy and in situ X-ray diffraction. *Journal of the American Chemical Society* **2020,** *142* (10), 4609-4615.
164. Vermoortele, F.; Bueken, B.; Le Bars, G.; Van de Voorde, B.; Vandichel, M.; Houthoofd, K.; Vimont, A.; Daturi, M.; Waroquier, M.; Van Speybroeck, V.; Kirschhock, C.; De Vos, D. E., Synthesis modulation as a tool to increase the catalytic activity of metal-organic frameworks: The unique case of UiO-66(Zr). *Journal of the American Chemical Society* **2013,** *135* (31), 11465-11468.
165. Mondloch, J. E.; Karagiaridi, O.; Farha, O. K.; Hupp, J. T., Activation of metal-organic framework materials. *CrystEngComm* **2013,** *15* (45), 9258-9264.
166. Nelson, A. P.; Farha, O. K.; Mulfort, K. L.; Hupp, J. T., Supercritical processing as a route to high internal surface areas and permanent microporosity in metal-organic framework materials. *Journal of the American Chemical Society* **2009,** *131* (2), 458-460.
167. Øien, S.; Wragg, D.; Reinsch, H.; Svelle, S.; Bordiga, S.; Lamberti, C.; Lillerud, K. P., Detailed structure analysis of atomic positions and defects in zirconium metal-organic frameworks. *Crystal Growth & Design* **2014,** *14* (11), 5370-5372.
168. Gandara, F.; Bennett, T. D., Crystallography of metal-organic frameworks. *IUCrJ* **2014,** *1* (6), 563-570.
169. Hirschle, P.; Preiß, T.; Auras, F.; Pick, A.; Völkner, J.; Valdepérez, D.; Witte, G.; Parak, W. J.; Rädler, J. O.; Wuttke, S., Exploration of MOF nanoparticle sizes using various physical characterization methods – is what you measure what you get? *CrystEngComm* **2016,** *18* (23), 4359-4368.
170. Ambroz, F.; Macdonald, T. J.; Martis, V.; Parkin, I. P., Evaluation of the BET theory for the characterization of meso and microporous MOFs. *Small Methods* **2018,** *2* (11), 1800173.
171. Park, J.; Howe, J. D.; Sholl, D. S., How reproducible are isotherm measurements in metal-organic frameworks? *Chemistry of Materials* **2017,** *29* (24), 10487-10495.
172. Wang, T. C.; Vermeulen, N. A.; Kim, I. S.; Martinson, A. B. F.; Stoddart, J. F.; Hupp, J. T.; Farha, O. K., Scalable synthesis and post-modification of a mesoporous metal-organic framework called NU-1000. *Nature Protocols* **2016,** *11* (1), 149-162.

173. Feng, D.; Jiang, H.-L.; Chen, Y.-P.; Gu, Z.-Y.; Wei, Z.; Zhou, H.-C., Metal-organic frameworks based on previously unknown Zr_8/Hf_8 cubic clusters. *Inorganic Chemistry* **2013,** *52* (21), 12661-12667.
174. Feng, D.; Gu, Z.-Y.; Chen, Y.-P.; Park, J.; Wei, Z.; Sun, Y.; Bosch, M.; Yuan, S.; Zhou, H.-C., A highly stable porphyrinic zirconium metal-organic framework with shp-a topology. *Journal of the American Chemical Society* **2014,** *136* (51), 17714-17717.
175. Feng, D.; Chung, W.-C.; Wei, Z.; Gu, Z.-Y.; Jiang, H.-L.; Chen, Y.-P.; Darensbourg, D. J.; Zhou, H.-C., Construction of ultrastable porphyrin Zr metal-organic frameworks through linker elimination. *Journal of the American Chemical Society* **2013,** *135* (45), 17105-17110.
176. Jiang, H.-L.; Feng, D.; Wang, K.; Gu, Z.-Y.; Wei, Z.; Chen, Y.-P.; Zhou, H.-C., An exceptionally stable, porphyrinic Zr metal-organic framework exhibiting pH-dependent fluorescence. *Journal of the American Chemical Society* **2013,** *135* (37), 13934-13938.
177. Fritzsche, M.; Jester, S.-S.; Höger, S.; Klaus, C.; Dingenouts, N.; Linder, P.; Drechsler, M.; Rosenfeldt, S., Self-organization of coil-ring-coil structures into tubular supramolecular polymer brushes: Synthesis, morphology, and growth. *Macromolecules* **2010,** *43* (20), 8379-8388.
178. Höger, S.; Rosselli, S.; Ramminger, A.-D.; Enkelmann, V., A facile synthesis of large extraannular-functionalized phenyl-ethynyl macrocycles containing m-terphenyl units. *Organic Letters* **2002,** *4* (24), 4269-4272.
179. Joyner, R. D.; Kenney, M. E., Phthalocyaninosilicon compounds. *Inorganic Chemistry* **1962,** *1* (2), 236-238.
180. Raboui, H.; Al-Amar, M.; Abdelrahman, A. I.; Bender, T. P., Axially phenoxylated aluminum phthalocyanines and their application in organic photovoltaic cells. *RSC Advances* **2015,** *5* (57), 45731-45739.
181. Brasseur, N.; Ouellet, R.; Madeleine, C. L.; Lier, J. E. V., Water-soluble aluminium phthalocyanine–polymer conjugates for PDT: photodynamic activities and pharmacokinetics in tumour-bearing mice. *British Journal of Cancer* **1999,** *80* (10), 1533-1541.
182. Beeby, A.; FitzGerald, S.; Stanley, C. F., A photophysical study of protonated (tetra-tert-butylphthalocyaninato)zinc. *Journal of the Chemical Society, Perkin Transactions 2* **2001,** (10), 1978-1982.
183. Semyannikov, P. P.; Basova, T. V.; Grankin, V. M.; Igumenov, I. K., Vapour pressure of some phthalocyanines. *Journal of Porphyrins and Phthalocyanines* **2000,** *4* (3), 271-277.
184. Wagner, H. J.; Loutfy, R. O.; Hsiao, C.-K., Purification and characterization of phthalocyanines. *Journal of Materials Science* **1982,** *17* (10), 2781-2791.
185. Takaishi, S.; DeMarco, E. J.; Pellin, M. J.; Farha, O. K.; Hupp, J. T., Solvent-assisted linker exchange (SALE) and post-assembly metallation in porphyrinic metal-organic framework materials. *Chemical Science* **2013,** *4* (4), 1509-1513.
186. Dodson, R. A.; Kalenak, A. P.; Matzger, A. J., Solvent choice in metal-organic framework linker exchange permits microstructural control. *Journal of the American Chemical Society* **2020,** *142* (49), 20806-20813.